DISSERTATION

TARGETING PROTEOSTATIC MAINTENANCE AND MITOCHONDRIAL FUNCTION WITH PHYTOCHEMICAL COMPOUNDS IN MODELS OF BRAIN AND SKELETAL MUSCLE AGING

Submitted by

Maureen Ann Walsh

Department of Health and Exercise Science

In partial fulfillment of the requirements

For the Degree of Doctor of Philosophy

Colorado State University

Fort Collins, Colorado

Spring 2024

Doctoral Committee:

Advisor: Karyn L. Hamilton

Brett W. Fling
Julie A. Moreno
Thomas J. LaRocca
Kelly S. Santangelo

ABSTRACT

TARGETING PROTEOSTATIC MAINTENANCE AND MITOCHONDRIAL FUNCTION WITH PHYTOCHEMICAL COMPOUNDS IN MODELS OF BRAIN AND SKELETAL MUSCLE AGING

There is a growing population of older adults (>65+ years) worldwide that is projected to increase in coming decades, presenting both a challenge and an opportunity. Specifically, age is the number one risk factor for chronic diseases like sarcopenia, the loss of muscle mass and function, and neurodegenerative diseases such as Alzheimer's Disease. The twelve hallmarks of aging are a collection of cellular changes that drive the aging process. Two highly interconnected hallmarks of aging that drive the development and progression of sarcopenia and neurodegeneration are loss of proteostasis (protein homeostasis) and mitochondrial dysfunction. While progress has been made in understanding the etiology of chronic diseases, treatments for age-related chronic diseases affecting skeletal muscle and the brain are lacking. One reason for the lack of effective treatments in humans is the absence of preclinical animal models that recapitulate human aging. However, our group previously identified the Hartley guinea pig as a novel model of brain and skeletal muscle aging. We then treated these guinea pigs with a phytochemical compound to delay the onset and/or slow the progression of brain and skeletal muscle aging. Through the experiments in this dissertation, I observed that: 1.) phytochemical compounds, branded as Protandim, can improve mechanisms of proteostasis independent of changes in mitochondrial respiration in muscle precursor cells; 2.) the phytochemical compound, branded as PB125, can improve mechanisms of skeletal muscle proteostasis in the Hartley guinea pig; 3.) PB125 can also decrease neuroinflammation in the Hartley guinea pig; and 4.) despite the lack of declines in hippocampal mitochondrial respiration with age, Hartley guinea pigs exhibit decreased mitochondrial efficiency. Collectively, this

dissertation builds on prior work suggesting that the Hartley guinea pig is a valuable model to test preclinical interventions.

ACKNOWLEDGEMENTS

This work was funded by NIH R21 AG054713-02, the Colorado Clinical and Translation Sciences Institute grant UM1TR004399, Rocky Mountain American College of Sports Medicine Graduate Research Grant, and the Colorado State University College of Health and Human Science Dean's Fellowship.

There are many people who have contributed to my intellectual and personal graduate school journey and, therefore, these words are for them. First and foremost a thank you to my mentor, Dr. Karyn Hamilton, who has been essential in my development as a scientist and person. Not only did you let me come back to learn from you, but you did with open arms. You have continued to be an incredible role model, strong woman in science, and an all-around exceptional human. Second, thank you to my committee members Drs. Brett Fling, Tom LaRocca, Julie Moreno, and Kelly Santangelo as well as Kimber Finan, my supervised college teaching mentor. Each of you have aided in my scientific and professional development. In every conversation with each of you individually or as a group, no matter how short or long, I have grasped so much advice that I will remember throughout my personal and professional journeys. I also found two people who I coined my science older sisters during my graduate school training. Thank you to Drs. Becky Scalzo and Sarah Wherry for your encouragement, support, and realistic outlooks on science and life.

Next, there is so much gratitude to express to the current and past members of the TRACD lab. Not only did I grow in my scientific skill set because of your help, but I grew as a person both inside and outside the lab always having fun and forming lasting memories. Dr. Qian Zhang thank you for teaching me all there is to know about cell culture and gas-chromatography mass spectrometry. You did so with patience and kindness all while sharing

great wisdom in our daily conversations. Dr. Robby Jacobs thank you for helping me establish new respirometry experiments and fostering an amazing collaboration while providing mentorship along the way. Finally, Dr. Rob Musci thank you for serving as a life-long mentor and friend. You helped me navigate the challenging waters of Utah and come out the other side more independent. Of course, an entire sentence should be dedicated to teaching me how to run an O2k.

I would also like to convey gratitude to my friends for supporting me on my hardest days, months, and years of graduate school. Dr. Meg Smith and I showed up at CSU from the same state not knowing each other. Maybe we were first bonded by our love of being from PA but since I thank you for listening, encouraging, and believing in me. I am excited for our journeys ahead as we return to our undergraduate institutions (#PAProf) to inspire the next generation of exercise scientists. The next thank you is for Master x 2 Moriah Brenneman. You helped me through literal house fires and figurative ones too. I do not think we truly knew the memories that we would make when we agree to be roommates but if I had to go through any of those terrible things, I am glad I did it with you and Strider too. Anyone who know me knows I love to run. However, there was a period in graduate school that running, and life were very challenging yet there was one exceptional person who reminded me of what a non-linear running journey (and life journey) looked like. Alissa Newman, thank you for your friendship, our Friday Five runs around the cemetery in rain, wind, or shine, and all the conversations along the way. You sat in the dirt with me on my worst days and celebrated the best ones. You are a remarkable human and helped me become a better version of myself. On the topic of running, I thank all my other friends who I have shared miles with including Kristen Glennie, Elena Lancioni, Sarah Morton, Sophie Seward, and Devin Wahl. Your positive outlooks on running and life will always resonate with me. Collectively, I tried to build a strong support network which indeed happened. However, it is never too late to grow a network and within my last year of graduate school the amazing

Kylee Van Horn was added to my team of supporters. Thank you, Kylee, for the encouragement, conversations, and smart ways to fuel, train, and PR in the final months of my graduate school journey.

The next significant thank you goes to my family for constantly offering words of support and encouragement. To my brother, Jonathan Walsh, you make me laugh when I need it most. You bring both humor and humility to our family, two qualities that have helped tremendously along the way. To my dad, Joe Walsh, you have taught me numerous life lessons. However, the greatest were the value of hard work and the exemplary team leadership skills through my years working alongside of you. I, of course, also want to acknowledge O'Neill Coffee Roasters for the copious amount of caffeine sent to Fort Collins, Colorado. To my mom, Dr. Christine Walsh, the inspiration behind it all. When you decided to pursue a Ph.D. when I was 8 years old, I did not really know what that meant. Fast forward almost 20 years later and I think I have a much better grasp on the matter. Nonetheless you embarked on an academic challenging setting the example. Because of yours and dad's encouragement, I held the belief that I could pursue challenges, demonstrate perseverance, and value life-long learning. You are a smart lady so you probably know that you wrote these words in your dissertation dedication unbeknownst they would come true years later. Now I cannot wait to be your colleague.

Four years ago, I defended my master's thesis, and this is where my acknowledgements ended. However, a lot has changed in those four years. In addition to collecting more data and writing more papers there is one other thing I found along the way. I found my best friend. Dr. Chris Rom you have changed my life in more ways than one. Within three days of moving back to Fort Collins to continue my Ph.D. at CSU I met you in a coffee shop. Thank you CeAnn Udovich for accidentally facilitating this one. Was this meant to be? I sure think so. The hard parts of my Ph.D. became more enjoyable with you by my side all the while you earned your Ph.D. as well. You showed me that "teamwork can make the dreamwork" and I am so excited to

be on your team living our dream.

TABLE OF CONTENTS

CHAPTER 1 – INTRODUCTION AND EXPERIMENTAL AIMS

DRIVERS OF AGING AND AGE-RELATED CHRONIC DISEASES

Aging comprises an organism's progressive structural and functional declines, culminating in disease and death. Whether or not one defines aging itself as a disease, there is no cure for aging. However, lifespan, the period from birth until death, has increased over the last century in part due to the development of vaccines, antibiotics, and improved sanitary practices. Currently, the leading causes of death are chronic diseases [1]. Healthspan, a subset of lifespan, is the period one remains free from chronic diseases [2]. While individuals are living longer, they are spending on average more of that time burdened by chronic diseases. Thus, a common goal in the field of geroscience is to extend human healthspan through targeting the biological processes that drive aging [2].

Through decades of research, geroscientists have identified twelve hallmarks of aging, which promote the development and progression of age-related chronic diseases [3]. There are three criteria for a biological process to be considered a hallmark of aging in animals and/or humans: 1. the proposed hallmark accompanies the aging process, 2. experimentally heightening the proposed hallmark accelerates the aging process, and 3. therapeutically targeting the proposed hallmark slows, stops, and/or reverses the aging process [3]. Furthermore, the twelve hallmarks are interconnected.

THE ENERGETIC BUDGET HELPS EXPLAIN THE INTERCONNECTED HALLMARKS OF AGING

The amount of ATP available to an organism in a day is defined as the energetic budget [4]. The energetic budget can be divided into four energy dependent processes related to: 1. life-sustaining processes (e.g., sodium-potassium pumps, cardiac contractions, etc.), 2. growth and maintenance repair (e.g., making new biomass and upkeeping existing biomass, respectively) [5,6], 3. allostasis (i.e., an organism's ability to adapt to stressful situations) [7],

and 4. the reserve (i.e., the energy transformation capacity not consumed by basal life-sustaining processes and normal allostasis) [4]. While humans have abundant energy stores (e.g., adipose tissue) the accessibility of these stores can become impaired with age [8].

Mitochondrial dysfunction, a hallmark of aging [3], constrains the energetic budget, which results in modification of the energy allocated to the growth and maintenance repair [4]. All of the cellular processes to maintain the proteome are referred to as proteostasis, which falls within the maintenance repair component of the energetic budget. When the processes that maintain the proteome are disrupted, protein homeostasis is impaired and this loss of proteostasis is another well-established hallmark of aging. The cellular mechanisms to maintain proteostasis are energetically costly components of cellular maintenance. Specifically, maintaining the proteome accounts for about 20% of basal metabolism, and is the most energetically costly process in cells [9,10]. Furthermore, when mitochondrial dysfunction creates an energetic constraint, it consequently leads to a decrease in ATP allocated for maintaining the proteome [11,12]. The aging process occurs partially due to the result of the accumulation of damage (a consequence of mitochondrial dysfunction and chronic inflammation, another hallmark of aging) through imperfect somatic (specifically proteostatic) maintenance. Collectively, mitochondrial dysfunction and loss of proteostasis (the two primary outcomes assessed in this dissertation) are interconnected and critical to cellular and organismal health.

MITOCHONDRIAL DYSFUNCTION WITH AGE: ARE MODELS TRANSLATABLE?

Mitochondrial function is multifaceted including respiration for ATP production [13], calcium handling [14], free radical production [13], fatty acid synthesis [15], and others. These processes are all energy dependent. Thus, ATP production via oxidative phosphorylation (i.e., mitochondrial respiration) remains a primary function of mitochondria, enabling them to energetically support all mitochondrial functions. Mitochondrial dysfunction includes impairments in the numerous functions of a single mitochondrial reticulum, but decreases in oxygen consumption, a measure of mitochondrial respiration, is a robust observation [3]. Specifically,

the Baltimore Longitudinal Aging study reported a significant negative correlation between human age and mitochondrial respiration [16]. Further evidence of this relationship arises from laboratory animal models developed to query contributors to cellular aging. For example, genetic knockout of superoxide dismutase ($Sod1^{-/-}$), a protein that scavenges free radicals, impairs mitochondrial function, and increases oxidative stress [17], which likely contributes to a 30% reduction in murine lifespan [18]. In contrast, targeting mitochondrial function can improve aspects of cellular aging. Genetically increasing mitochondrial peroxiredoxin 3 (mPRDX3), an endogenous antioxidant localized to the mitochondria, in the same $Sod1^{-/-}$ mouse ($Sod1^{-/-}$ x mPRDX3) resulted in an increase in mitochondrial function. However, the use of genetic manipulation to 1. model mitochondrial dysfunction associated with aging (the $Sod1^{-/-}$ mouse), and 2. treat age-related mitochondrial dysfunction (the $Sod1^{-/-}$ x mPRDX3 mouse) lacks translatability for humans. One challenge for accelerating translational aging research targeting mitochondrial function as a treatment is limited availability of preclinical models that recapitulate the human aging phenotype.

LOSS OF PROTEOSTASIS WITH AGE: ARE MODELS TRANSLATABLE?

Protein homeostasis (i.e., proteostasis) includes the cellular processes to maintain the proteome or all the proteins in an organism [19]. The complex proteostatic network includes machinery for synthesis, proper folding, chaperoning to correct cell locations for function, post-translational modifications, and degradation of proteins [19]. However, with age the mechanisms of proteostasis become impaired [20]. While it is highly debated if protein synthesis decreases with age [21], older adults have a blunted response to an anabolic stimulus, resistance exercise, compared to younger adults [22]. Further, genetic loss of nuclear erythroid factor related factor-2 (Nrf2), a transcription factor at the nexus of proteostasis and redox balance [23], impairs mechanisms of protein turnover and accelerates the age-related loss of skeletal muscle mass and function [24]. Conversely, mechanisms of proteostasis have been improved as evidenced by interventions like genetic manipulation to restrict growth [25]. However, like the models of

impairing or improving mitochondrial function noted in the section above, genetic manipulation in the case of growth restriction again does not translate to human aging. Our laboratory has also shown that mechanisms of proteostasis are improved following lifespan-extending treatments, including calorie restriction and treatment with rapamycin, an inhibitor of the mechanistic target of rapamycin complex one (mTORC1) protein kinase [26]. While limiting energy intake is known to improve mechanisms of proteostasis [26,27], adherence to substantial behavior change would be required to translate this healthspan-promoting treatment in humans. While adults had strong compliance with calorie restriction when food was provided and additional motivation was employed [28], this paradigm may lack translatability in our current society due to poor adherence over time [29]. Finally, while rapamycin is gaining traction as a geroprotector, further clinical trials are needed to ensure safety and efficacy in older adults [30]. Thus, while loss of proteostasis exists in older adults and contributes to cellular and organismal aging, there is a lack of preclinical models and translatable treatments to target this hallmark of aging.

THERAPUTICALLY TARGETING MITOCHONDRIAL DYSFUNCTION AND LOSS OF PROTEOSTASIS: WHAT WE KNOW AND WHAT WE DO NOT KNOW

In an experimental paradigm aimed at improving healthspan, a treatment targeting one hallmark of cellular aging (e.g., mitochondrial function), usually improves other hallmarks (e.g., mechanisms of proteostasis) due to their interconnected relationships [31]. One important example of this is chronic exercise training. Endurance exercise training, long known to promote skeletal muscle mitochondrial biogenesis [32–34], also attenuates the age-related decline in skeletal muscle mitochondrial function [35]. In addition to mitochondrial adaptations, exercise promotes skeletal muscle protein turnover [36] and improves other hallmarks of aging in tissues such as the brain [37] and heart [38]. Thus, the scientific community recognizes exercise as a powerful intervention for improving health outcomes and slowing the hallmarks of aging. However, older adults frequently have physical and psychological barriers to performing

exercise including exercise contraindications and low self-efficacy [39], respectively. Therefore, alternative avenues to augment exercise adaptations (i.e., exercise mimetics) might be favorable for those older adults who cannot or do not prefer exercise.

The wide-ranging beneficial adaptations to exercise are, at least in part, orchestrated by the transcription factor Nrf2 [40], which responds to cellular stress and promotes the hormetic adaptations to exercise that culminate in improved health [40,41]. Nrf2 regulates its own transcription, in addition to that of over 400 genes involved in cytoprotection [42,43], by binding to the antioxidant response elements (AREs) in promoter regions of target genes. One target gene is the transcription factor nuclear respiratory factor 1 (NRF1), which activates the expression of key metabolic genes regulating cellular growth and mitochondrial respiration [44,45]. Specifically, NRF1 is a critical transcriptional regulator of nuclear-encoded subunits in mitochondrial electron transfer complexes. NRF1 regulates transcription via binding with the coactivator PGC-1α, considered a master regulator of mitochondrial biogenesis. Expression of PGC-1α increases during periods of energy stress, including calorie restriction [46] and exercise [47]. Additionally, it has been suggested that Nrf2 and NRF1 are both regulated by this transcriptional coactivator, PGC-1α, and thus demonstrate crosstalk [48,49]. Therefore, our group believes that avenues to target Nrf2 and NRF1 pathways may improve mitochondrial function and mitochondrial protein turnover using phytochemical (plant-based) compounds that are also Nrf2 and NRF1 activators (Nrf2a and NRF1a).

SKELETAL MUSCLE AND BRAIN AGING: PRECLINICAL MODELS MATTER

Skeletal muscle and brain aging co-exist in older adults [50] and both are at least part driven by mitochondrial dysfunction and loss of proteostasis [12,51]. Furthermore, the tandem decline in memory and gait speed, respective functions of the brain and musculoskeletal systems, increases the risk for dementia in older adults [52]. However, there are not effective treatments

that slow the functional declines in cognition and mobility in the brain and skeletal muscle, respectively. One likely contributor to the low translational success rate of treatments that show promise in the laboratory to clinical populations is the heavy reliance on preclinical animal models that do now closely mimic the progressive decline in skeletal muscle and brain health in aging humans. For example, the $Nrf2^{-/-}$ mouse [24] experiences a drastic and rapid loss of skeletal muscle mass and function mimicking sarcopenia compared to older wild-type control mice. However, humans experience slow, progressive changes that elicit aging muscle characteristics. A similar paradigm is observed in models of human brain aging and Alzheimer's Disease (AD). Although, there are preclinical animals modeling familial AD [53]; however, 90-95% of human AD cases are sporadic (non-genetic), with an onset occurring later in life [54,55]. While more than 150 rodent models of AD exist, AD drug translation from the laboratory to human fails 99.6% of the time [56]. One reason contributing to this poor success rate for brain aging is likely the absence of laboratory models of spontaneous, progressive neurodegeneration, that also encompass the multimorbidities (i.e., >2 chronic illnesses) present with human aging [57].

Additionally, the underlying etiology of AD is still not understood [58]. One hypothesis is the mitochondrial cascade hypothesis, which postulates that multifaceted mitochondrial dysfunction contributes to amyloid beta (Aβ) dyshomeostasis, driving the development and progression of AD [59]. [59]. Specifically, various metrics of intact platelet mitochondrial respiration, including basal respiration, non-coupled respiration, and mitochondrial reserve capacity, are lower in older adults with AD compared to cognitively healthy older adults independent of plasma concentrations of Aβ [60]. However, this hypothesis had not been tested in a non-transgenic preclinical model that naturally develops progressive neurodegeneration characteristic of human brain aging along with other multimorbidities, including musculoskeletal decline and mobility impairment. Thus, identifying a preclinical model that recapitulates hallmarks of both skeletal muscle and brain aging would be valuable for sarcopenia and neurodegeneration separately but

also for the co-existence of these paralleling age-related changes and for accelerating translation to improve human health.

HARTLEY GUINEA PIGS MODEL BOTH SKELETAL MUSCLE AND BRAIN AGING

Hartley guinea pigs are emerging as a valuable and tractable model of both musculoskeletal aging and neurodegeneration. From a musculoskeletal research perspective, the Hartley guinea pig was first described as a model for progressive osteoarthritis. Beginning at 3-4 months (mo) of age, Hartley guinea pigs begin developing spontaneous osteoarthritis which is accompanied with local and systemic inflammation [61–63]. By ~18 mo, mobility is severely constrained, typically prompting euthanasia [62]. Because osteoarthritis and sarcopenia occur alongside one another in humans [64], we sought to examine myofiber remodeling in the Hartley model. We previously reported that, from 5 to 15 mo, Hartleys mimic myofiber remodeling in aging humans, with decreases in rates of skeletal muscle protein synthesis, declines in mitochondrial function, changes in myofiber distribution, and decreases in skeletal muscle density [65,66]. Hartleys can also develop vascular disease [67] and obesity [68] with age, which are often comorbidities of AD and Alzheimer's Disease Related Dementias (ADRDs) [69,70].

In a prior study, we sought to delay the onset and/or slow the progression of age-related changes in myofiber remodeling by treating Hartley guinea pigs for either 3 or 10 months with the phytochemical Nrf2a, PB125. We observed that 10 mo of daily PB125 treatment slowed the age-related decline in mitochondrial function and mechanisms of proteostasis in a primarily oxidative muscle. However, primarily glycolytic muscles that are more susceptible to age-related changes [71,72]. Thus, we have not examined how 10 mo of daily PB125 treatment affected a muscle composed of type II myofibers.

Recently we also reported that Hartleys have signs of progressive hippocampal neurodegeneration [73]. From 5 to 15 mo of age, there are increases in circulating neurofilament light chain (NFL), hyperphosphorylated tau, Aβ, and glial activation consistent

with human AD [73]. These comparisons were made against the control PigmEnTed (PET) guinea pig strain that exhibited hallmarks of typical human brain aging [73]. One of the most prominent hallmarks of neurodegeneration in the Hartley guinea pig is the presence of spongiosis in the cerebellum. Spongiosis (i.e., spongy brain), characterized by vacuoles in the grey matter, is a prominent aspect of prion disease but can also present in AD [74] and other forms of dementia [75]. While there is uncertainty as to what specifically causes spongiosis, impairments in protein breakdown, a component of proteostasis have been implicated as a contributor to spongiosis and subsequent neuron death [76].

A strength of both the Hartley and PET guinea pig strains for these studies is that they are non-transgenic. Because most of the skeletal muscle and brain aging preclinical models are genetically manipulated, observations in such models may have limitations for translation to human aging [77,78]. Therefore, Hartley and PET guinea pigs are excellent options to evaluate mechanisms of proteostasis and mitochondrial function in skeletal muscle and brain aging and test potential treatments.

SUMMARY, SPECIFIC AIMS, AND HYPOTHESES

Collectively, the following studies seek to contribute to current understanding of how mitochondrial function and loss of proteostasis are interconnected and can be targeted to prevent age-related decline in skeletal muscle and brain. The projects comprising this dissertation explore the potential for NRF1 and Nrf2 activation (through treatment with plant-based compounds) to improve mitochondrial function and mechanisms of proteostasis. They also further establish the translational value of Hartley guinea pigs for understanding mechanisms underlying both skeletal muscle and brain aging, and for identifying the value of targeting mitochondrial function and proteostasis to simultaneously slow the progression of age-related peripheral and central decline. Chapters 2, 3, 4, and 5 represent independent manuscript-style reports of my doctoral research: Chapter 2 is published [79]; Chapters 3 and 4 are in preparation; and Chapter 5 is in revision at Acta Physiologica. Finally, Appendix F

contains another arm of Chapter 3 that may not be included in the manuscript, but the data are helpful in discussing the parent project.

- Chapter 2 Specific Aim: Interrogate the effects of co-treatment with NRF1 and Nrf2 activators for improving mitochondrial respiration, mitochondrial protein content, and mechanisms of mitochondrial proteostasis in response to an oxidative challenge in muscle precursor cells. *I hypothesized that, in comparison to controls, treatment with the combination of NRF1 and Nrf2 activators would improve mechanisms of mitochondrial proteostasis and mitochondrial function to a greater extent than either compound alone, in conditions with or without an oxidative challenge.*
- Chapter 3 Specific Aims: 1.) Confirm that the skeletal muscle aging phenotype is more robust in the Hartley guinea pig strain compared to the PET guinea pig strain; 2.) Evaluate the impact of a 10-month treatment with PB125, a Nrf2 activator, on mechanisms of proteostasis in a predominantly glycolytic skeletal muscle, the tibialis anterior, in Hartley guinea pigs. *I hypothesized that 1.)* PET guinea pigs would not experience the same degree of declines in protein synthesis compared to age matched Hartley guinea pigs; 2.) *Daily PB125 treatment (from 5 to 15 mo) would increase mechanisms of proteostasis in the tibialis anterior, a myofiber more susceptible to age-related changes compared to the control animals.*
- Chapter 4 Specific Aims: 1.) Assess if the presence of an age-related cerebellar phenotype exists in Hartley guinea pigs; 2.) Determine if short-term (3 mo) PB125 treatment could delay the onset of cerebellar aging in Hartley guinea pigs; 3.) Determine if long-term (10 mo) PB125 treatment could slow the progression of cerebellar aging in Hartley guinea pigs. *I hypothesized 1.) Hartley guinea pigs would display decreased rates of cerebellar protein synthesis, progressive spongiosis, and increased gliosis from 5 to 15 mo; 2.) Short-term (3 mo) PB125 treatment would maintain rates of cerebellar protein synthesis while decreasing the degree of spongiosis and gliosis compared to the*

control animals; 3.) Long-term (10 mo) PB125 treatment would increase rates of cerebellar protein synthesis and decrease the degree of spongiosis and gliosis compared to the control animals.

- Chapter 5 Specific Aim: Evaluate hippocampal mitochondrial function (i.e., complex-specific mitochondrial respiration) and mitochondrial protein content in young versus older Hartley and PET guinea pigs. Compared to younger animals, *I hypothesized that 1.) Older Hartley guinea pigs would have lower mitochondrial respiration; however, PET guinea pigs would not have any age-related differences; 2.) Hartley guinea pigs would have an age-related decrease in mitochondrial protein content, but PET guinea pigs would have no age-related differences.*
- Appendix F Specific Aim: Evaluate the impact of 3-month (from 2 to 5 mo of age) PB125 treatment, a Nrf2 activator, on mechanisms of proteostasis in a predominantly glycolytic skeletal muscle in Hartley guinea pigs. *I hypothesized that treatment with PB125 would improve mechanisms of skeletal muscle proteostasis in a predominantly glycolytic muscle compared to the control animals.*

REFERENCES

1. Ahmad FB, Anderson RN. The Leading Causes of Death in the US for 2020. *JAMA*. 2021;325(18):1829-1830. doi:10.1001/jama.2021.5469

2. Seals DR, Justice JN, LaRocca TJ. Physiological geroscience: targeting function to increase healthspan and achieve optimal longevity. *J Physiology*. 2016;594(8):2001-2024. doi:10.1113/jphysiol.2014.282665

3. López-Otín C, Blasco MA, Partridge L, Serrano M, Kroemer and G. Hallmarks of aging: An expanding universe. *Cell*. Published online 2023. doi:10.1016/j.cell.2022.11.001

4. Bobba-Alves N, Juster RP, Picard M. The Energetic Cost of Allostasis and Allostatic Load. *Psychoneuroendocrino*. 2022;146:105951. doi:10.1016/j.psyneuen.2022.105951

5. Kapahi P. Protein Metabolism and Homeostasis in Aging. *Adv Exp Med Biol*. 2010;694:30-37. doi:10.1007/978-1-4419-7002-2_3

6. Hou C, Zuo W, Moses ME, Woodruff WH, Brown JH, West GB. Energy Uptake and Allocation During Ontogeny. *Science*. 2008;322(5902):736-739. doi:10.1126/science.1162302

7. Sterling, Eyer. *Allostasis: A New Paradigm to Explain Arousal Pathology. In Handbook of Life Stress, Cognition and Health*. New York: John Wiley & Sons; 1988.

8. Nguyen D, Samson SL, Reddy VT, Gonzalez EV, Sekhar RV. Impaired mitochondrial fatty acid oxidation and insulin resistance in aging: novel protective role of glutathione. *Aging Cell*. 2013;12(3):415-425. doi:10.1111/acel.12073

9. Waterlow JC. Protein turnover with special reference to man. *Q J Exp Physiol*. 1984;69(3):409-438. doi:10.1113/expphysiol.1984.sp002829

10. Rolfe DF, Brown GC. Cellular energy utilization and molecular origin of standard metabolic rate in mammals. *Physiol Rev*. 1997;77(3):731-758. doi:10.1152/physrev.1997.77.3.731

11. Shaulson ED, Cohen AA, Picard M. The somato-cognitive energy conservation theory of aging. Published online 2023. doi:10.31219/osf.io/zuey2

12. Musci RV, Hamilton KL, Miller BF. Targeting mitochondrial function and proteostasis to mitigate dynapenia. *Eur J Appl Physiol*. 2018;118(1):1-9. doi:10.1007/s00421-017-3730-x

13. Brand MD, Orr AL, Perevoshchikova IV, Quinlan CL. The role of mitochondrial function and cellular bioenergetics in ageing and disease. *Brit J Dermatol*. 2013;169:1-8. doi:10.1111/bjd.12208

14. Balderas E, Eberhardt DR, Lee S, et al. Mitochondrial calcium uniporter stabilization preserves energetic homeostasis during Complex I impairment. *Nat Commun*. 2022;13(1):2769. doi:10.1038/C1467-022-30236-4

15. Nowinski SM, Solmonson A, Rusin SF, et al. Mitochondrial fatty acid synthesis coordinates oxidative metabolism in mammalian mitochondria. *Elife*. 2020;9:e58041. doi:10.7554/elife.58041

16. Gonzalez-Freire M, Scalzo P, D'Agostino J, et al. Skeletal muscle ex vivo mitochondrial respiration parallels decline in vivo oxidative capacity, cardiorespiratory fitness, and muscle strength: The Baltimore Longitudinal Study of Aging. *Aging Cell*. 2018;17(2):e12725. doi:10.1111/acel.12725

17. Deepa SS, Bhaskaran S, Espinoza S, et al. A new mouse model of frailty: the Cu/Zn superoxide dismutase knockout mouse. *Geroscience*. 2017;39(2):187-198. doi:10.1007/s11357-017-9975-9

18. Deepa SS, Remmen HV, Brooks SV, et al. Accelerated sarcopenia in Cu/Zn superoxide dismutase knockout mice. *Free Radical Bio Med*. 2019;132(Geroscience 39 2 2017):19-23. doi:10.1016/j.freeradbiomed.2018.06.032

19. Balch WE, Morimoto RI, Dillin A, Kelly JW. Adapting Proteostasis for Disease Intervention. *Science*. 2008;319(5865):916-919. doi:10.1126/science.1141448

20. Santra M, Dill KA, Graff AMR de. Proteostasis collapse is a driver of cell aging and death. *Proc National Acad Sci*. Published online 2019:201906592. doi:10.1073/pnas.1906592116

21. O'Reilly CL, Bodine SC, Miller BF. Current limitations and future opportunities of tracer studies of muscle ageing. *J Physiol*. Published online 2023. doi:10.1113/jp285616

22. Brook MS, Wilkinson DJ, Mitchell WK, et al. Synchronous deficits in cumulative muscle protein synthesis and ribosomal biogenesis underlie age-related anabolic resistance to exercise in humans. *J Physiology*. 2016;594(24):7399-7417. doi:10.1113/jp272857

23. Gao L, Kumar V, Vellichirammal NN, et al. Functional, proteomic and bioinformatic analyses of Nrf2- and Keap1- null skeletal muscle. *J Physiology*. 2020;598(23):5427-5451. doi:10.1113/jp280176

24. Ahn B, Pharaoh G, Premkumar P, et al. Nrf2 deficiency exacerbates age-related contractile dysfunction and loss of skeletal muscle mass. *Redox Biol*. 2018;17(PLoS One 8 2013):47-58. doi:10.1016/j.redox.2018.04.004

25. Drake JC, Bruns DR, Peelor FF, et al. Long-lived Snell dwarf mice display increased proteostatic mechanisms that are not dependent on decreased mTORC1 activity. *Aging Cell*. 2015;14(3):474-482. doi:10.1111/acel.12329

26. Miller BF, Drake JC, Naylor B, Price JC, Hamilton KL. The measurement of protein synthesis for assessing proteostasis in studies of slowed aging. *Ageing Res Rev*. 2014;18:106-111. doi:10.1016/j.arr.2014.09.005

27. Miller BF, Robinson MM, Reuland DJ, et al. Calorie Restriction Does Not Increase Short-term or Long-term Protein Synthesis. *Journals Gerontology Ser*. 2013;68(5):530-538. doi:10.1093/gerona/gls219

28. Moreira EAM, Most M, Howard J, Ravussin E. Dietary Adherence to Long-Term Controlled Feeding in a Calorie-Restriction Study in Overweight Men and Women. *Nutr Clin Pr*. 2011;26(3):309-315. doi:10.1177/0884533611405992

29. Dorling JL, Das SK, Racette SB, et al. Changes in body weight, adherence, and appetite during 2 years of calorie restriction: the CALERIE 2 randomized clinical trial. *Eur J Clin Nutr*. 2020;74(8):1210-1220. doi:10.1038/C1430-020-0593-8

30. Konopka AR, Lamming DW, Grasso BA, et al. Blazing a trail for the clinical use of rapamycin as a geroprotecTOR. *GeroScience*. 2023;45(5):2769-2783. doi:10.1007/s11357-023-00935-x

31. Zhang Q, Walsh MA, Linden MA, Hamilton KL. Reference Module in Biomedical Sciences. *Encycl Biomed Gerontology*. 2019;(Oxidative Medicine and Cellular Longevity 2015):382-389. doi:10.1016/b978-0-12-801238-3.11447-3

32. Holloszy JO. Biochemical Adaptations in Muscle Effects of exercise on mitochondrial oxygen uptake and respiratory enzyme activity in skeletal muscle. *J Biol Chem*. 1967;242(9):2278-2282. doi:10.1016/s0021-9258(18)96046-1

33. MacInnis MJ, Zacharewicz E, Martin BJ, et al. Superior mitochondrial adaptations in human skeletal muscle after interval compared to continuous single-leg cycling matched for total work. *J Physiol*. 2017;595(9):2955-2968. doi:10.1113/jp272570

34. Scalzo RL, Peltonen GL, Binns SE, et al. Greater muscle protein synthesis and mitochondrial biogenesis in males compared with females during sprint interval training. *Faseb J*. 2014;28(6):2705-2714. doi:10.1096/fj.13-246595

35. Distefano G, Standley RA, Zhang X, et al. Physical activity unveils the relationship between mitochondrial energetics, muscle quality, and physical function in older adults. *J Cachexia Sarcopenia Muscle*. 2018;9(2):279-294. doi:10.1002/jcsm.12272

36. Tøien T, Nielsen JL, Berg OK, et al. The impact of life-long strength versus endurance training on muscle fiber morphology and phenotype composition in older men. *J Appl Physiol*. 2023;135(6):1360-1371. doi:10.1152/japplphysiol.00208.2023

37. Wahl D, Cavalier AN, Smith M, Seals DR, LaRocca TJ. Healthy Aging Interventions Reduce Repetitive Element Transcripts. *Journals Gerontology Ser*. 2020;76(5):805-810. doi:10.1093/gerona/glaa302

38. Murray KO, Mahoney SA, Venkatasubramanian R, Seals DR, Clayton ZS. Aging, aerobic exercise, and cardiovascular health: Barriers, alternative strategies and future directions. *Exp Gerontol*. 2023;173:112105. doi:10.1016/j.exger.2023.112105

39. Neupert SD, Lachman ME, Whitbourne SB. Exercise Self-Efficacy and Control Beliefs: Effects on Exercise Behavior after an Exercise Intervention for Older Adults. *J Aging Phys Act*. 2009;17(1):1-16. doi:10.1123/japa.17.1.1

40. Islam H, Bonafiglia JT, Turnbull PC, Simpson CA, Perry CGR, Gurd BJ. The impact of acute and chronic exercise on Nrf2 expression in relation to markers of mitochondrial biogenesis in human skeletal muscle. *Eur J Appl Physiol*. 2020;120(1):149-160. doi:10.1007/s00421-019-04259-7

41. Musci RV, Hamilton KL, Linden MA. Exercise-Induced Mitohormesis for the Maintenance of Skeletal Muscle and Healthspan Extension. *Sports*. 2019;7(7):170. doi:10.3390/sports7070170

42. Nguyen T, Nioi P, Pickett CB. The Nrf2-antioxidant response element signaling pathway and its activation by oxidative stress. *J Biological Chem*. 2009;284(20):13291-13295. doi:10.1074/jbc.r900010200

43. Nishimoto S, Koike S, Inoue N, Suzuki T, Ogasawara Y. Activation of Nrf2 attenuates carbonyl stress induced by methylglyoxal in human neuroblastoma cells: Increase in GSH levels is a critical event for the detoxification mechanism. *Biochem Bioph Res Co*. 2017;483(2):874-879. doi:10.1016/j.bbrc.2017.01.024

44. Scarpulla RC. Transcriptional activators and coactivators in the nuclear control of mitochondrial function in mammalian cells. *Gene*. 2002;286(1):81-89. doi:10.1016/s0378-1119(01)00809-5

45. Lu Y, Ding W, Wang B, et al. Positive regulation of human PINK1 and Parkin gene expression by nuclear respiratory factor 1. *Mitochondrion*. 2020;51:22-29. doi:10.1016/j.mito.2019.12.002

46. Wahl D, Solon-Biet SM, Wang QP, et al. Comparing the Effects of Low-Protein and High-Carbohydrate Diets and Caloric Restriction on Brain Aging in Mice. *Cell Reports*. 2018;25(8):2234-2243.e6. doi:10.1016/j.celrep.2018.10.070

47. Andrade-Souza VA, Ghiarone T, Sansonio A, et al. Exercise twice-a-day potentiates markers of mitochondrial biogenesis in men. *Faseb J*. 2020;34(1):1602-1619. doi:10.1096/fj.201901207rr

48. Gureev AP, Shaforostova EA, Popov VN. Regulation of Mitochondrial Biogenesis as a Way for Active Longevity: Interaction Between the Nrf2 and PGC-1α Signaling Pathways. *Frontiers Genetics*. 2019;10:435. doi:10.3389/fgene.2019.00435

49. Aquilano K, Baldelli S, Pagliei B, Cannata SM, Rotilio G, Ciriolo MR. p53 Orchestrates the PGC-1α-Mediated Antioxidant Response Upon Mild Redox and Metabolic Imbalance. *Antioxid Redox Sign*. 2013;18(4):386-399. doi:10.1089/ars.2012.4615

50. Morris JK, McCoin CS, Fuller KN, et al. Mild cognitive impairment and donepezil impact mitochondrial respiratory capacity in skeletal muscle. *Funct*. Published online 2021. doi:10.1093/function/zqab045

51. Jin M, Cai SQ. Mechanisms Underlying Brain Aging Under Normal and Pathological Conditions. *Neurosci Bull*. 2023;39(2):303-314. doi:10.1007/s12264-022-00969-9

52. Tian Q, Resnick SM, Mielke MM, et al. Association of Dual Decline in Memory and Gait Speed With Risk for Dementia Among Adults Older Than 60 Years. *JAMA Netw Open*. 2020;3(2):e1921636. doi:10.1001/jamanetworkopen.2019.21636

53. Bekris LM, Yu CE, Bird TD, Tsuang DW. Review Article: Genetics of Alzheimer Disease. *J Geriatr Psych Neur*. 2010;23(4):213-227. doi:10.1177/0891988710383571

54. HARMAN D. Alzheimer's Disease Pathogenesis. *Ann N York Acad Sci*. 2006;1067(1):454-460. doi:10.1196/annals.1354.065

55. Bali J, Gheinani AH, Zurbriggen S, Rajendran L. Role of genes linked to sporadic Alzheimer's disease risk in the production of β-amyloid peptides. *Proc Natl Acad Sci*. 2012;109(38):15307-15311. doi:10.1073/pnas.1201632109

56. Vitek MP, Araujo JA, Fossel M, et al. Translational animal models for Alzheimer's disease: An Alzheimer's Association Business Consortium Think Tank. *Alzheimer's Dement: Transl Res Clin Interv*. 2020;6(1):e12114. doi:10.1002/trc2.12114

57. Jankowsky JL, Zheng H. Practical considerations for choosing a mouse model of Alzheimer's disease. *Mol Neurodegener*. 2017;12(1):89. doi:10.1186/s13024-017-0231-7

58. Liu PP, Xie Y, Meng XY, Kang JS. History and progress of hypotheses and clinical trials for Alzheimer's disease. *Signal Transduct Target Ther*. 2019;4(1):29. doi:10.1038/C1392-019-0063-8

59. Swerdlow RH, Khan SM. A "mitochondrial cascade hypothesis" for sporadic Alzheimer's disease. *Méd Hypotheses*. 2004;63(1):8-20. doi:10.1016/j.mehy.2003.12.045

60. Fišar Z, Jirák R, Zvěřová M, et al. Plasma amyloid beta levels and platelet mitochondrial respiration in patients with Alzheimer's disease. *Clin Biochem*. 2019;72:71-80. doi:10.1016/j.clinbiochem.2019.04.003

61. Santangelo KS, Bertone AL. Effective reduction of the interleukin-1β transcript in osteoarthritis-prone guinea pig chondrocytes via short hairpin RNA mediated RNA interference influences gene expression of mediators implicated in disease pathogenesis. *Osteoarthr Cartilage*. 2011;19(12):1449-1457. doi:10.1016/j.joca.2011.09.004

62. Santangelo KS, Kaeding AC, Baker SA, Bertone AL. Quantitative Gait Analysis Detects Significant Differences in Movement between Osteoarthritic and Nonosteoarthritic Guinea Pig Strains before and after Treatment with Flunixin Meglumine. *Arthritis*. 2014;2014:503519. doi:10.1155/2014/503519

63. Santangelo KS, Pieczarka EM, Nuovo GJ, Weisbrode SE, Bertone AL. Temporal expression and tissue distribution of interleukin-1β in two strains of guinea pigs with varying propensity for spontaneous knee osteoarthritis. *Osteoarthr Cartilage*. 2011;19(4):439-448. doi:10.1016/j.joca.2011.01.004

64. Shorter E, Sannicandro AJ, Poulet B, Goljanek-Whysall K. Skeletal Muscle Wasting and Its Relationship With Osteoarthritis: a Mini-Review of Mechanisms and Current Interventions. *Curr Rheumatol Rep*. 2019;21(8):40. doi:10.1007/s11926-019-0839-4

65. Musci RV, Walsh MA, Konopka AR, et al. The Dunkin Hartley Guinea Pig Is a Model of Primary Osteoarthritis That Also Exhibits Early Onset Myofiber Remodeling That Resembles Human Musculoskeletal Aging. *Front Physiol*. 2020;11:571372. doi:10.3389/fphys.2020.571372

66. Musci RV, Andrie KM, Walsh MA, et al. Phytochemical compound PB125 attenuates skeletal muscle mitochondrial dysfunction and impaired proteostasis in a model of musculoskeletal decline. *J Physiology*. Published online 2022. doi:10.1113/jp282273

67. Krieglstein J, Kewitz T, Kirchhefer U, et al. Damage of Guinea Pig Heart and Arteries by a Trioleate-Enriched Diet and of Cultured Cardiomyocytes by Oleic Acid. *Plos One*. 2010;5(3):e9561. doi:10.1371/journal.pone.0009561

68. Radakovich LB, Marolf AJ, Culver LA, Santangelo KS. Calorie restriction with regular chow, but not a high-fat diet, delays onset of spontaneous osteoarthritis in the Hartley guinea pig model. *Arthritis Res Ther*. 2019;21(1):145. doi:10.1186/s13075-019-1925-8

69. Slomski A. Obesity Is Now the Top Modifiable Dementia Risk Factor in the US. *JAMA*. 2022;328(1):10-10. doi:10.1001/jama.2022.11058

70. Wang JH, Wu YJ, Tee BL, Lo RY. Medical Comorbidity in Alzheimer's Disease: A Nested Case-Control Study. *J Alzheimer's Dis*. 2018;Preprint(Preprint):1-9. doi:10.3233/jad-170786

71. Anderson EJ, Neufer PD. Type II skeletal myofibers possess unique properties that potentiate mitochondrial H2O2 generation. *Am J Physiol-cell Ph*. 2006;290(3):C844-C851. doi:10.1152/ajpcell.00402.2005

72. Nilwik R, Snijders T, Leenders M, et al. The decline in skeletal muscle mass with aging is mainly attributed to a reduction in type II muscle fiber size. *Exp Gerontol*. 2013;48(5):492-498. doi:10.1016/j.exger.2013.02.012

73. Wahl D, Moreno JA, Santangelo KS, et al. Non-Transgenic Guinea Pig Strains Exhibit Hallmarks of Human Brain Aging and Alzheimer's Disease. *Journals Gerontology Ser*. Published online 2022. doi:10.1093/gerona/glac073

74. Paquet C, Amin J, Mouton-Liger F, et al. Effect of active Aβ immunotherapy on neurons in human Alzheimer's disease. *J Pathol*. 2015;235(5):721-730. doi:10.1002/path.4491

75. Erkinjuntti T, Benavente O, Eliasziw M, et al. Diffuse Vacuolization (Spongiosis) and Arteriolosclerosis in the Frontal White Matter Occurs in Vascular Dementia. *Arch Neurol*. 1996;53(4):325-332. doi:10.1001/archneur.1996.00550040053014

76. Whatley BR, Li L, Chin LS. The ubiquitin–proteasome system in spongiform degenerative disorders. *Biochim Biophys Acta (BBA) - Mol Basis Dis*. 2008;1782(12):700-712. doi:10.1016/j.bbadis.2008.08.006

77. Jucker M. The benefits and limitations of animal models for translational research in neurodegenerative diseases. *Nat Med*. 2010;16(11):1210-1214. doi:10.1038/nm.2224

78. Tai LM, Weng JM, LaDu MJ, Brady ST. Relevance of transgenic mouse models for Alzheimer's disease. *Prog Mol Biol Transl Sci*. 2020;177:1-48. doi:10.1016/bs.pmbts.2020.07.007

79. Walsh MA, Zhang Q, Musci RV, Hamilton KL. The combination of NRF1 and Nrf2 activators in myoblasts stimulate mechanisms of proteostasis without changes in mitochondrial respiration. *Redox Muscle Physiology Exerc Sport*. Published online 2022:100001. doi:10.1016/j.rimpes.2022.100001

CHAPTER 2 – THE COMBINATION OF NRF1 AND NRF2 ACTIVATORS IN MYOBLASTS STIMULATE MECHANISMS OF PROTEOSTASIS WITHOUT CHANGES IN MITOCHONDRIAL RESPIRATION

INTRODUCTION

Cellular damage and dysfunction are indications of unresolved, persistent oxidative stress. However, oxidative stress is not solely the net imbalance of reactive oxygen species (ROS) and cellular antioxidants; it also includes impaired redox sensing and signaling pathways [1]. The multifaceted nature of cellular redox responsiveness is one reason why a direct scavenging antioxidant therapy (e.g., vitamin C or E) often yields equivocal benefits for disease treatment or augmentation of exercise adaptations [as extensively reviewed here [2,3]. One barrier to improving cellular stress responses and overall health is identifying targets to modulate cellular redox-sensitive processes effectively. This is especially difficult as cells respond to stress in various ways ranging from activation of cell survival pathways [4] to initiating programs aimed at eliminating cells with irreparable damage [5–7].

One way to contextualize cellular stress responses, particularly mitochondrial stress responses, is adaptive homeostasis. Adaptive homeostasis is a term used to describe "the transient expansion or contraction of the homeostatic range in response to exposure to sub-toxic, non-damaging, signaling molecules or events, or the removal or cessation of such events" [8]. Mechanisms to maintain protein homeostasis or proteostasis expand and contract to adapt to transient stressors [9]. However, this proteostatic adaptation has been shown to decline with age in multiple model organisms [10].

Targeting mitochondria through redox-sensitive pathways may be a powerful approach to improve skeletal muscle proteostasis and subsequently improve skeletal muscle function with advancing age [11–14]. Mitochondrial dysfunction, especially in skeletal muscle, is one driver of

[1] Published in Redox in Muscle Physiology, Exercise, and Sport: authored by Maureen A. Walsh, Robert V. Musci, Qian Zhang, Karyn L. Hamilton

age-related chronic diseases, where there is a decrease in ATP availability and a concomitant increase in ROS production [11,15,16]. ATP is requisite for proteostatic maintenance, which is an energetically costly process [17,18]. Consequently, a decrement in protein turnover drives the accumulation of protein aggregates and cellular dysfunction [19–22]. Experimental support for targeting mitochondrial function to improve lifespan includes observations that decrements in mitochondrial function precede protein dyshomeostasis in C. elegans, resulting in decreased lifespan [23]. Genetic CRISPR screenings identified Complex I of the electron transfer system as a significant determinant of mitochondrial ROS production and cellular fitness [24]. Therefore, mitochondrial targets are advantageous for improving overall cellular health.

Mitochondrial function and proteostasis are highly interconnected [13,14]. Therefore, identifying targets to improve one driver will likely improve multiple and possibly adaptive homeostasis. The transcription factor nuclear erythroid-related factor 2 (Nrf2) is at the nexus of redox homeostasis. Nrf2 regulates transcription of a gene program that modulates not only cellular antioxidant and detoxification responses [25] but also maintenance of proteostasis [26,27], mitochondrial function [28,29] and inflammatory responses][30]. Therefore, it is a signal transduction pathway that modulates adaptive homeostasis [extensively reviewed here – [27,31,32]. Nrf2 can be activated through numerous mechanisms, including aerobic exercise, oxidative stress, hydrogen sulfide, and a variety of phytochemical compounds [33–37].

Evidence that supports the use of a phytochemical Nrf2 activator (Nrf2a) for targeting drivers of cellular aging spans the translational spectrum. *In vitro* treatment of muscle precursor cells with the Nrf2a Protandim increased rates of mitochondrial proteins synthesized for proteome maintenance in the presence of an oxidative challenge [26]. Oral treatment with the Nrf2a Protandim increased median lifespan in male mice in the National Institutes of Aging Interventions Testing Program [38].

Additionally, we have previously reported that Protandim also increased synthesis of myofibrillar proteins in older men [39]. Finally, treatment with Protandim protected human coronary artery endothelial cells from oxidative stress and showed that Nrf2 activation is at least in part responsible for cytoprotection [40]. These observations collectively emphasize the importance of the present stressors (e.g., age, or an oxidative challenge) to observe the greatest beneficial effects of Nrf2a treatment to augment adaptive homeostatic responses [9,41–43].

Nrf2 regulates its own transcription in addition to that of over 400 genes involved in cytoprotection [44,45], by binding to the antioxidant response elements (AREs) in promoter regions of target genes. One target gene is the transcription factor nuclear respiratory factor 1 (NRF1), which activates the expression of key metabolic genes regulating cellular growth, mitochondrial respiration, mitophagy, and heme biosynthesis[46,47]. Specifically, NRF1 is a critical transcriptional regulator of nuclear-encoded subunits in mitochondrial electron transfer complexes. Disruption of NRF1 is lethal and likely a consequence of mitochondrial DNA depletion [48,49]. NRF1 regulates transcription via binding with the coactivator PGC-1α, considered a master regulator of mitochondrial biogenesis. Expression of PGC-1α increases during periods of energy stress, including calorie restriction [50] and exercise [51]. Additionally, it has been suggested that Nrf2 and NRF1 are both regulated by the transcriptional coactivator, PGC-1α, and thus demonstrate crosstalk [52,53]. Taken together, these observations suggest that NRF1 and Nrf2 can work together to regulate a transcriptional program to promote adaptive homeostasis in response to stressful stimuli. Therefore, targeting both NRF1 and Nrf2 simultaneously may represent a powerful approach for promoting beneficial stress responses.

To our knowledge, there has only been one published study examining the intersection of NRF1 and Nrf2. Using carbon monoxide to elicit cellular stress, Piantadosi et al. reported that NRF1 activation and subsequent mitochondrial biogenesis occurred through Nrf2 binding to the AREs in the NRF1 promoter [54]. This suggests that beneficial mitochondrial adaptations to redox stress at the transcriptional level may, under at least some circumstances, require

activation of both NRF1 and Nrf2. While evidence suggests that the use of exogenous Nrf2a may stimulate mitochondrial adaptations to stress [26], it is not known if the use of an exogenous NRF1 activator (NRF1a) together with a Nrf2a may promote even better mitochondrial stress adaptation. Therefore, we sought to interrogate the effect of co-treatment with NRF1a and Nrf2a for improving mitochondrial function and mechanisms of mitochondrial proteostasis in response to an oxidative challenge in muscle precursor cells. We hypothesized that the combination of NRF1a and Nrf2a activators would improve mechanisms of proteostasis and mitochondrial function to a greater extent than either transcriptional activator alone, in conditions with and without an oxidative challenge of hydrogen peroxide (H_2O_2).

METHODS

Cell Culture and Treatments

C2C12 myoblasts (CRL-1772; ATCC, Manassas, VA) were maintained in Dulbecco's modified Eagle's medium (DMEM; Sigma-Aldrich) supplemented with 1% penicillin/streptomycin (ATCC) and 10% fetal bovine serum (ATCC) in a 5% CO_2 humidified atmosphere at 37 °C for all experiments. We choose myoblasts over myotubes because we wanted address both primary culture outcomes (i.e., protein turnover and mitochondrial respiration) in the same culture model and others have shown that myotubes are not capable to being respired using our high-resolution methods [55]. To induce an oxidative challenge *in vitro*, we treated myoblasts with H_2O_2 (Sigma-Aldrich) diluted in DMEM supplemented with 1% penicillin/streptomycin (ATCC) and 10% fetal bovine serum (ATCC) to a concentration of 50 μM as previously described [26]. This concentration was chosen based on preliminary experiments showing acute decreases in DNA synthesis with H_2O_2 treatment without measurable cell detachment, a

metric of cell death, or changes in cell viability as assessed with the WST-1 assay (Roche, Mannhein, Germany) (Figure A.1) [56]. NRF1a and Nrf2a compounds provided by LifeVantage Corporation (Sandy, UT, USA) were prepared at 20 µg/µl in DMSO. This concentration for the NRF1a was chosen based on the gene expression of NRF1 and mitochondrial-related genes at 6 hrs of treatment (Figure A.2). The NRF1a activator was comprised of acetyl-l-carnitine HCl (85% purity; 12.2 µg/ml), quercetin dihydrate (≥ 95% purity; 2.8 µg/ml), alpha-lipoic acid (≥99% purity; 2.4 µg/ml), vinovia LS grape (74% grape seed extract, 24% grape skin/seed/pulp extract, 2% maltodextrin (corn); 1.8 µg/ml), and CoQ10 (≥98% purity; 0.8 µg/ml). The Nrf2a was comprised of milk thistle extract (70-80% purity; 6.7 µg/ml), bacopa extract (45% purity; 4.4 µg/ml), ashwagandha extract (98% purity; 4.4 µg/ml), green tea extract (45% purity; 2.2 µg/ml), and turmeric (95%; 2.2 µg/ml) [57]. The concentration for the Nrf2a, 20 µg/ml, has been used in prior studies [26].

Gene Expression

For gene expression studies, cells were seeded at 200,000 cells / well in 6-well tissue culture plates (Genesee Scientific, San Diego CA, Catalog #25-105) and exposed to test agent the following day. Following 6 hrs of incubation in NRF1a at 20 µg/ml, RNA was extracted using the PureLink RNA Mini Kit (Thermo-Fisher Scientific, Waltham MA, Cat #12183018A). Cells were lysed on the plate using 350 µL of lysis buffer; otherwise, all manufacturer's instructions were followed. RNA was eluted into 35µL of RNAse-free water and quantified on a NanoDrop 800 spectrophotometer (Thermo-Fisher Scientific). First-strand cDNA synthesis was carried out on 1µg of RNA, using the SuperScript VILO Master Mix (Thermo-Fisher Scientific, Cat # 11755050) according to the manufacturer's instructions. A four-fold dilution was made of each cDNA in PCR-grade water, and 2µL of this solution was carried forward into qRT-PCR. Mouse PCR primers for C2C12 cells were purchased from Thermo Fisher Scientific unless otherwise indicated as follows: MT-CO1 (mitochondrial subunit, cytochrome c): qMmuCEP0062613 (FAM

label) – Bio-Rad Laboratories, Hercules, CA, NRF-1: Mm01135606_m1 (FAM label), PPARGC1A (PGC-1α): Mm01208835_m1 (FAM label), Tfam: Mm00447485_m1 (FAM label), and β-actin control: 4352341E (VIC label). PCR reactions were performed using Taqman Gene Expression Master Mix (Thermo Fisher Scientific, Cat # 4369016). Reactions were run on an Applied Biosystems 7500 Fast Real-Time PCR Instrument (Thermo Fisher Scientific) under the following conditions: 50°C for 2 min, 95°C for 20 sec, 40 cycles of (95°C for 3 sec, 60°C for 30 seconds). Threshold cycle (C_T) was determined by the instrument software. Differences in threshold cycle between the gene of interest and actin (ΔC_T) were determined for each sample and used to determine fold induction of each gene of interest, compared to untreated controls.

Protein Synthesis

Cells were seeded in 10 cm plates at passage 7. For protein and DNA synthesis experiments, when cells reached 70% confluence, medium was removed and replaced with medium-enriched to 10% diluting 99.8% deuterium oxide (^2H_2O; Sigma Aldrich 756822) with treatments added [26,58]. Treatments included a vehicle control of DMSO (CON; 1 µl/ml), NRF1a (20 µg/ml), Nrf2a (20 µg/ml), and NRF1a + Nrf2a (both at 20 µg/ml). Each of these treatments was tested with and without co-treatment with 50 µM H_2O_2. Myoblasts were harvested at time points ranging from 8 to 16 hrs (n=3/time point/experiment; total n=9/treatment) (Figure 2.1a). Immediately before cell harvesting, 1 ml samples of media were taken to measure the media ^2H_2O-enrichment. Cells were rinsed with sterile PBS and then harvested in 1.2 ml of mitochondrial isolation buffer (100 mM KCl, 40 mM Tris·HCl, 10 mM Tris base, 5 mM $MgCl_2$, 1 mM EDTA, and 1 mM ATP, pH 7.50) with phosphatase and protease inhibitors (HALT; ThermoFisher Scientific, Salt Lake City, UT). The total volume was separated into a 1 ml aliquot for protein synthesis analysis and a 200 µl aliquot for DNA synthesis analysis.

For protein synthesis, 1 ml of harvested cells was centrifuged at 800 *g* for 10 min at 4 °C. The supernatant was removed and centrifuged at 10,000 *g* for 30 min at 4 °C to pellet the mitochondrial fraction. 400 µl of the subsequent supernatant was removed and mixed with an equal volume of 14% sulfosalicylic acid to yield the cytosolic fraction. The mixture was incubated on ice for 1 hr and then centrifuged at 16,000 *g* for 10 min at 4 °C to pellet the cytosolic protein fraction. The mitochondrial and cytosolic pellets were solubilized by incubation in 250 µl 1 M NaOH at 56 °C and shaking at 500 rpm for 15 min. Cell mitochondrial and cytosolic solubilized proteins were hydrolyzed by adding 1.5 ml 6 M HCl and incubated for 24 h at 120 °C. The resulting amino acids from hydrolysis were further purified by ion-exchanged, dried under vacuum, and then suspended in 500 µl Milli-Q biology grade H_2O. The suspended samples were derivatized by adding 500 µl acetonitrile, 50 µl 1M K_2HPO_4 (pH 11.0), and 20 µl pentafluorobenzyl bromide, and the sealed mixture was incubated at 100 °C for 1 hr. Derivatives were extracted in ethyl acetate, and the organic layer was removed and dried under N_2. The mitochondrial fraction was reconstituted in 180 µl ethyl acetate, and cytosolic fraction was reconstituted in 400 µl ethyl acetate. Using negative chemical ionization mode, derivatized amino acids were analyzed on an Agilent 7890 GC and 5977 single quad mass spec using an Agilent DB-5MS GC column (30 m x 0.25 mm x 0.25 µm). Samples (1 µl) were injected using splitless mode (inlet temperature 220°C). Helium was the carrier, and methane was the reagent gas. The mass-to-charge ratios (m/z) of 448, 449, and 450 were monitored for the pentafluorobenzyl-N,N-di(pentafluorobenzyl)alaninate derivative. In all cases, these mass-to-charge ratios represented the primary daughter ions that included all the original hydrocarbon bonds from the given amino acid, previously described [26].

DNA Synthesis

Whole-cell DNA was extracted from 200 µl of the initial cell lysates using the QIAmp DNA mini kit (Qiagen, Valencia, CA) following the manufacturer's instructions. DNA was suspended in nuclease-free water and hydrolyzed to free deoxyribonucleic acids by incubation

with nuclease S1 and potato acid phosphatase overnight at 37 °C. Hydrolysates were reacted with pentafluorobenzyl hydroxylamine and acetic acid and then acetylated with acetic anhydride and 1-methylimidazole. Methylene chloride was added, and the organic layer was removed to a GC vial. The DNA extracts were dried, resuspended in ethyl acetate, and analyzed on an Agilent 7890B GC coupled to an Agilent 5977A MS using an Agilent DB-17 GC column using helium as the carrier and methane as the reagent gas. The fractional molar isotope abundances at m/z 435 (M = 0 mass isotopomer) and 436 (M = 1) of the pentafluorobenzyl triacetyl derivative of purine dR were quantified using MassHunter software (Agilent Technologies, Santa Clara, CA) previously described [26,58–61].

Cell Media Deuterium Enrichment

To measure the deuterium enrichment of cell culture media, 100 µl of cell culture media was placed in the inner well of an o-ring screw-on cap and placed inverted on a heating block overnight at 80 °C. Next, 2 µl 10 M NaOH and 20 µl acetone were added to all samples and standards and capped immediately. Samples were vortexed at low speed and kept overnight at room temperature. Samples were extracted with 200 µl hexane, and the organic layer was transferred through anhydrous Na_2SO_4 into GC vials and analyzed via EI mode using a DB-17MS column. *In vitro* protein synthesis was calculated using the true precursor enrichment using plasma or media ^2H_2O enrichment and Mass Isotopomer Distribution Analysis (MIDA) adjustment. Protein synthesis rates were divided by time and expressed as fractional synthesis rates (FSR, %/hr). For DNA synthesis, the fraction new was calculated by dividing DNA enrichment from to media enrichment and MIDA adjustment by time (FSR, %/h), as previously described [26].

Cell Preparation for Mitochondrial Respiration

At passage 6 when cells reached 90% confluence, they were treated with either a vehicle control of DMSO (CON; 1 µl/ml), 50 µM H_2O_2, NRF1a + Nrf2a (both at 20 µg/ml), or NRF1a + Nrf2a (both at 20 µg/ml) + 50 µM H_2O_2. Myoblasts were harvested at time 8 hrs (Figure 2.1b). At harvest, media and treatments were removed. Cells were rinsed with 1 ml of 0.25% trypsin-EDTA and then incubated in 2 ml of trypsin in a 5% CO_2 humidified atmosphere at 37 °C for 1 min. Then, 6 ml of Dulbecco's modified Eagle's medium (DMEM; Sigma-Aldrich) supplemented with 1% penicillin/streptomycin (ATCC) and 10% fetal bovine serum (ATCC) was added to the cells to stop the trypsinization reaction and spun for 2 min at 150 g at 21 °C. The supernatant was removed, pellet rinsed with sterile PBS, and spun for 2 min at 150 g at 21 °C. The supernatant was removed, and cells were resuspended in MiR05 (mitochondrial respiration medium) buffer (0.5 mM EGTA, 3 mM $MgCl_2 \cdot 6H_2O$, 60 mM lactobionic acid, 20 mM taurine, 10 mM KH_2PO_4, 20 mM HEPES, 110 mM sucrose, 1 g/L bovine serum albumin, pH 7.10). Cell count was determined using the Invitrogen Countess II FL Automated Cell Counter (ThermoScientific, Salt Lake City, UT).

Mitochondrial Function Using High-Resolution Respirometry

The Oroboros Oxygraph 2000 (O2K) (Oroboros, Innsbruck, Austria) was used to complete high-resolution respirometry experiments at 37 °C. Instruments were air calibrated daily, and a low oxygen calibration was also performed daily. Cells (approximately 9.25 X 10^5 cells/ml) resuspended in MiR05 were added to each chamber along with catalase (112,000 U/ml) which is necessary for chamber re-oxygenation during the respirometry utilizing H_2O_2. Cells were permeabilized with digitonin (1.62 µM) and then equilibrated for 10 min. This digitonin concentration was selected based on a subset of experiments to optimize respiration without over-permeabilization (Figure A.3). We used an ADP titration protocol to determine ADP sensitivity (Km) and maximal oxidative capacity (Vmax) under Complex I supported respiration (Figure A.4) [34,62]. We measured Complex I supported leak respiration with the addition of 10

mM glutamate, 0.5 mM malate, and 5 mM pyruvate. Upon acquisition of leak respiration, we titrated progressively greater concentrations of ADP from 0.075 mM, 0.175 mM, 0.25 mM, 0.5 mM, 1 mM, 2 mM, 4 mM, to 8 mM, awaiting steady-state oxygen flux prior to adding the subsequent titration, to determine Complex I linked ADP Vmax and apparent Km (i.e., ADP sensitivity). After the ADP titration was completed, we added 5 mM cytochrome C to test mitochondrial membrane integrity. We excluded measurements that had a cytochrome C control factor of greater than 0.12 based on the threshold in which a relationship between the cytochrome C control factor and respiration existed (Figure A.5) [34]. After cytochrome C addition, we added 10 mM succinate to acquire maximal Complex I and II supported coupled respiration. We then added 0.5 µM FCCP sequentially until there was no increase in respiration to determine the capacity of the electron transfer system to consume oxygen or maximal uncoupled respiration. To measure maximal uncoupled respiration with the inhibition of Complex I, we added 5 µM rotenone. Finally, we added 2.5 µM Antimycin A to measure residual oxygen consumption. In line with best practices, technical replicates were averaged. Apparent Vmax and Km values were determined using Michaelis-Menten kinetics as previously described [34,62].

Protein Content

At passage 6 when cells reached 90% confluence, cells were either treated with a vehicle control of DMSO (CON; 1 µl/ml), NRF1a (20 µg/ml), Nrf2a (20 µg/ml), and NRF1a + Nrf2a (both at 20 µg/ml). Each of these treatments was tested with and without co-treatment with 50 µM H_2O_2. To measure protein content, cells were harvested after 8 hours after treatment in 1.5 ml of 1X PBS, centrifuged at 200 g for 6 min at 4 °C. Pellets were resuspended in radioimmunoprecipitation assay (RIPA) (150 mM NaCl, 0.1 mM EDTA, 50 mM Tris, 0.1% sodium deoxycholate, 0.1% SDS, 1% Triton X-100, pH 7.50)

with HALT protease inhibitors and incubated on ice for 2 hrs. Then, samples were diluted to 0.25 µg/ml with BioRad Laemmli Sample Buffer (950 µl) and B-mercaptoethanol (50 µl) as a reducing agent. Samples were then boiled at 50 °C for 10 min to denature proteins. Protein (2.5 µg) from each sample was separated on a 4%–20% gel and transferred to PVDF membranes for detection of Nrf2 (Santa Cruz Ab, Dallas, TX; Cat # 28379), NRF1 (Santa Cruz Ab, Dallas, TX; Cat # 365949), heme oxygenase-1 (HO-1) (Abcam, Cambridge, MA; Ab Cat # 13243), NAD(P)H dehydrogenase [quinone] 1 (NQO-1) (Novus Biologicals, Centennial, CO; Ab Cat # NB200-209), glutathione synthetase (Abcam, Cambridge, MA; Ab Cat # 91591), and glutathione reductase (Abcam, Cambridge, MA; Ab Cat # 16801), phosphorylated AMPK (Cell Signaling Technologies, Danvers, MA; Ab Cat # 2531L), total AMPK (Cell Signaling Technologies, Danvers, MA; Ab Cat # 2532L), and OXPHOS (Abcam, Cambridge, MA; Ab Cat# 110413). Primary antibodies were diluted 1:100-1,000 and secondary antibodies 1:10,000. Membranes were amido black stained and total protein staining quantified to control for protein loading and transfer quality. Protein content was assessed using densitometry as previously described with modifications [58].

Statistics

A one-way ANOVA with Dunnett's multiple-comparisons test was used to compare treatment groups for the ratio of protein to DNA synthesis rates and the fractional synthesis rates for protein and DNA synthesis at each time point. For the mitochondrial respiration analysis, the ADP titration was fit to Michaelis-Menten kinetics. A one-way ANOVA was used to examine treatment effects at each step of the titration. Because we observed a significant difference between CON and H_2O_2 treated myoblasts, we expanded our multiple comparisons by using a Tukey post-hoc analysis for our mitochondrial respiration data. Routine outlier tests (ROUT) were performed for all analyses. Significance was set a priori at $p<0.05$. Analyses were completed in Prism 8.0 (La Jolla, California, USA).

RESULTS

Protein and DNA Synthesis

Deuterium labeling of free amino acids including alanine, and incorporation of the labeled amino acids into proteins, is a validated [63] approach for measuring protein synthesis rates. Similarly, deuterium labeling of the deoxyribose moiety of purine deoxyribonucleotides in DNA provides a measure of dividing cells sensitive enough for monitoring very low rates of cell proliferation [64]. Here, we enriched cell culture medium with deuterium oxide (^2H_2O) to facilitate dynamic and simultaneous monitoring of rates of newly synthesized proteins and DNA. In both the mitochondrial and cytosolic fractions, the rates of protein synthesis were not different among treatment groups (Figure 2.2a and b). However, the NRF1a and Nrf2a, both individually as well as combined, significantly decreased the rate of cellular proliferation (Figure 2.2c) in the presence of H_2O_2 stress relative to cells exposed to H_2O_2 alone. Results were similar at the 16 hr time points (Figure A.6). In the presence of an oxidative challenge, there was a significantly greater proportion of newly synthesized mitochondrial and cytosolic proteins allocated to proteome maintenance with NRF1a treatment, Nrf2a treatment, and co-treatment, compared to H_2O_2 alone (Figure 2.2d and e); again, findings were similar at both the 12 and 16 hr time points (Figure A.7). While the ratio of mitochondrial protein synthesis to DNA synthesis still tended to be greater in cells treated with NRF1a + Nrf2a in the absence of H_2O_2, these differences only reached significance at the 16 hr time point in the mitochondrial fraction (Figure A.8). We conclude that co-treatment of the NRF1a and Nrf2a increased mechanisms promoting maintenance of proteostasis by maintaining rates of protein synthesis despite slower rates of cell proliferation.

Mitochondrial Respiration

Given that co-treatment with the NRF1a and Nrf2a activated mechanisms favoring mitochondrial proteome maintenance, we assessed mitochondrial function using high-resolution respirometry in co-treated samples. Michaelis-Menten plots were created for each sample and used to calculate ADP Vmax and Km values for each treatment group (Figure 2.3a). At a submaximal concentration of ADP very closely associated with the ADP concentration used to calculate the Km, we observed no significant differences between groups (Figure 2.3b). There was no difference between H_2O_2 alone and NRF1a + Nrf2a+ H_2O_2. There were no differences in ADP sensitivity as assessed by the Km value (Figure 2.3c). However, there was significantly lower maximal mitochondrial respiration in the cells exposed to H_2O_2 alone and cells treated with the combination of NRF1a + Nrf2a+ H_2O_2 compared to CON (Figure 2.3d). ADP-stimulated (i.e., State III) Complex I and Complex II respiration was only significantly different between CON and NRF1a + Nrf2a + H_2O_2, but not between H_2O_2 and NRF1a + Nrf2a + H_2O_2 (Figure 2.3e). There were no differences in the ratio of coupled to uncoupled respiration (Figure 2.3f). Complex I-IV supported uncoupled respiration was lower in the cells treated with H_2O_2 and NRF1a + Nrf2a + H_2O_2 compared to CON, indicating only an effect of H_2O_2 (Figure 2.3g). In Complex II-IV supported uncoupled respiration, there were no significant differences indicating that declines in maximal respiration might, in part, be due to Complex I activity (Figure 2.3h). We conclude that the declines due to H_2O_2 treatment in maximal mitochondrial respiration and Complex I-IV uncoupled mitochondrial respiration were not rescued by co-treatment with the NRF1a and Nrf2a.

Protein Content

Since we observed increases in proteostatic maintenance, we hypothesized this could be at least partially explained through increased activation of AMPK, based on other findings from our lab [58]. More specifically, in response to energy and potentially redox stresses [65] cells activate AMPK and subsequent energetic stress signaling. In our precious work [26,66], we

observed that this is associated with, reallocation of cellular resources to maintain the proteome at the expense of cell proliferation. Since we observed this “trade-off” leading to greater proteome maintenance the co-treatment of the NRF1a and Nrf2a (Figure 2.2d and e), we wanted to assess AMPK activation in response to treatment. However, we found no differences in AMPK activation among any of the treatments (Figure 2.5). While 8 hrs was a logical timepoint to select, a shorter or longer timepoint may have been required to detect AMPK activation. Additionally, to complement our measurements of mitochondrial protein synthesis and respiration, we measured mitochondrial electron transfer system protein content. After 8 hrs of treatment, we observed non-uniform changes in mitochondrial protein content, indicating that any differences in mitochondrial protein density likely do not explain the differences we observed in respiration (Figure 2.4). From these results, we conclude that activation of mechanisms promoting mitochondrial proteome maintenance (Figure 2.5d) were not accompanied by evidence of activation of the AMPK energy-sensing pathway, nor did they result in significantly greater mitochondrial protein content.

After 8 hours of treatment, we used western blotting to evaluate NRF1 and Nrf2 protein content as well as the expression of endogenous antioxidants regulated by Nrf2. There were no differences in NRF1 protein content (Figure 2.6a). Nrf2 protein content was lower with Nrf2a + H_2O_2 compared to H_2O_2 alone (Figure 2.6b). Consistent with previous work, HO-1 was significantly greater with Nrf2a + H_2O_2 treatment compared to H_2O_2 alone (Figure 2.6C) [41,67]. NQO1 and glutathione synthetase, which both have ARE repeats in the promoter regions, were not different between any treatment groups (Figure 2.6d and e). Finally, like Nrf2 protein content, glutathione reductase protein content decreased in Nrf2a + H_2O_2 compared to H_2O_2 alone (Figure 2.6f).

DISCUSSION

Adapting to oxidative stress is essential for cellular function and maintaining organismal health. Non-damaging oxidative challenges can result in positive adaptations (i.e., positive adaptive homeostasis) [8,43]. With advancing age, the ability to resolve oxidative stress is compromised, and, further, the stress exposures become more chronic in nature, collectively contributing to the development of age-related chronic diseases [43]. Consequently, unresolved oxidative stress serves as a feed-forward mechanism that drives further impairment in cellular function [14]. Therefore, developing interventions that do not directly scavenge ROS but instead augment the adaptive response to ROS offer a distinct and potentially better solution to age- and disease-related increases in oxidative stress. The purpose of this study was to identify if co-treatment with a NRF1a and a Nrf2a would enhance cellular adaptation to stress, with evidence of mitochondrial proteome maintenance, improved mitochondrial respiratory function, and greater endogenous antioxidant defenses (Figure 2.7). The primary findings were that in myoblasts treated with a combination of a NRF1a and Nrf2a in the presence of a stress, there was evidence of mitochondrial and cytosolic proteome maintenance independent of changes in mitochondrial respiration, AMPK activation, or antioxidant protein content.

NRF1a, Nrf2a, and co-treatment of NRF1a and Nrf2a increased mechanisms of mitochondrial proteostasis to adapt to an oxidative challenge (Figure 2.7 panel a)

The combination of a NRF1a and Nrf2a resulted in an increased allocation of protein synthetic resources toward proteome maintenance at the expense of myoblast proliferation (Figure 2.2 and 7a). We have previously reported that this “tradeoff” between proteome maintenance and cell proliferation occurs in tissues from murine models of life-/healthspan extension, including rapamycin treatment, calorie restriction, and disruption of growth hormone signaling in the Snell-dwarf model [59,60,66,68,69]. In contrast to these chronic *in vivo* models, the responses observed in the current study are acute adaptations to stress that may reflect cellular mechanisms contributing to the expansion of adaptive homeostasis. We chose

myoblasts as our culture model for two reasons. First, our primary outcomes for this study focused on simultaneous measurement of rates of protein synthesis and cell proliferation. Making these measurements simultaneously over an extended period of time (in this case, 16 hrs) enables us to gain insight into treatment-related "trade-offs" in how newly synthesized proteins are allocated; toward cell proliferation versus toward maintenance of the proteome (somatic maintenance). A proliferative cell model, rather than a terminally differentiated model, is best for this assessment. Additionally, high-resolution respirometry in differentiated myotubes in suspension is limited by the inability to maintain structural integrity during harvesting [55]. We selected exogenous H_2O_2 as a cell stressor, as we and other have observed it is a convenient mimetic of perturbed cellular dyshomeostasis [26,70].

We sought to interrogate potential mechanistic explanations for the tradeoff between investment of more newly synthesized proteins in proteome maintenance at the expense of cell proliferation, a finding we have previously observed when energetic signaling pathways are activated (e.g., AMPK activation or mTOR inhibition) [58]. For example, AMPK is central to energetic stress sensing and has also been shown to be increased with exogenous H_2O_2 treatment in fibroblasts [71]. However, there were no differences in phosphorylated AMPK, total AMPK, or the ratio of the two in any of the treatment groups (Figures 2.5 and A.9). Consistent with this finding, we have previously reported that chronic treatment with calorie restriction, rapamycin, and rapamycin with metformin – all known to target cellular energetic stress signaling – activates mechanisms favoring proteostatic maintenance in the absence of detectable AMPK activation in skeletal muscle [60].

Despite the significantly slower rates of cell proliferation with NRF1a and Nrf2a treatment, the rates of protein synthesis were maintained, indicating that mechanisms to maintain the cellular proteome (proteostasis) played a role in the adaptations to stress.

We observed little or no net accrual of the mitochondrial proteins we measured at the 8-hour timepoint. Therefore, we posit that over the 16 hr isotope tracer experiments, it is likely that rates of protein synthesis were matched by rates of degradation, contributing to the maintenance of the proteome rather than the accumulation of damage. Nrf2 has been suggested to assist in the adaptative homeostatic responses of the proteasome. Specifically, Nrf2 activates genes involved in stress protection and the activation of the 20S proteasome [72]. Additionally, p62, a classic autophagy receptor, interacts with Nrf2 [72], supporting that treatment with a Nrf2a may have improved mechanisms of autophagy in the present study. Further, Pomatto postulates that the protein dyshomeostasis that occurs with age compresses the range of adaptative homeostatic responses [9,43]. Therefore, further exploring the role of Nrf2 in multiple components of proteome maintenance, including autophagy and protein quality, is an important next step in understanding the mechanisms by which Nrf2 may mediate the adaptive homeostatic response to sublethal cell stresses.

Adaptation to an oxidative challenge was not dependent on an expanded endogenous antioxidant network following co-treatment with NRF1a and Nrf2a (Figure 2.7 panel b)

Activation of NRF1 and Nrf2 can regulate the expression of these transcription factors as well as many genes contributing to the endogenous antioxidant network and redox regulation. NRF1 protein content was not different between treatments. However, the half-life of NRF1 is 5 hours [73] and, therefore, it is not surprising that we did not observe changes in protein content at the end of the 8-hour treatment (Figure 2.6a). Furthermore, Nrf2 protein content was lower in the Nrf2a plus H_2O_2 treatment compared to H_2O_2 alone (Figure 2.6b). Again, because the half-life of Nrf2 is only 20 minutes, it is difficult to capture alterations in Nrf2 protein content [74], making protein assays of Nrf2 target genes a better reflection of Nrf2 activation. Indeed HO-1, a highly conserved antioxidant with multiple ARE repeats [75], was increased in the Nrf2a and H_2O_2 group compared to H_2O_2 alone (Figure 2.6c). HO-1 has been shown to increase in a

concentration-dependent manner in response to the treatment with the same Nrf2a used in this current study [76] We did not identify changes in NQO1 or glutathione synthetase as a result of treatment (Figure 2.6d and e); this finding is consistent with our previous observations that NQO1 content was unchanged in older individuals treated with the same Nrf2a used here [39]. Collectively, it seems unlikely that changes in endogenous antioxidant protein content played a substantial role in the adaptive response to combined NRF1a and Nrf2a treatments (Figure 2.7b).

An oxidative challenge decreased mitochondrial respiration, which was not rescued with the co-treatment of NRF1a and Nrf2a, suggesting unaltered ATP availability (Figure 2.7 panel c)

To our knowledge, this is the first study to report mitochondrial respiration using high-resolution respirometry in C2C12 myoblasts that were pre-treated with an oxidative challenge. Compared to CON cells, H_2O_2 treated myoblasts had a decline in maximal mitochondrial respiration but no change in ADP sensitivity (Figure 2.3b and c). This observation agrees with the reported decline in mitochondrial oxygen consumption rate (measured using a Seahorse metabolic flux analyzer) in C2C12 myotubes that were treated with the same concentration of H_2O_2 [70]. However, decrements in maximal mitochondrial oxidative capacity were not attenuated with the combination of the NRF1a and Nrf2a (Figure 2.3b). Further, the significant decline in uncoupled Complex I through Complex IV respiration was present in H_2O_2 treated cells and the combined NRF1a, Nrf2a, and H_2O_2 cells (Figure 2.3c). The H_2O_2 challenge, independent of co-treatment with transcription factor activators, decreased multiple metrics of maximal respiration through Complex I, as the significant differences were abolished upon addition of rotenone leading to Complex I inhibition (Figure 2.3c and d). It is important to note the physiological difference between submaximal versus maximal mitochondrial respiration. To elaborate, in both i*n vitro* and *in vivo* conditions, electron transfer systems do not

operate at maximal capacity, and so it may be more relevant to identify treatment-related differences in submaximal ADP stimulated respiration using lower ADP concentrations rather than ADP Vmax. Here we observed no differences in submaximal respiration between treatments (Figure 2.3c and d).

Key findings

Adaptive homeostasis is where acute exposures to sub-toxic stimuli initiate transient cellular responses necessary to reestablish homeostasis. Consistent with previous observations, the presence of a sub-toxic H_2O_2 stress [26] is required to demonstrate a beneficial effect of the NRF1 and Nrf2 activator treatment [26,39]. Contrary to our hypothesis, cells exposed to H_2O_2 stress alone and those treated with NRF1 and Nrf2 activators during that H_2O_2 stress had the same decrement in mitochondrial respiratory capacity compared to control cells. This observation implies equivalent ATP availability. However, an important observation is that, despite lower mitochondrial respiration in response to the oxidative challenge, co-treatment with NRF1 and Nrf2 activators stimulated mechanisms favoring the maintenance of the mitochondrial proteome with a trade-off of slower cell proliferation. Therefore, our findings suggest that treatment with NRF1 and Nrf2 activators promotes adaptation to acute stress characterized by mitochondrial proteome maintenance, independent of enhanced energy availability or endogenous antioxidant capacity.

Conclusions

This study was designed to provide insights into how targeting two transcription factors could improve adaptive homeostatic responses to a non-damaging stress. The co-treatment with NRF1 and Nrf2 activators improved proteostatic maintenance to a greater extent than either treatment alone, without improving mitochondrial respiration. Further investigation of whether transcriptional or translational fidelity of mitochondrial proteins in response to co-treatment with NRF1 and Nrf2 activators might help explain the observed improvements in

protein turnover without increases in mitochondrial respiration. Additional studies should interrogate whether this acute investment in proteostatic maintenance yields beneficial protection from future oxidative challenges. These future studies should also include investigation of mitochondrial function in differentiated myotubes or primary cells, as energetics are altered during the differentiation process [77]. Additionally, identifying the effect of targeting NRF1 and Nrf2 during exposure to repeated oxidative challenges could contribute to understanding the potential for improving cellular resilience. We suspect that the adaptations in the presence of the NRF1 and Nrf2 activator co-treatment may also contribute to long-term beneficial adaptations. For example, we have demonstrated that treatment with a Nrf2a favored mechanisms of proteome maintenance and permitted beneficial mitochondrial adaptations to exercise [26]. Additionally, we recently reported improvements in muscle mitochondrial respiration in a multimorbidity model treated orally with Nrf2a [34]. Therefore, we suspect the changes we observed in response to acute co-treatment with NRF1a and Nrf2a, would likely be mirrored by cytoprotection against the chronic oxidative stress that is typical with advancing age.

FIGURES

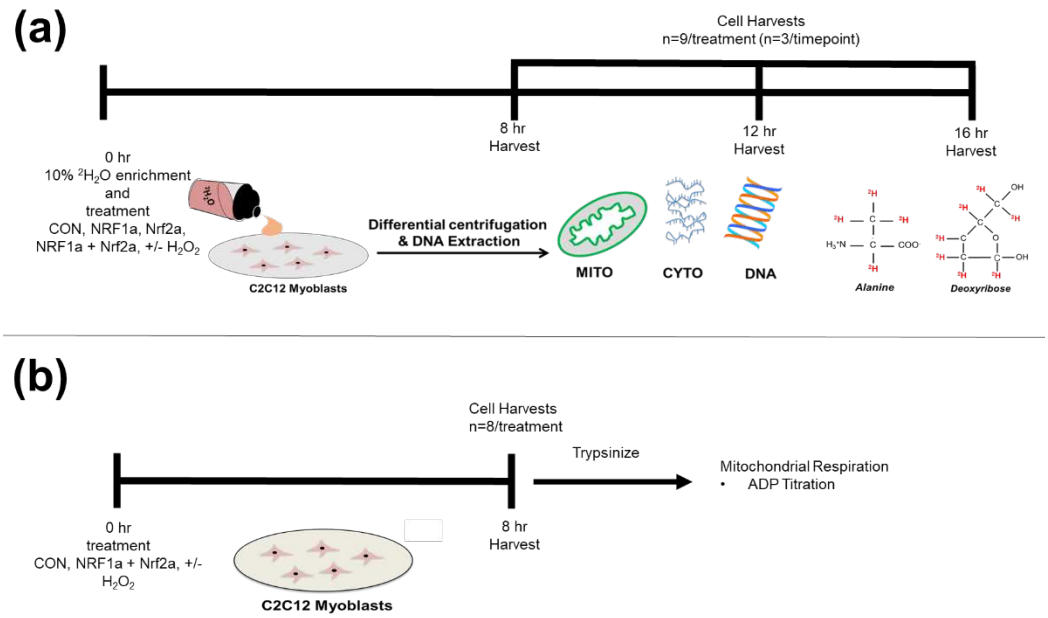

Figure 2.1. Experimental design for in vitro synthesis and mitochondrial respiration. For simultaneous assessment of protein and DNA synthesis rates, at time point 0 hr media was replaced with 10% ^2H_2O-enriched cell culture media with respective treatments of CON (DMSO), NRF1 activator (NRF1a) at 20 µg/ml, Nrf2a at 20 µg/ml, with and without hydrogen peroxide (H_2O_2) at 50 µM. Cells were harvested at 8, 12, and 16 hours. There was a total of n = 9/treatment and n = 3/timepoint (a). For assessment of mitochondrial respiration, at time point 0 hr, media was replaced with fresh cell culture media with respective treatments of CON (DMSO), NRF1a at 20 µg/ml and Nrf2a at 20 µg/ml, with and without H_2O_2 at 50 µM. Cells were trypsinized at 8 hrs and placed in mitochondrial respiration medium (MiR05) for high-resolution respirometry using an ADP titration protocol (b).

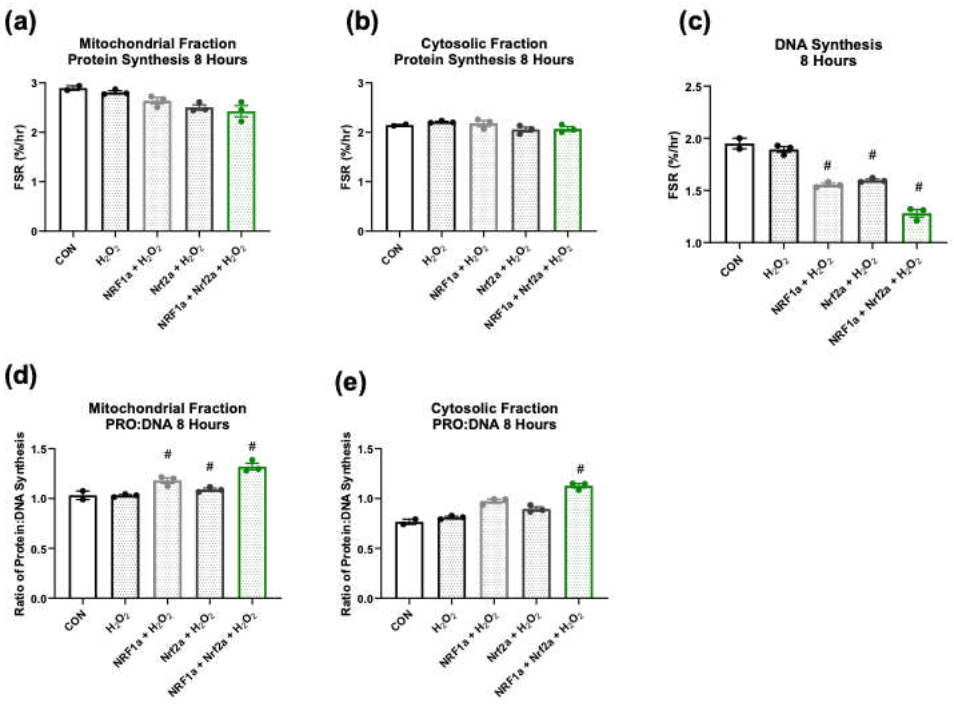

Figure 2.2. Combined treatment with NRF1 and Nrf2 activators promotes mechanisms favoring maintenance of both mitochondrial and cytosolic proteostasis. Using stable isotopic tracing with $^{2}H_2O$ enriched medium, we simultaneously monitored rates of new protein and DNA synthesis over 16 hrs of treatment with NRF1 and Nrf2 activators during a challenge with H_2O_2. Data here reflect 8 hrs of treatment. Rates of mitochondrial (a) and cytosolic (b) protein synthesis were maintained in all treatment groups. However, there were significantly slower rates of DNA synthesis (cell proliferation) in cells treated with NRF1a, Nrf2a, and the combination of NRF1a and Nrf2a compared to H_2O_2 alone (c). To gain insight into the effect of treatments on allocation of newly synthesized proteins for somatic maintenance versus for newly proliferating cells, we expressed the rates of protein synthesis relative to the rates of cell proliferation. There was a significantly greater ratio of rates of both cytosolic and mitochondrial protein synthesis to the rates of DNA synthesis when cells were treated with the combination of NRF1a and Nrf2a under an H_2O_2 challenge, indicating improved mechanisms of proteostasis (d and e). Mechanisms of mitochondrial proteome maintenance were also greater with monotreatment of NRF1a or Nrf2a (d). #$p<0.05$ compared to H_2O_2

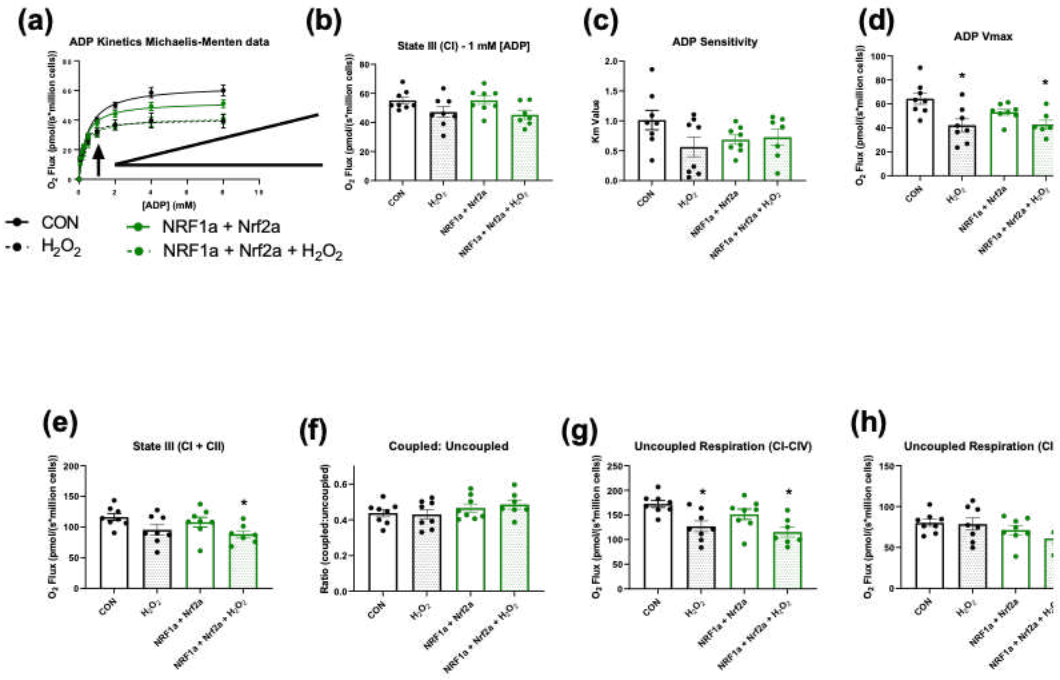

Figure 2.3. Treatment with NRF1 and Nrf2 activators does not rescue H_2O_2-induced declines in mitochondrial respiration. Using high-resolution respirometry during an ADP titration protocol, we measured mitochondrial oxygen consumption in cells treated for 8 hrs with NRF1 and Nrf2 activators during a challenge with H_2O_2. The ADP titrations were fit to Michaelis-Menten kinetics (a). At submaximal ADP concentrations up to and including 1 mM ADP there were no significant differences between treatment groups. This observation is identified within panel (a) by the arrow and then graphed in panel (b). There were no differences in ADP sensitivity as assessed by the Km value (c). Acutely exposing cells to H_2O_2 stress decreased maximal mitochondrial respiration, and the co-treatment of NRF1a + Nrf2a did not recover this acute decline (d). State III Complex I and II supported mitochondrial respiration was significantly lower in cells treated with NRF1a + Nrf2a + H_2O_2 compared to CON (e). There were no differences in the ratio of coupled to uncoupled respiration (f). Compared to CON, Complex I-IV supported uncoupled respiration was significantly lower in the cells treated with H_2O_2 and NRF1a + Nrf2a + H_2O_2, but there were no differences with the NRF1a and Nrf2a treatments without H_2O_2 (g). In Complex II-IV supported uncoupled respiration, there were no significant differences (h). *$p<0.05$ compared to CON

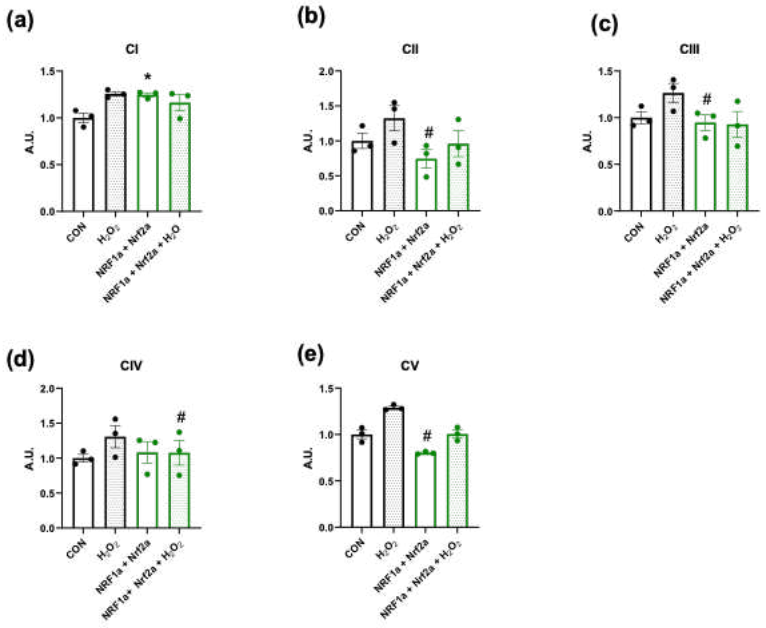

Figure 2.4. Treatment with a combination of NRF1 and Nrf2 activators, with or without a H_2O_2 challenge, does not uniformly alter mitochondrial protein content. Using western blot analyses we evaluated the effect of treatments on expression of 5 mitochondrial electron transfer chain complexes. Compared to CON, the combination of NRF1a + Nrf2a significantly increased CI protein content (a). However, the combination of NRF1a + Nrf2a significantly decreased CII, CIII, and CV protein content compared to H_2O_2 (b, c, and e). Finally, CIV protein content was significantly lower in NRF1a + Nrf2a + H_2O_2 compared to H_2O_2 alone (d). See representative blots in Figure S9. *$p<0.05$ compared to CON; #$p<0.05$ compared to H_2O_2

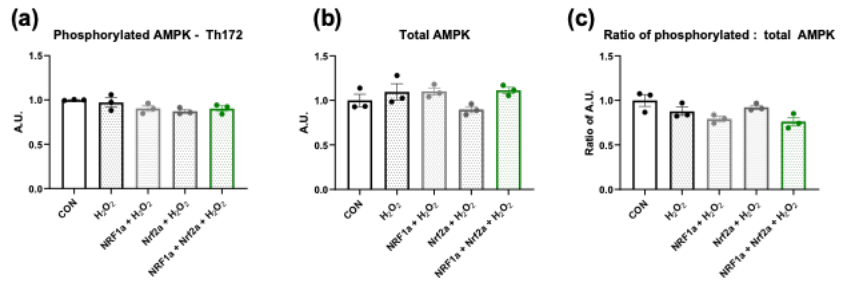

Figure 2.5. Treatment with NRF1 and Nrf2 activators during a H_2O_2 challenge does not alter AMPK signaling. Using western blot analyses, we identified no significant differences in the amount of phosphorylated AMPK, total AMPK, or the ratio of phosphorylated to total AMPK in response to 8 hrs of treatment with NRF1a, Nrf2a, or the combination of NRF1a + Nrf2a compared to CON or H_2O_2. See representative blots in Figure A.9.

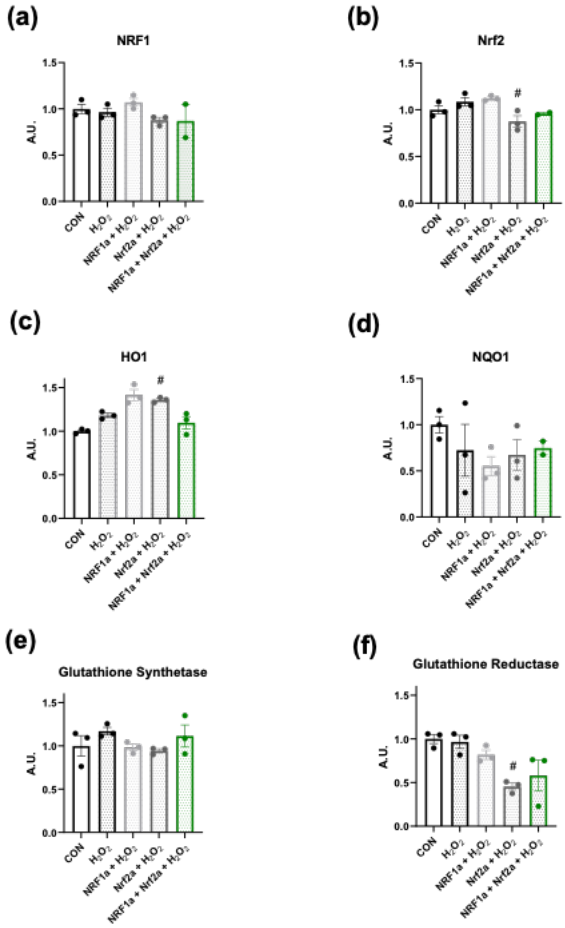

Figure 2.6. Protein content of NRF1, Nrf2, and ARE-regulated endogenous antioxidants. After 8 hrs of treatment, there were no significant differences in the content NRF1 protein (a). There was a significant decrease in Nrf2 protein content in Nrf2a + H_2O_2 treated cells compared to H_2O_2 alone (b). HO-1 content was significantly increased in Nrf2a + H_2O_2 compared to H_2O_2 alone (c). There were no significant differences in NQO1 or glutathione synthetase, two targets of Nrf2, between groups (d and e). Finally, there was a significant decrease in glutathione reductase protein content in Nrf2a + H_2O_2 compared to H_2O_2 alone (f). See representative blots in Figure S9. #$p<0.05$ compared to H_2O_2

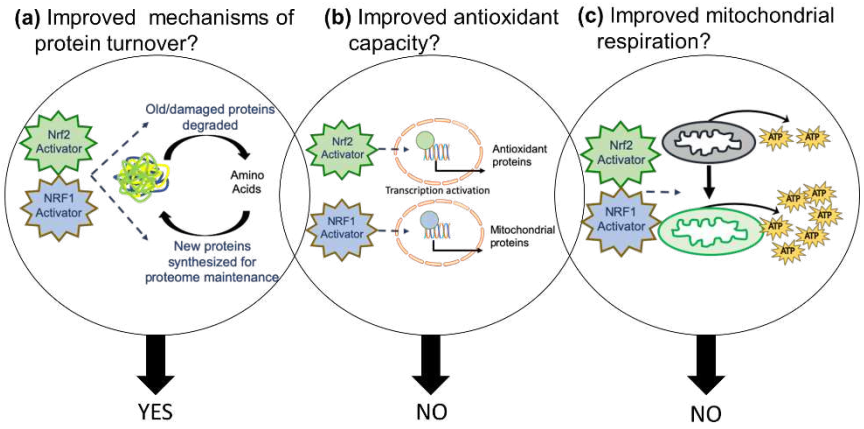

Figure 2.7. Mechanisms by which co-treatment of NRF1 and Nrf2 activators could contribute to adaptive stress responses. Here we summarize the adaptation to a H_2O_2 stress in cells treated with a combination of NRF1 and Nrf2 activators. (a) The co-treatment of the activators in the presence of an oxidative challenge improved mechanisms of protein turnover (Figure 2d-e). (b) Transcriptional regulation via NRF1 and Nrf2 activation has the potential to improve antioxidant capacity and redox regulation. However, at least with the short-term treatments used here, we observed non-uniform differences in downstream antioxidants (Figure 6). Both NRF1 and Nrf2 regulate the transcription of genes critical for mitochondrial biogenesis and function. There were no uniform differences in mitochondrial protein content, suggesting there was no net accrual of mitochondrial proteins (Figure 5). (c) We observed a decrease in maximal ADP-stimulated respiration with H_2O_2 treatment, that was unaltered by co-treatment with NRF1 and Nrf2 activators (Figure 3b). Key Finding: Because mitochondrial respiratory capacity was not different between H_2O_2 and the co-treatment with NRF1 and Nrf2 activators plus H_2O_2, we can imply that the cells had similar ATP availability. However, despite the similar ATP availability, treatment with NRF1 and Nrf2 activators shifted the energetic investment toward synthesis of proteins to maintain the mitochondrial proteome, with less for newly proliferating cells (Figure 2). Therefore, a key finding from this study is that co-treatment with NRF1 and Nrf2 activators promotes adaptation to an acute oxidative stress via reallocation of energetic resources to promote mitochondrial proteostasis.

REFERENCES

1. Jones DP. Redefining Oxidative Stress. *Antioxid Redox Sign*. 2006;8(9-10):1865-1879. doi:10.1089/ars.2006.8.1865

2. Bouayed J, Bohn T. Exogenous antioxidants—Double-edged swords in cellular redox state. *Oxid Med Cell Longev*. 2010;3(4):228-237. doi:10.4161/oxim.3.4.12858

3. Nikolaidis MG, Kerksick CM, Lamprecht M, McAnulty SR. Does vitamin C and E supplementation impair the favorable adaptations of regular exercise? *Oxid Med Cell Longev*. 2012;2012:707941. doi:10.1155/2012/707941

4. Tapia PC. Sublethal mitochondrial stress with an attendant stoichiometric augmentation of reactive oxygen species may precipitate many of the beneficial alterations in cellular physiology produced by caloric restriction, intermittent fasting, exercise and dietary phytonutrients: “Mitohormesis” for health and vitality. *Med Hypotheses*. 2006;66(4):832-843. doi:10.1016/j.mehy.2005.09.009

5. Drake JC, Laker RC, Wilson RJ, Zhang M, Yan Z. Exercise-induced mitophagy in skeletal muscle occurs in the absence of stabilization of Pink1 on mitochondria. *Cell Cycle*. Published online 2018. doi:10.1080/15384101.2018.1559556

6. Laker RC, Drake JC, Wilson RJ, et al. Ampk phosphorylation of Ulk1 is required for targeting of mitochondria to lysosomes in exercise-induced mitophagy. *Nat Commun*. 2017;8(1):548. doi:10.1038/C1467-017-00520-9

7. Drake JC, Wilson RJ, Laker RC, et al. Mitochondria-localized AMPK responds to local energetics and contributes to exercise and energetic stress-induced mitophagy. *P Natl Acad Sci Usa*. 2021;118(37). doi:10.1073/pnas.2025932118

8. Davies KJA. Adaptive homeostasis. *Mol Aspects Med*. 2016;49:1-7. doi:10.1016/j.mam.2016.04.007

9. Lomeli N, Bota DA, Davies KJA. Diminished stress resistance and defective adaptive homeostasis in age-related diseases. *Clin Sci*. 2017;131(21):2573-2599. doi:10.1042/cs20160982

10. Pomatto LCD, Davies KJA.Adaptive homeostasis and the free radical theory of ageing. *Free Radical Bio Med*. 2018;124:420-430. doi:10.1016/j.freeradbiomed.2018.06.016

11. Coen PM, Musci RV, Hinkley JM, Miller BF. Mitochondria as a Target for Mitigating Sarcopenia. *Front Physiol*. 2019;9:1883. doi:10.3389/fphys.2018.01883

12. Musci RV, Hamilton KL, Miller BF. Targeting mitochondrial function and proteostasis to mitigate dynapenia. *Eur J Appl Physiol*. 2018;118(1):1-9. doi:10.1007/s00421-017-3730-x

13. Kennedy BK, Berger SL, Brunet A, et al. Geroscience: Linking Aging to Chronic Disease. *Cell*. 2014;159(4):709-713. doi:10.1016/j.cell.2014.10.039

14. López-Otín C, Blasco MA, Partridge L, Serrano M, Kroemer G. The Hallmarks of Aging. *Cell*. 2013;153(6):1194-1217. doi:10.1016/j.cell.2013.05.039

15. Holloway GP, Holwerda AM, Miotto PM, Dirks ML, Verdijk LB, Loon LJC van. Age-Associated Impairments in Mitochondrial ADP Sensitivity Contribute to Redox Stress in Senescent Human Skeletal Muscle. *Cell Reports*. 2018;22(11):2837-2848. doi:10.1016/j.celrep.2018.02.069

16. Gonzalez-Freire M, Adelnia F, Moaddel R, Ferrucci L. Searching for a mitochondrial root to the decline in muscle function with ageing. *J Cachexia Sarcopenia Muscle*. 2018;9(3):435-440. doi:10.1002/jcsm.12313

17. Brand MD. Uncoupling to survive? The role of mitochondrial inefficiency in ageing. *Exp Gerontol*. 2000;35(6-7):811-820. doi:10.1016/s0531-5565(00)00135-2

18. Buttgereit F, Brand MD. A hierarchy of ATP-consuming processes in mammalian cells. *Biochem J*. 1995;312(1):163-167. doi:10.1042/bj3120163

19. Haus JM, Carrithers JA, Trappe SW, Trappe TA. Collagen, cross-linking, and advanced glycation end products in aging human skeletal muscle. *J Appl Physiol*. 2007;103(6):2068-2076. doi:10.1152/japplphysiol.00670.2007

20. Fernando R, Drescher C, Nowotny K, Grune T, Castro JP. Impaired proteostasis during skeletal muscle aging. *Free Radical Bio Med*. 2019;132(J Lab Clin Med 137 4 2001):58-66. doi:10.1016/j.freeradbiomed.2018.08.037

21. Korovila I, Hugo M, Castro JP, et al. Proteostasis, oxidative stress and aging. *Redox Biol*. 2017;13:550-567. doi:10.1016/j.redox.2017.07.008

22. Kaushik S, Cuervo AM. Proteostasis and aging. *Nat Med*. 2015;21(12):nm.4001. doi:10.1038/nm.4001

23. Gaffney CJ, Pollard A, Barratt TF, Constantin-Teodosiu D, Greenhaff PL, Szewczyk NJ. Greater loss of mitochondrial function with ageing is associated with earlier onset of sarcopenia in *C. elegans*. *Aging*. 2018;10(11):3382-3396. doi:10.18632/aging.101654

24. Kong H, Reczek CR, McElroy GS, et al. Metabolic determinants of cellular fitness dependent on mitochondrial reactive oxygen species. *Sci Adv*. 2020;6(45):eabb7272. doi:10.1126/sciadv.abb7272

25. Gao L, Kumar V, Vellichirammal NN, et al. Functional, proteomic and bioinformatic analyses of Nrf2- and Keap1- null skeletal muscle. *J Physiology*. 2020;598(23):5427-5451. doi:10.1113/jp280176

26. Bruns DR, Ehrlicher SE, Khademi S, et al. Differential Effects of Vitamin C or Protandim on Skeletal Muscle Adaptation to Exercise. *J Appl Physiol*. Published online 2018. doi:10.1152/japplphysiol.00277.2018

27. Pajares M, Cuadrado A, Rojo AI. Modulation of proteostasis by transcription factor NRF2 and impact in neurodegenerative diseases. *Redox Biol*. 2017;11:543-553. doi:10.1016/j.redox.2017.01.006

28. Gao L, Kumar V, Hackfort B, et al. Proteomic and Functional Analyses of Keap1-Nrf2 Pathway in Skeletal Muscle. *Faseb J*. 2019;33(S1):868.30-868.30. doi:10.1096/fasebj.2019.33.1_supplement.868.30

29. Coleman V, Sa-Nguanmoo P, Koenig J, et al. Partial involvement of Nrf2 in skeletal muscle mitohormesis as an adaptive response to mitochondrial uncoupling. *Sci Rep-uk*. 2018;8(1):2446. doi:10.1038/C1598-018-20901-4

30. Chen LG, Zhang YQ, Wu ZZ, Hsieh CW, Chu CS, Wung BS. Peanut arachidin-1 enhances Nrf2-mediated protective mechanisms against TNF-α-induced ICAM-1 expression and NF-κB activation in endothelial cells. *Int J Mol Med*. 2018;41(1):541-547. doi:10.3892/ijmm.2017.3238

31. Cuadrado A, Rojo AI, Wells G, et al. Therapeutic targeting of the NRF2 and KEAP1 partnership in chronic diseases. *Nat Rev Drug Discov*. 2019;18(4):295-317. doi:10.1038/C1573-018-0008-x

32. Dinkova-Kostova AT, Abramov AY. The emerging role of Nrf2 in mitochondrial function. *Free Radical Bio Med*. 2015;88(Pt B):179-188. doi:10.1016/j.freeradbiomed.2015.04.036

33. Musci RV, Hamilton KL, Linden MA. Exercise-Induced Mitohormesis for the Maintenance of Skeletal Muscle and Healthspan Extension. *Sports*. 2019;7(7):170. doi:10.3390/sports7070170

34. Musci RV, Andrie KM, Walsh MA, et al. Phytochemical Nrf2 activator attenuates skeletal muscle mitochondrial dysfunction and impaired proteostasis in a preclinical model of musculoskeletal aging. doi:10.1101/2021.06.11.448143

35. Konopka AR, Castor WM, Wolff CA, et al. Skeletal muscle mitochondrial protein synthesis and respiration in response to the energetic stress of an ultra-endurance race. *J Appl Physiol*. 2017;123(6):1516-1524. doi:10.1152/japplphysiol.00457.2017

36. Islam H, Bonafiglia JT, Turnbull PC, Simpson CA, Perry CGR, Gurd BJ. The impact of acute and chronic exercise on Nrf2 expression in relation to markers of mitochondrial biogenesis in human skeletal muscle. *Eur J Appl Physiol*. 2020;120(1):149-160. doi:10.1007/s00421-019-04259-7

37. Xie L, Gu Y, Wen M, et al. Hydrogen Sulfide Induces Keap1 S-sulfhydration and Suppresses Diabetes-Accelerated Atherosclerosis via Nrf2 Activation. *Diabetes*. 2016;65(10):3171-3184. doi:10.2337/db16-0020

38. Strong R, Miller RA, Antebi A, et al. Longer lifespan in male mice treated with a weakly estrogenic agonist, an antioxidant, an α-glucosidase inhibitor or a Nrf2-inducer. *Aging Cell*. 2016;15(5):872-884. doi:10.1111/acel.12496

39. Konopka AR, Laurin JL, Musci RV, et al. Influence of Nrf2 activators on subcellular skeletal muscle protein and DNA synthesis rates after 6 weeks of milk protein feeding in older adults. *Geroscience*. 2017;39(2):175-186. doi:10.1007/s11357-017-9968-8

40. Ungvari Z, Bagi Z, Feher A, et al. Resveratrol confers endothelial protection via activation of the antioxidant transcription factor Nrf2. *Am J Physiol-heart C*. 2010;299(1):H18-H24. doi:10.1152/ajpheart.00260.2010

41. Donovan EL, McCord JM, Reuland DJ, Miller BF, Hamilton KL. Phytochemical Activation of Nrf2 Protects Human Coronary Artery Endothelial Cells against an Oxidative Challenge. *Oxid Med Cell Longev*. 2012;2012:132931. doi:10.1155/2012/132931

42. Pomatto LCD, Sun PY, Davies KJA. To Adapt or not to Adapt: Consequences of Declining Adaptive Homeostasis and Proteostasis with Age. *Mech Ageing Dev*. 2018;177:80-87. doi:10.1016/j.mad.2018.05.006

43. Pomatto LCD, Davies KJA. The role of declining adaptive homeostasis in ageing. *J Physiology*. 2017;595(24):7275-7309. doi:10.1113/jp275072

44. Nguyen T, Nioi P, Pickett CB. The Nrf2-antioxidant response element signaling pathway and its activation by oxidative stress. *J Biological Chem*. 2009;284(20):13291-13295. doi:10.1074/jbc.r900010200

45. Nishimoto S, Koike S, Inoue N, Suzuki T, Ogasawara Y. Activation of Nrf2 attenuates carbonyl stress induced by methylglyoxal in human neuroblastoma cells: Increase in GSH levels is a critical event for the detoxification mechanism. *Biochem Bioph Res Co*. 2017;483(2):874-879. doi:10.1016/j.bbrc.2017.01.024

46. Scarpulla RC. Transcriptional activators and coactivators in the nuclear control of mitochondrial function in mammalian cells. *Gene*. 2002;286(1):81-89. doi:10.1016/s0378-1119(01)00809-5

47. Lu Y, Ding W, Wang B, et al. Positive regulation of human PINK1 and Parkin gene expression by nuclear respiratory factor 1. *Mitochondrion*. 2020;51:22-29. doi:10.1016/j.mito.2019.12.002

48. Huo L, Scarpulla RC. Mitochondrial DNA Instability and Peri-Implantation Lethality Associated with Targeted Disruption of Nuclear Respiratory Factor 1 in Mice. *Mol Cell Biol*. 2001;21(2):644-654. doi:10.1128/mcb.21.2.644-654.2001

49. Scarpulla RC. Nuclear Control of Respiratory Chain Expression by Nuclear Respiratory Factors and PGC-1-Related Coactivator. *Ann Ny Acad Sci*. 2008;1147(1):321-334. doi:10.1196/annals.1427.006

50. Wahl D, Solon-Biet SM, Wang QP, et al. Comparing the Effects of Low-Protein and High-Carbohydrate Diets and Caloric Restriction on Brain Aging in Mice. *Cell Reports*. 2018;25(8):2234-2243.e6. doi:10.1016/j.celrep.2018.10.070

51. Andrade-Souza VA, Ghiarone T, Sansonio A, et al. Exercise twice-a-day potentiates markers of mitochondrial biogenesis in men. *Faseb J*. 2020;34(1):1602-1619. doi:10.1096/fj.201901207rr

52. Gureev AP, Shaforostova EA, Popov VN. Regulation of Mitochondrial Biogenesis as a Way for Active Longevity: Interaction Between the Nrf2 and PGC-1α Signaling Pathways. *Frontiers Genetics*. 2019;10:435. doi:10.3389/fgene.2019.00435

53. Aquilano K, Baldelli S, Pagliei B, Cannata SM, Rotilio G, Ciriolo MR. p53 Orchestrates the PGC-1α-Mediated Antioxidant Response Upon Mild Redox and Metabolic Imbalance. *Antioxid Redox Sign*. 2013;18(4):386-399. doi:10.1089/ars.2012.4615

54. Piantadosi CA, Carraway MS, Babiker A, Suliman HB. Heme Oxygenase-1 Regulates Cardiac Mitochondrial Biogenesis via Nrf2-Mediated Transcriptional Control of Nuclear Respiratory Factor-1. *Circ Res*. 2008;103(11):1232-1240. doi:10.1161/01.res.0000338597.71702.ad

55. Robinson MM, Sather BK, Burney ER, et al. Robust intrinsic differences in mitochondrial respiration and H2O2 emission between L6 and C2C12 cells. *Am J Physiology Cell Physiology*. Published online 2019. doi:10.1152/ajpcell.00343.2018

56. Cummings BS, Schnellmann RG. Measurement of Cell Death in Mammalian Cells. *Curr Protoc Pharmacol*. 2004;25(1):12.8.1-12.8.22. doi:10.1002/0471141755.ph1208s25

57. Nelson SK, Bose SK, Grunwald GK, Myhill P, McCord JM. The induction of human superoxide dismutase and catalase in vivo: A fundamentally new approach to antioxidant therapy. *Free Radical Bio Med*. 2006;40(2):341-347. doi:10.1016/j.freeradbiomed.2005.08.043

58. Wolff CA, Reid JJ, Musci RV, et al. Differential Effects of Rapamycin and Metformin in Combination with Rapamycin on Mechanisms of Proteostasis in Cultured Skeletal Myotubes. *Journals Gerontology Ser*. Published online 2019. doi:10.1093/gerona/glz058

59. Drake JC, Peelor FF, Biela LM, et al. Assessment of Mitochondrial Biogenesis and mTORC1 Signaling During Chronic Rapamycin Feeding in Male and Female Mice. *Journals Gerontology Ser*. 2013;68(12):1493-1501. doi:10.1093/gerona/glt047

60. Miller BF, Robinson MM, Bruss MD, Hellerstein M, Hamilton KL. A comprehensive assessment of mitochondrial protein synthesis and cellular proliferation with age and caloric restriction. *Aging Cell*. 2012;11(1):150-161. doi:10.1111/j.1474-9726.2011.00769.x

61. Robinson MM, Turner SM, Hellerstein MK, Hamilton KL, Miller BF. Long-term synthesis rates of skeletal muscle DNA and protein are higher during aerobic training in older humans than in sedentary young subjects but are not altered by protein supplementation. *Faseb J*. 2011;25(9):3240-3249. doi:10.1096/fj.11-186437

62. Konopka AR, Laurin JL, Schoenberg HM, et al. Metformin inhibits mitochondrial adaptations to aerobic exercise training in older adults. *Aging Cell*. 2019;18(1):e12880. doi:10.1111/acel.12880

63. Belloto E, Diraison F, Basset A, Allain G, Abdallah P, Beylot M. Determination of protein replacement rates by deuterated water: validation of underlying assumptions. *Am J Physiol-endoc M*. 2007;292(5):E1340-E1347. doi:10.1152/ajpendo.00488.2006

64. Voogt JN, Awada M, Murphy EJ, Hayes GM, Busch R, Hellerstein MK. Measurement of very low rates of cell proliferation by heavy water labeling of DNA and gas chromatography/pyrolysis/isotope ratio–mass spectrometric analysis. *Nat Protoc*. 2007;2(12):3058-3062. doi:10.1038/nprot.2007.421

65. Shao D, Oka S ichi, Liu T, et al. A Redox-Dependent Mechanism for Regulation of AMPK Activation by Thioredoxin1 during Energy Starvation. *Cell Metab*. 2014;19(2):232-245. doi:10.1016/j.cmet.2013.12.013

66. Drake JC, Bruns DR, Peelor FF, et al. Long-lived Snell dwarf mice display increased proteostatic mechanisms that are not dependent on decreased mTORC1 activity. *Aging Cell*. 2015;14(3):474-482. doi:10.1111/acel.12329

67. Reuland D, McCord J, Hamilton K. Upregulation of heme oxygenase-1 through activation of Nrf2 by the phytochemicals in Protandim. *Faseb J*. 2010;24:1001.1-1001.1. doi:10.1096/fasebj.24.1_supplement.1001.1

68. Drake JC, Peelor FF, Biela LM, Miller RA, Hamilton KL, Miller BF. Assessment of protein synthesis and cellular proliferation in long-lived crowded litter mice. *Faseb J*. 2013;27:1202.25-1202.25. doi:10.1096/fasebj.27.1_supplement.1202.25

69. Drake JC, Bruns DR, Peelor FF, et al. Long-lived crowded-litter mice have an age-dependent increase in protein synthesis to DNA synthesis ratio and mTORC1 substrate phosphorylation. *Am J Physiol-endoc M*. 2014;307(9):E813-E821. doi:10.1152/ajpendo.00256.2014

70. Shuler KT, Wilson BE, Muñoz ER, Mitchell AD, Selsby JT, Hudson MB. Muscle Stem Cell-Derived Extracellular Vesicles Reverse Hydrogen Peroxide-Induced Mitochondrial Dysfunction in Mouse Myotubes. *Cells*. 2020;9(12):2544. doi:10.3390/cells9122544

71. Choi SL, Kim SJ, Lee KT, et al. The Regulation of AMP-Activated Protein Kinase by H2O2. *Biochem Bioph Res Co*. 2001;287(1):92-97. doi:10.1006/bbrc.2001.5544

72. Komatsu M, Kurokawa H, Waguri S, et al. The selective autophagy substrate p62 activates the stress responsive transcription factor Nrf2 through inactivation of Keap1. *Nat Cell Biol*. 2010;12(3):213-223. doi:10.1038/ncb2021

73. Chepelev NL, Bennitz JD, Huang T, McBride S, Willmore WG. The Nrf1 CNC-bZIP Protein Is Regulated by the Proteasome and Activated by Hypoxia. *Plos One*. 2011;6(12):e29167. doi:10.1371/journal.pone.0029167

74. Kobayashi M, Yamamoto M. Nrf2–Keap1 regulation of cellular defense mechanisms against electrophiles and reactive oxygen species. *Adv Enzyme Regul*. 2006;46(1):113-140. doi:10.1016/j.advenzreg.2006.01.007

75. Loboda A, Damulewicz M, Pyza E, Jozkowicz A, Dulak J. Role of Nrf2/HO-1 system in development, oxidative stress response and diseases: an evolutionarily conserved mechanism. *Cell Mol Life Sci*. 2016;73(17):3221-3247. doi:10.1007/s00018-016-2223-0

76. Reuland DJ, Khademi S, Castle CJ, et al. Upregulation of phase II enzymes through phytochemical activation of Nrf2 protects cardiomyocytes against oxidant stress. *Free Radical Bio Med*. 2013;56:102-111. doi:10.1016/j.freeradbiomed.2012.11.016

77. Malinska D, Kudin AP, Bejtka M, Kunz WS. Changes in mitochondrial reactive oxygen species synthesis during differentiation of skeletal muscle cells. *Mitochondrion*. 2012;12(1):144-148. doi:10.1016/j.mito.2011.06.015

CHAPTER 3 – PHYTOCHEMICAL COMPOUND, PB125, IMPROVES MECHANISMS OF SKELETAL MUSCLE PROTEOSTASIS IN A PRECLINICAL MODEL OF MUSCULOSKELETAL DECLINE: MUSCLE SPECIFICITY MATTERS

INTRODUCTION

Musculoskeletal disorders are the top cause of disability in older adults [1]. The musculoskeletal system includes bone, articular cartilage, skeletal muscle, and associated connective tissues [2]. Specifically, each component of the musculoskeletal system is susceptible a different age-related chronic disease such as osteoporosis [3], osteoarthritis [4], and sarcopenia [5] for bone, articular cartilage, and skeletal muscle, respectively. These conditions co-exist, with osteoarthritis increasing the prevalence of sarcopenia [6] and low skeletal muscle mass increasing the risk of developing osteoarthritis [7]. Having an age-related chronic disease of the musculoskeletal system also increases risks for other age-related co-morbidites [8]. Therefore, by slowing the progression of musculoskeletal diseases we hope to improve healthy aging in older adults.

The components of the musculoskeletal system work together to produce movement (i.e., walking or mobility). However, mobility impairments (i.e., decreased gait speed, coordination, and balance) in older adults are associated with markers of biological aging, specifically the hallmarks of aging [9–11]. While no single study has tracked mobility changes across all the life stages [11], habitual walking speed (i.e., gait speed) decreases with advancing age in both men and women and occurs prior to substantial changes in skeletal muscle mass [12]. It was recently demonstrated that mitochondrial dysfunction, a hallmark of aging, predicts gait speed declines in a longitudinal study [10] further bolstering the concept that biological processes drive functional declines.

The age-related loss of skeletal muscle mass and strength/function (i.e., sarcopenia) is also driven by loss of proteostasis, another hallmark of aging [10]. Proteostasis is the collection of cellular processes involved in the synthesis, folding, chaperoning, post-translational

modifications, and degradation of proteins [13]. However, with age proteins become damaged, for example, through increased and prolonged production of free radicals (i.e., oxidative stress). Specifically, genetic loss of superoxide dismutase ($Sod1^{-/-}$), an endogenous antioxidant, results in increased oxidative stress and protein damage which contributes to sarcopenia in mice [14,15]. However, when the $Sod1^{-/-}$ whole body mouse was crossed to constitutively overexpress the hydrogen peroxide scavenger peroxiredoxin 3 in skeletal muscle, it led to an attenuation of sarcopenic hallmarks [16]. Therefore, improving mechanisms of skeletal muscle redox balance and protein health consequently improved skeletal muscle function.

Cellular senescence, another hallmark of aging, negatively affects skeletal muscle health [17]. Despite the lack of cell division in senescent cells, they have a pro-inflammatory phenotype that is detrimental to the surrounding cells and have therefore been coined “zombie cells” [18]. Senescence in skeletal muscle is different from other tissues in that the greatest percentage of nuclei in a muscle homogenate are in the myofibers (individual multinucleated muscle cells). However, even though myonuclei can synthesize new DNA, the proportion of new DNA synthesized by myonuclei is substantially smaller than the percentage of new DNA from surrounding cells in skeletal muscle including pericytes, endothelial cells, fibroblasts, satellite cells, and immune cells over a period of time [19]. Therefore, it is likely important to discern senescence in myofibers versus the surrounding cells. Specifically, increases in p21 drive myofiber senescence while the cells that surround myofibers within a whole skeletal muscle are driven by increases in p16 [20]. Additionally, suppressing skeletal muscle cellular senescence through senolytic treatment improved skeletal muscle function. In summary, musculoskeletal aging is multifaceted; however, targeting mitochondrial function, maintain proteome maintenance, and cellular senescence might be viable therapeutic targets [21,22].

Therapies that have high translational capacity (i.e., fast discovery from lab bench to patient bedside) to help older adults with sarcopenia are lacking [23]. For example, resistance exercise has been the only treatment shown to improve skeletal muscle health in older adults

[24,25]. Despite ~40% of clinical trials having an exercise intervention [as extensively reviewed here [23]] exercise lacks translatability. Specifically, there is evidence that physical activity participation is low in older adults even when they are educated about the benefits of activity due to barriers like lack of interest and pain associated with exercise [26]. Therefore, non-exercise alternatives such as nutraceuticals that target similar cellular pathways as exercise might be advantageous for slowing the age-related decline in skeletal muscle.

However, when nutraceuticals are tested in human clinical trials, they fail to elicit meaningful benefits in skeletal muscle health [in the 13 trials reviewed in [23]. One reason that might explain why human clinical trials failed is because, when the proposed nutraceutical interventions were tested in preclinical animal models, these animals did not closely resemble the human skeletal muscle aging phenotype. Our group has identified that the Hartley guinea pig may serve as a model that more closely mimics the insidious, progressive musculoskeletal decline that occurs in conjunction with other age-related morbidities in humans [27]. At 3 to 4 months of age Hartley guinea pigs begin developing osteoarthritis [28], wherein by 18 months their mobility is constrained [29]. Because osteoarthritis and age-related skeletal muscle loss (i.e., sarcopenia) co-exist in humans [6,7] we further characterized how the Hartley guinea pigs myofibers change with age. Hartley guinea pigs exhibit a decrease in skeletal muscle density indicative of an increased in fat deposition [27], decreased rates of protein synthesis [27,30], decreases in mitochondrial function [30], and a greater percentage of small myofibers [27], which mimics human aging [31–34].

We have been investigating combinations of plant-derived compounds shown to synergistically target and activate a transcription factor that influences expression of genes involved in proteostasis, mitochondrial function, and cell proliferation [30,35–38]. For example, we demonstrated that, in older men, there was a trend to increase mechanisms of skeletal muscle proteostasis following six weeks of treatment with Protandim, a phytochemical compound (the same compound used in Chapter 2) developed to activate the transcription

factor nuclear factor erythroid 2-related factor 2 (Nrf2). Nrf2 is at the nexus of redox homeostasis, mitochondrial energetics, and proteome maintenance [39]. A newer Nrf2 activator, Pathways Bioscience 125 (PB125), shows a greater degree of Nrf2 activation than Protandim (unpublished data), with associated protection against oxidative induced injury in hepatocytes [40].

In an NIH-funded preclinical intervention trial, we examined if treatment with the phytochemical compound PB125 could slow the progression of musculoskeletal decline in Hartley guinea pigs. Because Hartleys have compromised mobility associated with progressive musculoskeletal decline [29], and mitochondrial function can predict mobility declines [10], we investigated if a 10-month daily treatment of PB125 attenuated the age-related decline in mitochondrial respiration. Musci et al., observed that the age-related declines in maximal and noncoupled skeletal muscle mitochondrial respiration were attenuated with 10 mo of PB125 treatment which was coupled with an increase in voluntary movement (i.e., one metric of mobility) [30]. Further,10 mo of PB125 attenuated the age-related decline in rates of contractile protein synthesis [30]. It is noteworthy that these effects were observed in the soleus, a muscle comprised primarily of type I myofibers, which is less susceptible to age-related decline [31,41].

However, there is also mounting evidence that the greatest benefits to Nrf2 activator treatment are observed when a stress is imposed. In Chapter 2, treating muscle precursor cells with low-dose oxidative stress combined with a Nrf2 activator (Protandim) resulted in the greatest increase in mechanisms of proteostasis, compared to when the stress was absent. In rodents participating in lifelong aerobic exercise (i.e., a hormetic Nrf2 activator) [42], the greatest benefits were observed in muscles with of a mixed myofiber composition as compared to solely type I myofibers [43]. Type II myofibers are also the most susceptible to age-related remodeling [31,41,44], contributing to decreases in force production. Further, the age-related muscle changes in the Hartley were predominantly seen in the gastrocnemius, a mixed myofiber muscle, as compared to the soleus [27]. The tibialis anterior, a muscle comprised essentially

entirely of type II myofibers, is important for mobility and highly susceptible to age-related changes. The tibialis anterior is active during the swing phase of the gait cycle by clearing the toes off the ground [45], and then activates again as the ankle is generating positive power [46]. Inadequate ankle dorsiflexion may risk unintentional ground contact, resulting in trips and falls in older adults [47,48]. However, the age, sex, and PB125 treatment effects have not been examined in muscles with predominantly type II myofibers such at the tibialis anterior.

To confirm that the skeletal muscle changes we observe in the Hartley guinea pig model are reflective of age and treatment, rather than related to the species, we aimed to identify an appropriate comparison strain. In our prior work, we made comparisons between the Hartleys and Strain 13 guinea pigs; however, Strain 13 is inbred compared to the outbred Hartley strain [27]. Additionally, we had previously only made 5 and 15 mo cross-sectional comparisons in the gastrocnemius and soleus from male animals. However, in our prior PB125 published work there were sex-specific differences in the responses to treatment [30]. Therefore, we wanted to confirm that the skeletal muscle aging phenotypes were more robust in the Hartley guinea pig compared to the outbred PigmEnTed (PET) strain that is less prone to progressive joint degeneration at an early age (unpublished work from our group). Therefore, we first hypothesized that PET guinea pigs would not experience the same degree of myofiber remodeling aging compared to age matched Hartley guinea pigs.

To address the primary objective of the study, which was to identify the potential benefit of PB125 for promoting muscle proteostasis in a predominantly type II fiber muscle, we then examined the long (from 5 to 15 mo; total treatment duration = 10 mo) term effects of daily PB125 treatment on tibialis anterior mechanisms of proteostasis. Thus, our second hypothesis was that PB125 would increase mechanisms of proteostasis in the tibialis anterior, a myofiber more susceptible to age-related changes in older guinea pigs (5 to 15 mo daily treatment) in Hartley guinea pigs.

METHODS

Husbandry

All procedures were approved by the Colorado State University Institutional Animal Care and Use Committee (Protocol # 1213) and were performed in accordance with the NIH Guide for the Care and Use of Laboratory Animals. To test hypothesis #1, male and female PET guinea pigs were obtained from Elm Hill Laboratories (Chelmsford, MA, USA) at approximately 2 and 12 months of age and sacrificed at 5 and 15 mo of age, respectively; 4 male and female guinea pigs were utilized in each age (total n = 32) as these animals were a part of a small pilot study. Male and female Hartley guinea pigs were obtained from Charles River Laboratories (Wilmington, MA, USA) at approximately 1 and 4 mo of age and sacrificed at 5 and 15 mo of age, respectively (14 males and females per age; total n = 56). The 4 mo old male and female Hartleys also served as control animals to test hypothesis #2. To test the effect of PB125 on tibialis anterior proteostasis, 4 mo male and female (n = 14/sex) additional Hartley guinea pigs were obtained from Charles River Laboratories, providing 14 males and 14 females for each of the 10-mo treatment regimens; vehicle control and PB125. This study was powered to detect differences in mechanisms of proteostasis at a power of 0.80 and significance (chance of Type I error) set at p=0.05 (Lenth power calculator). Based on data from a prior study, we calculated an n=13 animals/group, and increased the number to n=14/group to account for premature losses due to morbidity (total n =112). Animals were maintained at Colorado State University's Laboratory Animal Resources housing facilities and were monitored daily by veterinary staff. All guinea pigs were singly housed in solid bottom cages, maintained on a 12-12 hour light-dark cycle, and provided *ad libitum* access to food and water. All animals were fasted for 12 hours prior to euthanasia.

Daily PB125 treatment in Hartley guinea pigs

PB125 (Pathways Bioscience, Aurora, CO) is a phytochemical compound comprised of rosemary, ashwagandha, and luteolin powders, which contain the three active ingredients

carnosol, withaferin A, and luteolin at a mixed ratio of 15:5:2 by mass, respectively [40]. In a prior publication we demonstrated the feasibility of selecting 8.0 mg/kg of daily dosing [30]. After a one-month acclimation to housing conditions, male and female Hartley guinea pigs in each treatment group were randomized to receive a daily oral dose of PB125 suspended in OraSweet (Perrigo, Dublin, Ireland) or an equivalent volume of OraSweet only, which was the vehicle control (CON) beginning at 5 mo of age until 15 mo of age (Figure 3.1). Hartley guinea pigs were not dosed the morning of necropsy as we wanted to assess the long-term and not acute effects of PB125 treatment.

Deuterium oxide labeling in PET and Hartley guinea pigs

To simultaneously assess long-term rates of skeletal muscle protein, DNA, and RNA synthesis, all guinea pigs were given a subcutaneous injection of 0.9% saline enriched with 99% deuterium (^2H_2O) equivalent to 3% of their body weight 30 days prior to euthanasia [27,30]. Drinking water was enriched to 8% ^2H_2O for the purpose of maintaining ^2H_2O enrichment of the body water pool during the 30-day labelling period. At the time of euthanasia and tissue harvest, the guinea pigs were 5 mo or 15 mo.

Euthanasia and tissue collection in PET and Hartley guinea pigs

In accordance with the standards of the American Veterinary Medical Association, animals were anesthetized with a mixture of isoflurane and oxygen; thoracic cavities were opened, and blood was collected via direct cardiac puncture. Whole blood was centrifuged (1200 *g*, 4^{o}C, 15 min) to separate plasma, which was frozen at -80^{o}C until further analysis. After blood collection, the anesthetized animals were transferred to a chamber filled with carbon dioxide for euthanasia. The soleus, gastrocnemius, and tibialis anterior were trimmed of tendons and connective tissue, weighed, and flash frozen in liquid nitrogen.

Two control females, two PB125 females, one control male, and two PB125 males required humane euthanasia prior to final analysis due to underlying issues unrelated to treatment (Hartley guinea pig final n = 105). Gross necropsy findings by veterinarians did not

raise significant concern as the cause of death in these cases were consistent with what would be expected in conventionally raised guinea pigs. We did not lose any PET guinea pigs prior to euthanasia. However, the 5 mo PET male tibialis anterior samples were lost prior to analysis.

Sample preparation and analysis via Gas Chromatography-Mass Spectroscopy (GC-MS): proteins

The tibialis anterior muscle was homogenized and fractionated following established laboratory protocols [27,30,49]. Briefly, tissues (20 – 40 mg) were homogenized at 1:10 in isolation buffer (100 mM KCl, 40 mM Tris HCl, 10 mM Tris Base, 5 mM $MgCl_2$, 1 mM EDTA, 1 mM ATP, pH – 7.50) with phosphatase and protease inhibitors (HALT Thermo Scientific, Rockford, IL, USA) using a tissue homogenizer (Bullet Blender, Next Advance Inc., Averill Park, NY, USA) with zirconium beads (Next Advance Inc., Averill Park, NY, USA). After homogenization, subcellular fractions were isolated via differential centrifugation as previously described [27,30]. Once fractionated pellets were isolated and purified, 250 µl 1 M NaOH was added, and pellets were incubated for 15 min at 50 ^{o}C and 900 RPM.

Protein subfractions were hydrolyzed in 6 M HCl for 24 hours at 120 ^{o}C after which the hydrolysates were ion-exchanged, dried *in vacuo*, and then resuspended in 1 mL of MiliQ H_2O. Half of the suspension was derivatized with 500 µL acetonitrile, 50 µL 1 M K_2HPO_4, and 20 µl of pentafluorobenzyl bromide and incubated at 100 ^{o}C for 60 min. Derivatives were extracted into ethyl acetate and the organic layer was transferred into vials which were then dried under nitrogen. Samples were reconstituted in ethyl acetate (400 µL – 800 µL).

The derivative of alanine was analyzed on an Agilent 7890A GC coupled to an Agilent 5977A MS as previously described [27,30,35]. The newly synthesized fraction (f) of proteins was calculated from the true precursor enrichment (p) based upon plasma analyzed for $^{2}H_2O$ enrichment and adjusted using mass isotopomer distribution analysis [50]. Protein synthesis of each subfraction was calculated as the fraction of deuterium-labeled over unlabeled alanine proteins over the entire labeling period (30 days) and expressed as the fractional synthesis rate

(FSR). Thus, we divided fraction new by our labeling period (30 days) and multiplied by 100 to express FSR as %/day. Our isotope approach and analysis followed the established procedures detailed in this Core of Reproducibility in Physiology publication [51].

Sample preparation and analysis via GC-MS: body water

80 µL of plasma was placed into the inner well of an o-ring cap that was screwed to tube and inverted on a heating block overnight at 100°C. After incubation, 2 µL of 10 M NaOH and 20 µL of acetone were added to the samples and $^{2}H_2O$ standards (0 – 20%) and capped immediately, vortexed, and incubated at room temperature overnight. Samples were extracted with 200 µL hexane and the organic layer was transferred through pipette tips filled with anhydrous Na_2SO_4 into GC vials and analyzed via EI mode using a DB-17MS column.

Sample preparation and analysis via GC-MS: DNA

Incorporation of ^{2}H into purine deoxyribose (dR) of DNA was measured following procedures previously described with slight modifications [52–54]. DNA was isolated from tissue homogenates. Because DNA quality is not a priority, we employed a faster and more cost-effective method of isolating DNA through sonication. Briefly samples (< 5 mg of powdered tissue suspended in 200 ul of MiliQ water) were sonicated for 10 seconds 6 times allowing samples to cool on ice in between repetitions. To confirm that the fraction new of the deoxyribose derivative is similar a subset of samples was analyzed using sonication and a Qiagen DNA Kit extraction (QIAmp DNA Kit) for the tibialis anterior (Supplemental Figure B.1) $p>0.05$ indicating the methods were not different. DNA isolated from tissue was hydrolyzed with nuclease S1 and potato acid phosphatase at 37°C shaking at 150 RPM overnight. These hydrolysates were derivatized with pentafluorobenzyl hydroxylamine and acetic acid and incubated at 100 °C for 30 min. After incubation, samples were acetylated with acetic anhydride and 1-methylimidazole. Dichloromethane was added, mixed, and then extracted, dried *in vacuo*, and resuspended in ethyl acetate, and analyzed by GC/MS as previously described [52–54]. The newly synthesized fraction (f) of proteins was calculated from the true precursor enrichment

(p) based upon plasma analyzed for $^{2}H_2O$ enrichment and adjusted using mass isotopomer distribution analysis [50].

Sample preparation and analysis via GC-MS: RNA

Incorporation of ^{2}H into purine ribose (dR) of DNA was measured following procedures previously described with slight modifications [55,56]. RNA was isolated from tissue using Trizol and chloroform as previously described [56]. Samples were then hydrolyzed with nuclease S1 and potato acid phosphatase at 37°C shaking at 150 RPM overnight. These hydrolysates were derivatized with pentafluorobenzyl hydroxylamine and acetic acid and incubated at 100 °C for 30 min. After incubation, samples were acetylated with acetic anhydride and 1-methylimidazole. Dichloromethane was added, mixed, and then extracted, dried *in vacuo*, and resuspended in ethyl acetate, and analyzed by GC/MS as previously described [52–54]. The newly synthesized fraction (f) of proteins was calculated from the true precursor enrichment (p) based upon plasma analyzed for $^{2}H_2O$ enrichment and adjusted using mass isotopomer distribution analysis [50]. It has been previously reported that incorporation of deuterium into purine ribose of RNA assessed ribosome turnover as 80-85% of total RNA is ribosomal RNA and the other types, mRNA and tRNA are fully turned over within 24 hours [57,58] while labeling period in this study was 30 days.

Assessing protein synthesis related to mechanisms of proteostasis

To evaluate protein synthesis related to protein maintenance versus new cell proliferation (new DNA), we calculated the ratio of protein synthesis to DNA synthesis [59–61]. Increases in the ratio of PRO:DNA can be interpreted as a greater proportion of protein synthesis related to protein turnover to maintain the proteome and a smaller proportion of protein synthesis dedicated to proliferation [62].

Protein content

Western blotting was used to measure relative content of Nrf2, NAD(P)H dehydrogenase [quinone] 1 (NQO1), OXPHOS, eukaryotic initiation factor 2 (eIF2;) phosphorylated (Ser51) and

total), p21, cyclin D, and Phospho-histone H2A.X (Phospho-H2AX) (Ser139) in a subset of tissues. See Supplemental Table B.1 for all western blotting conditions. 50-70 mg portions of the tibialis anterior (n = 9-12 per treatment group) were powdered under liquid nitrogen and homogenized in a Bullet Blender with zirconium beads and 1.0 mL of radioimmunoprecipitation assay (RIPA) buffer (150 mM NaCl, 0.1 mM EDTA, 50 mM Tris, 0.1% sodium deoxycholate, 0.1% SDS, 1% Triton X-100, pH = 7.50) with HALT protease inhibitors. Protein concentration was determined with BCA assay (ThermoFisher 23225). Samples were reduced (50 µL of B-mercaptoethanol) and heated at 50^{o}C for 10 min (for OXPHOS) or at 95^{o}C for 5 min for all other antibodies. Approximately 20 µg of protein was loaded into a 4% - 20% Criterion pre-cast gel (Bio-Rad, Hercules, CA, USA) and resolved at 120 V for 120 min. The proteins were then transferred at 100 V for 75 min in transfer buffer (20% w/v methanol, 0.02% w/v SDS, 25 mM Tris Base, 192 mM glycine, pH 8.3). Membranes were then blocked and incubated with primary antibodies on a shaker overnight in 4^{o}C. Membranes were rinsed and then incubated with appropriate secondary antibodies. After the membranes were rinsed, Western Lightening ECL Enhanced (Perkin Elm NEL 104001EA) was applied and the membranes were subsequently imaged using a FluorChem E Chemiluminescence Imager (Protein Simple, San Diego, CA, USA). Analysis of densitometry was completed using AlphaView SA Software. Units are expressed as density of primary antibody relative to density of Ponceau S or amido black and normalized to the 5 month male control animals as previously described [30,35]. Full labeled and unedited blots are in the supplemental figures as well as total protein stains.

Statistical analysis

To compare the effect of sex and PB125 treatment on anthropometrics, isotope tracer data, and protein content a two-way ANOVA was used with Tukey post-hoc analyses. Because guinea pigs are experiencing increases in body mass from 5 to 15 mo [27,30] we also ran a two-way ANOVA with Tukey post-hoc test to assess age-related differences in skeletal muscle mass and relative skeletal muscle mass. To highlight the fiber type-dependent effects of

age/treatment, we compared the effects of age and PB125 on proteostasis in the tibialis anterior (comprised almost entirely of type II myofibers), the gastrocnemius (mixed myofiber types), and the soleus (mostly type I myofibers), by to re-analyzing data from previously published outcomes using a two-way ANOVA and Tukey post-hoc [27,30]. We used independent t-tests to compare the effect of age in PET and Hartley guinea pigs. Due to the fact we lost all the 5 mo male tibialis anterior samples, we were unable to make sex-comparisons in the PET guinea pigs. Additionally, in outcomes that had both a robust sex and treatment effects, independent t-tests were used to examine treatment effects within a sex to differentiate different mechanisms by which PB125 treatment improved mechanisms of proteostasis. Finally, we assessed if PB125 treatment could attenuate any age-related changes (from 5 to 15 mo) with a one-way ANOVA and Tukey post-doc as previously described [30]. ROUT outlier tests were performed on all data sets and identified outliers were removed. We set statistical significance a priori at $p<0.05$ but also report trends at $p<0.10$. Data are presented as mean +/- SD. All statistics were performed in Prism 9.0 (La Jolla, California, USA).

RESULTS

Hartley guinea pigs as a model of myofiber remodeling: Further explorations

Previously we reported significant decreases in rates of protein synthesis in the gastrocnemius and soleus from 5 to 15 mo of age in Hartley guinea pigs [27]. Similarly, there were significant declines in rates of myofibrillar and mitochondrial protein synthesis in the tibialis anterior (Figure B.2A-B). To identify if another guinea pig strain less prone to joint degeneration had similar decreases in rates of skeletal muscle protein synthesis over the same age range, we cross-sectionally examined rates of tibialis anterior and gastrocnemius protein synthesis at 5 and 15 mo in the outbred PET (control) strain of guinea pig. Similar to the Hartleys (Figures B.2A and B), PET guinea pigs had significantly slower rates of tibialis anterior myofibrillar (Figure B.2C) and mitochondrial (Figure B.2D) protein synthesis at 15 compared to 5 mo. Reproducing our prior findings, Hartley guinea pigs had significant decreases rates of

gastrocnemius myofibrillar (Figure B.3A) and mitochondrial (Figure B.3B) protein synthesis from 5 to 15 mo of age. However, in PETs, gastrocnemius myofibrillar (Figure B.3C) and mitochondrial (Figure B.3D) protein synthesis rates were maintained from 5 to 15 mo of age. Taken together, we again confirm that the Hartley guinea pig is a feasible model to examine age-related myofibrillar remodeling. The PET guinea pig may serve as a valuable control in future studies in that mixed myofibers (e.g., the gastrocnemius) did not show age-related myofiber remodeling over the age-range during which Hartleys begin to develop a phenotype mimicking muscle aging in humans. Therefore, this preclinical intervention focused on long-term PB125 treatment to slow the progression of myofiber remodeling in the tibialis anterior of Hartley guinea pigs.

Anthropometrics of PB125 intervention

There was no effect of PB125 treatment on body mass (Figure 3.2A), tibialis anterior muscle mass, (Figure 3.2B), or relative tibialis anterior muscle mass (Figure 3.2C). However, there was an overall effect of sex, with male guinea pigs being larger than females (Figure 3.2A). Because we have previously reported that Hartley guinea pigs are still experiencing increases in body mass from 5 to 15 months [30], we also looked at the effect of age on muscle mass. Specifically, there was an age-related increase in tibialis anterior mass (Figure B.4A); however, a trend ($p = 0.0503$) for an age-related decrease in relative tibialis anterior skeletal muscle mass (Figure B.4B) which is similar to what we observed in the gastrocnemius, but not the soleus from 5 to 15 mo [30], suggesting again that type II myofibers are more susceptible to remodeling.

Allocation of newly synthesized proteins toward proteostatic maintenance after long term PB125 treatment

Deuterium labeling of free amino acids including alanine, and incorporation of the labeled amino acids into proteins, is a validated method allowing for long term, dynamic and simultaneous monitoring of rates of newly synthesized proteins, RNA, and DNA [63]. We aimed

to determine if 10 mo of daily PB125 treatment slowed the progression of skeletal muscle decline in Hartley guinea pigs. Rates of protein synthesis were maintained with PB125 treatment in the myofibrillar (Figure 3.3A), mitochondrial (Figure 3.3B), cytosolic (Figure 3.3C), and collagen (Figure 3.3D) fractions. We also semi-quantitatively analyzed OXPHOS proteins and confirmed there were no differences with PB125 treatment in mitochondrial protein content, supporting the isotope data (Figures B.5 (quantified), B.10 (unedited blot) and B.11 (total protein)). However, PB125 treated male guinea pigs had a significant increase in rates of ribosomal biogenesis while female guinea pigs had no difference (Figure 3.4A). Interestingly, there was significant decrease in rates of DNA synthesis in PB125 treated guinea pigs which was primarily driven by females (Figure 3.4B).

It is important to consider changes in protein synthesis relative to cellular proliferation [62]. Thus, when expressing the rates of protein to DNA synthesis as a ratio, two interesting findings emerged. First, there was an overall effect of sex in the tibialis anterior, in that control-treated female guinea pigs had a lower ratio of protein to DNA synthesis rates compared to males in all four subcellular fractions (Figure 3.5A-D). Second, there was an overall effect of 10 mo of PB125 treatment in the tibialis anterior to increase the ratio of protein to DNA synthesis rates which was primarily driven by the females in the myofibrillar (Figure 3.5A), mitochondrial (Figure 3.5B), cytosolic (Figure 3.5C), and collagen (Figure 3.5D) fractions. Because we had previously analyzed the gastrocnemius, a mixed myofiber type muscle, and the soleus, a muscle with mostly type I myofibers [30], we re-analyzed those data to examine the muscle specificity of PB125 treatment by expressing protein to DNA synthesis rates as a ratio. We found that there were no effects of 10 mo of PB125 on mechanisms of proteostasis in any subcellular fraction of the gastrocnemius or soleus (Figure 3.5E-L). Taken together, our data show that 10 mo of PB125 treatment suppresses rates of DNA synthesis while maintaining rates of protein synthesis to ultimately increases mechanisms of proteostasis in the tibialis anterior.

However, this effect is primarily observed in female guinea pigs and only in the tibialis anterior, a muscle composed of type II myofibers and susceptible to age-related remodeling [31,41,44].

PB125 does not alter Nrf2 accumulation in the tibialis anterior

The phytochemical compound, PB125, composed of carnosol, luteolin, and withaferin A, is a purported Nrf2 activator and we previously confirmed that these active ingredients are detectable in the blood of treated Hartleys [30]. To discern if Nrf2 activation contributed to the improved mechanisms of proteostasis, we probed for Nrf2 protein content in the tibialis anterior. There was no effect of treatment on Nrf2 protein content (Figures B.6A (quantified), B.12 (unedited blot), B.13 (total protein)) or NQO1, an antioxidant transcriptionally regulated by Nrf2 activation (Figures B.6B (quantified), B.14 (unedited blot), B.15 (total protein)). In other studies by our group (Chapter 2 of this dissertation published as [35]) and others [43], there was also no differences in Nrf2 protein content following treatments known to activate Nrf2. The half-life of Nrf2 is 20 minutes [64], making it challenging to assess activation. Finally, this parent project was designed to capture long-term PB125 treatment effects and not acute changes in Nrf2 protein content, lending to the fact guinea pigs were not dosed with PB125 the morning of euthanasia.

PB125 does not alter cell cycle regulation

Because there was a robust effect of PB125 treatment on decreasing rates of DNA synthesis, we examined a pathway that regulates cell cycle progression. Specifically, Nrf2 can bind to protein kinase RNA-like ER kinase (PERK) which in increases the phosphorylation of eIF2 subsequently decreasing cyclin D leading to cell cycle arrest [65]. There was an overall effect of PB125 treatment to decrease phosphorylated eIF2 with PB125 treatment (Figures B.7A (quantified), B.16 (unedited blot), B.18 (total protein)), but no differences in total eIF2 (Figures B.7B (quantified), B.17 (unedited blot), B.18 (total protein)) or the ratio of phosphorylated to total eIF2 (Figure B.7C (quantified)), collectively suggesting that eIF2 activation did not change. There was a significant sex by treatment interaction for cyclin D protein content, wherein cyclin

D was higher in males but lower in females (Figures B.9B (quantified), B.19 (unedited blot), B.20 (total protein)). However, when cyclin D was analyzed within a sex there were no treatment differences (data not shown). Taken together, it appears that these regulators of the cell cycle were not affected by PB125 treatment.

PB125 may alter skeletal muscle cellular senescence

Nrf2 is also known to interact with p21, a marker of skeletal muscle cellular senescence [65]. We observed an overall effect of sex, with females having lower p21 content compared to males (Figures B.8A (quantified), B.21 (unedited blot), B.22 (total protein)). There was also an overall effect of treatment to decrease phospho-H2AX protein content, a marker of senescence associated DNA damage (Figures B.9B (quantified), B.23 (unedited blot), B.24 (total protein)). One interesting finding was that p21, cyclin D, and phospho-H2AX, appear at three times the predicted molecular weight in the guinea pig species (Figures S.19 (p21), B.21 (cyclin D), and B.23 (phospho-H2AX)). To ensure proper western blotting methods, we ran guinea pig and mouse samples on the same gel/membrane and probed for p21 and cyclin D (Figure B.25). We found there was one single band for the guinea pig but two bands for the mouse. While we cannot be certain, we speculate that the band detected in guinea pig using these antibodies might be homotrimers. Collectively, it appears that there were divergent treatment effects on markers of cellular senescence and senescence associated DNA damage in male versus female guinea pigs.

To confirm the divergence in PB125 treatment effects on measures of cellular senescence in male and female Hartley guinea pigs, we analyzed the PB125 effects within each sex. Interestingly, there was no effect of 10 mo PB125 treatment on p21 (Figure 3.6A) or phospho-H2AX (Figure 3.6B) protein content in male guinea pigs. Furthermore, there were no PB125 treatment effects on rates of DNA synthesis (Figure 3.6C) or mechanisms of myofibrillar proteostasis in male guinea pigs (Figure 3.6D). The lack of a difference in mechanisms of proteostasis persisted in the mitochondrial fraction (Figure B.9A) and the cytosolic fraction

(Figure B.9B) in male Hartley guinea pigs. The findings in male Hartley guinea pigs contrasted with female Hartley guinea pigs. Specifically, PB125 treated female Hartley guinea pigs had lower p21 content ($p = 0.0580$) (Figure 3.6E), significantly lower phospho-H2AX (Figure 3.6F), and significantly lower rates of DNA synthesis (Figure 3.6G). These changes may have driven the significant increase in the ratio of myofibrillar protein to DNA synthesis rates (Figure 3.6H) which also occurred in the mitochondrial fraction (Figure S.3.9D), cytosolic fraction (Figure 3.9E), and collagen fraction (Figure 3.9F) in female Hartley guinea pigs. Collectively, these findings suggest that long term 10 mo PB125 treatment had the most robust effects in female guinea pigs.

Our final analysis was to discern if 10 mo of PB125 treatment attenuated any age-related effects on indirect markers of cellular senescence, associated damage, and mechanisms of proteostasis. In males Hartley guinea pigs, there were age-related increases in p21 and phospho-H2AX indicating increased markers of cellular senescence and DNA damage. However, the phospho-H2AX was attenuated with 10 mo PB125 treatment in male guinea pigs (Figure 3.7B). Male guinea pigs also had a significant decrease in rates of DNA synthesis with age that was altered with 10 mo of PB125 treatment (Figure 3.7C). There were no effects on mechanisms of myofibrillar proteostasis with age or treatment in male guinea pigs (Figure 3.7D). In female Hartley guinea pigs 10 mo of PB125 treatment attenuated the age-related increase in p21 (Figure 3.7E) and phospho-H2AX (Figure 3.7F). Additionally, PB125 decreased rates of DNA synthesis in the 10 mo treated guinea pigs (Figure 3.7G) and increased mechanisms of myofibrillar proteostasis (Figure 3.7H) compared to the age-matched controls. Taken together, our data suggest that 10 mo of PB125 treatment in female guinea pigs increased mechanisms of proteostasis through decreased cellular senescence and decreased senescence associate DNA damage, allowing lower rates of DNA turnover to ultimately increasing allocation of newly synthesized muscle proteins for proteostatic maintenance.

DISCUSSION

Skeletal muscle aging in humans is multifaceted. For example, the age-related loss of skeletal muscle mass and function is driven by mitochondrial dysfunction, loss of proteostasis, and increases in cellular senescence [66]. However, we lack effective treatments for sarcopenia in humans. One potential reason why treatments succeed in laboratory animal models [67] but fail in human clinical trials [68] is there are differences in skeletal muscle age-related changes between rodents [69] and humans [12]. To circumvent this issue our group has been using the Hartley guinea pig as a model of musculoskeletal aging, which encompasses myofiber remodeling [27] and other multimorbidities associated with older age [70,71]. In the present study, we further characterized myofiber remodeling in Hartleys and used this model to evaluate the efficacy of a treatment for slowing the progression of myofiber remodeling in a muscle comprised of type II myofibers, the tibialis anterior. Our long-term 10-month preclinical intervention was a daily treatment with PB125, a purported Nrf2 activator. The current study builds on a growing body of knowledge about the promise of this PB125 intervention for improving skeletal muscle health in a muscle with type I myofibers [30] and in bones, using the Hartley model [72]. Our key findings from the present study were that: 1. age-related declines in skeletal muscle protein synthesis were more prominent in the Hartley guinea pig strain comparted to the PET guinea pig strain; 2. PB125 improved mechanisms of proteostasis in a sex and muscle specific manner; 3. Decreases in tibialis anterior cellular senescence may have been the mechanism by which PB125 increased mechanisms of proteostasis in females.

Key finding #1: Age-related declines in skeletal muscle protein synthesis were more prominent in the Hartley guinea pig strain comparted to the PET guinea pig strain

When our group initially characterized the musculoskeletal decline of Hartley guinea pigs, we compared them to an inbred strain of guinea pig, the Strain 13. However, Strain 13 animals are not commercially available, which left us in search of a new control strain and one that also circumvented the limitations of the Strain 13 [see [27]. We identified the PET outbred

strain of guinea pig, which might be a superior control strain to the Hartley guinea pigs (discussed in more detail in chapters 4 and 5) [73]; however, we had yet to characterize its skeletal muscle myofiber remodeling.

In the present study we observed two interesting findings. The first was that compared to PET guinea pigs, Hartley guinea pigs have decreases in rates of gastrocnemius protein synthesis from 5 to 15 mo of age (Figure B.3). Second, both PET and Hartley guinea pigs have decreases in rates of tibialis anterior protein synthesis from 5 to 15 mo (Figure B.2), highlighting that type II myofibers exhibit a greater degree of myofiber remodeling with age. Future studies should focus on other characteristics of myofiber remodeling (e.g., cross-sectional area, myofiber size distribution, collagen accumulation, and force production) between PET and Hartley guinea pigs. After verifying the aging phenotype, we leveraged the Hartleys to test the preclinical intervention of long-term PB125 treatment improving mechanisms of proteostasis in the tibialis anterior, the focus for the rest of this discussion.

Key finding #2: PB125 improved mechanisms of proteostasis in a muscle specific manner

Our first publication established the efficacy of PB125 for improving mitochondrial respiration and protein synthesis in the soleus, a muscle comprised of type I myofibers [30]. In that study, we also examined rates of protein synthesis in the gastrocnemius, a mixed myofiber type muscle. In a Journal Club Commentary article about our publication, the authors posed the question of how PB125 might improve mechanisms of proteostasis in a strictly type II myofiber muscle, more susceptible to age-related decline [74]. Here, we observed that PB125 improved mechanisms of proteostasis in all four subcellular fractions (Figure 3.5A-D) in the tibialis anterior. However, when we reanalyzed gastrocnemius (Figure 3.5E-H) and soleus (Figure 3.5 I-L) expressing rates of protein synthesis relative to cellular proliferation (DNA synthesis) from our prior publication [30], there were no differences in mechanisms of proteostasis.

While it may seem surprising that specific skeletal muscles responded so differently to PB125 treatment, a purported Nrf2, we are not the first to observe this finding. Specifically,

Wang and colleagues found that exercise training, a stress also capable of activating Nrf2, resulted in increased Nrf2 activation and expression of downstream targets in the rectus femoris [43], a muscle comprised of mixed myofiber types [75]. However, there was no evidence of Nrf2 activation in the oxidative soleus muscle [43]. Additionally, we postulate that a "stress" must be imposed for purported Nrf2 activators to result in the most robust benefits. Specifically, we refer to stress in this context as a state where an organism is exhibiting challenges to homeostasis that consequently could confer positive adaptative homeostatic benefits (e.g., exercise training) [42] or negative adaptative homeostatic benefits (e.g., accelerated muscle aging/disease) [76–78]. From the study by Wang and colleagues, the stress of running (their exercise intervention) activates different muscles that could have resulted in varying degrees of Nrf2 activation [43]. Specifically, when running, the quadriceps work at a larger percentage of their maximal voluntary contraction compared to the soleus [79]. Further, prior work from our lab showed that PB125 treatment in healthy middle-aged (10-15 mo) mice did not influence protein turnover or downstream targets of Nrf2, leading us to conclude that the beneficial PB125 outcomes are observed only when a stress such as an age-related stress is posed [80,81]. Collectively, this suggests that the positive effects we observed on mechanisms of proteostasis in tibialis anterior were likely due, at least in part, to the fact this muscle is more susceptible to age-related declines compared to the gastrocnemius and soleus in Hartleys and humans [82].

Key finding #3: Decreases in tibialis anterior cellular senescence might be explain how PB125 increased mechanisms of proteostasis in females but not males

Because we observed that PB125 suppressed rates of tibialis anterior DNA synthesis (Figure 3.4B) while maintaining rates of protein synthesis (Figure 3.3), we concluded that treatment improved mechanisms of proteostasis (Figure 3.5A-D). The ratio of protein to DNA synthesis rates captures trade-offs [62] between protein synthesis to meet the requirements of new cell proliferation versus greater allocation of new proteins for somatic maintenance. We have observed higher ratios of protein to DNA synthesis rates associated with healthspan

extending interventions [62]. Here, we sought to understand potential mechanism(s) that influence this trade-off. Because PB125 altered rates of DNA synthesis, we sought to interrogate markers of cellular senescence.

We choose to assess semi-quantitative measures of cellular senescence with western blotting by probing for p21 and phospho-H2AX, which were recommended in a recent perspective on skeletal muscle cellular senescence [18]. Further, p21 in myofibers is the most prominent hallmark of skeletal muscle senescence [20] and has been shown to be altered with treatment of senolytics in the tibialis anterior [83]. Interestingly we observed that from 5 to 15 mo of age both p21 and phospho-H2AX increased in male (Figure 3.7A and B) and female (Figure 3.7 E and F) Hartleys, potentially confirming the presence of myofiber senescence in this unique model of musculoskeletal decline. Further, in both males and females the age-related increase in phospho-H2AX (Figure 3.7 B and F) but not p21 (Figure 3.7 A and E) was attenuated with 10 mo of PB125 treatment. In females treated with PB125 we believe that the decreases in cellular senescence may explain the decreased rates of DNA synthesis (Figure 3.7G) with treatment and thus increased mechanisms of proteostasis with increased ratios of protein to DNA synthesis rates (Figure 3.7H and Figures B.9 D-F). However, when the males were analyzed separated from females there was no effect of PB125 treatment for increasing mechanisms of proteostasis (Figure 3.7D and Figures B.9A and B).

It is important to note the unique nature of skeletal muscle DNA synthesis rates. For example, only about 10% of DNA synthesis includes myonuclei replication and therefore the remaining 90% of DNA turnover from skeletal muscle includes other cell types such as pericytes, endothelial cells, fibroblasts, satellite cells, and immune cells [19]. Thus, in a skeletal muscle tissue homogenate, where there are many cell types it is difficult to discern which cell types drove the decreased rates of DNA replication with PB125 treatment because of the measured synthesis of the homogenate is the culmination of turnover rates and abundance of all cells. We speculate that the perceived decrease in DNA synthesis rates were driven by a

decrease in the proliferation of inflammatory cells within PB125 treated skeletal muscle of female guinea pigs. In support of this idea, we observed lower phospho-H2AX, a measure of senescence associated DNA damage in these same tissues. While the current data provide some insight about why mechanisms of proteostasis were improved in female Hartley guinea pigs, future studies should try to discern the mechanism(s) by which rates of DNA synthesis increased in female Hartley guinea pigs with age. Further, future research ought to specifically interrogate the senescent status of the cell type subsets in skeletal muscle. Collectively, these findings suggest that long term 10 mo PB125 treatment had the most robust effects in female guinea pigs.

Limitations

It is important to note that, because knee osteoarthritis and myofiber remodeling was progressing from 5 to 15 mo of age in these animals [27], we cannot discern the effect of age itself from disease progression. Additionally, Hartleys are still experiencing long bone and soft tissue growth until ~10 mo [84], potentially influencing changes observed during treatment from 5 to 15 mo of age. Additionally, sarcopenia is defined as the age-related loss of skeletal muscle mass and function [85]. However, due to study constraints we did not assess measures of muscle function such as *ex vivo* force production. We have reported that PB125 improved metrics of mobility [30], but we cannot extrapolate the findings of the current study to skeletal muscle function.

Conclusions and future directions

These data contribute to the greater body of work from our group that the Hartley guinea pig is a valuable model mimicking multimorbidities of human aging, including musculoskeletal decline and brain aging (to be supported in Chapters 4 and 5). Further, the current study supports that PB125 might improve mechanisms of proteostasis in muscles most susceptible to age-related changes. Future studies should examine why the observed muscle specific differences occurred to hopefully translate PB125 into human clinical trials.

FIGURES

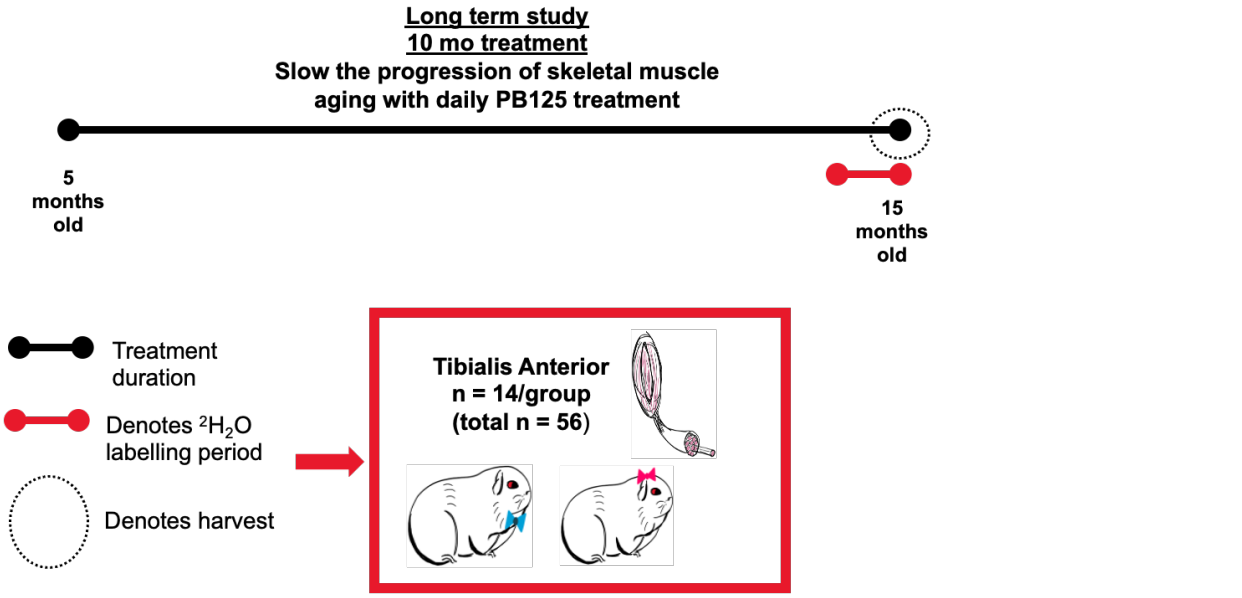

Figure 3.1. Study design. Male (n = 14/group) and Female (n = 14/group) Hartley guinea pigs were either treated with PB125 or a vehicle control for 10 mo (from 5 to 15 mo) to slow the progression of skeletal muscle aging (black line). During the final month of treatment (red line line) guinea pigs were labeled with deuterium oxide (^2H_2O) to assess long-term rates of protein, RNA, and DNA synthesis. Guinea pigs were sacrificed at 15 mo of age and plasma, tibialis anterior, gastrocnemius, and soleus samples were collected for analysis. We also sacrificed 5 mo male and female animals to examine the age-related changes from 5 to 15 mo independent of treatment (n=14/group).

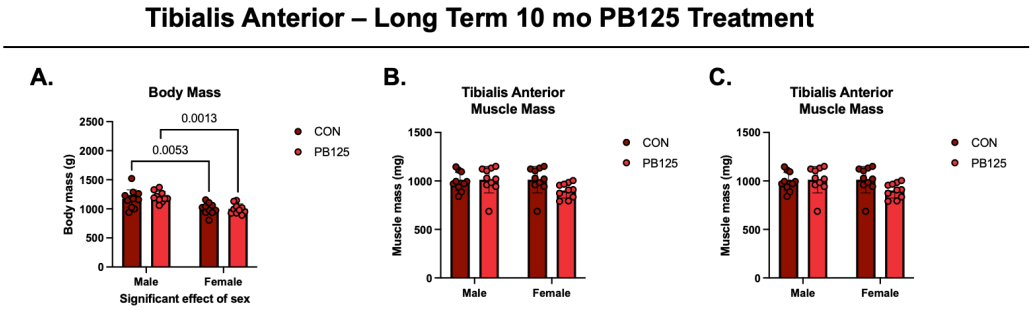

Figure 3.2. Long-term 10 mo PB125 treatment does not affect body mass or skeletal muscle mass. There was an overall effect for of sex for body mass that male Hartley guinea pigs were larger than female guinea pigs (A). However, there was no effect of treatment on body mass (A), tibialis anterior muscle mass (B), or relative tibialis anterior muscle mass (C).

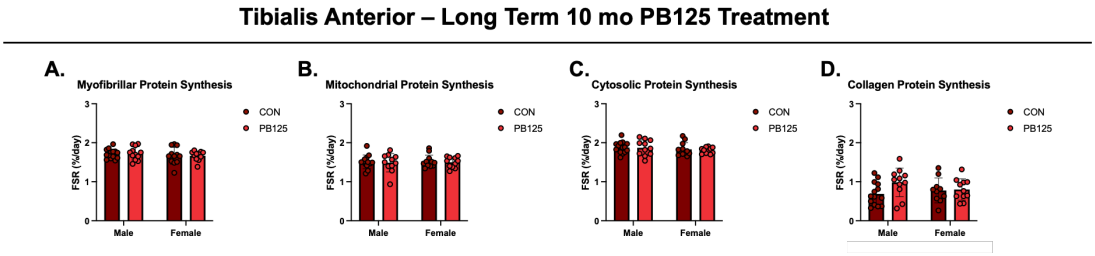

Figure 3.3. Long-term 10 mo PB125 treatment maintains rates of tibialis anterior protein synthesis. Rates of myofibrillar (A), mitochondrial (B), cytosolic (C), and collagen (D) protein synthesis were maintained with 10 mo of daily PB125 treatment.

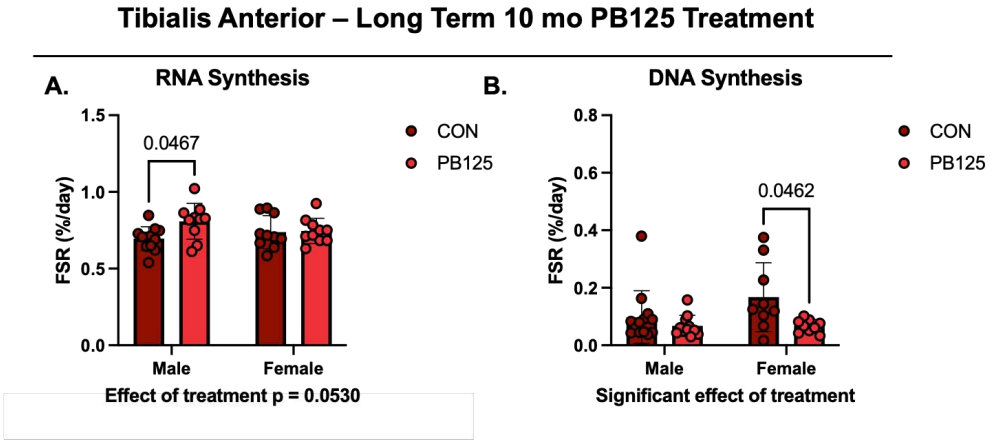

Figure 3.4. Long-term 10 mo PB125 treatment increases ribosomal biogenesis and decreased rates of DNA synthesis in a sex-specific manner. Because 85% of total RNA is ribosomal RNA it has been previously described that labeling with deuterium oxide capture changes in ribosomal biogenesis with a given treatment intervention. PB125 treated guinea pigs had a trend ($p = 0.0530$) to increase ribosomal biogenesis and it appears this effect was driven by the male Hartley guinea pigs (A). Conversely, 10 mo of PB125 treatment significantly decreased rates of DNA synthesis where the effect was primarily driven in the female Hartley guinea pigs (B).

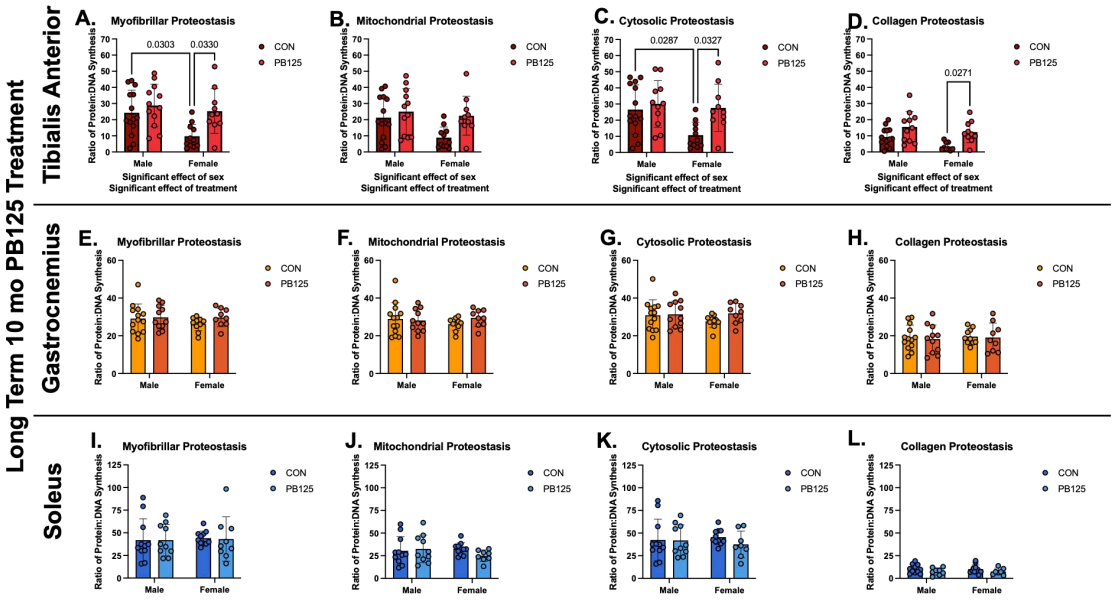

Figure 3.5. Long-term 10 mo PB125 treatment increases mechanisms of proteostasis in a muscle-specific manner. We have previously highlighted the importance of considering protein synthesis rates relative to cellular proliferation when interpreting mechanisms of proteostatic maintenance [62]. Therefore, we expressed rates of protein synthesis relative to DNA synthesis as a ratio. Additionally, we re-analyzed previously published data in the gastrocnemius and soleus from these same guinea pigs [30], to compare responses to treatment with a Nrf2 activator between muscles of different fiber types [43]. We found that PB125 increased the ratio of protein to DNA synthesis rates in the tibialis anterior myofibrillar (A), mitochondrial (B), cytosolic (C), and collagen (D) fractions suggesting that allocation of newly synthesized proteins was likely for proteome maintenance. Additionally, in the tibialis anterior there was an overall effect of sex that male Hartley guinea pigs had higher ratios of protein to DNA synthesis rates compared to female Hartley guinea pigs in all fractions (A-D). Specifically, it appears that PB125 treatment rescued the sex-effect between male and female Hartley guinea pigs ultimately driving the overall treatment effect in all fractions as the Tukey multiple comparison was significant in the female Hartley guinea pigs but not the male for the myofibrillar (A), cytosolic (C), and collagen (D) fractions. Conversely, there were no effects of PB125 treatment or sex in all fractions of the gastrocnemius or soleus (E – L).

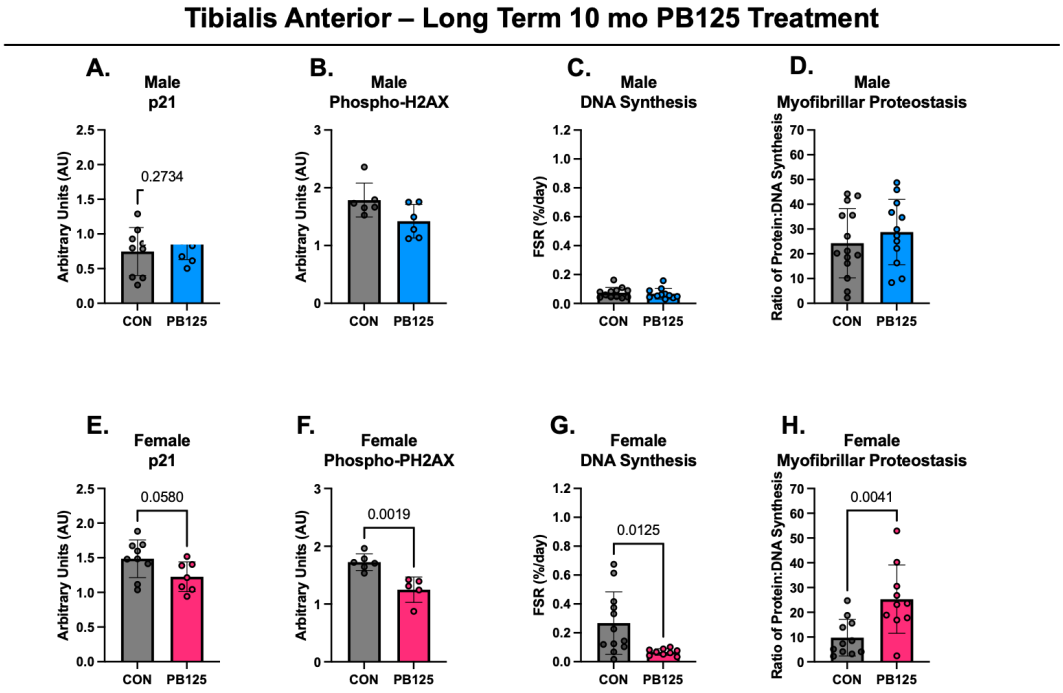

Figure 3.6. Long-term 10 mo PB125 decreases markers of skeletal muscle cellular senescence and senescence-associated DNA damage in in female but not male Hartley guinea pigs. There was no effect of PB125 treatment in male Hartley guinea pigs on p21 protein content (A), phospho-H2AX protein content (B), rates of DNA synthesis (C), or mechanisms of myofibrillar proteostasis (D) in the tibialis anterior. Conversely, 10 mo of PB125 treatment trended to decrease (p = 0.0580) p21 protein content (E), significantly decreased phospho-H2AX protein content (F), significantly decreased rates of DNA synthesis (G), and significantly increased mechanisms of myofibrillar proteostasis (H) in the tibialis anterior.

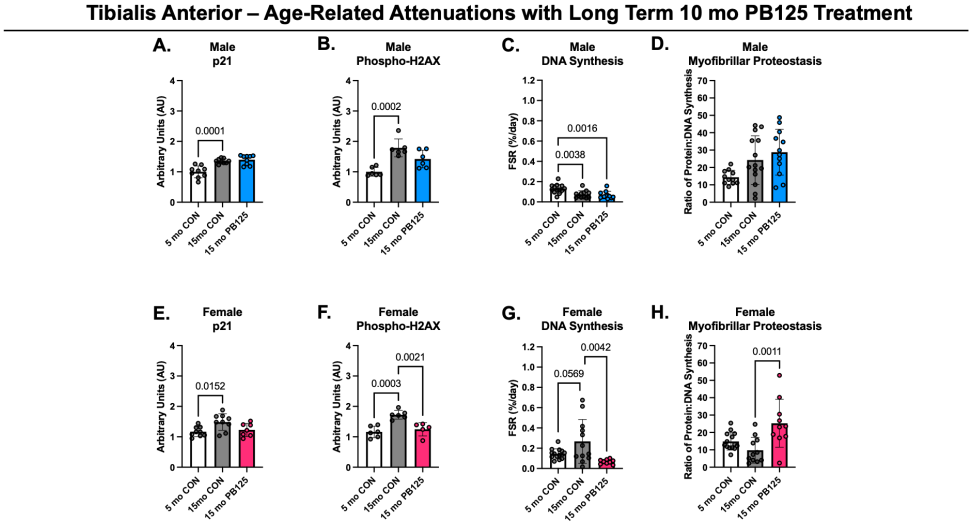

Figure 3.7. Long-term 10 mo PB125 attenuates the age-related increase markers of cellular senescence in Hartley guinea pigs. From 5 to 15 mo p21 increases in both males (A) and females (D) but this increase was attenuated with 10 mo of PB125 treatment in both sexes. Additionally, from 5 to 15 mo phospho-H2AX increases in both males (B) and females (F) but this increase is attenuated with 10 mo of PB125 treatment in both sexes. Rates of tibialis anterior DNA synthesis significantly decreased from 5 to 15 mo in male Hartley guinea pigs and such change was further decreased by PB125 treatment (C). Conversely, rates of tibialis anterior DNA synthesis in female Hartley guinea trended to increase ($p = 0.0569$) from 5 to 15 mo but significantly decreased with PB125 treatment (G). Finally, there were no differences in mechanisms of myofibrillar proteostasis in male Hartley guinea pigs (D) but there was a significant increase in mechanisms of myofibrillar proteostasis in female Hartley guinea pigs treated with PB125 compared to 15 mo control animals (H). Collectively, these findings suggest that long term 10 mo PB125 treatment had the most robust effects in female guinea pigs.

REFERENCES

1. Chen N, Fong DYT, Wong JYH. Health and Economic Outcomes Associated With Musculoskeletal Disorders Attributable to High Body Mass Index in 192 Countries and Territories in 2019. JAMA Netw Open. 2023;6(1):e2250674. doi:10.1001/jamanetworkopen.2022.50674

2. Azzolino D, Spolidoro GCI, Saporiti E, Luchetti C, Agostoni C, Cesari M. Musculoskeletal Changes Across the Lifespan: Nutrition and the Life-Course Approach to Prevention. Front Med. 2021;8:697954. doi:10.3389/fmed.2021.697954

3. Gregson CL, Armstrong DJ, Bowden J, et al. UK clinical guideline for the prevention and treatment of osteoporosis. Arch Osteoporos. 2022;17(1):58. doi:10.1007/s11657-022-01061-5

4. Palazzo C, Nguyen C, Lefevre-Colau MM, Rannou F, Poiraudeau S. Risk factors and burden of osteoarthritis. Ann Phys Rehabilitation Med. 2016;59(3):134-138. doi:10.1016/j.rehab.2016.01.006

5. Fuggle N, Shaw S, Dennison E, Cooper C. Sarcopenia. Best Pract Res Clin Rheumatology. 2017;31(2):218-242. doi:10.1016/j.berh.2017.11.007

6. Kemmler W, Teschler M, Goisser S, et al. Prevalence of sarcopenia in Germany and the corresponding effect of osteoarthritis in females 70 years and older living in the community: results of the FORMoSA study. Clin Interv Aging. 2015;10:1565. doi:10.2147/cia.s89585

7. Lee SY, Ro HJ, Chung SG, Kang SH, Seo KM, Kim DK. Low Skeletal Muscle Mass in the Lower Limbs Is Independently Associated to Knee Osteoarthritis. Plos One. 2016;11(11):e0166385. doi:10.1371/journal.pone.0166385

8. Goates S, Du K, Arensberg MB, Gaillard T, Guralnik J, Pereira SL. Economic Impact of Hospitalizations in US Adults with Sarcopenia. J Frailty Aging. Published online 2019:1-8. doi:10.14283/jfa.2019.10

9. López-Otín C, Blasco MA, Partridge L, Serrano M, Kroemer and G. Hallmarks of aging: An expanding universe. Cell. Published online 2023. doi:10.1016/j.cell.2022.11.001

10. Tian Q, Mitchell BA, Zampino M, Fishbein KW, Spencer RG, Ferrucci L. Muscle mitochondrial energetics predicts mobility decline in well-functioning older adults: The baltimore longitudinal study of aging. Aging Cell. Published online 2022:e13552. doi:10.1111/acel.13552

11. Ferrucci L, Cooper R, Shardell M, Simonsick EM, Schrack JA, Kuh D. Age-Related Change in Mobility: Perspectives From Life Course Epidemiology and Geroscience. J Gerontol: Ser A. 2016;71(9):1184-1194. doi:10.1093/gerona/glw043

12. Suetta C, Haddock B, Alcazar J, et al. The Copenhagen Sarcopenia Study: lean mass, strength, power, and physical function in a Danish cohort aged 20–93 years. J Cachexia Sarcopenia Muscle. Published online 2019. doi:10.1002/jcsm.12477

13. Balch WE, Morimoto RI, Dillin A, Kelly JW. Adapting Proteostasis for Disease Intervention. Science. 2008;319(5865):916-919. doi:10.1126/science.1141448

14. Jang YC, Lustgarten MS, Liu Y, et al. Increased superoxide in vivo accelerates age-associated muscle atrophy through mitochondrial dysfunction and neuromuscular junction degeneration. Faseb J Official Publ Fed Am Soc Exp Biology. 2009;24(5):1376-1390. doi:10.1096/fj.09-146308

15. Muller FL, Song W, Liu Y, et al. Absence of CuZn superoxide dismutase leads to elevated oxidative stress and acceleration of age-dependent skeletal muscle atrophy. Free Radic Biol Med. 2006;40(11):1993-2004. doi:10.1016/j.freeradbiomed.2006.01.036

16. Ahn B, Ranjit R, Kneis P, et al. Scavenging mitochondrial hydrogen peroxide by peroxiredoxin 3 overexpression attenuates contractile dysfunction and muscle atrophy in a murine model of accelerated sarcopenia. Aging Cell. Published online 2022:e13569. doi:10.1111/acel.13569

17. Xiang Y, You Z, Huang X, et al. Oxidative stress-induced premature senescence and aggravated denervated skeletal muscular atrophy by regulating progerin–p53 interaction. Skelet Muscle. 2022;12(1):19. doi:10.1186/s13395-022-00302-y

18. Dungan CM, Wells JM, Murach KA. The life and times of cellular senescence in skeletal muscle: friend or foe for homeostasis and adaptation? Am J Physiol-Cell Physiol. 2023;325(1):C324-C331. doi:10.1152/ajpcell.00553.2022

19. Borowik AK, Davidyan A, Peelor FF, et al. Skeletal muscle nuclei in mice are not post-mitotic. Funct. Published online 2022. doi:10.1093/function/zqac059

20. Zhang X, Habiballa L, Aversa Z, et al. Characterization of cellular senescence in aging skeletal muscle. Nat Aging. Published online 2022:1-15. doi:10.1038/C3587-022-00250-8

21. Coen PM, Musci RV, Hinkley JM, Miller BF. Mitochondria as a Target for Mitigating Sarcopenia. Front Physiol. 2019;9:1883. doi:10.3389/fphys.2018.01883

22. Musci RV, Hamilton KL, Miller BF. Targeting mitochondrial function and proteostasis to mitigate dynapenia. Eur J Appl Physiol. 2018;118(1):1-9. doi:10.1007/s00421-017-3730-x

23. Lo JH tung, U KP, Yiu T, Ong MT yun, Lee WY wai. Sarcopenia: Current treatments and new regenerative therapeutic approaches. J Orthop Transl. 2020;23:38-52. doi:10.1016/j.jot.2020.04.002

24. Wang J, Mogensen AMG, Thybo F, et al. Low-load blood flow-restricted resistance exercise produces fiber type-independent hypertrophy and improves muscle functional capacity in older individuals. J Appl Physiol. 2023;134(4):1047-1062. doi:10.1152/japplphysiol.00789.2022

25. Fairfield WD, Minton DM, Elliehausen CJ, et al. Small-Scale Randomized Controlled Trial to Explore the Impact of β-Hydroxy-β-Methylbutyrate Plus Vitamin D3 on Skeletal Muscle Health in Middle Aged Women. Nutrients. 2022;14(21):4674. doi:10.3390/nu14214674

26. Crombie IK, Irvine L, Williams B, et al. Why older people do not participate in leisure time physical activity: a survey of activity levels, beliefs and deterrents. Age Ageing. 2004;33(3):287-292. doi:10.1093/ageing/afh089

27. Musci RV, Walsh MA, Konopka AR, et al. The Dunkin Hartley Guinea Pig Is a Model of Primary Osteoarthritis That Also Exhibits Early Onset Myofiber Remodeling That Resembles Human Musculoskeletal Aging. Front Physiol. 2020;11:571372. doi:10.3389/fphys.2020.571372

28. Jimenez PA, Glasson SS, Trubetskoy OV, Haimes HB. Spontaneous osteoarthritis in Dunkin Hartley guinea pigs: histologic, radiologic, and biochemical changes. Lab Anim Sci. 1997;47(6):598-601.

29. Santangelo KS, Kaeding AC, Baker SA, Bertone AL. Quantitative Gait Analysis Detects Significant Differences in Movement between Osteoarthritic and Nonosteoarthritic Guinea Pig Strains before and after Treatment with Flunixin Meglumine. Arthritis. 2014;2014:503519. doi:10.1155/2014/503519

30. Musci RV, Andrie KM, Walsh MA, et al. Phytochemical compound PB125 attenuates skeletal muscle mitochondrial dysfunction and impaired proteostasis in a model of musculoskeletal decline. J Physiology. Published online 2022. doi:10.1113/jp282273

31. Spendiff S, Vuda M, Gouspillou G, et al. Denervation drives mitochondrial dysfunction in skeletal muscle of octogenarians. J Physiology. 2016;594(24):7361-7379. doi:10.1113/jp272487
32. Scott D, Trbojevic T, Skinner E, et al. Associations of calf inter- and intra-muscular adipose tissue with cardiometabolic health and physical function in community-dwelling older adults. J Musculoskel Neuron. 2015;15(4):350-357.

33. Visser M, Goodpaster BH, Kritchevsky SB, et al. Muscle Mass, Muscle Strength, and Muscle Fat Infiltration as Predictors of Incident Mobility Limitations in Well-Functioning Older Persons. Journals Gerontology Ser. 2005;60(3):324-333. doi:10.1093/gerona/60.3.324

34. Gonzalez-Freire M, Scalzo P, D'Agostino J, et al. Skeletal muscle ex vivo mitochondrial respiration parallels decline in vivo oxidative capacity, cardiorespiratory fitness, and muscle strength: The Baltimore Longitudinal Study of Aging. Aging Cell. 2018;17(2):e12725. doi:10.1111/acel.12725

35. Walsh MA, Zhang Q, Musci RV, Hamilton KL. The combination of NRF1 and Nrf2 activators in myoblasts stimulate mechanisms of proteostasis without changes in mitochondrial respiration. Redox Muscle Physiology Exerc Sport. Published online 2022:100001. doi:10.1016/j.rimpes.2022.100001

36. Konopka AR, Laurin JL, Musci RV, et al. Influence of Nrf2 activators on subcellular skeletal muscle protein and DNA synthesis rates after 6 weeks of milk protein feeding in older adults. Geroscience. 2017;39(2):175-186. doi:10.1007/s11357-017-9968-8

37. Donovan EL, McCord JM, Reuland DJ, Miller BF, Hamilton KL. Phytochemical Activation of Nrf2 Protects Human Coronary Artery Endothelial Cells against an Oxidative Challenge. Oxid Med Cell Longev. 2012;2012:132931. doi:10.1155/2012/132931

38. Bruns DR, Ehrlicher SE, Khademi S, et al. Differential Effects of Vitamin C or Protandim on Skeletal Muscle Adaptation to Exercise. J Appl Physiol. Published online 2018. doi:10.1152/japplphysiol.00277.2018

39. Gao L, Kumar V, Vellichirammal NN, et al. Functional, proteomic and bioinformatic analyses of Nrf2- and Keap1- null skeletal muscle. J Physiology. 2020;598(23):5427-5451. doi:10.1113/jp280176

40. Hybertson BM, Gao B, Bose S, McCord JM. Phytochemical Combination PB125 Activates the Nrf2 Pathway and Induces Cellular Protection against Oxidative Injury. Antioxidants. 2019;8(5):119. doi:10.3390/antiox8050119

41. Nilwik R, Snijders T, Leenders M, et al. The decline in skeletal muscle mass with aging is mainly attributed to a reduction in type II muscle fiber size. Exp Gerontol. 2013;48(5):492-498. doi:10.1016/j.exger.2013.02.012

42. Musci RV, Hamilton KL, Linden MA. Exercise-Induced Mitohormesis for the Maintenance of Skeletal Muscle and Healthspan Extension. Sports. 2019;7(7):170. doi:10.3390/sports7070170

43. Wang Z, Xu H, Zhou H, et al. Long term detraining reverses the improvement of lifelong exercise on skeletal muscle ferroptosis and infammation in aging rats: fber type dependence of the Keap1/Nrf2 pathway. Biogerontology. Published online 2023. doi:10.1007/s10522-023-10042-1

44. Lexell J, Taylor CC, Sjöström M. What is the cause of the ageing atrophy? Total number, size and proportion of different fiber types studied in whole vastus lateralis muscle from 15- to 83-year-old men. J Neurol Sci. 1988;84(2-3):275-294. doi:10.1016/0022-510x(88)90132-3

45. Chleboun GS, Busic AB, Graham KK, Stuckey HA. Fascicle Length Change of the Human Tibialis Anterior and Vastus Lateralis During Walking. J Orthop Sports Phys Ther. 2007;37(7):372-379. doi:10.2519/jospt.2007.2440

46. Maharaj JN, Cresswell AG, Lichtwark GA. Tibialis anterior tendinous tissue plays a key role in energy absorption during human walking. J Exp Biol. 2019;222(11):jeb191247. doi:10.1242/jeb.191247

47. Kemoun G, Thoumie P, Boisson D, Guieu JD. Ankle dorsiflexion delay can predict falls in the elderly. J Rehabilitation Med. 2002;34(6):278-283. doi:10.1080/165019702760390374

48. Begg RK, Sparrow WA. Ageing effects on knee and ankle joint angles at key events and phases of the gait cycle. J Méd Eng Technol. 2006;30(6):382-389. doi:10.1080/03091900500445353

49. Martinez W, Zhang Q, Linden MA, et al. Rates of protein synthesis are maintained in brain but reduced in skeletal muscle during dietary sulfur amino acid restriction. Frontiers Aging. 2022;3:975129. doi:10.3389/fragi.2022.975129

50. Busch R, Kim YK, Neese RA, et al. Measurement of protein turnover rates by heavy water labeling of nonessential amino acids. Biochimica Et Biophysica Acta Bba - Gen Subj. 2006;1760(5):730-744. doi:10.1016/j.bbagen.2005.12.023

51. Miller BF, Reid JJ, Price JC, Lin HJL, Atherton PJ, Smith K. CORP: The use of deuterated water for the measurement of protein synthesis. J Appl Physiol. 2020;128(5):1163-1176. doi:10.1152/japplphysiol.00855.2019

52. Busch R, Neese RA, Awada M, Hayes GM, Hellerstein MK. Measurement of cell proliferation by heavy water labeling. Nat Protoc. 2007;2(12):nprot.2007.420. doi:10.1038/nprot.2007.420

53. Drake JC, Peelor FF, Biela LM, Miller RA, Hamilton KL, Miller BF. Assessment of protein synthesis and cellular proliferation in long-lived crowded litter mice. Faseb J. 2013;27:1202.25-1202.25. doi:10.1096/fasebj.27.1_supplement.1202.25

54. Miller BF, Robinson MM, Bruss MD, Hellerstein M, Hamilton KL. A comprehensive assessment of mitochondrial protein synthesis and cellular proliferation with age and caloric restriction. Aging Cell. 2012;11(1):150-161. doi:10.1111/j.1474-9726.2011.00769.x

55. Brook MS, Wilkinson DJ, Mitchell WK, et al. A novel D2O tracer method to quantify RNA turnover as a biomarker of de novo ribosomal biogenesis, in vitro, in animal models, and in human skeletal muscle. Am J Physiol-endoc M. 2017;313(6):E681-E689. doi:10.1152/ajpendo.00157.2017

56. Sieljacks P, Wang J, Groennebaek T, et al. Six Weeks of Low-Load Blood Flow Restricted and High-Load Resistance Exercise Training Produce Similar Increases in Cumulative Myofibrillar Protein Synthesis and Ribosomal Biogenesis in Healthy Males. Front Physiol. 2019;10:649. doi:10.3389/fphys.2019.00649

57. Mathis AD, Naylor BC, Carson RH, et al. Mechanisms of In Vivo Ribosome Maintenance Change in Response to Nutrient Signals*. Mol Cell Proteomics. 2017;16(2):243-254. doi:10.1074/mcp.m116.063255

58. Lawrence MM, Pelt DWV, Confides AL, et al. Massage as a mechanotherapy promotes skeletal muscle protein and ribosomal turnover but does not mitigate muscle atrophy during disuse in adult rats. Acta Physiol. 2020;229(3):e13460. doi:10.1111/apha.13460

59. Miller BF, Hamilton KL. A perspective on the determination of mitochondrial biogenesis. Am J Physiol-endoc M. 2012;302(5):E496-E499. doi:10.1152/ajpendo.00578.2011

60. Drake JC, Bruns DR, Peelor FF, et al. Long-lived Snell dwarf mice display increased proteostatic mechanisms that are not dependent on decreased mTORC1 activity. Aging Cell. 2015;14(3):474-482. doi:10.1111/acel.12329

61. Drake JC, Bruns DR, Peelor FF, et al. Long-lived crowded-litter mice have an age-dependent increase in protein synthesis to DNA synthesis ratio and mTORC1 substrate phosphorylation. Am J Physiol-endoc M. 2014;307(9):E813-E821. doi:10.1152/ajpendo.00256.2014

62. Miller BF, Drake JC, Naylor B, Price JC, Hamilton KL. The measurement of protein synthesis for assessing proteostasis in studies of slowed aging. Ageing Res Rev. 2014;18:106-111. doi:10.1016/j.arr.2014.09.005

63. Belloto E, Diraison F, Basset A, Allain G, Abdallah P, Beylot M. Determination of protein replacement rates by deuterated water: validation of underlying assumptions. Am J Physiol-endoc M. 2007;292(5):E1340-E1347. doi:10.1152/ajpendo.00488.2006

64. Kobayashi M, Yamamoto M. Nrf2–Keap1 regulation of cellular defense mechanisms against electrophiles and reactive oxygen species. Adv Enzyme Regul. 2006;46(1):113-140. doi:10.1016/j.advenzreg.2006.01.007

65. Márton M, Tihanyi N, Gyulavári P, Bánhegyi G, Kapuy O. NRF2-regulated cell cycle arrest at early stage of oxidative stress response mechanism. Plos One. 2018;13(11):e0207949. doi:10.1371/journal.pone.0207949

66. Granic A, Suetterlin K, Shavlakadze T, Grounds MD, Sayer AA. Hallmarks of ageing in human skeletal muscle and implications for understanding the pathophysiology of sarcopenia in women and men. Clin Sci. 2023;137(22):1721-1751. doi:10.1042/cs20230319

67. Kovacheva EL, Hikim APS, Shen R, Sinha I, Sinha-Hikim I. Testosterone Supplementation Reverses Sarcopenia in Aging through Regulation of Myostatin, c-Jun NH2-Terminal Kinase, Notch, and Akt Signaling Pathways. Endocrinology. 2010;151(2):628-638. doi:10.1210/en.2009-1177

68. Shehzad B, D. CA, G. TT, et al. Adverse Events Associated with Testosterone Administration. New Engl J Med. 2010;363(2):109-122. doi:10.1056/nejmoa1000485

69. Graber TG, Kim JH, Grange RW, McLoon LK, Thompson LV. C57BL/6 life span study: age-related declines in muscle power production and contractile velocity. Age Dordrecht Neth. 2015;37(3):9773. doi:10.1007/s11357-015-9773-1

70. Krieglstein J, Kewitz T, Kirchhefer U, et al. Damage of Guinea Pig Heart and Arteries by a Trioleate-Enriched Diet and of Cultured Cardiomyocytes by Oleic Acid. Plos One. 2010;5(3):e9561. doi:10.1371/journal.pone.0009561

71. Radakovich LB, Marolf AJ, Culver LA, Santangelo KS. Calorie restriction with regular chow, but not a high-fat diet, delays onset of spontaneous osteoarthritis in the Hartley guinea pig model. Arthritis Res Ther. 2019;21(1):145. doi:10.1186/s13075-019-1925-8

72. Andrie KM, Palmer DR, Wahl O, et al. Treatment with PB125® Increases Femoral Long Bone Strength in 15-Month-Old Female Hartley Guinea Pigs. Ann Biomed Eng. Published online 2023:1-11. doi:10.1007/s10439-023-03415-7

73. Wahl D, Moreno JA, Santangelo KS, et al. Non-Transgenic Guinea Pig Strains Exhibit Hallmarks of Human Brain Aging and Alzheimer's Disease. Journals Gerontology Ser. Published online 2022. doi:10.1093/gerona/glac073

74. Rahman FA, Hian-Cheong DJ, Thoms JP. Plants powering muscle: The effects of phytochemical PB125 on mitochondrial function and skeletal muscle health. J Physiology. Published online 2022. doi:10.1113/jp283779

75. Díaz-Herrera P, García-Castellano JM, Torres A, Morcuende JA, Calbet JAL, Sarrat R. Effect of high-intensity running in rectus femoris muscle fiber in rats. J Orthop Res. 2001;19(2):229-232. doi:10.1016/s0736-0266(00)00031-0

76. Pomatto LCD, Davies KJA. Adaptive homeostasis and the free radical theory of ageing. Free Radical Bio Med. 2018;124:420-430. doi:10.1016/j.freeradbiomed.2018.06.016

77. Pomatto LCD, Davies KJA. The role of declining adaptive homeostasis in ageing. J Physiology. 2017;595(24):7275-7309. doi:10.1113/jp275072

78. Pomatto LCD, Sun PY, Davies KJA. To Adapt or not to Adapt: Consequences of Declining Adaptive Homeostasis and Proteostasis with Age. Mech Ageing Dev. 2018;177:80-87. doi:10.1016/j.mad.2018.05.006

79. Tsuji K, Ishida H, Oba K, Ueki T, Fujihashi Y. Activity of lower limb muscles during treadmill running at different velocities. J Phys Ther Sci. 2015;27(2):353-356. doi:10.1589/jpts.27.353

80. Laurin J. Evaluation of a novel phytochemical Nrf2 activator on cytoprotective gene expression and proteostasis in vivo, Mountain Scholar Thesis, Published online 2017.

81. Valenti Z. Effect of treatment with a Nrf2 activator on in vivo proteostasis in mice. Mountain Scholar Thesis Published online 2019.

82. Barber LA, Barrett RS, Gillett JG, Cresswell AG, Lichtwark GA. Neuromechanical properties of the triceps surae in young and older adults. Exp Gerontol. 2013;48(11):1147-1155. doi:10.1016/j.exger.2013.07.007

83. Borowik AK, Lawrence MM, Peelor FF, et al. Senolytic treatment does not mitigate oxidative stress-induced muscle atrophy but improves muscle force generation in CuZn superoxide dismutase knockout mice. GeroScience. Published online 2024:1-15. doi:10.1007/s11357-024-01070-x

84. Watson PJ, Hall LD, Malcolm A, Tyler JA. Degenerative joint disease in the guinea pig. Use of magnetic resonance imaging to monitor progression of bone pathology. Arthritis Rheumatism. 1996;39(8):1327-1337. doi:10.1002/art.1780390810

85. Cruz-Jentoft AJ, Bahat G, Bauer J, et al. Sarcopenia: revised European consensus on definition and diagnosis. Age Ageing. 2018;48(1):16-31. doi:10.1093/ageing/afy169

CHAPTER 4 – EFFECTS OF PB125 ON CEREBELLAR AGING IN HARTLEY GUINEA PIGS

INTRODUCTION

The cerebellum contains 60-80% of the neurons in the brain and is the region responsible for motor movement regulation and balance control [1,2]. Therefore, the cerebellum is important for mobility, a physical function imperative to maintain and support healthy aging [3,4]. Despite the cerebellar contribution to total neuronal content and mobility, it is an understudied brain region compared to the cerebral cortex, specifically in the context of aging and age-related chronic diseases [2,5]. A recent consensus statement summarized that very little is known about the aging cerebellum with the exception that age-related reductions in volume are correlated with cognitive decline [1]. Interestingly, there are differing phenotypes in "typical" cerebellar aging (i.e., age-associated changes in the absence of disease) versus pathological cerebellar aging [1]. One barrier to making more progress in describing structural and functional changes in the aging cerebellum is the lack of preclinical animal models that additionally recapitulate human brain aging. Specifically, cerebellar aging is typically observed later in age/disease progression [1]. Here, we further propose the Hartley guinea pig as a potential preclinical model to assess hallmarks of cerebellar brain aging and neuropathology. Additionally, we even postulate the possibility to test interventions to delay the onset or slow the progression of cerebellar brain aging.

The Hartley guinea pig, as extensively described in Chapter 3, displays multimorbidities (i.e., >2 or more chronic diseases) of aging including osteoarthritis [6,7], myofiber remodeling [8], obesity [9], and vascular disease [10]. Our group has additionally characterized the Hartley guinea pig as a model of that may naturally develop features of human neuropathology [11]. In addition to our ongoing in-depth characterization of progressive neuropathology in this model, we have shown significant decreases in rates of protein synthesis in the frontal cortex, increases in hippocampal amyloid beta and phosphorylated tau, and gliosis that progresses

from 5 to 15 mo [11]. We speculate the Hartley guinea pig might model Alzheimer's Disease or an Alzheimer's Disease Related Dementia phenotype suggesting accelerated neuropathology as compared to the control PigmEnTed (PET) guinea pig strain (also from Chapter 3) especially since evidence suggests that the effects of aging on the cerebellum likely extend beyond modifications in motor coordination [1].

One surprising finding to date is that both younger (5 month) and older (15 month) Hartley guinea pigs display spongiosis (spongy brain) in the cerebellum, a histopathology finding characterized by holes (average radius ~ 1.0 μm) in the brain. These holes may be evidence of neuron loss and dysfunction of the supporting brain cells (i.e., gliosis) [12]. This pathology occurs alongside other morbidities of aging in Hartleys, often culminating in early euthanasia due to severe mobility impairment. This highlights the importance of growing the current understanding of cerebellar aging in this model. Additionally, if a cerebellar aging phenotype exists in the Hartley guinea pigs, we have already shown proof of concept that Pathways Bioscience 125 (PB125), a purported Nrf2 activator, improves aspects of skeletal muscle health (Chapter 3 and [13]), cartilage (Andrie et al., unpublished), and bone [14] which culminated in an improved metric of mobility [13]. Further, recent evidence suggests peripheral tissue changes (e.g., skeletal muscle) can impair neural communication as evidenced by impaired nerve-stimulated force production [15]. Thus, PB125 may have potentially improved cerebellar aging in these same guinea pigs.

Therefore, the purposes of this study were three-fold. 1. To assess the presence of an age-related cerebellar phenotype in Hartley guinea pigs. We hypothesized that Hartley guinea pigs will display decreased rates of cerebellar protein synthesis, progressive spongiosis, and increased gliosis from 5 to 15 mo compared to the PET guinea pigs. 2. To determine if short-term (3 mo) PB125 treatment could delay the onset of cerebellar pathology in Hartley guinea pigs. We hypothesized that short-term PB125 treatment will maintain rates of cerebellar protein synthesis and decrease the degree of spongiosis and gliosis 3. To determine if long-term (10

mo) PB125 treatment could slow the progression of cerebellar pathology in Hartleys. We hypothesized that long-term PB125 treatment will increase rates of cerebellar protein synthesis while decreasing the degree of spongiosis and gliosis.

METHODS

Husbandry

All procedures were approved by the Colorado State University Institutional Animal Care and Use Committee (Protocol # 1213) and were performed in accordance with the NIH Guide for the Care and Use of Laboratory Animals. To test hypothesis #1, male and female PET guinea pigs were obtained from Elm Hill Laboratories (Chelmsford, MA, USA) at approximately 2 and 12 months of age and sacrificed at 5 and 15 mo of age, respectively; 4 male and female guinea pigs were utilized in each age (total n = 32) as these animals were a part of a small pilot study. We additionally obtained male and female Hartley guinea pigs were obtained from Charles River Laboratories (Wilmington, MA, USA) at approximately 1 and 4 months of age and sacrificed at 5 and 15 mo of age, respectively; 14 male and female guinea pigs were utilized in each age (total n = 56); these animals also served as the control animals for comparison to PB125 treatment groups. To test hypotheses #2 and 3, Hartley guinea pigs were obtained from Charles River Laboratories (Wilmington, MA, USA) at 1 and 4- months of age (mo) for each treatment regimen to determine if PB125 could delay the onset (short-term treatment from 2 to 5 mo to test hypothesis #2) or slow the progression (long-term treatment from 5 to 15 mo to test hypothesis #3) in the cerebellum [11] (Figure 4.1). This study was powered to detect differences in mechanisms of proteostasis at a power of 0.80 and significance (chance of Type I error) set at p=0.05 (Lenth power calculator). Based on data from a prior study (associated with hypotheses 2 and 3), we calculated an n=13 animals/group, and increased the number to n=14/group to account for unanticipated losses (total n =112). Animals were maintained at Colorado State University's Laboratory Animal Resources housing facilities and were monitored daily by veterinary staff. All guinea pigs were singly housed in solid bottom cages, maintained

on a 12-12 hour light-dark cycle, and provided *ad libitum* access to food and water. Animals were fasted for 12 hours prior to euthanasia. These were the same animals used in Chapter 3.

Daily PB125 treatment in Hartley guinea pigs

PB125 (Pathways Bioscience, Aurora, CO) is a phytochemical compound comprised of rosemary, ashwagandha, and luteolin powders, which contain the three active ingredients carnosol, withaferin A, and luteolin at a mixed ratio of 15:5:2 by mass, respectively [16]. In a prior publication we demonstrated the feasibility of selecting 8.0 mg/kg of daily dosing [13]. After a one-month acclimation to housing conditions, male and female Hartley guinea pigs in each treatment group were randomized to receive a daily oral dose of PB125 suspended in OraSweet (Perrigo, Dublin, Ireland) or an equivalent volume of OraSweet only (CON) beginning at 5 mo of age until 15 mo of age (Figure 4.1). Hartley guinea pigs were not dosed the morning of necropsy as we wanted to assess the long-term and not acute effects of PB125 treatment.

Deuterium oxide labeling in PET and Hartley guinea pigs

To assess long-term rates of cerebellar protein synthesis, all guinea pigs (including the PETs) were given a subcutaneous injection of 0.9% saline enriched with 99% deuterium (^2H_2O) equivalent to 3% of their body weight 30 days prior to euthanasia [8,13]. Drinking water was enriched to 8% ^2H_2O for the purpose of maintaining ^2H_2O enrichment of the body water pool during the 30-day labelling period. At the time of harvest, the guinea pigs were 5 mo or 15 mo.

Euthanasia and tissue collection in PET and Hartley guinea pigs

In accordance with the standards of the American Veterinary Medical Association, animals were anesthetized with a mixture of isoflurane and oxygen; thoracic cavities were opened, and blood was collected via direct cardiac puncture. Whole blood was centrifuged (1200 *g*, 4^{o}C, 15 min) to separate plasma, which was frozen at -80^{o}C until further analysis. After blood collection, the anesthetized animals were transferred to a chamber filled with carbon dioxide for euthanasia. The right half the cerebellum and flash frozen in liquid nitrogen and the left half was placed in formalin.

Two control females, two PB125 females, one control male, and two PB125 males required humane euthanasia prior to final analysis due to underlying issues unrelated to treatment (Hartley guinea pig final n = 105). Gross necropsy findings by veterinarians did not raise significant concern as the cause of death in these cases were consistent with what would be expected in conventionally raised guinea pigs. We did not lose any PET guinea pigs prior to euthanasia.

Sample preparation and analysis via Gas Chromatography-Mass Spectroscopy (GC-MS): proteins

The cerebellum was homogenized and fractionated following established laboratory protocols [8,13,17]. Briefly, tissues (20 – 40 mg) were homogenized at 1:10 in isolation buffer (100 mM KCl, 40 mM Tris HCl, 10 mM Tris Base, 5 mM MgCl2, 1 mM EDTA, 1 mM ATP, pH – 7.50) with phosphatase and protease inhibitors (HALT Thermo Scientific, Rockford, IL, USA) using a tissue homogenizer (Bullet Blender, Next Advance Inc., Averill Park, NY, USA) with zirconium beads (Next Advance Inc., Averill Park, NY, USA). After homogenization, subcellular fractions were isolated via differential centrifugation as previously described [8,13]. Once fractionated pellets were isolated and purified, 250 µl 1 M NaOH was added, and pellets were incubated for 15 min at 50 ^{o}C and 900 RPM.

Protein subfractions were hydrolyzed in 6 M HCl for 24 hours at 120 ^{o}C after which the hydrolysates were ion-exchanged, dried *in vacuo*, and then resuspended in 1 mL of MiliQ H_2O. Half of the suspension was derivatized with 500 µL acetonitrile, 50 µL 1 M K_2HPO_4, and 20 µl of pentafluorobenzyl bromide and incubated at 100 ^{o}C for 60 min. Derivatives were extracted into ethyl acetate and the organic layer was transferred into vials which were then dried under nitrogen. Samples were reconstituted in ethyl acetate (400 µL – 800 µL).

The derivative of alanine was analyzed on an Agilent 7890A GC coupled to an Agilent 5977A MS as previously described [8,13,18]. The newly synthesized fraction (f) of proteins was calculated from the true precursor enrichment (p) based upon plasma analyzed for $^{2}H_2O$

enrichment and adjusted using mass isotopomer distribution analysis [19]. Protein synthesis of each subfraction was calculated as the fraction of deuterium-labeled over unlabeled alanine proteins over the entire labeling period (30 days) and expressed as the fractional synthesis rate (FSR). Thus, we divided fraction new by our labeling period (30 days) and multiplied by 100 to express FSR as %/day. Our isotope approach and analysis followed the established procedures detailed in this Core of Reproducibility in Physiology publication [20].

Sample preparation and analysis via GC-MS: body water

80 µL of plasma was placed into the inner well of an o-ring cap that was screwed to tube and inverted on a heating block overnight at 100°C. After incubation, 2 µL of 10 M NaOH and 20 µL of acetone were added to the samples and $^{2}H_2O$ standards (0 – 20%) and capped immediately, vortexed, and incubated at room temperature overnight. Samples were extracted with 200 µL hexane and the organic layer was transferred through pipette tips filled with anhydrous Na_2SO_4 into GC vials and analyzed via EI mode using a DB-17MS column.

Tissue processing for histopathology and spongiosis

Brains (n = 3/age/sex/treatment; total N = 24) of Hartley guinea pigs were extirpated en bloc and fixed whole in 10% buffered formalin or 4% paraformaldehyde at room temperature for at least 48 h. Tissues were processed using a Leica TP1020 Automatic Benchtop Tissue Processor and embedded in paraffin wax (Cancer Diagnostics, Cat #: EEPAR56). They were then sectioned on a Thermo Scientific HM 325–2 Manual Microtome at 5 µm thickness and mounted on positively charged glass slides (Superfrost Plus, Cancer Diagnostics, Cat #: 4951) for staining and analysis. One whole-tissue section per animal was stained with hematoxylin and eosin (H&E) for determination of morphological and histopathological changes (i.e., spongiosis analyses). See “Quantification of spongiosis panel” for more details below.

Immunohistochemistry for Iba1

Tissue sections were deparaffinized in xylene and rehydrated through graded ethanol, followed by chemical and heat induced antigen retrieval using EDTA buffer (1 mM EDTA

disodium salt dihydrate, 0.05% Tween; pH 8.0) for 20 min at 100°C. This was followed by removal of endoperoxides by 0.3% hydrogen peroxide for 30 min at room temperature. Tissue was permeabilized (0.1% Triton-X in 1 M Tris Buffered Saline (TBS)) and blocking was performed in 10% serum diluted in 1 M TBS. Primary antibodies were diluted to their optimized concentrations in 1 M TBS and incubated on the tissue at 4°C overnight. Blocking and antibody information is in Supplemental Table C.1. Wash steps were performed using 2% bovine serum albumin and 2% Triton-X in 1 M TBS and then secondary antibody incubation for 1 hour. An ABC HRP peroxidase detection kit (Vector Laboratories, Cat #: pk-4,000) and ImmPACT DAB Substrate, Peroxidase (HRP) Kit (Vector Laboratories, Cat #: sk-4,105) was used as chromogen and slides were counterstained with hematoxylin (Thermo Fisher Scientific, Cat #: 7231) and bluing solution (Cancer Diagnostics, Cat #: FX2107). All slides for each antigen of interest received the same immunoreaction period also noted in Supplemental Table C.1. Slides were secured with a coverslip in mounting medium and stored at room temperature until imaging. Whole tissue images were taken using an Olympus BX53 microscope with an Olympus DP70 camera using an Olympus UPlanSApo 20x objective (N.A. = 0.75). Representative images were taken using an Olympus BX53 microscope with an Olympus DP70 camera using an Olympus UPlanFL N 40x objective (N.A. = 0.75). Manual thresholding within the Count and Measure module of CellSens was applied to batch analysis macros for mean intensity measurements of Iba1 [21]. Images were quantified by a blinded observer.

Immunofluorescence – C3+S100β

Paraffin embedded brain sections were deparaffinized in xylene and rehydrated through graded ethanol, followed by chemical and heat induced antigen retrieval using EDTA buffer (1 mM EDTA disodium salt dihydrate, 0.05% Tween; pH 8.0) for 20 min at 100°C. This was followed by permeabilization using 0.01% Triton X diluted in 1 M TBS. Blocking was performed with 2% serum diluted in 1 M TBS. Astrocyte stains used anti-S100 calcium-binding protein β (S100β), anti-glial fibrillary acidic protein (GFAP), and complement 3 protein (C3). See

Supplemental Table C.1 for all blocking and antibody conditions. Following DAPI, slides were mounted on glass coverslips in ProLong Gold Antifade mounting medium, fixed for 24 h at room temperature, and then stored at 4°C until imaging. Images were captured using an Olympus BX63 fluorescence microscope equipped with a motorized stage and Hamamatsu ORCA-flash 4.0 LT CCD camera using a 40x Olympus X-Apochromat air objective air objective (N.A. = 0.80). All slides quantified were imaged on the same day with the same exposure per channel. Specifically, S100β events were then converted to ROIs and the intensity of C3 positivity was interrogated on a cell-by-cell basis for the most accurate representation of astrocyte reactivity within a consistent 1 x 1mm area of the cerebellum. Due to the size of these files this was the largest area that was able to be quantified. Manual thresholding within the Count and Measure module of CellSens was applied to batch analysis macros for mean intensity measurements of C3 [22]. Images were quantified by a blinded observer. For representative images each channel was imaged with the same Olympus BX63 fluorescence microscope 40x at the same exposure time across all groups. Threshold was determined by background intensity and setting that as the minimum threshold. The maximum was adjusted based on the clarity of the image/staining.

Quantification of spongiosis panel

H&E whole tissue images were taken using an Olympus BX53 microscope with an Olympus DP70 camera using an Olympus UPlanSApo 20x objective (N.A. = 0.75). Representative images were taken using an Olympus BX53 microscope with an Olympus DP70 camera using an Olympus UPlanSApo 40x objective (N.A. = 0.75). Within CellSens images were converted to greyscale images and manual thresholding within the Count and Measure module of CellSens was applied to batch analysis macros for the percent of holes (i.e., white area), number of holes within the base of the arbor vitae of the cerebellum which was normalized to area, the mean hole radius, and the mean hole area. The base of the arbor vitae was selected as it was the region of the cerebellum where the spongiosis is the most

pronounced and resulted in the least amount of bias with quantification. Images were quantified by a blinded observer.

Protein content for Nrf2 and NQO1

Western blotting was used to measure relative content of Nrf2 and NQO1 proteins. 50-70 mg portions of the cerebellum (n=12 per treatment group) were powdered under liquid nitrogen and homogenized in a Bullet Blender with zirconium beads and 1.0 mL of radioimmunoprecipitation assay (RIPA) buffer (150 mM NaCl, 0.1 mM EDTA, 50 mM Tris, 0.1% sodium deoxycholate, 0.1% SDS, 1% Triton X-100, pH = 7.50) with HALT protease inhibitors. Protein concentration was determined with BCA assay (ThermoFisher 23225). Samples were at 95^{o}C for 5 min. Approximately 20 µg of protein was loaded into a 4% - 20% Criterion pre-cast gel (Bio-Rad, Hercules, CA, USA) and resolved at 120 V for 120 min. The proteins were then transferred at 100 V for 75 min in transfer buffer (20% w/v methanol, 0.02% w/v SDS, 25 mM Tris Base, 192 mM glycine, pH 8.3). Membranes were then blocked and incubated with primary antibodies against Nrf2 (Santa Cruz 13032) and NQO1 (Novus 200-208) on a shaker overnight in 4^{o}C. Membranes were rinsed and then incubated with appropriate secondary antibodies (Santa Cruz 2005) for Nrf2 and NQO1. See Supplemental Table C.2 for all blocking and antibody conditions. After the membranes were rinsed, Western Lightening ECL Enhanced (Perkin Elm NEL104001EA) was applied and the membranes were subsequently imaged using a FluorChem E Chemiluminescence Imager (Protein Simple, San Diego, CA, USA). Analysis of densitometry was completed using AlphaView SA Software. Units are expressed as density of primary antibody relative to density of amido black as previously described [18].

Statistical analysis

To compare the effect of age from 5 to 15 mo on metrics of cerebellar neuropathology, independent t-tests were used in the Hartley and PET strains as there was no effect of sex in any of the outcomes (data not shown). To compare the effect of treatment on protein synthesis, spongiosis, and gliosis in the two studies (i.e., short and long-term PB125 treatment studies),

independent t-tests were also used again because there was no effect of sex in any of the outcomes (data not shown). Finally, we assessed if PB125 treatment could attenuate any age-related changes (from 5 to 15 mo) with a one-way ANOVA and Tukey post-doc as previously described [13]. We set statistical significance a priori at $p<0.05$. However, we also report differences with $p<0.10$ as non-significant trends to highlight potential directions for future studies. ROUT outlier tests were performed on all data sets and identified outliers were removed. Data are presented as mean +/- SD. All statistics were performed in Prism 8.0 (La Jolla, California, USA).

RESULTS

Cerebellar protein synthesis differs from 5 to 15 mo in Hartley guinea pigs

Prior work shows evidence of declining rates of protein synthesis in the prefrontal cortex, and protein misfolding with gliosis in the hippocampus in Hartley guinea pigs; however, we were uncertain how the cerebellum changes with age. Here we observe that from 5 to 15 mo, rates of cerebellar structural/mixed protein synthesis significantly decrease with age (Figure 4.2A) while rates of mitochondrial (Figure 4.2B) and cytosolic (Figure 4.2C) proteins were maintained from 5 to 15 mo. These findings contrast with the maintained rates of structural/mixed (Figure C.1A), mitochondrial (Figure C.1B), and cytosolic (Figure C.1C) proteins in the PET guinea pigs, highlighting that the Hartleys have progressive pathology from 5 to 15 mo and the PET strain may serve as a valuable control in future studies regarding cerebellar aging.

The severity of cerebellar spongiosis does not change from 5 to 15 mo in Hartley guinea pigs

Because our preliminary observations suggested the presence of spongiosis in the cerebellum of Hartley guinea pigs we sought to determine a quantifiable outcome of this unique pathology. Interestingly from 5 to 15 mo, there were no differences in the percent holes (Figure 4.3A), number of holes (Figure 4.3B), the mean hole radius (Figure 4.3C), or the mean hole area (Figure 4.3D) in the cerebellum. Representative images are shown in Figure 4.3E. Future

studies should seek to determine why, at such a young age, Hartley guinea pigs have such robust spongiosis.

Hartleys have increased gliosis from 5 to 15 mo

Spongiosis can be accompanied with gliosis [12] and our prior studies documented age-related increases in gliosis markers in the hippocampus [11]. Therefore, we quantified how Iba1 in microglia and C3 expression in S100β-positive astrocytes changed with age in the cerebellum. From 5 to 15 mo there was a significant increase in both Iba1 (Figure 4.4A (quantified) and 4.4B (representative images)) and C3 expression in S100β-positive astrocytes (Figure 4.4C (quantified) 4.4D (representative images)). Taken together, these results confirm that the Hartley guinea pig is a feasible model for examining cerebellar inflammation.

Short-term PB125 treatment does not alter hallmarks of cerebellar aging

To examine if short-term PB125 treatment (from 2 to 5 mo of age) delayed the onset of markers of cerebellar brain aging, we assessed of rates of protein synthesis, quantified of spongiosis, and identified markers of gliosis in PB125, and vehicle treated Hartleys. There were no treatment differences in rates of structural/mixed (Figure 4.5A), mitochondrial (Figure 4.5B), and cytosolic (Figure 4.5C) proteins. Similarly, spongiotic percent holes (Figure 4.6A), number of holes (Figure 4.6B), mean hole radius (Figure 4.6C), mean hole area (Figure 4.6D) were not different in the cerebellum after 3 mo of PB125 treatment compared to vehicle controls (representative images Figure 4.6E). Iba1 (Figure 4.7A (quantified) and 4.7B (representative images)) and C3 expression in S100β-positive astrocytes (Figure 4.7C (quantified) 4.7D (representative images)) were also not different between treatment groups. Even though there were no differences, we also wanted to determine if 3 mo of PB125 treatment increased Nrf2 activation. We found again found no differences in Nrf2 protein content (Figure C.2A (quantified) unedited blot (Figure C.4) total protein (Figure C.5)) or NQO1 protein content, a downstream target of Nrf2, (Figure C.2B (quantified) unedited blot (Figure C.6) total protein (Figure C.7)). Taken together, 3 mo of PB125 treatment did not alter rates of protein synthesis, spongiosis, or

gliosis in the cerebellum of Hartley guinea pigs; however, because we did not age these guinea pigs after the 5-mo treatment stopped we are not certain of any longstanding treatment effects.

Long-term PB125 treatment does not impact hallmarks of cerebellar aging

To examine if long-term PB125 treatment (from 5 to 15 mo of age) slows the onset of cerebellar brain aging, we assessed rates of protein synthesis, quantification of spongiosis, and markers of gliosis. There was no treatment difference in rates of structural/mixed (Figure 4.8A), mitochondrial (Figure 4.8B), and cytosolic (Figure 4.8C) proteins. Spongiotic percent holes (Figure 4.9A), number of holes (Figure 4.9B), and mean hole radius (Figure 4.9C) in the cerebellum were not different after 10 mo of PB125 treatment compared to vehicle control. The mean hole area (Figure 4.9D) was significantly higher in PB125 treated guinea pigs; however, we collectively conclude that the spongiotic phenotype did not change with 10 mo if PB125 treatment (representative images Figure 4.9E). There were also no differences in Iba1 (Figure 4.10A (quantified) and 4.10B (representative images)) and C3 expression in S100β astrocytes (Figure 4.10C (quantified) 4.10D (representative images)). Even though there were no statistical differences in our neuropathology outcomes, we also wanted to determine if 10 mo of PB125 treatment increased Nrf2 activation. We again found no differences in Nrf2 protein content (Figure C.3A (quantified) unedited blot (Figure C.4) total protein (Figure C.5)) or NQO1 protein content, a downstream target of Nrf2, (Figure C.3B (quantified) unedited blot (Figure C.6) total protein (Figure C.7)). Taken together, 10 mo of PB125 treatment did not alter rates of cerebellar protein synthesis, spongiosis, or gliosis.

Long-term PB125 treatment attenuates some cerebellar age-related declines

Despite the absence of effects with 3 or 10 mo of PB125 treatment on delaying the onset or slowing the progression of cerebellar aging, respectively, we did notice that in some outcomes the effect of PB125 treatment yielded non-significantly lower measures. Therefore, we sought to determine if 10 mo of PB125 treatment attenuated age-related changes in the rates of structural/mixed protein synthesis, Iba1 expression, and C3 expression in S100β-

positive astrocytes. We found that 10 mo of PB125 treatment did not attenuate the age-related decline in rates of structural/mixed protein synthesis (Figure 4.11A). However, treatment did significantly attenuate the age-related increase in cerebellar Iba1 (Figure 4.11B (quantified) Figure 4.11C (representative images)). Long-term treatment also attenuated the age-related increase ($p = 0.0704$) in C3 expressing S100β-positive astrocytes, a prominent hallmark of reactive astrocytes (Figure 4.11D (quantified) Figure 4.11E (representative images)) [23].

DISCUSSION

The cerebellum is an understudied brain region in the context of aging, neurodegeneration, and neuropathology [2,5]. However, its role in motor movement regulation [24] and balance control [25] is important for mobility and fall prevention. Gait speed is arguably one of the most important functions to maintain with age to ensure independence and decreases in gait speed are predictive of morbidity and mortality [4]. In this study we examined the age-related changes in cerebellar aging using a novel non-transgenic guinea pig model that mimics neuropathology changes observed in aging humans [11]. Additionally, we also assessed short- (3 mo) and long- (10 mo) term treatment effects of PB125 in delaying the onset or slowing the progression of cerebellar brain aging, respectively in Hartley guinea pigs. Our key findings include 1. Rates of structural/mixed protein synthesis in the cerebellum are dramatically decreased with age in Hartleys, 2. PB125 treatment attenuated the age-related increase in cerebellar gliosis despite not altering rates of protein synthesis or the degree of spongiosis.

Key finding #1: Rates of structural/mixed protein synthesis are decreased with age in Hartleys

Our prior work examined how rates of prefrontal cortex protein synthesis rates changed from 5 to 15 mo in Hartley guinea pigs where we found approximately a 14% decrease in the fraction of newly synthesized proteins in 30-day labeling period [11]. While this finding was statistically significant, its magnitude of decrease was much lower than the 72% decrease in rates of cerebellar structural/mixed protein synthesis from 5 to 15 mo in the present study (Figure 4.2A).

The use of deuterium oxide allows us to capture rates of protein synthesis over a 30-day period which overcomes limitations to acutely assessing protein synthesis rates and/or protein content as a snapshot measure. However, it is noteworthy to comment on the nature of the bulk fraction protein synthesis (i.e., the rates of protein synthesis in an entire subcellular fraction accomplished through differential centrifugation). Specifically, we note age-related declines in structural/mixed protein synthesis as compared to cytosolic or mitochondrial bulk protein synthesis rates that did not change from 5 to 15 mo (Figures 4.2B and C, respectively). In a prior study by our group using kinetic proteomics, we showed that in a given set of samples, bulk protein synthesis rates can decrease, for example, but rates of specific individual proteins may be increased or decreased [26]. While kinetic proteomics was not feasible for this present study, we can speculate what important proteins may have been in the structural/mixed fraction including GFAP, an intermediate filament-III protein [27], and Iba1 which has actin binding activity [28]. Additionally, isotopic labeling captures a synthesis rate which is typically matched to degradation in healthy tissues if protein content is maintained. However, taken without our histology data (one assessment of protein content) we observed an age-related increase in Iba1 (Figure 4.4A) and reactive astrocytes Figure 4.4C) suggesting that protein clearance was decreased to a greater extent than synthesis leading to accumulation of functional proteins. Given that astrocytes aid in protein clearance specifically amyloid beta clearance [29] targeting astrocyte reactivity could be a potential avenue to peruse when trying to slow the age-related decline in mixed/structural protein synthesis rates in Hartley guinea pigs. To confirm this hypothesis future studies that include kinetic proteomic analyses could shed light on how aging alters rates of synthesis of specific structural cerebellar proteins. However, this is the first documentation of using the deuterium oxide tracer to measure rates of protein synthesis in the cerebellum.

Key finding #2: PB125 treatment attenuated the age-related increase in cerebellar gliosis despite not altering rates of protein synthesis or the degree of spongiosis

Because we observed substantial decreases in cerebellar rates of protein synthesis and increases in gliosis from 5 to 15 mo, we wanted to determine if these decreases were attenuated with 10 mo of PB125 treatment. Prior work by our group has shown 10 mo of PB125 treatment attenuated age-related decreases in skeletal muscle mitochondrial respiration [13], skeletal muscle protein synthesis [13], and indirect measures of skeletal muscle cellular senescence (Chapter 3) suggesting PB125 has the potential to attenuate hallmarks of cellular aging. Furthermore, recent evidence suggests weakened neural conduction impairs skeletal muscle health which preceded cognitive dysfunction [15] suggesting a possible bidirectional relationship between brain and skeletal muscle.

We found that indeed 10 mo of PB125 treatment attenuated the age-related increase in Iba1 (Figure 4.11B) and C3 (Figure 4.11D) suggesting PB125 decreased a pro-inflammatory phenotype that is often accompanied by reactive astrocytes in neurodegenerative diseases [23]. However, PB125 did not attenuate the robust age-related decline in cerebellar mixed/structural protein synthesis (Figure 4.11A). Thus, it appears that, despite the lack of improved structural integrity with PB125 treatment (i.e., no differences in spongiotic severity), the remaining functional cells exhibit a diminished “reactive” (and pro-inflammatory) phenotype. It is important to note that both reactive microglia and astrocytes exist on a continuum and recent position statements have focused on how to best assess “reactivity [30,31].”

While a limitation of this current study was the lack of functional outcomes glial cells and measures of cognition, these data are an important first step in preclinically modeling cerebellar aging and showing again that PB125 treatment may improve hallmarks of aging. Another limitation worth noting is, while we detected the active ingredients of PB125 in system circulation [13], we did not make measurements specifically in the brain. PB125 is composed of three active ingredients including carnosol, luteolin, and withaferin A which all are speculated or confirmed to cross the blood brain barrier [32–34]. However, these ingredients are also metabolized rapidly. Specifically, luteolin is absorbed from the gut and metabolized rapidly to

gluconurides, [35,36] with luteolin-7-O-glucuronide accounting for ~77% of luteolin metabolites [37]. Further, luteolin-7-O-glucouronide can also activate Nrf2, with resultant anti-inflammatory and antioxidant responses [38]. Including metabolomic analyses in future studies could help identify the role of metabolites in the therapeutic efficacy of PB125 treatment.

The current findings parallel those in Chapter 3, in that 10 mo of PB125 treatment attenuated the age-related increases in markers of skeletal muscle cellular senescence which is also associated with a pro-inflammatory phenotype. However, in contrast to the findings in Chapter 3, there were no sex-differences in the cerebellum. While not directly assessed in Chapter 3 or in this study (Chapter 4), there is a strong interconnection between skeletal muscle and brain aging [39]. Future studies should directly examine the parallel declines in the brain and skeletal muscle in Hartley guinea pigs as well as the neuromuscular junction.

Conclusions and future directions

With the projected increased global population of older adults, there will undoubtedly be an increase in the prevalence of neurodegenerative diseases. Therefore, identifying safe and effective treatments that target the hallmarks of brain aging rather than merely the symptoms of diseases, might be a strong step in improving healthy aging. Because older adults present with numerous multimorbidities future studies should test interventions in preclinical models like the Hartley guinea pig that best recapitulate human brain aging.

FIGURES

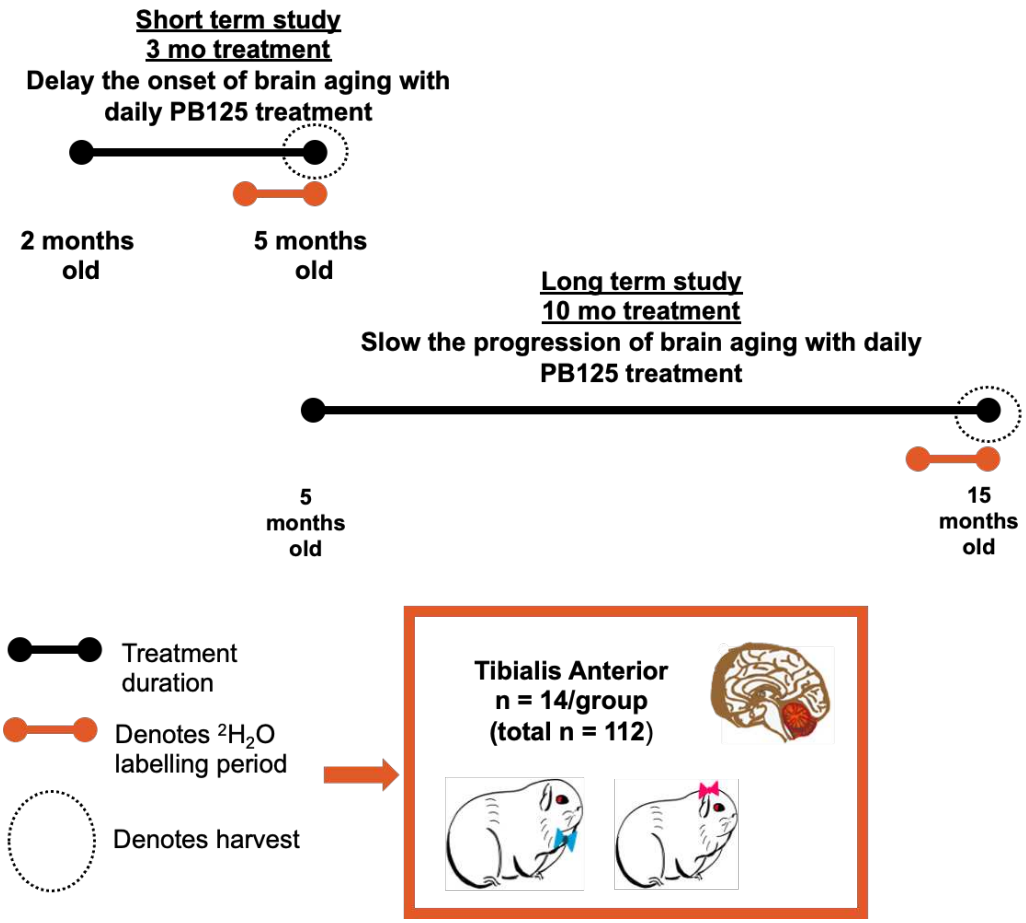

Figure 4.1. Study design. Male (n = 14/group) and Female (n = 14/group) Hartley guinea pigs were either treated with PB125 or a vehicle control for 3 mo (from 2 to 5 mo) or 10 mo (from 5 to 15 mo) to delay the onset of brain aging (short term study) or slow the progression of brain aging (long term study) (black lines), respectively. During the final month of treatment (orange lines) guinea pigs were labeled with deuterium oxide (^2H_2O) to assess long-term rates of protein and DNA synthesis. Guinea pigs were sacrificed at 5 and 15 mo of age and plasma, and cerebellum samples were collected for analysis.

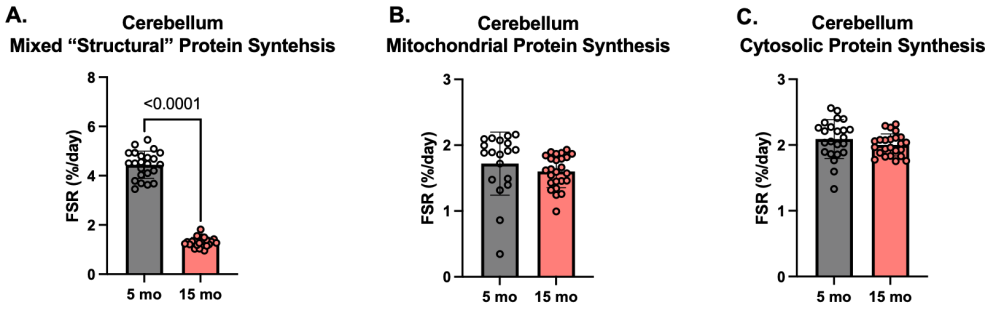

Figure 4.2. Age-related changes in cerebellar protein synthesis in Hartley guinea pigs. From 5 to 15 mo of age rates of mixed or structural protein synthesis were significantly decreased with age (A). However, rates of mitochondrial (B) and cytosolic (C) protein synthesis were maintained from 5 to 15 mo in Hartley guinea pigs.

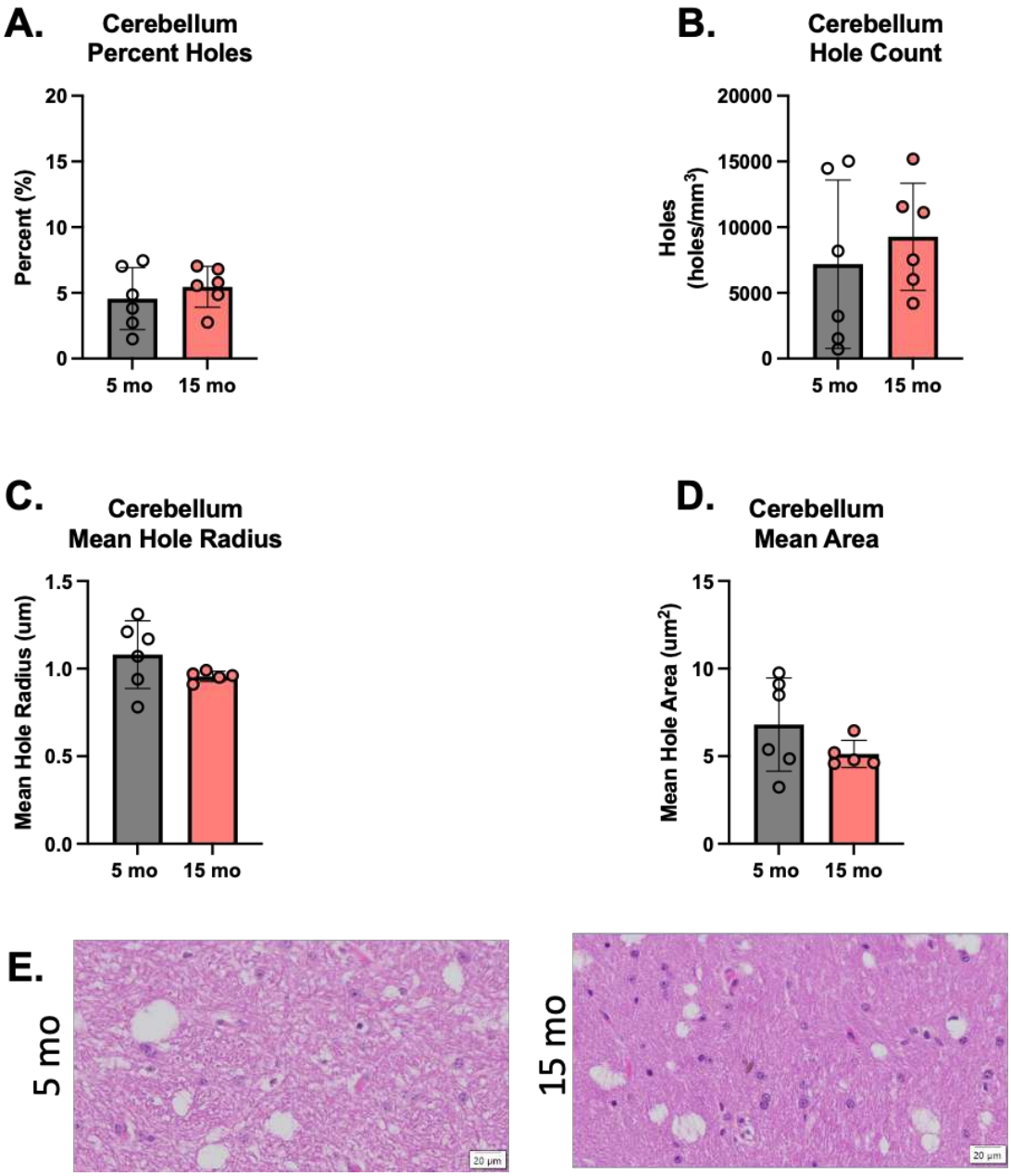

Figure 4.3. Age-related changes in cerebellar spongiosis in Hartley guinea pigs. From 5 to 15 mo there were no changes in the percent holes (A), number of holes (B), the mean hole radius (C), or the mean hole area (D) in the cerebellum of Hartley guinea pigs. Representative images are shown in panel E. Scale bar 20 μm.

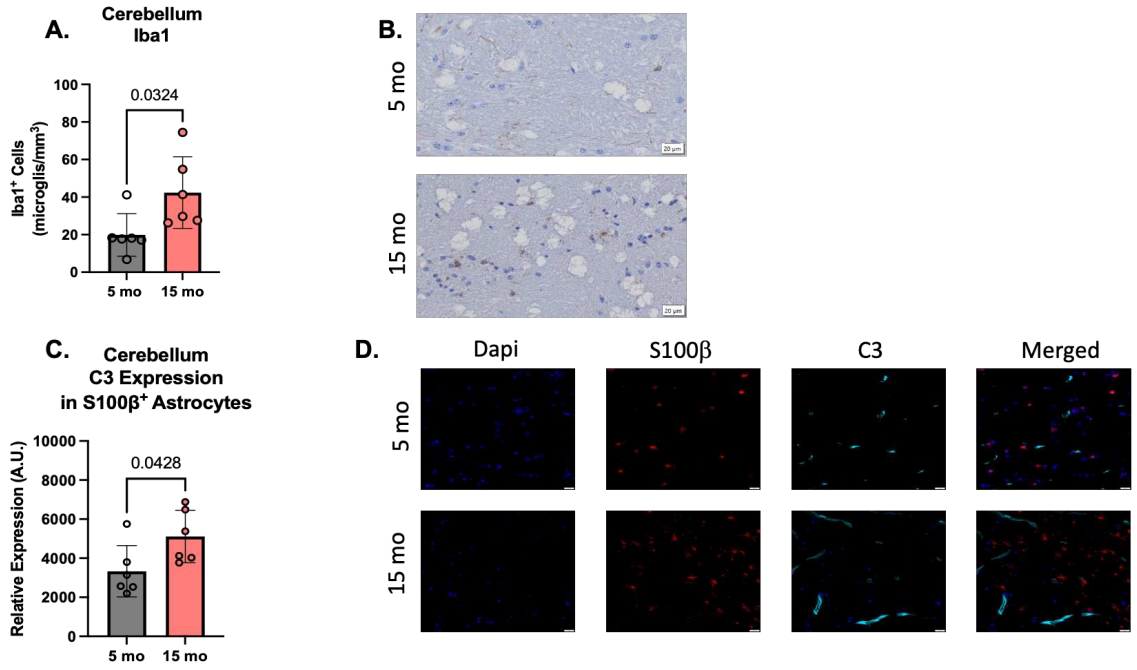

Figure 4.4. Age-related changes in cerebellar microgliosis and reactive astrocytes in Hartley guinea pigs. From 5 to 15 mo there was a significant increase in Iba1 in the cerebellum of Hartley guinea pigs (A). Iba1 representative images are shown in panel B. Additionally, from 5 to 15 mo there was a significant increase in the amount of C3 expressed in astrocytes in the cerebellum in Hartley guinea pigs (B). C3 expression representative images are shown in panel D. Scale bar 20 μm.

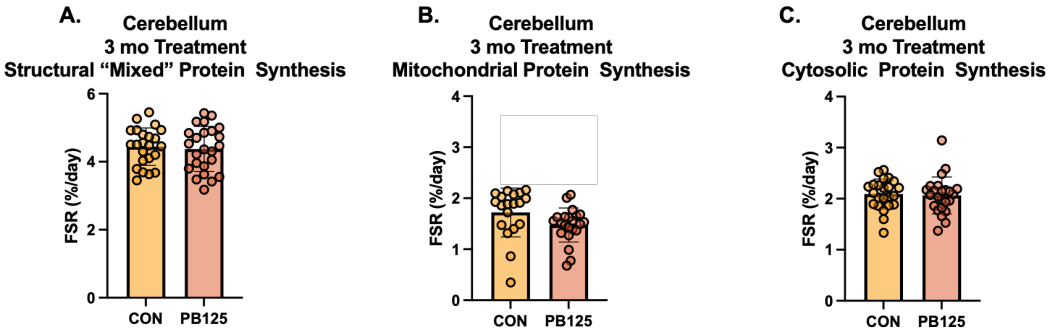

Figure 4.5. Short-term PB125 does not alter rates of cerebellar protein synthesis. 3 mo of PB125 treatment in the cerebellum of Hartley guinea pigs did not alter rates of structural or mixed (A), mitochondrial (B), and cytosolic (C) protein synthesis.

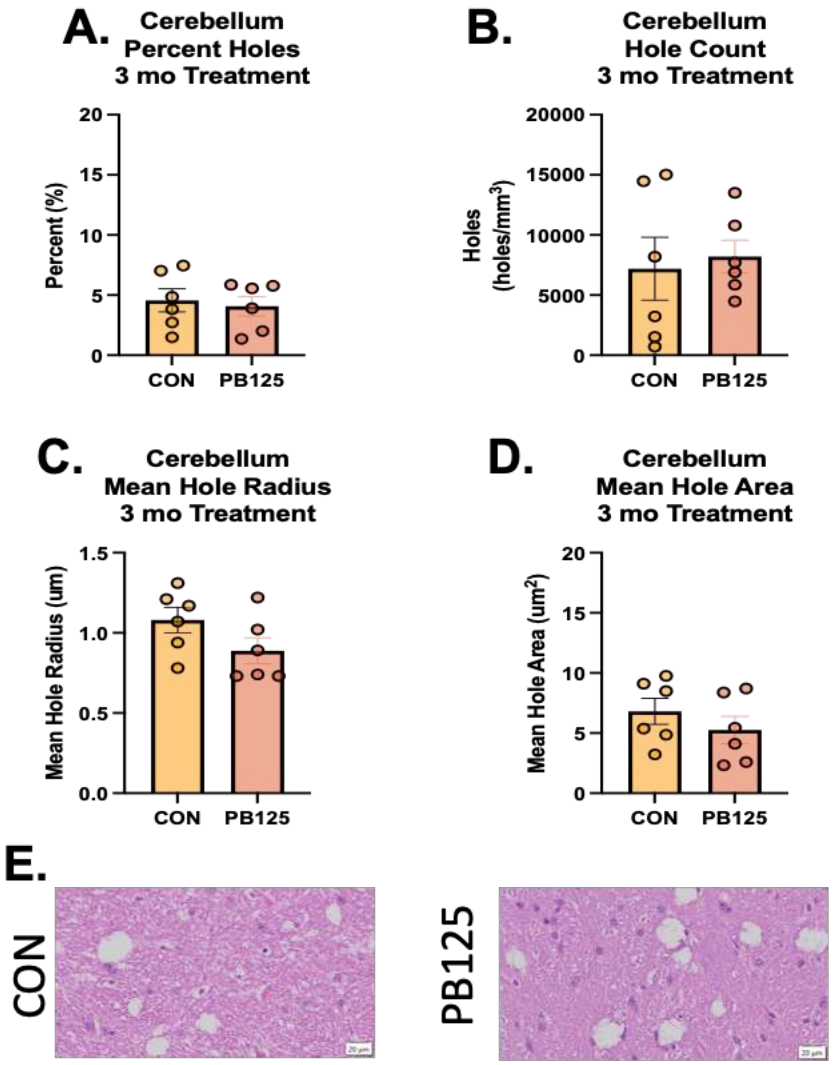

Figure 4.6. Short-term PB125 treatment does not alter the degree of cerebellar spongiosis. Measure of hole percentage (A), number of holes (B), the mean hole radius (C), or the mean hole area (D) did not change after 3 mo of PB125 treatment in the cerebellum of Hartley guinea pigs. Representative images are shown in panel E. Scale bar 20 μm.

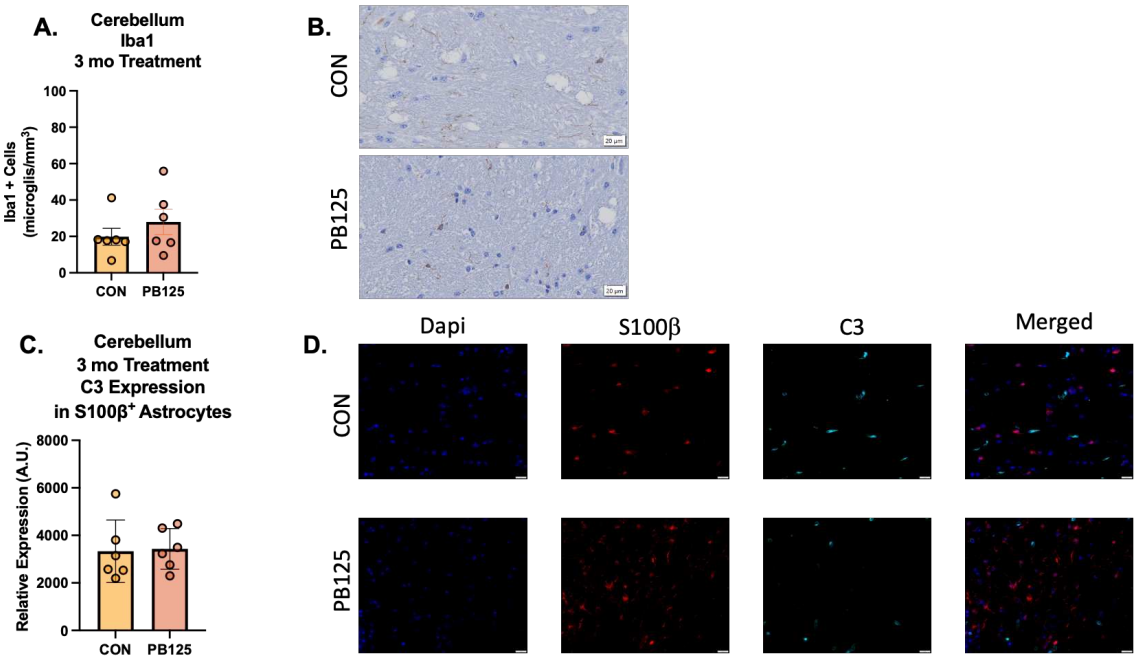

Figure 4.7. Short-term PB125 treatment does not alter Iba1 in microglia or C3 expression in astrocytes. Iba1, a measure of microgliosis, did not change with 3 mo of PB125 treatment in the cerebellum of Hartley guinea pigs (A). Iba1 representative images are shown in panel B. Additionally, C3 in astrocytes did not change with 3 mo of PB125 treatment in the cerebellum of Hartley guinea pigs (C). C3 expression representative images are shown in panel D. Scale bar 20 μm.

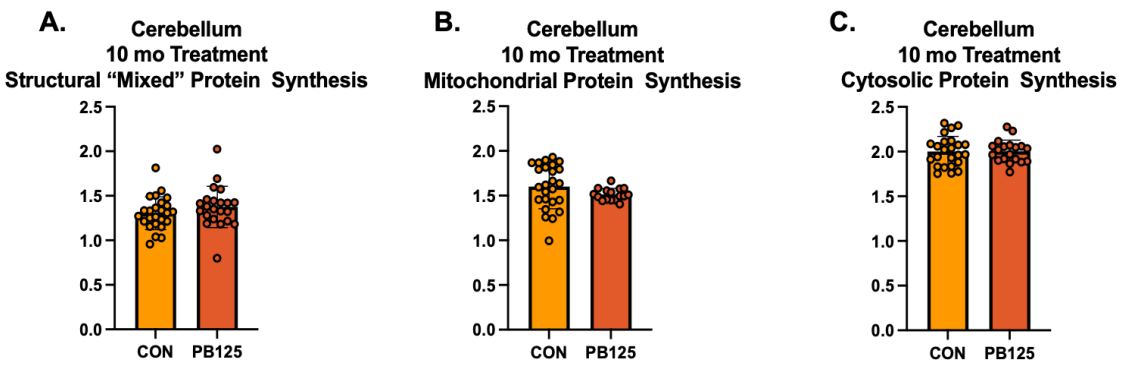

Figure 4.8. Long-term PB125 does not alter rates of cerebellar protein synthesis. 10 mo of PB125 treatment in the cerebellum of Hartley guinea pigs did not alter rates of structural or mixed (A), mitochondrial (B), and cytosolic (C) protein synthesis.

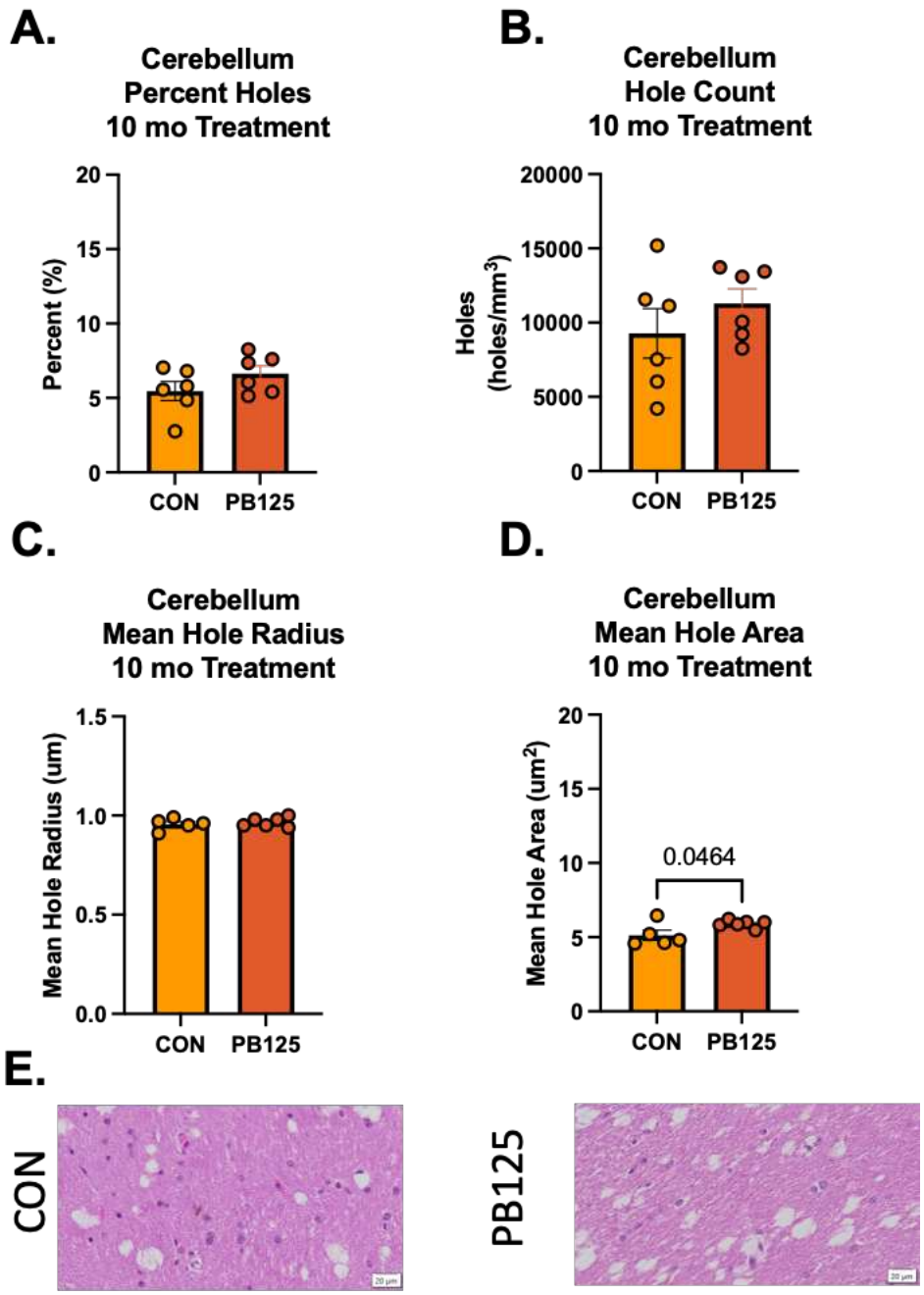

Figure 4.9. Long-term PB125 treatment does not alter the degree of cerebellar spongiosis. Measure of hole percentage (A), number of holes (B) or the mean hole radius (C) after 10 mo of PB125 treatment in the cerebellum of Hartley guinea pigs. However, PB125 did significantly increase or the mean hole area (D). However, collectively, the spongiotic phenotype did not change with 10 mo of PB125 treatment. Scale bar 20 μm.

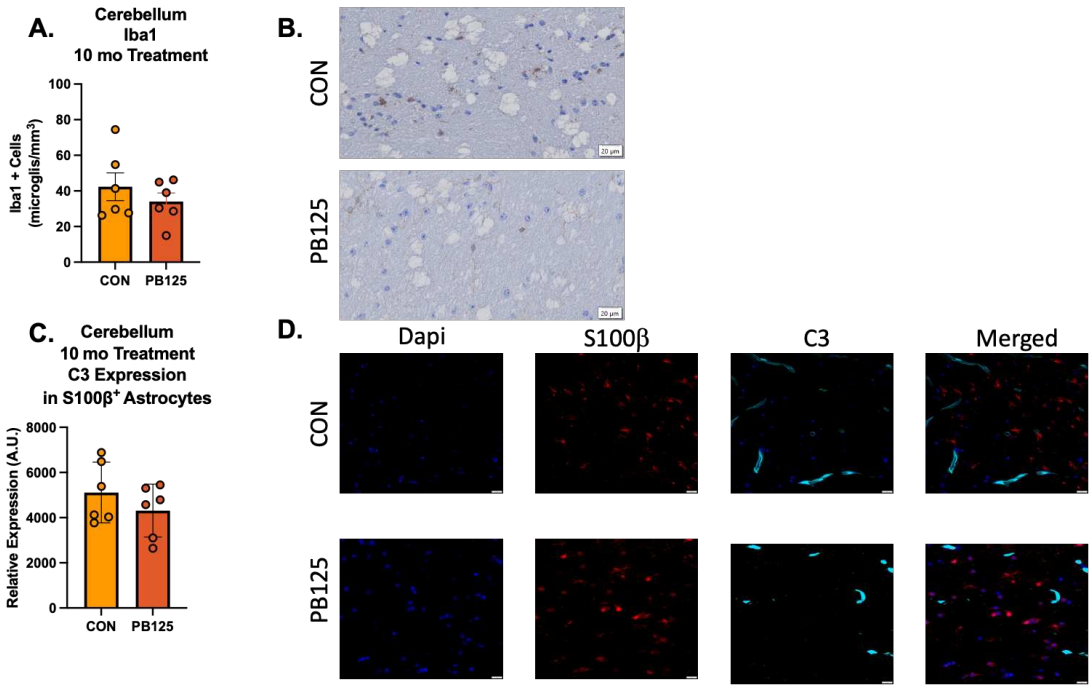

Figure 4.10. Long-term PB125 treatment does not alter Iba1 in microglia or C3 expression in astrocytes. Iba1, a measure of microgliosis, did not change with 10 mo of PB125 treatment in the cerebellum of Hartley guinea pigs (A). Iba1 representative images are shown in panel B. Additionally, C3 in astrocytes did not change with 3 mo of PB125 treatment in the cerebellum of Hartley guinea pigs (C). C3 expression representative images are shown in panel D. Scale bar 20 μm.

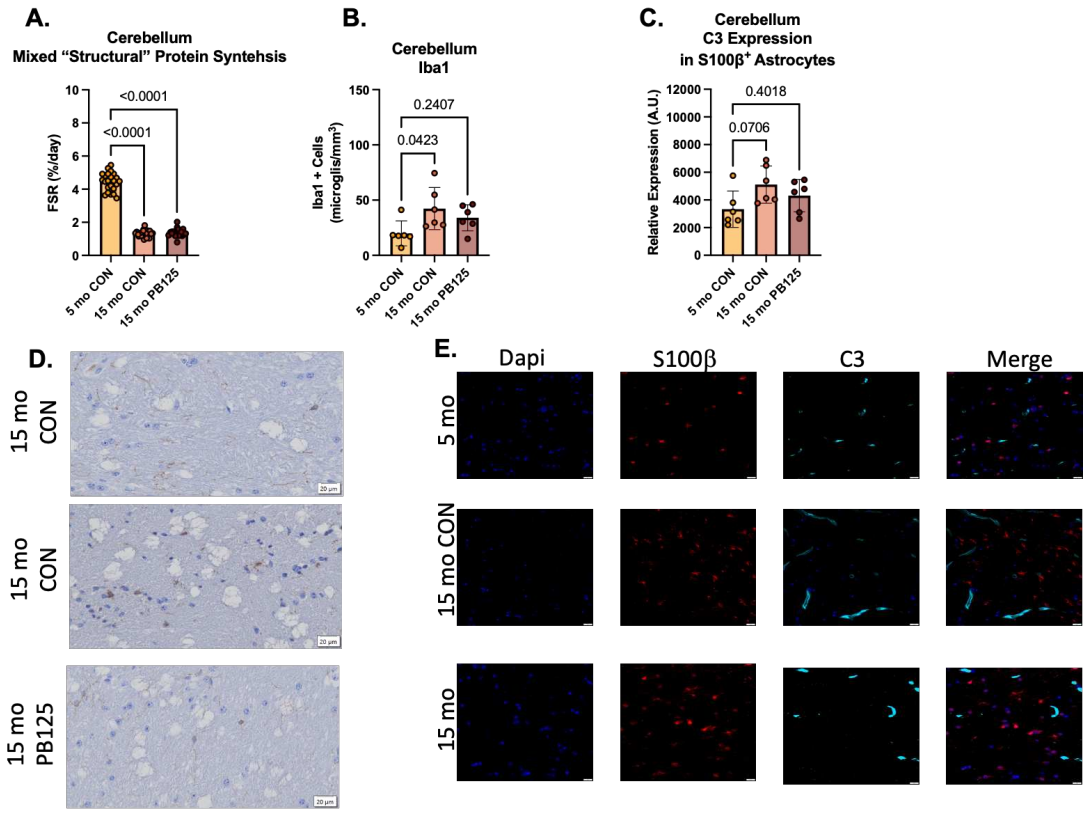

Figure 4.11. Long-term PB125 attenuates some markers of cerebellar brain aging. From 5 to 15 mo rates of structural or mixed protein synthesis significantly decreased with age and this was not attenuated with PB125 treatment in the cerebellum (A). However, Iba1 also increased from 5 to 15 mo, but it was attenuated with 10 mo of PB125 treatment in the cerebellum (B). Similarly, astrocytes expressing C3 trended to increase ($p = 0.0706$) from 5 to 15 mo, but it was attenuated with 10 mo of PB125 treatment in the cerebellum (C). Representative images for Iba1 and astrocytes expressing C3 are shown respectively in panels C and E. Scale bar 20 μm.

REFERENCES

1. Arleo A, Bareš M, Bernard JA, et al. Consensus Paper: Cerebellum and Ageing. Cerebellum. Published online 2023:1-31. doi:10.1007/s12311-023-01577-7

2. Haldipur P, Millen KJ, Aldinger KA. Human Cerebellar Development and Transcriptomics: Implications for Neurodevelopmental Disorders. Annu Rev Neurosci. 2022;45(1):515-531. doi:10.1146/annurev-neuro-111020-091953

3. Studenski S, Perera S, Patel K, et al. Gait Speed and Survival in Older Adults. JAMA. 2011;305(1):50-58. doi:10.1001/jama.2010.1923

4. Stanaway FF, Gnjidic D, Blyth FM, et al. How fast does the Grim Reaper walk? Receiver operating characteristics curve analysis in healthy men aged 70 and over. Bmj Br Medical J. 2011;343(dec15 1):d7679. doi:10.1136/bmj.d7679

5. Bernard JA. Don't forget the little brain: A framework for incorporating the cerebellum into the understanding of cognitive aging. Neurosci Biobehav Rev. 2022;137:104639. doi:10.1016/j.neubiorev.2022.104639

6. Santangelo KS, Bertone AL. Effective reduction of the interleukin-1β transcript in osteoarthritis-prone guinea pig chondrocytes via short hairpin RNA mediated RNA interference influences gene expression of mediators implicated in disease pathogenesis. Osteoarthr Cartilage. 2011;19(12):1449-1457. doi:10.1016/j.joca.2011.09.004

7. Santangelo KS, Kaeding AC, Baker SA, Bertone AL. Quantitative Gait Analysis Detects Significant Differences in Movement between Osteoarthritic and Nonosteoarthritic Guinea Pig Strains before and after Treatment with Flunixin Meglumine. Arthritis. 2014;2014:503519. doi:10.1155/2014/503519

8. Musci RV, Walsh MA, Konopka AR, et al. The Dunkin Hartley Guinea Pig Is a Model of Primary Osteoarthritis That Also Exhibits Early Onset Myofiber Remodeling That Resembles Human Musculoskeletal Aging. Front Physiol. 2020;11:571372. doi:10.3389/fphys.2020.571372

9. Radakovich LB, Marolf AJ, Culver LA, Santangelo KS. Calorie restriction with regular chow, but not a high-fat diet, delays onset of spontaneous osteoarthritis in the Hartley guinea pig model. Arthritis Res Ther. 2019;21(1):145. doi:10.1186/s13075-019-1925-8

10. Krieglstein J, Kewitz T, Kirchhefer U, et al. Damage of Guinea Pig Heart and Arteries by a Trioleate-Enriched Diet and of Cultured Cardiomyocytes by Oleic Acid. Plos One. 2010;5(3):e9561. doi:10.1371/journal.pone.0009561

11. Wahl D, Moreno JA, Santangelo KS, et al. Non-Transgenic Guinea Pig Strains Exhibit Hallmarks of Human Brain Aging and Alzheimer's Disease. Journals Gerontology Ser. Published online 2022. doi:10.1093/gerona/glac073

12. Díaz-Delgado J, Whitley DB, Storts RW, Heatley JJ, Hoppes S, Porter BF. The Pathology of Wobbly Hedgehog Syndrome. Vet Pathol. 2018;55(5):711-718. doi:10.1177/0300985818768033

13. Musci RV, Andrie KM, Walsh MA, et al. Phytochemical compound PB125 attenuates skeletal muscle mitochondrial dysfunction and impaired proteostasis in a model of musculoskeletal decline. J Physiology. Published online 2022. doi:10.1113/jp282273

14. Andrie KM, Palmer DR, Wahl O, et al. Treatment with PB125® Increases Femoral Long Bone Strength in 15-Month-Old Female Hartley Guinea Pigs. Ann Biomed Eng. Published online 2023:1-11. doi:10.1007/s10439-023-03415-7

15. Brisendine MH, Nichenko AS, Bandara AB, et al. Neuromuscular dysfunction precedes cognitive impairment in a mouse model of Alzheimer's Disease. Function. Published online 2023:zqad066. doi:10.1093/function/zqad066

16. Hybertson BM, Gao B, Bose S, McCord JM. Phytochemical Combination PB125 Activates the Nrf2 Pathway and Induces Cellular Protection against Oxidative Injury. Antioxidants. 2019;8(5):119. doi:10.3390/antiox8050119

17. Martinez W, Zhang Q, Linden MA, et al. Rates of protein synthesis are maintained in brain but reduced in skeletal muscle during dietary sulfur amino acid restriction. Frontiers Aging. 2022;3:975129. doi:10.3389/fragi.2022.975129

18. Walsh MA, Zhang Q, Musci RV, Hamilton KL. The combination of NRF1 and Nrf2 activators in myoblasts stimulate mechanisms of proteostasis without changes in mitochondrial respiration. Redox Muscle Physiology Exerc Sport. Published online 2022:100001. doi:10.1016/j.rimpes.2022.100001

19. Busch R, Kim YK, Neese RA, et al. Measurement of protein turnover rates by heavy water labeling of nonessential amino acids. Biochimica Et Biophysica Acta Bba - Gen Subj. 2006;1760(5):730-744. doi:10.1016/j.bbagen.2005.12.023

20. Miller BF, Reid JJ, Price JC, Lin HJL, Atherton PJ, Smith K. CORP: The use of deuterated water for the measurement of protein synthesis. J Appl Physiol. 2020;128(5):1163-1176. doi:10.1152/japplphysiol.00855.2019

21. Latham AS, Geer CE, Ackart DF, et al. Gliosis, misfolded protein aggregation, and neuronal loss in a guinea pig model of pulmonary tuberculosis. Frontiers Neurosci. 2023;17:1157652. doi:10.3389/fnins.2023.1157652

22. Rocha SM, Kirkley KS, Chatterjee D, Aboellail TA, Smeyne RJ, Tjalkens RB. Microglia-specific knock-out of NF-κB/IKK2 increases the accumulation of misfolded α-synuclein through the inhibition of p62/sequestosome-1-dependent autophagy in the rotenone model of Parkinson's disease. Glia. 2023;71(9):2154-2179. doi:10.1002/glia.24385

23. Liddelow SA, Guttenplan KA, Clarke LE, et al. Neurotoxic reactive astrocytes are induced by activated microglia. Nature. 2017;541(7638):481-487. doi:10.1038/nature21029

24. Brach JS, Lowry K, Perera S, et al. Improving Motor Control in Walking: A Randomized Clinical Trial in Older Adults With Subclinical Walking Difficulty. Arch Phys Med Rehabilitation. 2015;96(3):388-394. doi:10.1016/j.apmr.2014.10.018

25. Nascimento M de M, Gouveia ÉR, Gouveia BR, et al. Associations of Gait Speed, Cadence, Gait Stability Ratio, and Body Balance with Falls in Older Adults. Int J Environ Res Public Heal. 2022;19(21):13926. doi:10.3390/ijerph192113926

26. Wolff CA, Lawrence MM, Porter H, et al. Sex differences in changes of protein synthesis with rapamycin treatment are minimized when metformin is added to rapamycin. Geroscience. Published online 2020:1-20. doi:10.1007/s11357-020-00243-8

27. Eng LF, Ghirnikar RS, Lee YL. Glial Fibrillary Acidic Protein: GFAP-Thirty-One Years (1969–2000). Neurochem Res. 2000;25(9-10):1439-1451. doi:10.1023/a:1007677003387

28. Ohsawa K, Imai Y, Sasaki Y, Kohsaka S. Microglia/macrophage-specific protein Iba1 binds to fimbrin and enhances its actin-bundling activity. J Neurochem. 2004;88(4):844-856. doi:10.1046/j.1471-4159.2003.02213.x

29. Davis N, Mota BC, Stead L, et al. Pharmacological ablation of astrocytes reduces Aβ degradation and synaptic connectivity in an ex vivo model of Alzheimer's disease. J Neuroinflammation. 2021;18(1):73. doi:10.1186/s12974-021-02117-y

30. Paolicelli RC, Sierra A, Stevens B, et al. Microglia states and nomenclature: A field at its crossroads. Neuron. 2022;110(21):3458-3483. doi:10.1016/j.neuron.2022.10.020

31. Escartin C, Galea E, Lakatos A, et al. Reactive astrocyte nomenclature, definitions, and future directions. Nat Neurosci. 2021;24(3):312-325. doi:10.1038/C1593-020-00783-4

32. Rezaie T, McKercher SR, Kosaka K, et al. Protective Effect of Carnosic Acid, a Pro-Electrophilic Compound, in Models of Oxidative Stress and Light-Induced Retinal Degeneration. Investigative Opthalmology Vis Sci. 2012;53(12):7847. doi:10.1167/iovs.12-10793

33. Sawmiller D, Li S, Shahaduzzaman M, et al. Luteolin Reduces Alzheimer's Disease Pathologies Induced by Traumatic Brain Injury. Int J Mol Sci. 2014;15(1):895-904. doi:10.3390/ijms15010895

34. Ram N, Peak SL, Perez AR, Jinwal UK. Implications of Withaferin A in neurological disorders. Neural Regen Res. 2020;16(2):304-305. doi:10.4103/1673-5374.290894

35. Manach C, Williamson G, Morand C, Scalbert A, Rémésy C. Bioavailability and bioefficacy of polyphenols in humans. I. Review of 97 bioavailability studies 2. Am J Clin Nutr. 2005;81(1):230S-242S. doi:10.1093/ajcn/81.1.230s

36. Hostetler GL, Ralston RA, Schwartz SJ. Flavones: Food Sources, Bioavailability, Metabolism, and Bioactivity. Adv Nutr. 2017;8(3):423-435. doi:10.3945/an.116.012948

37. Boersma MG, Woude H van der, Bogaards J, et al. Regioselectivity of Phase II Metabolism of Luteolin and Quercetin by UDP-Glucuronosyl Transferases. Chem Res Toxicol. 2002;15(5):662-670. doi:10.1021/tx0101705

38. Cho YC, Park J, Cho S. Anti-Inflammatory and Anti-Oxidative Effects of luteolin-7-O-glucuronide in LPS-Stimulated Murine Macrophages through TAK1 Inhibition and Nrf2 Activation. Int J Mol Sci. 2020;21(6):2007. doi:10.3390/ijms21062007

39. Arosio B, Calvani R, Ferri E, et al. Sarcopenia and Cognitive Decline in Older Adults: Targeting the Muscle–Brain Axis. Nutrients. 2023;15(8):1853. doi:10.3390/nu15081853

CHAPTER 5 – NON-TRANSGENIC GUINEA PIG STRAINS EXHIBIT DIVERGENT AGE-RELATED CHANGES IN HIPPOCAMPAL MITOCHONDRIAL RESPIRATION

INTRODUCTION

Alzheimer's disease (AD) is the most common form of dementia and advancing age is the number one risk factor for AD. The incidence of AD is expected to increase three-fold in the next 30 years, paralleling the increase in older adults [1]. However, there has not been a matched increase in disease-modifying treatments for AD leading to a ~150% increase in AD mortality [2]. While more than 150 rodent models of AD are used in laboratories [3], translation of promising drugs for AD treatment from the laboratory to humans typically fails [4–6]. One reason contributing to this poor translation rate is the absence of laboratory models of spontaneous, progressive neurodegeneration that also encompass the multi-morbidities (>2 chronic illnesses) characteristic of human aging [7]. While there are preclinical animals modeling familial AD [8], 90-95% of human AD cases are sporadic (non-genetic), with an onset occurring later in life [9,10]. Although current murine AD models have helped expand the basic understanding of brain aging and AD pathophysiology, they have not assisted in compressing the translational gap for treatment development. Arguably, an ideal translational preclinical model would be a non-transgenic animal that mimics the spontaneous, progressive, age-related neurodegeneration observed in humans alongside other multi-morbidities of aging.

While the pathological hallmarks of AD including amyloid beta (Aβ) deposition, neurofibrillary tangles, and cerebral atrophy are well characterized, the exact etiology of AD remains in question [11]. Furthermore, in the absence of diagnosed AD, older adults can present with some of these same hallmark pathologies [12]. Therefore, several hypotheses

[2] In revision at Acta Physiologica authored by Maureen A. Walsh, Amanda S. Latham, Qian Zhang, Robert A. Jacobs, Thomas J. LaRocca, Julie A. Moreno, Kelly S. Santangelo, Karyn L. Hamilton

have been developed to explain the spatial and temporal nature of brain aging and AD hallmarks. Prominent among these is the mitochondrial cascade hypothesis was proposed ~20 years ago, postulating that multifaceted mitochondrial dysfunction contributes to Aβ dyshomeostasis driving the development and progression of AD [13]. While mitochondria have numerous functions [14], decreases in respiration, increases in reactive oxygen species production, calcium handling impairments, and mitophagy defects [15,16] are all implicated as contributors to neuroinflammation in the hippocampus which precedes Aβ accumulation [17]. While all these mitochondrial functions impacted in AD are important, they are also all energy dependent. Specifically, using post-mortem brain samples those with AD had significantly lower complex II and complex IV oxygen consumption compared to age-matched controls [15]. Additionally, peripheral mitochondrial respiration declines with age and neurodegenerative disease progression [15,18,19]. Therefore, mitochondrial respiration is arguably the most critical mitochondrial function to assess as it could be a therapeutic target to delay the onset and/or prevent the progression of brain aging and AD [13,20]. Further, assessing complex-specific respiration in addition to overall mitochondrial respiratory potential is pertinent in preclinical models. Various metrics of intact platelet mitochondrial respiration including basal respiration, non-coupled respiration, and mitochondrial reserve capacity are lower in older adults with AD compared to cognitively healthy older adults independent of plasma concentrations of Aβ [21]. Further, hallmarks of brain aging encompass similar multifaceted mitochondrial changes such as reticular enlargement or fragmentation, increased damage to mitochondrial DNA [22] from oxidants, reduced respiration, and compromised calcium handling suggesting that even in the absence of diagnosed AD, dysfunctional mitochondria may drive neurodegeneration.

The Hartley guinea pig (HGP) is a non-transgenic model that displays multi-morbidities characteristic of human aging. Beginning at 3-4 month (mo) of age, HGPs develop progressive osteoarthritis, which is accompanied by local and systemic inflammation [23–25]. From 5 to 15 mo, we have observed decreased mechanisms to maintain skeletal muscle proteostasis,

changes in myofiber distribution, and decreases in skeletal muscle density [26], all mimicking the skeletal muscle remodeling typically accompanying advancing age [27] and osteoarthritis in humans [28]. By ~18 mo, mobility is severely constrained, typically prompting euthanasia. HGPs additionally develop vascular disease [29] and obesity [30] with age which can also be present in AD [31,32]. Evidence suggests that, in humans, musculoskeletal decline and cognitive impairment associated with age-related neurodegeneration frequently coexist, with one disability increasing the rate of progression of the other [33]. Specifically, declines in mitochondrial respiration occur in both central and peripheral tissues. We have previously shown that there is an age-related decline in peripheral skeletal muscle mitochondrial respiration [34] but have not assessed it in the brain. When preclinically modeling brain aging and AD-related mitochondrial dysfunction it is imperative that the animal recapitulates both central and peripheral metabolic declines observed in humans. Therefore, the HGP might be a valuable model for studying age-related neurodegeneration and AD.

Our group recently reported that HGPs have signs of progressive hippocampal neurodegeneration [35]. From 5 to 15 mo of age, there are increases in circulating neurofilament light chain, neurofibrillary tangles, Aβ accumulation, and glial activation consistent with human AD [35]. Guinea pigs also share the same Aβ amino acid sequence homology with humans [36]. Because of these similarities, we examined brain transcriptomic changes in older 15 mo HGPs and compared them to another 15 mo outbreed PigmEnTed (PET) guinea pig strain. We found that gene expression relating to mitochondrial function was particularly decreased in older HGPs compared to older PETs [35]. However, PET guinea still exhibited some hallmarks of typical brain aging compared to older adults without AD [35] (suggesting their utility as a control strain for disentangling brain aging from neurodegeneration characteristic of AD). To date there has not been a study assessing comprehensive aspects of mitochondrial respiratory control in non-transgenic guinea pigs that additionally model neurodegeneration and other multi-morbidities of aging.

Based on the observations above, the purpose of this study was to evaluate complex-specific changes in hippocampal mitochondrial respiration and protein content in PET and HGPs from 5 to 12 mo. We hypothesized that older HGPs but not PET guinea pigs compared to their younger counterparts would have 1) impaired complex I supported ADP kinetics; 2) lower submaximal and maximal complex I and II respiration; 3) lower maximal complex II respiration; 4) lower maximal complex IV respiration; 5) decreased mitochondrial protein content.

METHODS

Husbandry

All procedures were approved by the Colorado State University Institutional Animal Care and Use Committee and were performed in accordance with the NIH Guide for the Care and Use of Laboratory Animals. Hartley and PET male guinea pigs were obtained from Elm Hill Laboratories (Chelmsford, MA, USA) at 4- and 11- mo of age and housed for one mo (n=12/group; total n = 48); final harvest ages were 5 and 12 mo (Figure 5.1A). Animals were housed at Colorado State University's Laboratory Animal Resources facilities and were monitored daily by veterinary staff. All guinea pigs were singly housed in solid bottom cages, maintained on a 12-12-hour (hr) light-dark cycle, and provided *ad libitum* access to food and water. Animals were fasted for 6 hrs prior to euthanasia. In accordance with the standards of the American Veterinary Medical Association, animals were anesthetized with a mixture of isoflurane and oxygen; thoracic cavities were opened, and blood was collected via direct cardiac puncture. One 12-month-old guinea pig died prior to final tissue collection due to reasons unrelated to the study; no gross pathology was observed on necropsy.

Mitochondrial respirometry

Immediately after euthanasia, ~50 mg of the hippocampus was placed in BIOPS (10 mM Ca-EGTA buffer, 0.1 μM free calcium, 20 mM imidazole, 20 mM taurine, 50 mM K-MES, 0.5 mM DTT, 6.56 mM MgCl2, 5.77 mM ATP, 15 mM phosphocreatine; pH 7.10 at 0° C) and kept on ice for transport. Samples did not sit in BIOPS on ice longer than ~6 hrs prior to respiration.

Approximately ~5 mg (wet weight) samples of hippocampus were placed in mitochondrial respiration medium, MiR05, (0.5 mM EGTA, 3 mM $MgCl_2$ * $6H_2O$, 60 mM lactobionic acid, 20 mM taurine, 10 mM KH_2PO_4, 20 mM HEPES, 110 mM D-sucrose, 1 g/L fatty acid-free BSA; pH 7.10 at 21° C in an Oxygraph-2k (O2k) (Oroboros, Innsbruck, Austria) for high-resolution respirometry. To control for oxygen flux at higher concentrations of oxygen, each morning of respirometry analysis, we conducted high oxygen concentration calibrations at 650, 550, 450, 350, 250, and 167 (i.e., concentration of room air) nmol/ml O_2 [37]. During the experiments, oxygen concentrations were maintained between 225 – 650 nmol/ml O_2. High-resolution respirometry measurements were performed in duplicate using two different protocols. Please refer to Supplemental Table D.1 for a detailed explanation of the protocols.

Tissue was placed in each O2k chamber with subsequent hyper-oxygenation to ~650 nmol/ml O_2. Chemical permeabilization after tissue had been placed in each O2k chamber with 50 µg/µl of freshly prepared saponin according to previously reported methods [38]. The first protocol, a Substrate Uncoupler Inhibitor Titration (SUIT 1), was an ADP titration protocol to test hypothesis 1, that older HGPs but not PETs would have impaired complex I supported ADP kinetics. The ADP titration determines maximal oxidative capacity (Vmax) and ADP sensitivity (Km), the amount of ADP to achieve ½ Vmax and measure of ADP sensitivity under complex I supported respiration. We measured complex I supported leak respiration (State $2_{[PGM]}$) with the addition of 10 mM glutamate, 0.5 mM malate, and 5 mM pyruvate. Upon acquisition of State $2_{[PGM]}$, we titrated progressively greater concentrations of ADP from 0.05 mM, 0.1 mM, 0.15 mM, 0.2 mM, 0.25 mM, 0.5 mM, 1 mM, 2 mM, 4 mM, 8 mM (State $3_{[PGM]}$), awaiting steady-state oxygen flux prior to adding the subsequent titration to determine complex I linked ADP Vmax and apparent Km (i.e., ADP sensitivity). After the ADP titration was completed, we added 5 mM cytochrome C to test mitochondrial membrane integrity. After cytochrome C addition, we added 10 mM succinate to acquire maximal complex I and II supported coupled respiration (State $3_{[PGMS]}$). We then added 0.5 µM FCCP sequentially until there was no increase in respiration to

determine the capacity of the electron transport system to consume oxygen, or maximal non-coupled respiration ($ETS_{[CI-CIV]}$). Finally, we added 5 μM rotenone to measure maximal non-coupled respiration with the inhibition of complex I ($ETS_{[CII-CIV]}$), followed by 2.5 μM Antimycin A to measure residual oxygen consumption (ROX). We then calculated the respiratory control ratio (RCR) as State $3_{[PGM]}$/State $2_{[PGM]}$ as a measure of mitochondrial coupling efficiency where a higher ratio is indicative of greater mitochondrial efficiency of oxygen consumption coupled to ATP production [34]. When fitting the Michaelis-Menten kinetics we noticed that at higher concentrations of ADP >1mM with the ADP titration there were inhibitory effects on oxygen consumption (data not shown), but this is well reported in the literature [39]. Therefore, the kinetics data was fit to the step where there was a plateau in oxygen consumption which was 1 mM ADP. We selected to go beyond 1 mM with our titration to ensure if there was a robust age or strain difference it would be captured.

The second protocol (SUIT 2) was designed to test the hypotheses 2, 3, and 4 to assess complex I and II submaximal and maximal respiration, maximal complex II respiration, and maximal complex IV respiration, respectively. First, oxygen consumption was measured after stimulating maximal leak respiration with pyruvate, glutamate, malate, and succinate. Next, submaximal (0.5 mM: State 3 CI – CIV $_{[PGMS + 0.5D]}$) and maximal (1 mM: State 3 CI – CIV $_{[PGMS + 1D]}$), boluses of ADP were added followed by a supra-saturating bolus of ADP (6.0 mM: State 3 CI – CIV $_{[PGMS+ 6D]}$). Next, 5 mM cytochrome C was added to test mitochondrial membrane integrity. The cytochrome C control flux control factor was 0.25 based on a threshold of a negative linear relationship between the cytochrome C control flux factor and State 3 respiration in the SUIT protocols (Figure D.1). Upon eliminating respirometry trials that had a cytochrome C control factor of greater than 0.25, the negative linear relationship no longer existed, and all samples included in analysis were not biased by over-permeabilization, which is what the cytochrome C control factor approximates (Figure D.1) [40]. This is also the threshold that was calculated in permeabilized skeletal muscle of guinea pigs [34]. After cytochrome C, 5 μM

rotenone (i.e., inhibitor of complex I) was added to determine maximal complex II coupled respiration (State 3 CII – CIV $_{[PGMS+ 6D]}$) followed by sequential titrations of 0.5 µM FCCP until respiration no longer increased to determine maximal supported non-coupled respiration (ETS CII – CIV $_{[PGMS+ 6D]}$). and added 2.5 µM antimycin A to measure ROX. Maximal complex IV respiration was achieved by titrating 2 mM ascorbate and 0.5 mM TMPD as previously described [38]. To correct for background autooxidation we perform a background experiment with the SUIT 2 substrates without a sample for each POS sensor and subtracted the background flux from the flux calculated in experimental conditions [38].

Protein content

Western blotting was used to test hypothesis #5 by measuring relative content of OXPHOS protein content in a subset of tissues as previously described by our group [41]. An n=6 animals/group were used to ensure all comparisons were made on the same gel/membrane. 15 - 30 mg portions of the hippocampus were homogenized in a Bullet Blender with zirconium beads and 0.3 mL of radioimmunoprecipitation assay (RIPA) buffer (150 mM NaCl, 0.1 mM EDTA, 50 mM Tris, 0.1% sodium deoxycholate, 0.1% SDS, 1% Triton X-100, pH = 7.50) with HALT protease inhibitors. Protein concentration was determined with BCA assay (ThermoFisher 23225). Samples were reduced (50 µL of B-mercaptoethanol and 950 µL of 2x laemmli sample buffer BioRad 1610737) and heated at 50^{o}C for 10 min. Approximately 20 µg of protein was loaded into a 4% - 20% Criterion pre-cast gel (Bio-Rad, Hercules, CA, USA) and resolved at 120 V for 120 min. The proteins were then transferred at 60 V for 105 min in transfer buffer (20% w/v methanol, 0.02% w/v SDS, 25 mM Tris Base, 192 mM glycine, pH = 8.3). Membranes were then blocked (5% BSA in TBST) and incubated with primary antibodies (1% non-fat milk in PBS; 1:1,000) against total OXPHOS proteins (Abcam 110413, Lot # Q5039) on a shaker overnight in 4^{o}C. Membranes were rinsed and then incubated with appropriate secondary antibodies for (5% BSA in TBST; 1:10,000) OXPHOS (goat anti-mouse Santa Cruz 2005, Lot # D1614). After the membranes were rinsed, Western Lightening ECL Enhanced

(Perkin Elm NEL104001EA) was applied and the membranes were subsequently imaged using a FluorChem E Chemiluminescence Imager (Protein Simple, San Diego, CA, USA). Analysis of densitometry was completed using AlphaView SA Software. Units are expressed as density of primary antibody relative to density of amido black as previously described [41].

Statistical analysis

In line with best practices, technical replicates were averaged for the mitochondrial respiration data [42]. Apparent Km and Vmax values were determined using Michaelis-Menten kinetics as previously described [34,41]. For anthropometrics, mitochondrial respiration, and protein content 2-way ANOVAs were used to measure the interaction of age and strain. Post-hoc analyses were performed using Tukey's post-hoc test. If a significant interaction was determined, strains were separated, and an independent t-test was used to determine the effect of age within a given strain. Because this was a pilot study with first-ever measurements of hippocampal mitochondrial respirometry in HGPs, we reported significant differences at a p-value < 0.05, but also included statistical trends p-value < 0.10. All statistical analyses were performed in Prism 8.0 (La Jolla, California, USA).

RESULTS

Anthropometrics

Body mass was greater at 12 mo compared to 5 mo in both PET and HGPs (Figure 5.1B), with no age-related differences in brain weight (Figure 5.1C). However, when brain mass was expressed relative to body mass, this ratio was significantly lower at 12 mo compared to 5 mo in both strains (Figure 5.1D).

Mitochondrial respiration

Two separate SUIT protocols were used to determine ADP kinetics (SUIT 1) and complex-specific respiration (SUIT 2) through carefully planned titrations of submaximal and maximal boluses of adenylates as well as complex-specific inhibitors. For SUIT 1, an ADP titration, each sample was fit to a Michaelis-Menten plot to calculate ADP Vmax and Km (Figure

5.2B). There was a significant age by strain interaction for ADP Vmax (Figure 5.2C) wherein PET guinea pigs had a significant increase in maximally stimulated ADP Vmax from 5 to 12 mo of age paralleling the increase of body mass and growth (Figure 5.2D). However, HGPs had a non-significant decrease in ADP Vmax (Figure 5.2E). ADP sensitivity as assessed by the Km values highlights differences at submaximal respirometry potential [34,41]. Similarly, to the ADP Vmax there was a significant age by strain interaction in ADP sensitivity (Figure 5.2F), but age-changes within strains were not different for PET and HGPs (Figure 5.2G and H) suggesting the interaction was driven by the age-related changes in ADP Vmax and not submaximal capacity which has been observed before [34]. The respiratory control ratio (RCR) is the ratio of maximally stimulated ATP production to LEAK respiration and a metric of mitochondrial coupling efficiency (higher ratio is indicative of greater mitochondrial efficiency of oxygen consumption coupled to ATP production). There was a trend ($p = 0.0812$) or an age by strain interaction in RCR (Figure 5.2I). HGPs had a significant decrease in RCR from 5 to 12 mo (Figure 5.2K) while there was no change for the PET guinea pigs (Figure 5.2J).

The SUIT 2 protocol allowed us to interrogate complex-specific mitochondrial respiration as well as submaximal and maximal complex I and II stimulated respiration testing the hypothesis that HGPs would have complex I, II, and IV impaired respiration with age compared to the PET guinea pigs (Figure 5.3B). At a submaximal bolus of 0.5 mM ADP under complex I and II supported respiration with pyruvate, glutamate, malate, and succinate there were no age or strain differences (Figure 5.3C). The lack of differences also persisted with maximal (1 mM ADP) and supra-maximal (6 mM ADP) complex I and II supported respiration (Figures 5.3D and E, respectively). To determine if any differences were present at the level of complex I, rotenone, was added to inhibit complex I and again there were no age or strain differences (Figure 5.3F). Next, the protonophore, FCCP, was added to examine the reserve capacity through uncoupling the electrochemical gradient of the inner mitochondrial membrane and there were also no differences (Figure 5.3G). Finally, complex IV specific respiration was achieved

through addition of ascorbate and TMPD where there were also no differences (Figure 5.3H). Thus, the collective respirometry findings suggest that maximally stimulated complex I specific respiration (Figure 5.2C) and complex I mitochondrial efficiency (Figure 5.2K) may mediate the pathological changes observed in the hippocampi of HGPs with age.

Mitochondrial protein content

Because there were divergent changes in mitochondrial respiration in HGPs and PET guinea pigs, we sought to determine if they were driven by an increase or maintenance (for the PETs) and/or a decrease (for the HGPs) in mitochondrial protein content. Using an OXPHOS western blot, which semi-quantitively determines the relative protein content of one component of each of the five distinct mitochondrial protein complexes, we found an overall effect of age to increase mitochondrial protein content in complexes I (Figure 5.4A), II (Figure 5.4D), IV (Figure 5.4J) as well as a trend ($p = 0.0700$) for complex V (Figure 5.4M). Because of the significant age by strain interaction in the respiration data, we also examined age differences within a strain. The age-related increases in protein content were entirely driven by the HGPs for complexes I, II, IV, and V (Figure 5.4C, F, L, O), with no differences in the PET guinea pigs between 5 and 12 mo (Figures 5.4B, E, H, K, N).

DISCUSSION

Although AD is the most common form of dementia, there is no cure. Decades of research have theorized the prominent cellular drivers of AD, including the mitochondrial cascade hypothesis [13]. In post-mortem human AD samples, evidence indicates a decrease in prefrontal cortex mitochondrial respiration [15]. Additionally, in humans with cognitive decline, skeletal mitochondrial respiration is impaired suggesting that peripheral declines in energetics parallel, are related to, and/or precede pathological AD [33]. However, to date there has not been a non-transgenic preclinical model that reflects the age/disease-related changes in brain mitochondrial respiration. Our lab has shown that the non-transgenic HGPs display hallmarks of AD similar to humans [35]. HGPs also develop progressive impairments in cartilage [24,25] and

skeletal muscle [26], two additional multi-morbidities of aging and risk factors for AD [43,44], Additionally, HGPs have age-related declines in peripheral skeletal muscle mitochondrial respiration [34]. Here we present three key findings regarding hippocampal mitochondrial function to strengthen the HGP as a model for brain aging and AD: 1. Despite increases in growth, HGPs do not have increased mitochondrial respiration with age, which is in contrast to the control PET guinea pigs; 2. With age, HGPs have a significant decrease in complex I efficacy; 3. Despite a decrease in mitochondrial efficiency, HGPs have a significant increase in mitochondrial protein content suggesting a mitohormetic compensatory change.

Key point #1. Divergent age-related changes in hippocampal ADP kinetics between Hartley and PET guinea pigs

The present study is the first in which guinea pig hippocampal samples were respired in an O2k using planned titrations to test our hypotheses in line with best practices [40]. The ADP titration (SUIT 1) is unique because it assesses both submaximal and maximal mitochondrial capacity through the provision of various substrates, inhibitors, and uncouplers. Specifically, when assessing mitochondrial respiration, it is critical that the *ex vivo* assays closely recapitulate *in vivo* conditions to increase the translational capacity of findings. In transgenic rodent models of AD there is a decrease in maximal complex I and complex II [45] respiration compared to the wildtype control; however, it is also important to note that these differences were exacerbated with age [45]. In our study, HGPs did not have any age-related changes in maximal stimulated complex I (Figure 5.2E) and complex I and II (Figure 5.3D and E) respiration, contrary to our hypotheses #1 and #2. However, because this was the first investigation of age-related changes in guinea pig hippocampal mitochondrial function, we also made comparisons with the non-transgenic PET guinea pig that has less severe brain age-related changes. PET guinea pigs had a significant increase in maximally stimulated complex I respiration (Figure 5.2D) suggesting that growth from 5 to 12 mo would in turn result in an increase in bioenergetic potential. Unlike post-mortem brain samples from humans with AD that

had lower complex II and complex IV oxygen age-matched controls, there were no age-related differences in complex II (Figures 5.3F) or complex IV (Figures 5.3H) respiration in either guinea pig strain (hypotheses #3 and #4). However, the human experiments referenced were carried out in previously frozen tissue in the absence of adenylates, hence limiting the translatability to human *in vivo* bioenergetics [15].

Key point #2. Complex I mitochondrial efficiency is impaired with age in Hartley but not PET guinea pigs

Mitochondrial efficiency is defined as the ratio of phosphorylated ATP: oxygen consumed (P:O). The O2k directly measures oxygen consumed, an indirect measure of ATP production. Others have developed sensitive methods for tandemly assessing ATP production and oxygen consumption [46]; however, those methods were not feasible for this study. One calculated measure of mitochondrial efficiency is RCR, the ratio of maximally stimulated State 3 complex I respiration relating to State 2 respiration in the presence of reducing equivalents but absence of adenylates [42]. Here we observed that HGPs had a significant decrease in complex I RCR from 5 to 12 mo (Figure 5.2K) while PET guinea pigs (Figure 5.2J) did not have any age-related differences. A decrease in RCR with age also parallels what we have reported in permeabilized skeletal muscle in male HGPs from 5 to 15 mo [34]. Taken together, these observations indicate that HGPs, even while they are still growing, develop histopathological changes in the hippocampus [35] and decreased complex I mitochondrial function. These findings also parallel data showing cartilage degeneration [24,25] and myofiber remodeling [26] between these same ages, highlighting that HGPs also recapitulate other morbidities of advancing age.

Key point #3. Despite decreases in mitochondrial efficiency, Hartley but not PET guinea pigs have a compensatory increase in mitochondrial protein content

Since mitochondrial respiration is a hallmark of AD, it is imperative to disentangle where impairments lie in the intricate nuclear and mitochondrial encoded reticulum of five distinct

protein complexes. If impairments exist, determining the location is critical to target therapies at specific mitochondrial complexes. Because there was a difference in mitochondrial respiration in PET and HGPs, it is necessary to discern if these changes were in part due to changes in protein content. For example, in humans with AD evidence indicates a significant decrease in serum nuclear-encoded mitochondrial genes, but an increase in mitochondrial-encoded genes compared to age-matched controls with no cognitive impairment [47]. For example, in humans with AD compared to age-matched controls, expression of nuclear-encoded mitochondrial genes was lower, but mitochondrial-encoded genes were greater [47]. In our data, the complex IV subunit, MTCO1, (CIV protein in Abcam OXPHOS blot) is a mitochondrially encoded protein complex which was higher in older 12 mo HGPs compared to the younger 5 mo HGPs (Figure 5.4L) paralleling what is observed in humans. Additionally, in our current study, we observed a significant decrease in complex I efficiency likely resulted in a compensatory increase in signals to increase mitochondrial biogenesis. Collectively, this increase in protein content suggests a potential maladaptive hormetic change to compensate for decreases in respiration. Future studies should further interrogate the increase in OXPHOS proteins as well as measures of mitophagy which are also implicated in neurodegeneration and AD [48].

Limitations

Because this was a pilot study, it is important to acknowledge some limitations. First, this study was only conducted in males whereas our prior work was performed in both males and females. Because we have observed sex differences in skeletal muscle mitochondrial respiration [34] and other physiological parameters [49] in HGPs, this study should be repeated in females. Another critical consideration is the concentration of substrates used in the O2k assays. For example, the concentration of ADP in the mammalian brain is 0.021 mM [50]. However, most mitochondrial assays in rodent and human AD models are carried out with 2 mM ADP, a supraphysiological concentration, added as the first and often only titration of ADP in the assay [45,51]. In contrast, we opted to begin with a concentration approximately two times

higher than resting ADP, but our maximal ADP kinetics were calculated at a 1 mM ADP concentration. Additionally, cognitive decline is clinically assessed with measures of cognitive function, which we could not carry out within the confines of this study. Finally, we glean the histopathology data including increases in Aβ, phosphorylation of tau, and gliosis from prior analyses in 5 and 15 mo old HGPs and PET guinea pigs [35]; however, these high-resolution mitochondrial respirometry data were collected in hippocampus tissue from 12 mo animals. Inclusion of histopathological findings from 12 mo animals will be helpful for future studies.

Conclusions and Future Directions

Decreased mitochondrial respiration is a hallmark of brain aging and AD. The HGP could be used as a preclinical model of brain aging and possibly AD to test potential therapies targeting mitochondrial respiration. Given HGPs had significant decreases in complex I efficiency, targeting specific components of complex I to increase efficiency might be a valuable first avenue. PET guinea pigs serve as an insightful control group as they develop some hallmarks of brain aging [35] but not to the same degree as HGPs, helping to disentangle the differences of age versus disease related changes. Finally, by better modeling age-related chronic diseases preclinically, more progress can be made to translate findings into human clinical trials.

FIGURES

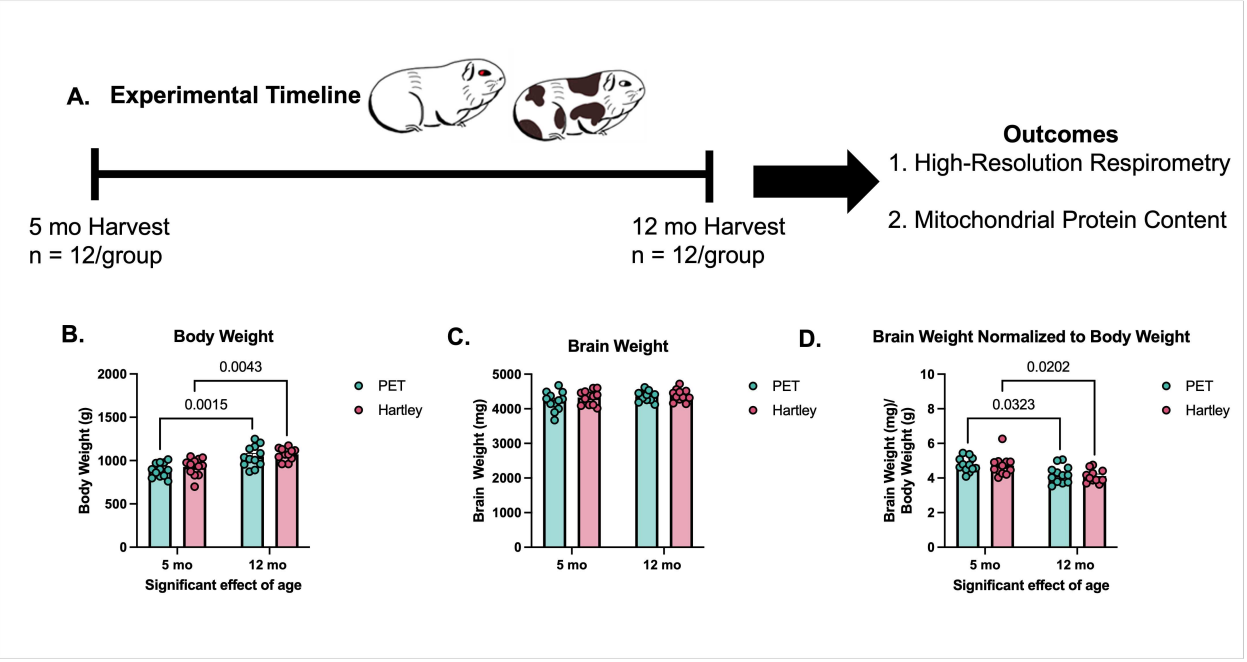

Figure 5.1. Study Design and Anthropometrics. Hippocampal samples from male PET and HGPs were collected at 5 and 12 mo of age (n = 12/age/strain; total N = 48 guinea pigs) to assess complex-specific mitochondrial oxygen consumption and protein content (A). Both PET and HGPs were heavier at 12 versus 5 mo of age (B), but there was no difference in whole brain weight (C). Interestingly, compared to their 5 mo counterparts 12 mo PET and HGPs had significantly lower relative brain weights (D). 5 mo PET n = 12; 5 mo Hartley n = 12; 12 mo PET n = 12; 12 mo Hartley n = 11 for all panels.

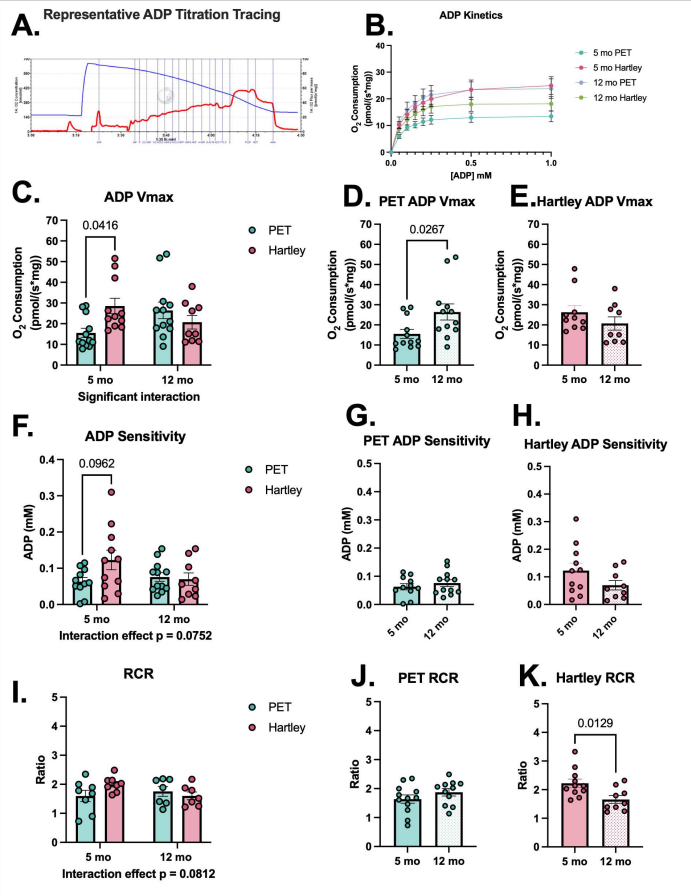

Figure 5.2. PET but not HGPs experience an age-related increase in complex I supported maximal mitochondrial respiration. The SUIT 1 ADP Titration assesses complex I supported (with glutamate, malate, and pyruvate) submaximal to maximal respiration to calculate the Vmax and Km values for maximal respiratory potential and ADP sensitivity, respectively. Panel A displays a raw tracing of the Oroboros O2k and Supplemental Table D.1 reports the protocols in detail. Averages of the Michaelis Menten curves are shown in panel B for each of the 4 groups. Interestingly, there was a significant age by strain interaction for ADP Vmax (C). Specifically, 5 mo HGPs had a significantly higher ADP Vmax compared to 5 mo PET guinea pigs. PET guinea pigs have a significant increase in ADP Vmax from 5 to 12 mo of age (D). However, HGPs had a non-significant decrease in ADP Vmax with age (E). There was a similar finding with ADP sensitivity, the amount of ADP required to achieve ½ Vmax, that there was an age by strain trend ($p = 0.0752$) for a significant interaction likely driven by the trend ($p = 0.0962$) that 5 mo HGPs had a lower ADP sensitivity versus 5 mo PETs (F). However, there were no differences in the PETs (G) or HGPs (H) from 5 to 12 mo. To understand where these changes lie in the mitochondrial reticulum the respiratory control ratio (RCR), as State 3 $_{[PGM]}$/State 2$_{[PGM]}$, a measure of mitochondrial coupling efficiency, where a higher ratio is indicative of greater mitochondrial efficiency of oxygen consumption coupled to ATP production. There was also a trend ($p = 0.0812$) for an age by strain interaction for RCR (I) where PET guinea pigs had no change in RCR (J) from 5 to 12 mo but HGPs had a significant decrease in complex I supported mitochondrial efficiency (K). 5 mo PET n = 12; 5 mo Hartley n = 12; 12 mo PET n = 12; 12 mo Hartley n = 9 for all panels. Two 12 mo HGPs were excluded from analysis because of cytochrome C responses. See methods and Figure D.1 to see how these thresholds were established in line with best practices [40].

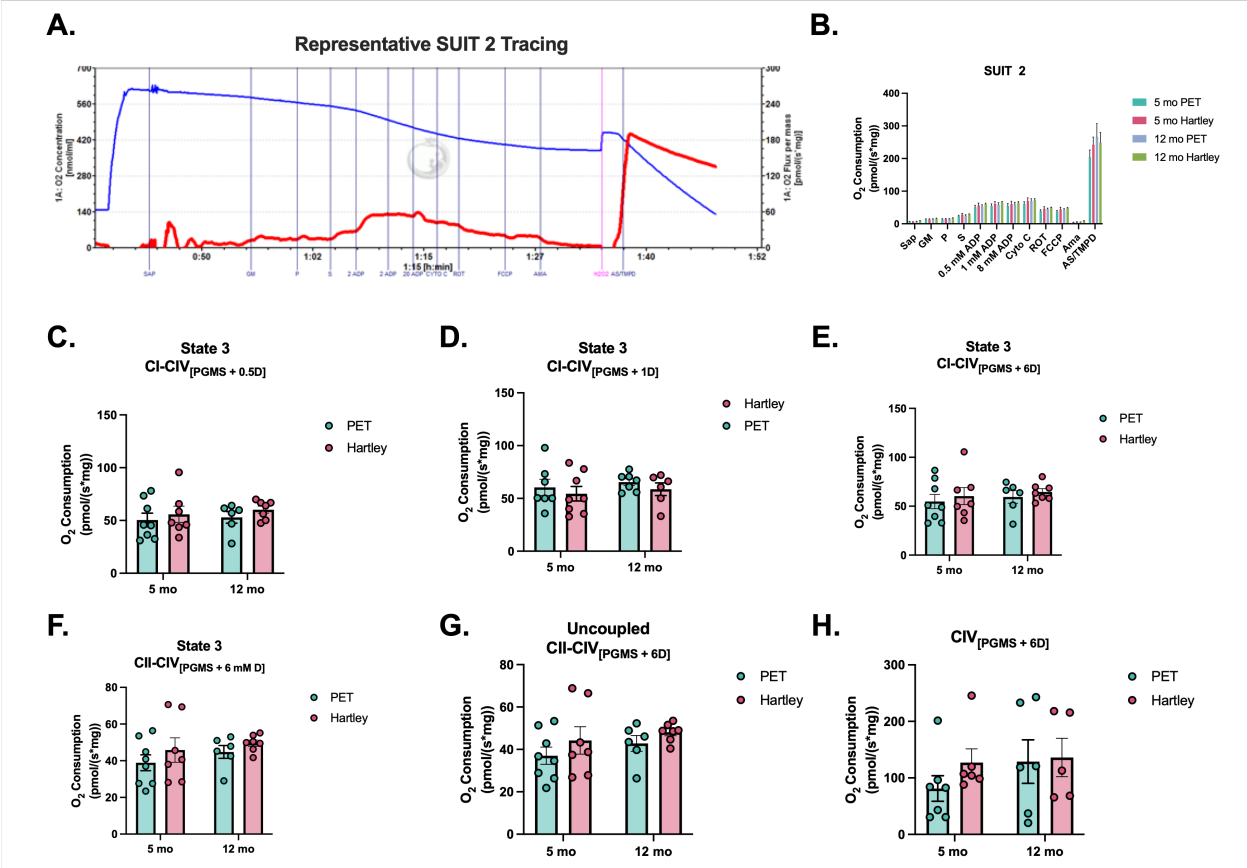

Figure 5.3. PET and HGPs do not have age-related changes in submaximal or maximal complex I and II supported mitochondrial respiration. The SUIT 2 protocol examined complex I (glutamate, malate, and pyruvate) and complex II (succinate) submaximal and maximal mitochondrial respiration prior examining non-coupled respiratory capacity. Panel A displays a raw tracing of the Oroboros O2k and Supplemental Table D.2 reports the protocols in detail. Changes in oxygen consumption for each titration step are displayed in panel B. There were no age or strain differences in submaximal complexes I through IV 0.5 mM ADP phosphorylating conditions (C). Further, there were no differences in maximal 1 mM ADP (D) or supramaximal 6 mM ADP phosphorylating conditions (E). When rotenone was added to inhibit complex I and examine complex II through IV maximal respiration there were also no differences (F). There were also no differences in non-coupled mitochondrial respiration when FCCP was added to non-couple the electrochemical gradient (G). Finally, when examining complex IV specific respiration there were also no difference in age and strain (H). 5 mo PET n = 6; 5 mo Hartley n = 6; 12 mo PET n = 6; 12 mo Hartley n = 6 for all panels. The n-value is lower due to the necessity for the same technician to respire all samples and decrease variability in line with best practices [40]. Further, O2k samples but be freshly respired decreasing the number of assays that can be performed in each day.

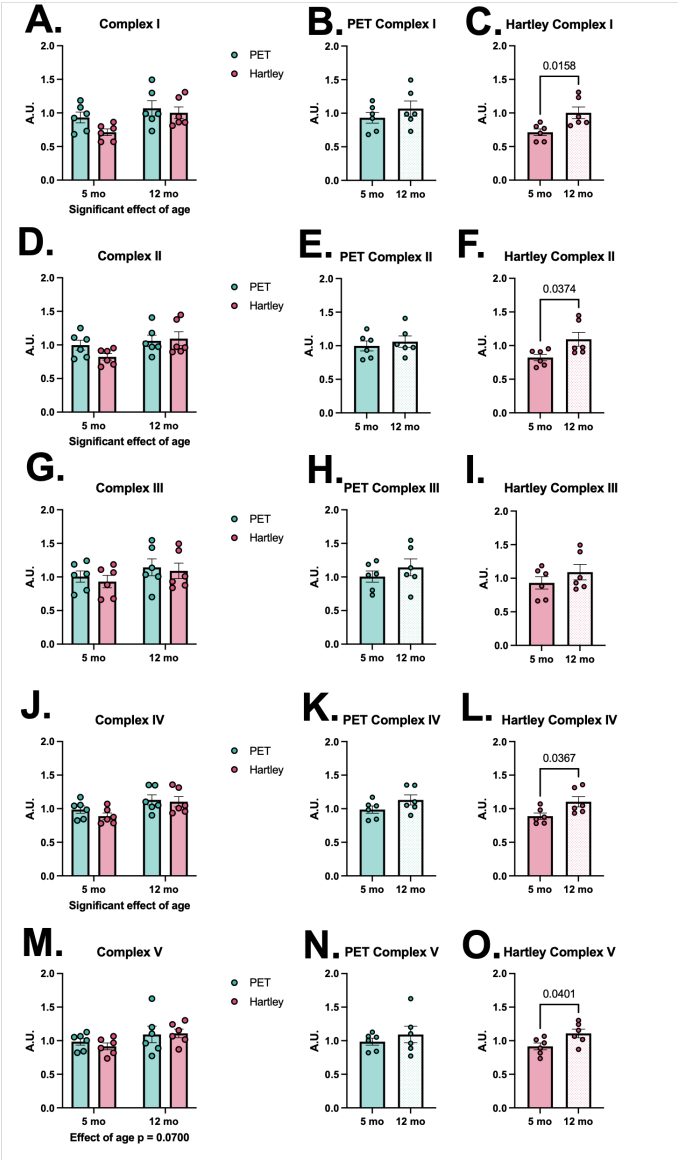

Figure 5.4. Hartley but not PET guinea pigs experience an age-related increase in mitochondrial protein content. An OXPHOS western blot quantified subunits for each of the 5 mitochondrial protein complexes. When examining age by strain differences for the OXPHOS proteins there was an effect of age to increase mitochondrial protein content for complex I (A), complex II (D), and complex IV (J). There was also a trend to increase complex V protein content with age (p = 0.0700) (M). However, when the strains were analyzed separately, PET guinea pigs had no significant differences in mitochondrial protein content for all complexes (B, E, H, K, N) while HGPs had significant increases in complex I (C), complex II (F), complex IV (L), and complex V (O) while a non-significant increase in complex III (I). 5 mo PET n = 6; 5 mo Hartley n = 6; 12 mo PET n = 6; 12 mo Hartley n = 6 for all panels. To have all animals compared on one membrane the n was reduced in line with best practices.

REFERENCES

1. Collaborators G 2019 DF, Nichols E, Steinmetz JD, et al. Estimation of the global prevalence of dementia in 2019 and forecasted prevalence in 2050: an analysis for the Global Burden of Disease Study 2019. *Lancet Public Heal*. 2022;7(2):e105-e125. doi:10.1016/s2468-2667(21)00249-8

2. *2022 Alzheimer's Disease Facts and Figures Special Report More Than Normal Aging: Understanding Mild Cognitive Impairment*.; 2022.

3. Vitek MP, Araujo JA, Fossel M, et al. Translational animal models for Alzheimer's disease: An Alzheimer's Association Business Consortium Think Tank. *Alzheimer's Dement: Transl Res Clin Interv*. 2020;6(1):e12114. doi:10.1002/trc2.12114

4. Drummond E, Wisniewski T. Alzheimer's disease: experimental models and reality. *Acta Neuropathol*. 2017;133(2):155-175. doi:10.1007/s00401-016-1662-x

5. Banik A, Brown RE, Bamburg J, et al. Translation of Pre-Clinical Studies into Successful Clinical Trials for Alzheimer's Disease: What are the Roadblocks and How Can They Be Overcome?1. *J Alzheimer's Dis*. 2015;47(4):815-843. doi:10.3233/jad-150136

6. Cummings JL, Morstorf T, Zhong K. Alzheimer's disease drug-development pipeline: few candidates, frequent failures. *Alzheimer's Res Ther*. 2014;6(4):37. doi:10.1186/alzrt269

7. Jankowsky JL, Zheng H. Practical considerations for choosing a mouse model of Alzheimer's disease. *Mol Neurodegener*. 2017;12(1):89. doi:10.1186/s13024-017-0231-7

8. Bekris LM, Yu CE, Bird TD, Tsuang DW. Review Article: Genetics of Alzheimer Disease. *J Geriatr Psych Neur*. 2010;23(4):213-227. doi:10.1177/0891988710383571

9. HARMAN D. Alzheimer's Disease Pathogenesis. *Ann N York Acad Sci*. 2006;1067(1):454-460. doi:10.1196/annals.1354.065

10. Bali J, Gheinani AH, Zurbriggen S, Rajendran L. Role of genes linked to sporadic Alzheimer's disease risk in the production of β-amyloid peptides. *Proc Natl Acad Sci*. 2012;109(38):15307-15311. doi:10.1073/pnas.1201632109

11. Liu PP, Xie Y, Meng XY, Kang JS. History and progress of hypotheses and clinical trials for Alzheimer's disease. *Signal Transduct Target Ther*. 2019;4(1):29. doi:10.1038/C1392-019-0063-8

12. Zolochevska O, Taglialatela G. Non-Demented Individuals with Alzheimer's Disease Neuropathology: Resistance to Cognitive Decline May Reveal New Treatment Strategies. *Curr Pharm Des*. 2016;22(26):4063-4068. doi:10.2174/1381612822666160518142110

13. Swerdlow RH, Khan SM. A "mitochondrial cascade hypothesis" for sporadic Alzheimer's disease. *Méd Hypotheses*. 2004;63(1):8-20. doi:10.1016/j.mehy.2003.12.045

14. Picard M, Shirihai OS. Mitochondrial signal transduction. *Cell Metab*. 2022;34(11):1620-1653. doi:10.1016/j.cmet.2022.10.008

15. Troutwine BR, Strope TA, Franczak E, et al. Mitochondrial function and Aβ in Alzheimer's disease postmortem brain. *Neurobiol Dis*. Published online 2022:105781. doi:10.1016/j.nbd.2022.105781

16. Yao J, Irwin RW, Zhao L, Nilsen J, Hamilton RT, Brinton RD. Mitochondrial bioenergetic deficit precedes Alzheimer's pathology in female mouse model of Alzheimer's disease. *Proc National Acad Sci*. 2009;106(34):14670-14675. doi:10.1073/pnas.0903563106

17. Liddelow SA, Guttenplan KA, Clarke LE, et al. Neurotoxic reactive astrocytes are induced by activated microglia. *Nature*. 2017;541(7638):481-487. doi:10.1038/nature21029

18. Gonzalez-Freire M, Scalzo P, D'Agostino J, et al. Skeletal muscle ex vivo mitochondrial respiration parallels decline in vivo oxidative capacity, cardiorespiratory fitness, and muscle strength: The Baltimore Longitudinal Study of Aging. *Aging Cell*. 2018;17(2):e12725. doi:10.1111/acel.12725

19. Holloway GP, Holwerda AM, Miotto PM, Dirks ML, Verdijk LB, Loon LJC van. Age-Associated Impairments in Mitochondrial ADP Sensitivity Contribute to Redox Stress in Senescent Human Skeletal Muscle. *Cell Reports*. 2018;22(11):2837-2848. doi:10.1016/j.celrep.2018.02.069

20. Swerdlow RH. Mitochondria and Mitochondrial Cascades in Alzheimer's Disease. *J Alzheimer's Dis*. 2017;Preprint(Preprint):1-14. doi:10.3233/jad-170585

21. Fišar Z, Jirák R, Zvěřová M, et al. Plasma amyloid beta levels and platelet mitochondrial respiration in patients with Alzheimer's disease. *Clin Biochem*. 2019;72:71-80. doi:10.1016/j.clinbiochem.2019.04.003

22. Mattson MP, Arumugam TV. Hallmarks of Brain Aging: Adaptive and Pathological Modification by Metabolic States. *Cell Metab*. 2018;27(6):1176-1199. doi:10.1016/j.cmet.2018.05.011

23. Santangelo KS, Bertone AL. Effective reduction of the interleukin-1β transcript in osteoarthritis-prone guinea pig chondrocytes via short hairpin RNA mediated RNA interference influences gene expression of mediators implicated in disease pathogenesis. *Osteoarthr Cartilage*. 2011;19(12):1449-1457. doi:10.1016/j.joca.2011.09.004

24. Santangelo KS, Kaeding AC, Baker SA, Bertone AL. Quantitative Gait Analysis Detects Significant Differences in Movement between Osteoarthritic and Nonosteoarthritic Guinea Pig Strains before and after Treatment with Flunixin Meglumine. *Arthritis*. 2014;2014:503519. doi:10.1155/2014/503519

25. Santangelo KS, Pieczarka EM, Nuovo GJ, Weisbrode SE, Bertone AL. Temporal expression and tissue distribution of interleukin-1β in two strains of guinea pigs with varying propensity for spontaneous knee osteoarthritis. *Osteoarthr Cartilage*. 2011;19(4):439-448. doi:10.1016/j.joca.2011.01.004

26. Musci RV, Walsh MA, Konopka AR, et al. The Dunkin Hartley Guinea Pig Is a Model of Primary Osteoarthritis That Also Exhibits Early Onset Myofiber Remodeling That Resembles Human Musculoskeletal Aging. *Front Physiol*. 2020;11:571372. doi:10.3389/fphys.2020.571372

27. Spendiff S, Vuda M, Gouspillou G, et al. Denervation drives mitochondrial dysfunction in skeletal muscle of octogenarians. *J Physiology*. 2016;594(24):7361-7379. doi:10.1113/jp272487

28. Shorter E, Sannicandro AJ, Poulet B, Goljanek-Whysall K. Skeletal Muscle Wasting and Its Relationship With Osteoarthritis: a Mini-Review of Mechanisms and Current Interventions. *Curr Rheumatol Rep*. 2019;21(8):40. doi:10.1007/s11926-019-0839-4

29. Krieglstein J, Kewitz T, Kirchhefer U, et al. Damage of Guinea Pig Heart and Arteries by a Trioleate-Enriched Diet and of Cultured Cardiomyocytes by Oleic Acid. *Plos One*. 2010;5(3):e9561. doi:10.1371/journal.pone.0009561

30. Radakovich LB, Marolf AJ, Culver LA, Santangelo KS. Calorie restriction with regular chow, but not a high-fat diet, delays onset of spontaneous osteoarthritis in the Hartley guinea pig model. *Arthritis Res Ther*. 2019;21(1):145. doi:10.1186/s13075-019-1925-8

31. Attems J, Jellinger KA. The overlap between vascular disease and Alzheimer's disease - lessons from pathology. *BMC Med*. 2014;12(1):206. doi:10.1186/s12916-014-0206-2

32. Charisis S, Lin H, Ray R, et al. Obesity impacts the expression of Alzheimer's disease–related genes: The Framingham Heart Study. *Alzheimer's Dement*. 2023;19(8):3496-3505. doi:10.1002/alz.12954

33. Morris JK, McCoin CS, Fuller KN, et al. Mild cognitive impairment and donepezil impact mitochondrial respiratory capacity in skeletal muscle. *Funct*. Published online 2021. doi:10.1093/function/zqab045

34. Musci RV, Andrie KM, Walsh MA, et al. Phytochemical compound PB125 attenuates skeletal muscle mitochondrial dysfunction and impaired proteostasis in a model of musculoskeletal decline. *J Physiology*. Published online 2022. doi:10.1113/jp282273

35. Wahl D, Moreno JA, Santangelo KS, et al. Non-Transgenic Guinea Pig Strains Exhibit Hallmarks of Human Brain Aging and Alzheimer's Disease. *Journals Gerontology Ser*. Published online 2022. doi:10.1093/gerona/glac073

36. Johnstone EM, Chaney MO, Norris FH, Pascual R, Little SP. Conservation of the sequence of the Alzheimer's disease amyloid peptide in dog, polar bear and five other mammals by cross-species polymerase chain reaction analysis. *Mol Brain Res*. 1991;10(4):299-305. doi:10.1016/0169-328x(91)90088-f

37. Pesta D, Gnaiger E. Mitochondrial Bioenergetics, Methods and Protocols. *Methods Mol Biology*. 2011;810:25-58. doi:10.1007/978-1-61779-382-0_3

38. Jacobs RA, Aboouf MA, Koester-Hegmann C, et al. Erythropoietin promotes hippocampal mitochondrial function and enhances cognition in mice. *Commun Biology*. 2021;4(1):938. doi:10.1038/C2003-021-02465-8

39. McLaughlin KL, Hagen JT, Coalson HS, et al. Novel approach to quantify mitochondrial content and intrinsic bioenergetic efficiency across organs. *Sci Rep-uk*. 2020;10(1):17599. doi:10.1038/C1598-020-74718-1

40. Walsh MA, Musci RV, Jacobs RA, Hamilton KL. A practical perspective on how to develop, implement, execute, and reproduce high-resolution respirometry experiments: The physiologist's guide to an Oroboros O2k. *FASEB J*. 2023;37(12). doi:10.1096/fj.202301644rr

41. Walsh MA, Zhang Q, Musci RV, Hamilton KL. The combination of NRF1 and Nrf2 activators in myoblasts stimulate mechanisms of proteostasis without changes in mitochondrial respiration. *Redox Muscle Physiology Exerc Sport*. Published online 2022:100001. doi:10.1016/j.rimpes.2022.100001

42. Jacques M, Kuang J, Bishop DJ, et al. Mitochondrial respiration variability and simulations in human skeletal muscle: The Gene SMART study. *Faseb J Official Publ Fed Am Soc Exp Biology*. Published online 2020. doi:10.1096/fj.201901997rr

43. Beeri MS, Leugrans SE, Delbono O, Bennett DA, Buchman AS. Sarcopenia is associated with incident Alzheimer's dementia, mild cognitive impairment, and cognitive decline. *J Am Geriatr Soc*. 2021;69(7):1826-1835. doi:10.1111/jgs.17206

44. Weber A, Mak S hung, Berenbaum F, et al. Association between osteoarthritis and increased risk of dementia. *Medicine*. 2019;98(10):e14355. doi:10.1097/md.0000000000014355

45. Viel C, Brandtner AT, Weißhaar A, Lehto A, Fuchs M, Klein J. Effects of Magnesium Orotate, Benfotiamine and a Combination of Vitamins on Mitochondrial and Cholinergic Function in the TgF344-AD Rat Model of Alzheimer's Disease. *Pharm*. 2021;14(12):1218. doi:10.3390/ph14121218

46. Lark DS, Torres MJ, Lin CT, Ryan TE, Anderson EJ, Neufer PD. Direct real-time quantification of mitochondrial oxidative phosphorylation efficiency in permeabilized skeletal muscle myofibers. *Am J Physiol-cell Ph*. 2016;311(2):C239-C245. doi:10.1152/ajpcell.00124.2016

47. Lunnon K, Keohane A, Pidsley R, et al. Mitochondrial genes are altered in blood early in Alzheimer's disease. *Neurobiol Aging*. 2017;53:36-47. doi:10.1016/j.neurobiolaging.2016.12.029

48. Mary A, Eysert F, Checler F, Chami M. Mitophagy in Alzheimer's disease: Molecular defects and therapeutic approaches. *Mol Psychiatry*. 2023;28(1):202-216. doi:10.1038/C1380-022-01631-6

49. Andrie KM, Palmer DR, Wahl O, et al. Treatment with PB125® Increases Femoral Long Bone Strength in 15-Month-Old Female Hartley Guinea Pigs. *Ann Biomed Eng*. Published online 2023:1-11. doi:10.1007/s10439-023-03415-7

50. Erecińska M, Silver IA. ATP and Brain Function. *J Cereb Blood Flow Metab*. 1988;9(1):2-19. doi:10.1038/jcbfm.1989.2

51. Grimm A, Eckert A. Brain aging and neurodegeneration: from a mitochondrial point of view. *J Neurochem*. 2017;143(4):418-431. doi:10.1111/jnc.14037

CHAPTER 6 – DISCUSSION OF OVERALL FINDINGS, SPECULATION OF WHAT SINGLE QUESTION NEEDS TO BE ANSWERED IN HUMAN BIOENERGETICS, AND STEPS MOVING FORWARD FOR ME AS AN INDEPENDENT THINKER

SUMMARY OF MY DOCTORAL WORK

Collectively this dissertation examined how loss of proteostasis and mitochondrial dysfunction, two hallmarks of aging, drive the development and progression of chronic diseases using novel *in vitro* and *in vivo* models. Protein homeostasis and mitochondrial function are highly interconnected given that protein turnover is an energetically costly process and mitochondria are the primary energy converter in cells.

Specifically, loss of skeletal muscle mass and function with age (sarcopenia) and neurodegeneration are, at least in part, due to loss of proteostasis and mitochondrial dysfunction [1,2]. While decades of research have grown the current understanding of sarcopenia and neurodegeneration, there is a lack effective treatments for older adults [3,4]. I speculated in this dissertation that one barrier to making progress in treatment development is that the preclinical animal models currently utilized for understanding the pathology do not model the age-related changes observed in older adults. For example, genetic manipulation is frequently used to model sarcopenia and neurodegeneration in rodents, yet older adults do not have a gene switch “on/off” to one day quickly develop these insidious age-related pathologies [5–8]. Furthermore, older adults frequently have multimorbidities (>2+ chronic illnesses) that accompany the aging process, yet the current preclinical animal models do not have these same phenotypes.

Therefore, in my dissertation I examined avenues to fill these gaps in knowledge. I examined how a unique non-transgenic guinea pig model recapitulates both skeletal muscle and brain aging in humans. Additionally, I examined how short and long-term treatment of a phytochemical compound, known to improve mechanisms of proteostasis and mitochondrial energetics in other tissues, affected a skeletal muscle highly susceptible to age-related changes as well as the cerebellum, the brain region responsible for motor movement regulation and

balance control. In demonstrating proof of concept that phytochemical compounds could improve mechanisms of mitochondrial proteostasis, I also showed that these improvements could occur independently to changes in mitochondrial function (Chapter 2). Therefore, potential healthspan extending interventions may or may not directly improve mitochondrial function. In Chapter 5 I assessed mitochondrial function in the hippocampus of Hartley guinea pigs where I hypothesized that as Hartleys develops hippocampal neurodegeneration, they would have impaired mitochondrial function. Contrary to my hypothesis, there were no age-related decreases in mitochondrial function in Hartleys over an age range where we have previously observed increases in neuroinflammation and neurodegeneration. Taken together, mitochondrial are critical organelles. However, mitochondrial function and/or dysfunction might not always be the "end all be all." Later in this chapter I will re-discuss these findings through a new lens.

To elaborate, at completion of these four projects outlined in Chapters 2, 3, 4, and 5, I began to question the phrases mitochondrial function versus dysfunction. Specifically, a mitochondrion that is coined to be "dysfunctional" is still producing ATP so is it not still functioning? Therefore, in this final chapter I would like to 1. Discuss how my mitochondrial dissertation data support or refute the binary concept of mitochondrial function versus dysfunction and 2. Use my doctoral work to (re)-answer a question that was posed to me 6 years ago as a first-semester graduate student. Collectively, through addressing these points, I believe I demonstrate my ability to think independently and discuss certain aspects of my doctoral work in the larger context of scientific literature.

PART 1: MITOCHONDRIAL FUNCTION AND DYSFUNCTION DO NOT EXIST AS A BINARY

Initially referred to as the "powerhouse of the cell [9]," decades of subsequent research led to the coining of a new term to describe the mitochondrial reticulum: the mitochondrial information processing system (MIPS) [10]. The reason for this change is that mitochondria

have multifaceted roles including respiration for ATP production [11], calcium handling [12], electron leak [11], fatty acid synthesis [13] and others. These processes are all energy dependent. Thus, ATP production via oxidative phosphorylation (i.e., mitochondrial respiration) remains a primary function of mitochondria, enabling them to energetically support all MIPS functions. Therefore, mitochondrial respiration was one primary outcome in my research.

Throughout the studies in this document and in other studies outside my dissertation, I have made hundreds of measures of mitochondrial respiration using the Oroboros Oxygraph 2000 (O2k). In my early writing and thinking as a graduate student, I always referred to this O2k readout as “mitochondrial function” and this is also how I described my Chapter 2 and 5 findings (which might make some mitochondriacs cringe). However, there have been instances, in my graduate research experiences, where increased O2k mitochondrial oxygen consumption did not always translate to increased whole body function or organismal health. Additionally, oxygen consumption measures in an O2k are only one measure of mitochondrial respiration, which is, in turn, only one mitochondrial function. Additionally, it is assessed *ex vivo* with supraphysiological concentrations of reagents. While I have also described in a perspective I published (Appendix E), ways to improve the development, implementation, execution, and reproducibility of O2k assays, a critical eye should be taken when examining mitochondrial respiration data and how they relate to mitochondrial function. Even more broadly, what is mitochondrial function? What is the difference between mitochondrial function versus dysfunction? Should researchers even be using these terms? These questions might not have concrete answers; however, there is a need to provide more clarity, context, and frame of reference of biological assays as they relate to human health.

The shift in thinking to mitochondrial function being a continuum (in contrast to function versus dysfunction) has also been discussed by others and there has been recent work arguing for the removal of mitochondrial function/dysfunction vocabulary in scientific studies [14]. Because mitochondria have numerous facets, deeming a reticular network functional or

dysfunctional is vague and misleading. Specifically, Monzel et al. suggest that coining the mitochondria the powerhouse of the cell creates a monofunctional limitation and impedes progress in shaping the field of mitochondrial biology [14]. However, mitochondria are the most studied organelle in biomedical sciences and show promise as potential therapeutic targets [10]. So, what is the best way to discuss mitochondrial research?

Recent work suggests that mitochondria exist as a hierarchy of needs (like Maslow's Hierarchy of Needs, often represented as a triangle) which interacts within the organism. The mitochondrial hierarchy of roles triangle begins with molecules, then is followed by features, activities, functions, and peaking at behaviors demonstrating the pleiotropic nature (i.e., producing more than 1 effect) of the mitochondrial reticulum [14]. Thus, to answer the question, "What is mitochondrial function?" neglects four other components. Specifically, mitochondrial behaviors, the apex of the mitochondrial hierarchy of roles triangle, (i.e., cellular goal driven activity) largely impact cell, tissue, and organism health and should be included whenever possible. Additionally, the language around mitochondrial respiration (the primary outcome of Chapters 2 and 5, not mitochondrial function) should entail a substantial degree of detail for readers. Again, reflecting on my early work, this degree of detail was neglected, but through growth and development my insights have changed.

New view of how mitochondria change with age

This chapter started by reporting that mitochondrial dysfunction is a hallmark of aging, yet the contribution of mitochondria to aging has recently been described as "murky [15]." In support of this supposition, Rinaldi highlights that there isn't linearity to mitochondrial dysfunction as first hypothesized, for example, that mitochondrial ROS are bad and drive disease [15]. Interestingly, there are albeit weak correlations between mitochondrial oxygen consumption and age when accounting for activity levels, sex, and body composition [16]. So, while mitochondrial dysfunction has been reported to exist in various age-related chronic diseases, the type of dysfunction is not always the same. Next, I will return to what I shared

above from Chapters 2 and 5, but this time discussing the findings with this new mindset of the greater context of mitochondrial research.

Revised conclusion for chapter 2

In Chapter 2 I assessed how the co-treatment of phytochemical compounds that are purported nuclear respiratory factor 1 (NRF1) and nuclear factor erythroid 2-related factor 2 (Nrf2) activators might improve mechanisms of proteostasis and mitochondrial function using immortalized muscle precursor cells (i.e., C2C12 myoblasts) in the presence of an oxidative challenge. Incorporating the new mindset of mitochondrial function as a continuum, I see now is that I assessed submaximal and maximal mitochondrial respiration (Figure 2.3) (one mitochondrial function) and OXPHOS protein content (Figure 2.4) (one mitochondrial feature). However, I did not assess mitochondrial molecules, activities, and behaviors, the other three components of the mitochondrial hierarchy of roles triangle [14]. Further, these immortalized cells are predominantly glycolytic in nature and recent reports have demonstrated robust differences in mitochondrial respiration (one of many mitochondrial functions) and mitochondrial protein content and organization (one of many mitochondrial features) [17]. Further, mitochondrial energetics change during the differentiation process as previously described [18]. Additionally, even submaximal mitochondrial respiration in C2C12 myoblasts, assessed via high-resolution respirometry in an O2k, is very different than how skeletal muscle mitochondria "function" in an older adult. Therefore, my revised conclusion regarding Chapter 2 is that co-treatment with phytochemical compounds that are purported NRF1 and Nrf2 activators, improves mechanisms of mitochondrial proteostasis in glycolytic muscle precursor cells, but does not directly alter submaximal or maximal oxygen consumption. Future studies should examine this treatment paradigm with outcomes pertaining to mitochondrial behaviors (e.g., mitochondrial-nuclear signaling).

Revised conclusion for chapter 5

When re-visiting the data in Chapter 5, we see that the mitochondrial dysfunction hypothesized to accompany hippocampal neurodegeneration Hartley guinea pigs was absent. Or was it? Indeed, there was no statistical difference in hippocampal mitochondrial oxygen consumption (one mitochondrial function) between younger and older Hartley guinea pigs. However, we also assessed mitochondrial oxygen consumption in PET guinea pigs that do not display robust hippocampal pathology over the age range when Hartleys do. Compared to younger PET guinea pigs, older PETs had significantly higher rates of oxygen consumption (Figure 5.2D), suggesting that the lack of an increase of mitochondrial oxygen consumption with age was detrimental to the Hartleys. I went one step further and assess content of mitochondrial OXPHOS proteins (one mitochondrial feature) in both guinea pig strains. Here I found that PET guinea pigs, despite the age-related increase in mitochondrial respiration (Figure 5.2D), did not have any changes in OXPHOS protein content (Figure 5.4B, E, H, K, N). Conversely, with age Hartley guinea pigs had a significant increase in OXPHOS proteins (Figure 5.4C, F, I, L, O), which suggests a compensatory effect due to less efficient mitochondria (evidenced by lower respiratory control ratios, a measure of mitochondrial efficiency; Figure 5.2K).

After pondering these results in the greater context of bioenergetics, there are a few assumptions I will highlight. The first is that there is mitochondrial diversity between different tissues with varied fuel preferences and capacities [14,19]. In Chapter 5 I assume that hippocampal mitochondria are similar to other tissues to a certain degree. Because of the lack of non-invasive methods to assess brain oxygen consumption in humans, we cannot understand the degree of mitochondrial dynamics, a mitochondrial behavior, as compared to tissues that are easier to assess (e.g., skeletal muscle with biopsies). Another assumption is in how we assessed mitochondrial efficiency, as coupled respiration (the presence of reducing equivalents and adenylates) divided by leak respiration (the presence of reducing equivalents but absence of adenylates). Mitochondrial efficiency is the relationship between ATP produced and oxygen consumed [20]. However, here (and throughout this entire dissertation) we only

assess the denominator (oxygen consumption) as a readout of ATP production. Yet nowhere do we directly measure ATP production, one of the primary functions of OXPHOS. While there are strengths to assessing oxygen consumption to discern disease/treatment benefits (See Appendix E), it is crucial in the context of "mitochondrial function" to highlight this limitation. Therefore, my revised conclusion about Chapter 5 is that, with age, Hartley guinea pigs compared to PET guinea pigs do not have an increase in submaximal or maximal mitochondrial oxygen consumption. Yet, during this same age range they have increased mitochondrial protein content and a lower coupled-to-leak respiration, an indirect measure of mitochondrial efficiency. Future studies should examine additional outcomes pertaining to additional mitochondrial functions (e.g., calcium handling and mitochondrial transition pore opening) and mitochondrial behaviors (e.g., fission/fusion dynamics).

Takeaways about mitochondrial function and dysfunction

While mitochondria are paramount for human health, there is not simply mitochondrial function and dysfunction. However, because a single mitochondrial reticulum has so many molecules, features, activities, functions, and behaviors there is not one simple assessment for mitochondrial health [14]. So, what does this mean moving forward? Well, it means that research efforts should prioritize measures of mitochondrial health that are easy to administer and that reflect *in vivo* bioenergetics in humans to a greater degree as compared to *ex vivo* supraphysiogical assessments of mitochondrial oxygen consumption. Additionally, multiple assessments should be examined in each study. By making assessments easier to administer it will push boundaries in the science of mitochondrial health and human bioenergetics and seek to ask the critical "big picture" questions in ways that have the greatest translational impact on human health.

PART 2: (RE)-ANSWER A QUESTION THAT WAS POSED TO ME 6 YEARS AGO AS A FIRST-SEMESTER GRADUATE STUDENT USING MY DOCTORAL WORK

At the time I entered the Master of Science degree program in Health and Exercise Science, at Colorado State University, all first-semester graduate students enrolled in Dr. Matt Hickey's Exercise Bioenergetics course (HES 610). Reflecting on the last 24 years of my education, this course was the most challenging course to date but also the most beneficial in terms of the knowledge and abilities that I gained. In this course we were challenged with take-home exams consisting of multi-part questions that did not always have "correct" answers. When pondering what should be included in my last dissertation chapter, I thought about how my data "fit into" the greater scientific body of literature. Serendipitously, one of these HES 610 take-home exam questions appeared to be an excellent framework for speculating what unanswered questions and unquestioned answers remain in the realm of human bioenergetics. To accomplish this, below I seek to "re-answer" this exam question from 6 years ago.

Dr. Hickey's Question:

"Dr. Alfred Knowbell has endowed the "Knowbell Prize" (from monies he earned during the dot-com revolution as founder of the famed internet search engine "FROOGLE"). The Prize is awarded each year to significant theoretical and/or practical advances in the understanding of biological thermodynamics. You have been designated as a finalist for the 2020 Knowbell Prize (which carries a stipend of $250,000/year for life, or until he runs out of money, whichever comes first). You will compete for this award with other equally famous scientists by summarizing your work on biological thermodynamics. You must: Identify the single most important question in biological thermodynamics that has yet to be adequately answered (even if the rest of the world thinks it has…) (a). Defend your selection in (a) above by making a case for the import of directing research efforts (and funding!) toward your target question. What aspects of basic, applied, comparative, or clinical science would be enhanced if your question were "solved"? Provide (and discuss) the single published work that best supports your

thesis/proposed question. Discuss how the work helps make the case for your response to (a) and (b) above."

My Answer:

Biological thermodynamics is a science that explains the nature of general laws of thermodynamic processes occurring in living organisms as nonequilibrium thermodynamic systems. Human bioenergetics falls within the umbrella of biological thermodynamics. While there are other questions regarding the basic nature of biological thermodynamics, I believe that narrowing the scope to human bioenergetics would yield the greatest return on investment if I answered this question. As detailed above, mitochondria serve numerous roles within an individual. Mitochondrial networks also function on a sensor to stress, adaptation, and functional outcome continuum, but within this framework there are both positive (i.e., eu-) and negative (i.e., dis-) levels of stress [21,22]. Therefore, the single question in human bioenergetics that has yet to be answered is, "What is the tipping point where mitochondrial eustress (i.e., a mitohormetic adaptations) becomes mitochondrial distress?" (Figure 6.1).

Mitochondrial eustress versus distress

First, I need to define mitochondrial eustress from mitochondrial distress. Importantly, I refer to mitochondrial distress rather than mitochondrial dysfunction for reasons explained in the above section. Mitochondria receive stress signals every moment of every day. Even under basal conditions (i.e., the under-stimulated an example of low mitochondrial stress), mitochondria produce reactive oxygen species (ROS) (i.e., about 2% of all oxygen becomes superoxide, a deleterious free radical) [23]. Acutely ROS production increases with exercise and serve as primary signaling molecules to activate pathways like peroxisome proliferator-activated receptor-γ coactivator 1-α (PGC1α) and Nrf2 to increase mitochondrial biogenesis and redox defenses, respectively [24]. However, under basal conditions and even with acute aerobic exercise, this ROS production does not become distressing (i.e., mitochondrial eustress). Rather mitochondrial eustress, response, and adaptation associated with chronic exercise

training has also been coined adaptative homeostatic or hormesis (or mitohormesis) responses which were discussed in Chapter 2. The adaptative homeostatic responses serve as protective mechanisms resulting in improved function, in the case of exercise performance, and/or protection against age-related chronic diseases [25–28].

Conversely, mitochondrial distress, in my opinion, is when the mitochondrial reticulum fails to demonstrate adequate stress resistance or resilience leading to damage and possibly disease. However, what is the “tipping point” in which is mitochondrial eustress becomes distress? Can we identify it? There is significant value in answering my question because as extensively described throughout this dissertation mitochondrial distress (previously referred to mitochondrial dysfunction) drives the development and progression of age-related chronic diseases suggesting that this tipping point was exceeded. However, mitochondrial distress can also occur in other physiological perturbations including excessive exercise training without adequate recovery [29] and in scenarios of psychological distress [30,31]. Thus, I also speculate that there are differences in this proposed tipping point for various mitochondrial eustress to distress continuums. Here I will postulate one potential hypothesis to answer my question and a brief overview of the methods employed to test such hypothesis. While this example might seem “out of left field” it further highlights my abilities to take my knowledge and apply it to other physiological paradigms.

As mentioned above, this hypothetical tipping point can present with exercise training, where chronic bouts of high intensity exercise without adequate recovery can result in impaired mitochondrial oxygen consumption and glucose metabolism [29]. In the world of exercise physiology this tipping point is sometimes called over training syndrome. However, there is heterogeneity within over training syndrome suggesting that cellular stress tipping points are not conserved across individuals [32]. Because of the variability of stress, response, and adaptation among perturbations (e.g., physical exercise, biological aging, or psychological distress) it makes the most sense to begin with a consistent physiological stress and population with the

fewest number of confounding variables to determine if/where this tipping point exists in a prospective study. For example, Army basic training is an intensive 10-week long physical training program that is the first step to becoming a soldier. However, approximately 20% of females participating in basic training experience stress fractures (i.e., small bone fracture typically due to overuse or respective force) during this 10-week period impairing training and threatening military readiness [33]. Specifically mitochondrial distress (previously referred to as mitochondrial function) impairs osteogenesis (bone formation) and increases osteoclast activity (bone breakdown) [34] which might be associated with intense physical training in the absence of proper recovery in our target population. Therefore, I proposed to test the hypothesis that there will be an acute rise in hypermetabolism (as assessed by resting whole body oxygen consumption) for reasons described below in female army soldiers prior to the development of a stress fracture during basic training. This rise in energy expenditure at rest will be related to decreases in glucose handling, increases in submaximal and maximal complex I and II supported mitochondrial respiration, and decreases in the 2 mile-run (a standard military performance assessment) in those who developed stress fractures during basic training.

When testing this hypothesis, I would propose longitudinal time points examining multiple outcomes of the mitochondrial hierarchy of roles triangle (molecules, features, activities, functions, and behaviors) in mitochondria from at least two cell types (e.g., peripheral blood mononuclear cells and skeletal muscle). I also would include whole-body measures of health and metabolism (e.g., resting energy expenditure, oral glucose tolerance test) and physical function/performance (e.g., maximal whole-body oxygen consumption and 2-mile run test). The proposed *ex vivo* and *in vivo* physiological assessments will be administered at baseline and then every two weeks throughout basic training at all five basic training locations in the United States. While this is simply an overview such information of determining if/when a rise in energy expenditure occurred (indicating hypermetabolism) might be a symptom that mitochondrial eustress is bridging to distress prior to stress fractures occurring. The implication or “so what” of

answering this specific “sub-question" to my overarching broad question could identify females who are at risk of later developing a stress fracture, alter training before the fracture occurred, and improve attrition to basic training.

If my broad question were answered (Figure 6.1), who would it help?

I use an analogy that mitochondrial distress is a house fire, potentially even “burning” through energetic resources (as observed by hypermetabolism which is discussed below; I promise it is coming) while producing cellular damage via unwelcomed cellular byproducts like smoke (e.g., ROS). However, every house fire has a different cause and burns in a different manner. The same could be said for this individual variability of this proposed tipping point (as mentioned above).

If the scientific community was able to solve my question of “What is the tipping point where mitochondrial eustress (i.e., a mitohormetic adaptations) becomes mitochondrial distress?” it would help basic, applied, and clinical scientists to ultimately improve human health. Continuing with the fire analogy, Figure 6.2 demonstrates how a science fire crew would seek to address my broader question (not the specific sub-question in the proposed study above). Basic scientists would obtain insights into what bioenergetic components “ignited the fire” in driving mitochondrial eustress to mitochondrial distress. Specifically, where did the fire start? Was it initiated by mitochondrial DNA damage? Or was it because the cells did not undergo mitophagy soon enough? Upon knowing where the fire started applied scientists could develop therapeutic targets to prevent mitochondrial eustress from distress. What if they gave drugs to decrease DNA damage? Or gave drugs to spark mitophagy? Finally, and most importantly, answering my question would hopefully help clinical scientists (i.e., medical professionals) who treats different fires every day. Importantly, while it would benefit basic, applied, and clinical scientists this question is translational in nature and cannot be answered without the collaborative commitment of basic, applied, and clinical scientists.

The single published work that best supports my proposed question in Figure 6.1 is entitled, “Cellular allostatic load is linked to increased energy expenditure and accelerated biological aging [35].” In short, Bobba-Alves and colleagues took primary human skin fibroblasts from human donors and treated them with a control or dexamethasone, a corticosteroid known to elicit cellular stress, for 250 days [36]. During the treatment duration, authors serially assessed multiple mitochondrial molecules, features, activities, functions, and behaviors highlighting the comprehensive nature of assessing bioenergetics. They concluded that the dexamethasone increased energy expenditure resulting in accelerated biological aging as assessed by mitochondrial DNA deletions, mitochondrial DNA mutations, decreased telomere length, and an increase in cell death. The work by Bobba-Alves and colleagues highlights that even in culture a tipping point exists (although not pin-pointed in this study) from mitochondrial eustress to distress, and it appears to be driven by an over-active metabolic rate that drives “early” aging. However, their paper still fails to answer my proposed question because, while it was performed in human primary fibroblasts, it was within one cell type as compared to the multiple cell types, tissues, organs, organ systems which comprise the human organism. Further, these were cells from three individuals which does not sufficiently encompass human heterogeneity. The study does, however, highlight the limitations posited above about the use of single assessments of mitochondrial health.

FINAL CONCLUSIONS AND TAKEAWAYS

The field of geroscience has greatly evolved, even since I first started my graduate training. For example, additional hallmarks of aging were identified [37], a world-wide pandemic came and went, and numerous papers relevant to my doctoral research were published. My dissertation contributed to information about the drivers of brain and skeletal muscle aging and how phytochemicals compounds targeting the NRF1 and Nrf2 proteins might modulate these drivers. Additionally, it assisted in helping to standardize assessments of mitochondrial

respiration. However, these data and their associated manuscripts make up a miniscule percentage of total data collected by scientists, as over 5 million scientific papers were published in 2022 alone. I say this not to undervalue my dissertation but highlight how the scientific field works and evolves. Most importantly this dissertation was the means to shape me as a tenacious thinker, curious scientist, enthusiastic teacher, and collaborative team member.

FIGURES

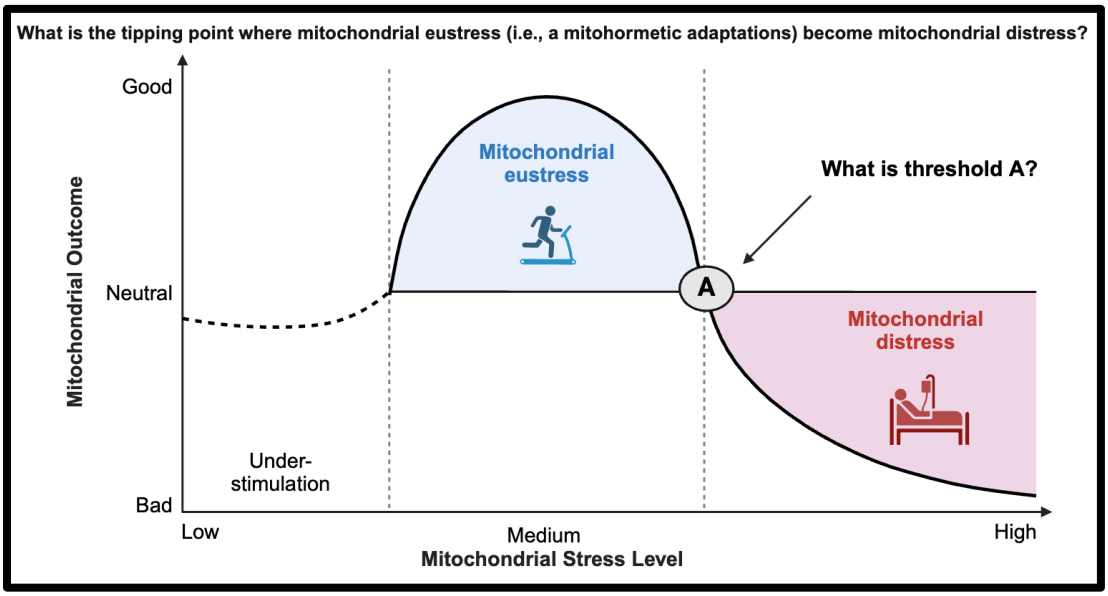

Figure 6.1. The single question in biological thermodynamics that has yet to be answered. Here I present a continuum with generalized “mitochondrial stress levels” (i.e., low, medium, high) on the x-axis and “mitochondrial outcome” (i.e., bad, neutral, good) on the y-axis. The “mitochondrial outcome” could be any mitochondrial molecule, feature, activity, function, or behavior within the mitochondrial hierarchy of roles triangle. Under conditions of low mitochondrial stress there is a negligible mitochondrial outcome. However, when mitochondria experience a medium (eu-) stress (e.g., aerobic exercise) they activate their sensor and adaptation abilities to yield a positive functional outcome (i.e., mitohormesis). Finally, when mitochondria are subjected to high levels of stress but do not have the ability to display stress resistance and resilience, they become distressed mitochondria. The proposed question seeks to answer what it the threshold when/where a mitochondria adapts versus when it becomes distressed?

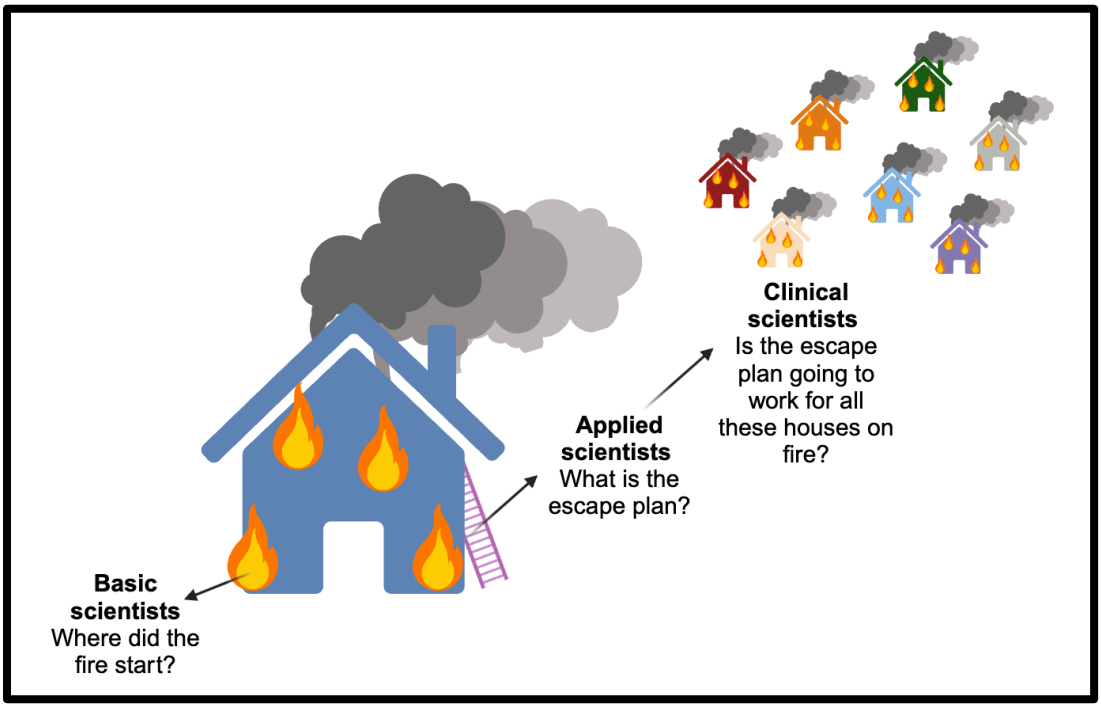

Figure 6.2. The house fire analogy. If my question were to be answered, who would it benefit? What is the role of basic, applied, and clinical scientists.

REFERENCES

1. Mattson MP, Arumugam TV. Hallmarks of Brain Aging: Adaptive and Pathological Modification by Metabolic States. *Cell Metab*. 2018;27(6):1176-1199. doi:10.1016/j.cmet.2018.05.011

2. Musci RV, Hamilton KL, Miller BF. Targeting mitochondrial function and proteostasis to mitigate dynapenia. *Eur J Appl Physiol*. 2018;118(1):1-9. doi:10.1007/s00421-017-3730-x

3. Lo JH tung, U KP, Yiu T, Ong MT yun, Lee WY wai. Sarcopenia: Current treatments and new regenerative therapeutic approaches. *J Orthop Transl*. 2020;23:38-52. doi:10.1016/j.jot.2020.04.002

4. Wang J, Hu WW, Jiang Z, Feng MJ. Advances in treatment of neurodegenerative diseases: Perspectives for combination of stem cells with neurotrophic factors. *World J Stem Cells*. 2020;12(5):323-338. doi:10.4252/wjsc.v12.i5.323

5. Jang YC, Lustgarten MS, Liu Y, et al. Increased superoxide in vivo accelerates age-associated muscle atrophy through mitochondrial dysfunction and neuromuscular junction degeneration. *Faseb J Official Publ Fed Am Soc Exp Biology*. 2009;24(5):1376-1390. doi:10.1096/fj.09-146308

6. Muller FL, Song W, Liu Y, et al. Absence of CuZn superoxide dismutase leads to elevated oxidative stress and acceleration of age-dependent skeletal muscle atrophy. *Free Radic Biol Med*. 2006;40(11):1993-2004. doi:10.1016/j.freeradbiomed.2006.01.036

7. Xu H, Bhaskaran S, Piekarz KM, et al. Age Related Changes in Muscle Mass and Force Generation in the Triple Transgenic (3xTgAD) Mouse Model of Alzheimer's Disease. *Front Aging Neurosci*. 2022;14:876816. doi:10.3389/fnagi.2022.876816

8. Oddo S, Caccamo A, Kitazawa M, Tseng BP, LaFerla FM. Amyloid deposition precedes tangle formation in a triple transgenic model of Alzheimer's disease. *Neurobiol Aging*. 2003;24(8):1063-1070. doi:10.1016/j.neurobiolaging.2003.08.012

9. Siekevitz P. Powerhouse of the Cell. *Scientific American*. 1957;197(1). https://www.jstor.org/stable/24940890

10. Picard M, Shirihai OS. Mitochondrial signal transduction. *Cell Metab*. 2022;34(11):1620-1653. doi:10.1016/j.cmet.2022.10.008

11. Brand MD, Orr AL, Perevoshchikova IV, Quinlan CL. The role of mitochondrial function and cellular bioenergetics in ageing and disease. *Brit J Dermatol*. 2013;169:1-8. doi:10.1111/bjd.12208

12. Balderas E, Eberhardt DR, Lee S, et al. Mitochondrial calcium uniporter stabilization preserves energetic homeostasis during Complex I impairment. *Nat Commun*. 2022;13(1):2769. doi:10.1038/C1467-022-30236-4

13. Nowinski SM, Solmonson A, Rusin SF, et al. Mitochondrial fatty acid synthesis coordinates oxidative metabolism in mammalian mitochondria. *Elife*. 2020;9:e58041. doi:10.7554/elife.58041

14. Monzel AS, Enríquez JA, Picard M. Multifaceted mitochondria: moving mitochondrial science beyond function and dysfunction. *Nat Metab*. 2023;5(4):546-562. doi:10.1038/C2255-023-00783-1

15. Rinaldi A. The fountain of youth of mitochondrial research. *EMBO Rep*. 2023;24(10):e58118. doi:10.15252/embr.202358118

16. Distefano G, Standley RA, Dubé JJ, et al. Chronological Age Does not Influence Ex-vivo Mitochondrial Respiration and Quality Control in Skeletal Muscle. *Journals Gerontology Ser Biological Sci Medical Sci*. Published online 2016:glw102. doi:10.1093/gerona/glw102

17. Edman S, Flockhart M, Larsen FJ, Apró W. Need for Speed: Human fast-twitch mitochondria favor power over efficiency. *Mol Metab*. Published online 2023:101854. doi:10.1016/j.molmet.2023.101854

18. Malinska D, Kudin AP, Bejtka M, Kunz WS. Changes in mitochondrial reactive oxygen species synthesis during differentiation of skeletal muscle cells. *Mitochondrion*. 2012;12(1):144-148. doi:10.1016/j.mito.2011.06.015

19. McLaughlin KL, Kew KA, McClung JM, Fisher-Wellman KH. Subcellular proteomics combined with bioenergetic phenotyping reveals protein biomarkers of respiratory insufficiency in the setting of proofreading-deficient mitochondrial polymerase. *Sci Rep-uk*. 2020;10(1):3603. doi:10.1038/C1598-020-60536-y

20. Lark DS, Torres MJ, Lin CT, Ryan TE, Anderson EJ, Neufer PD. Direct real-time quantification of mitochondrial oxidative phosphorylation efficiency in permeabilized skeletal muscle myofibers. *Am J Physiol-cell Ph*. 2016;311(2):C239-C245. doi:10.1152/ajpcell.00124.2016

21. Bobba-Alves N, Juster RP, Picard M. The Energetic Cost of Allostasis and Allostatic Load. *Psychoneuroendocrino*. 2022;146:105951. doi:10.1016/j.psyneuen.2022.105951

22. Musci RV, Hamilton KL, Linden MA. Exercise-Induced Mitohormesis for the Maintenance of Skeletal Muscle and Healthspan Extension. *Sports*. 2019;7(7):170. doi:10.3390/sports7070170

23. Cadenas E, Davies KJA. Mitochondrial free radical generation, oxidative stress, and aging11This article is dedicated to the memory of our dear friend, colleague, and mentor Lars Ernster (1920–1998), in gratitude for all he gave to us. *Free Radic Biol Med*. 2000;29(3-4):222-230. doi:10.1016/s0891-5849(00)00317-8

24. Kasai S, Shimizu S, Tatara Y, Mimura J, Itoh K. Regulation of Nrf2 by Mitochondrial Reactive Oxygen Species in Physiology and Pathology. *Biomol*. 2020;10(2):320. doi:10.3390/biom10020320

25. Pomatto LCD, Davies KJA. The role of declining adaptive homeostasis in ageing. *J Physiology*. 2017;595(24):7275-7309. doi:10.1113/jp275072

26. Pomatto LCD, Sun PY, Davies KJA. To Adapt or not to Adapt: Consequences of Declining Adaptive Homeostasis and Proteostasis with Age. *Mech Ageing Dev*. 2018;177:80-87. doi:10.1016/j.mad.2018.05.006

27. Davies KJA. Adaptive homeostasis. *Mol Aspects Med*. 2016;49:1-7. doi:10.1016/j.mam.2016.04.007

28. Pomatto LCD, Davies KJA. ADAPTIVE HOMEOSTASIS AND THE FREE RADICAL THEORY OF AGEING. *Free Radical Bio Med*. 2018;124:420-430. doi:10.1016/j.freeradbiomed.2018.06.016

29. Flockhart M, Nilsson LC, Tais S, Ekblom B, Apró W, Larsen FJ. Excessive exercise training causes mitochondrial functional impairment and decreases glucose tolerance in healthy volunteers. *Cell Metab*. Published online 2021. doi:10.1016/j.cmet.2021.02.017

30. Rosenberg AM, Saggar M, Monzel AS, et al. Brain mitochondrial diversity and network organization predict anxiety-like behavior in male mice. *Nat Commun*. 2023;14(1):4726. doi:10.1038/C1467-023-39941-0

31. Hollis F, Kooij MA van der, Zanoletti O, Lozano L, Cantó C, Sandi C. Mitochondrial function in the brain links anxiety with social subordination. *Proc National Acad Sci*. 2015;112(50):15486-15491. doi:10.1073/pnas.1512653112

32. Cadegiani FA, Silva PHL da, Abrao TCP, Kater CE. Diagnosis of Overtraining Syndrome: Results of the Endocrine and Metabolic Responses on Overtraining Syndrome Study: EROS-DIAGNOSIS. *J Sports Med*. 2020;2020:3937819. doi:10.1155/2020/3937819

33. Topakas N. Performance Readiness Bars prevent stress fractures. Published February 9, 2023. Accessed January 22, 2024. https://home.army.mil/jackson/about/news2/performance-readiness-bars-prevent-stress-fractures#:~:text=As%20many%20as%205%25%20of,consuming%20a%20nutrient%2Dpoor%20diet.

34. Dobson PF, Dennis EP, Hipps D, et al. Mitochondrial dysfunction impairs osteogenesis, increases osteoclast activity, and accelerates age related bone loss. *Sci Rep*. 2020;10(1):11643. doi:10.1038/C1598-020-68566-2

35. Bobba-Alves N, Sturm G, Lin J, et al. Cellular allostatic load is linked to increased energy expenditure and accelerated biological aging. *Psychoneuroendocrinology*. 2023;155:106322. doi:10.1016/j.psyneuen.2023.106322

36. Trumpff C, Marsland AL, Basualto-Alarcón C, et al. Acute psychological stress increases serum circulating cell-free mitochondrial DNA. *Psychoneuroendocrino*. 2019;106:268-276. doi:10.1016/j.psyneuen.2019.03.026

37. López-Otín C, Blasco MA, Partridge L, Serrano M, Kroemer and G. Hallmarks of aging: An expanding universe. *Cell*. Published online 2023. doi:10.1016/j.cell.2022.11.001

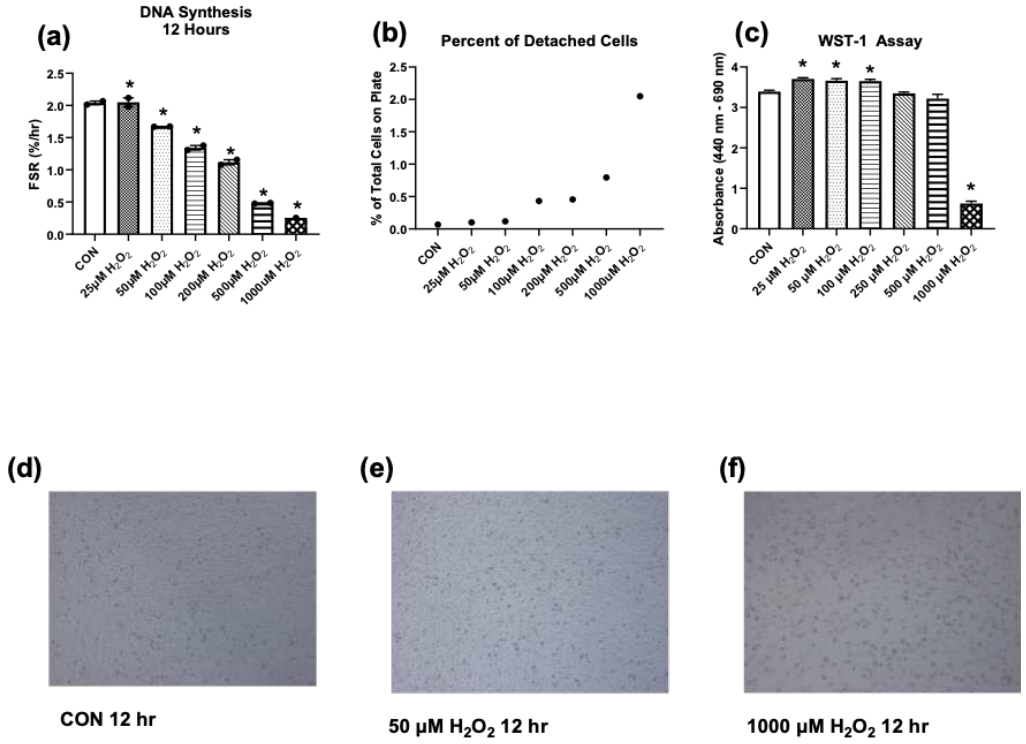

Figure A.1. Selection of an oxidative challenge that does not result in cell death. We carried out a concentration-response experiment with 0-1000 mM H_2O_2 in myoblasts. We selected 50 μM H_2O_2 as an exogenous oxidative challenge to couple with NRF1a and Nrf2a, as it resulted in a significant decrease in DNA synthesis (a) in the absence of increases in detached cells (b) or a decline in cell viability as detected by the WST-1 assay (c). Representative images were taken to demonstrate no difference in cell confluence or morphology between CON and 50 μM H_2O_2 (d-e). However, at the highest concentrations, morphology is altered along with confluence (f). *p<0.05 compared to CON

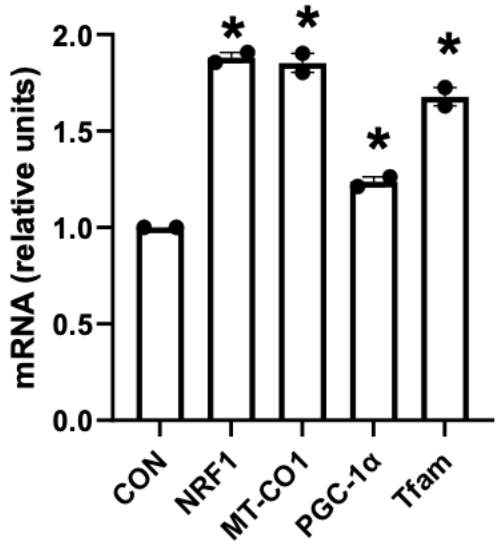

Figure A.2. Expression of NRF1-regulated genes increases following treatment of C2C12 cells with NRF1 activator. After 6 hours of treatment with 20 μg/ml NRF1a, there was a robust increase in genes related to mitochondrial biogenesis relative to CON. Genes included nuclear respiratory factor 1 (NRF1), mitochondrially encoded cytochrome oxidase 1 (MT-CO1), peroxisome proliferator-activated receptor-gamma coactivator 1-alpha (PGC-1α), and transcription factor A mitochondrial (T-fam) *$p<0.05$ compared to CON

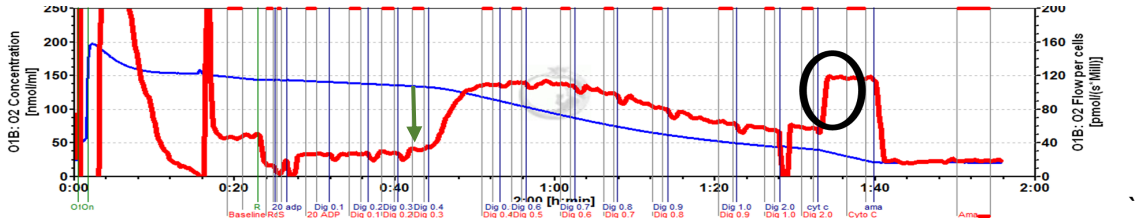

Figure A.3. Digitonin titration O2K tracing. Mitochondrial oxygen consumption was measured via high-resolution respirometry in C2C12s treated with increasing concentrations of digitonin to permeabilize the plasma membrane. Respiration was maximized at a digitonin concentration of 1.62 μM shown right after the 50 min mark (green arrow). Thereafter, an oxygen dependence is observed with the parallel decreasing blue line (oxygen concentration; left y-axis) and red line (flux derivative; right y-axis). Consequently, after the addition of cytochrome c (circled in black), there was a robust increase in flux, implying over permeabilization at the higher concentrations of digitonin. Therefore, 1.62 μM digitonin was chosen for all experimental respiration measurements.

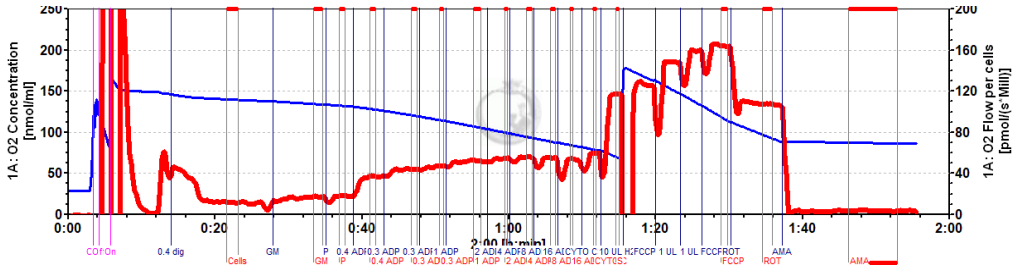

Figure A.4. Representative tracing of an experimental ADP titration during high-resolution respirometry. At ~20 min, cells were placed in the respirometry chamber, followed by titration of 1.62 µM of digitonin. After 10 minutes, substrate titrations were initiated. Over time, as the mitochondria consume oxygen, the blue line (oxygen concentration; left y-axis) decreases with concomitant increases in the red line (flux derivative; right y-axis). Marks labeled in red were recorded for each step of the titration, and oxygen flux was normalized to cell count (pmol/s*million cells). When the oxygen concentration decreased to ~60 nmol/ml, the chamber was re-oxygenated with hydrogen peroxide, which is rapidly converted to oxygen by the catalase in the respiration buffer.

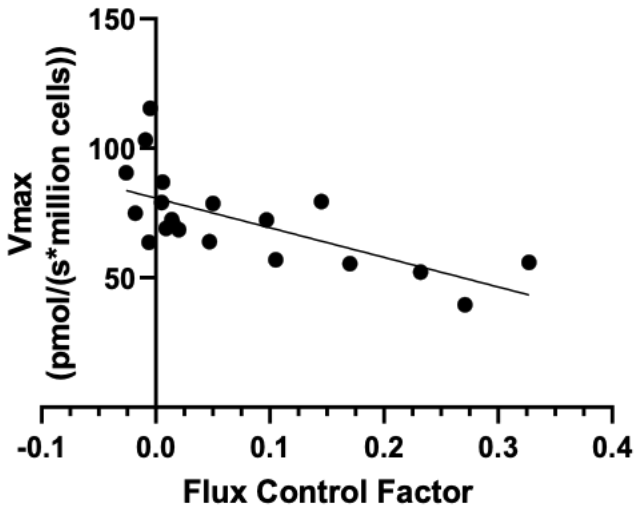

Figure A.5. Flux control factor to assessment membrane integrity. During mitochondrial high-resolution respirometry measurements, cytochrome c is titrated into the respirometry chambers to evaluate mitochondrial membrane integrity. Flux control factors were calculated in a subset of initial CON cell experiments. Specifically, the difference in the flux derivative just prior to and then immediately after stabilization following the addition of cytochrome c, was plotted against ADP Vmax. This relationship was used to identify the cut-off point at which a higher flux control factor decreased the ADP Vmax. Based on this assessment, for all experiments, we used a flux control factor cut-off of 0.12, a point below which ADP Vmax is unaltered.

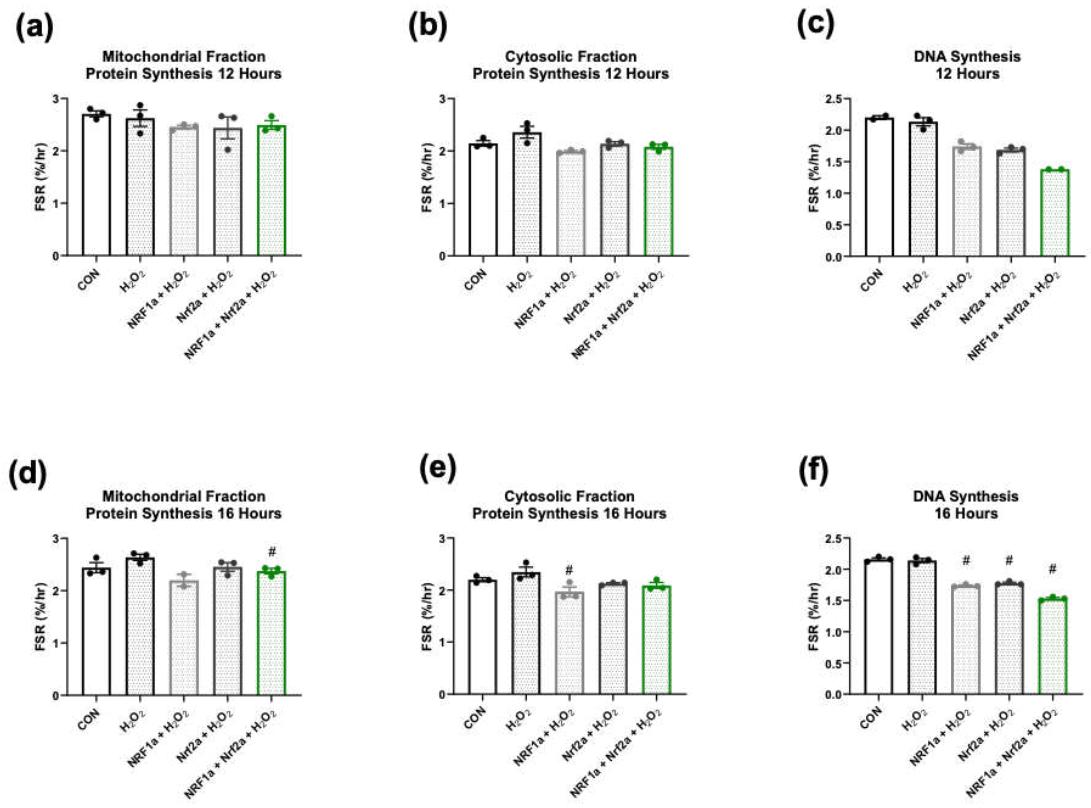

Figure A.6. Protein and DNA fractional synthesis rates. Using stable isotopic tracing with $^{2}H_2O$ enriched medium, we simultaneously monitored rates of new protein and DNA synthesis over 16 hrs of treatment with NRF1 and Nrf2 activators during a challenge with H_2O_2. Data reflecting 8 hrs of treatment are shown in Figure 2a-c, with data from the 12 hr and 16 hr time points shown here. Rates of protein and DNA synthesis were not significantly different among treatment groups at 12 hrs (a-c). At 16 hrs, there was a small but significant decline in mitochondrial protein synthesis, but no differences in cytosolic protein synthesis rates, in the combined NRF1a and Nrf2a treated cells (d and e). There were significant declines in DNA synthesis rates at 16 hrs in the NRF1a, the Nrf2a and the co-treatment of the NRF1a and Nrf2a compared to 50 μM H_2O_2 alone (f). #$p<0.05$ compared to H_2O_2

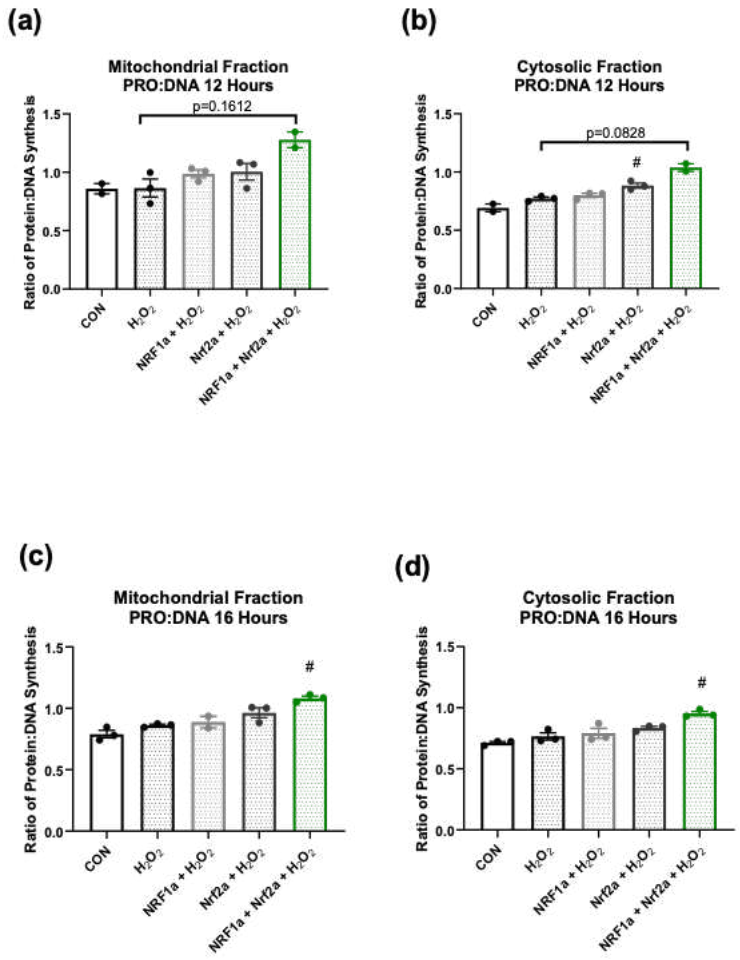

Figure A.7. Treatment with NRF1 and Nrf2 activators promotes mechanisms favoring maintenance of proteostasis during an oxidative challenge. To gain insight into the effect of treatments on allocation of newly synthesized proteins for somatic maintenance (proteostasis) versus for newly proliferating cells, we expressed the rates of protein synthesis relative to the rates of cell proliferation. Data reflecting 8 hrs of treatment are shown in Figure 2d-e, with data from the 12 hr and 16 hr time points shown here. There were no significant differences in the ratio of protein to DNA synthesis rates at 12 hours in the mitochondrial fraction (a). However, there was a significant increase in the ratio of protein synthesis to DNA synthesis in the cytosolic fraction in cells treated with the Nrf2a (b). It should be noted that the ratios for CON and NRF1a + Nrf2a + H_2O_2, only at the 12 hr time point, are based on n =2 due to low deoxyribose deuterium enrichment for GC/MS analysis. The p-value is p=0.1612 in the mitochondrial fraction and p=0.0828 in the cytosolic fraction between NRF1a + Nrf2a + H_2O_2 and H_2O_2 alone (a and b). There was a significantly greater ratio of both mitochondrial and cytosolic protein synthesis rates to DNA synthesis rates at 16 hrs in cells treated with a combination of NRF1a and Nrf2a under an oxidative challenge of H_2O_2, indicating greater allocation of newly synthesized proteins for proteome maintenance. Additionally, this improvement could not be explained by either NRF1a or Nrf2a alone (c and d). #p<0.05 compared to H_2O_2

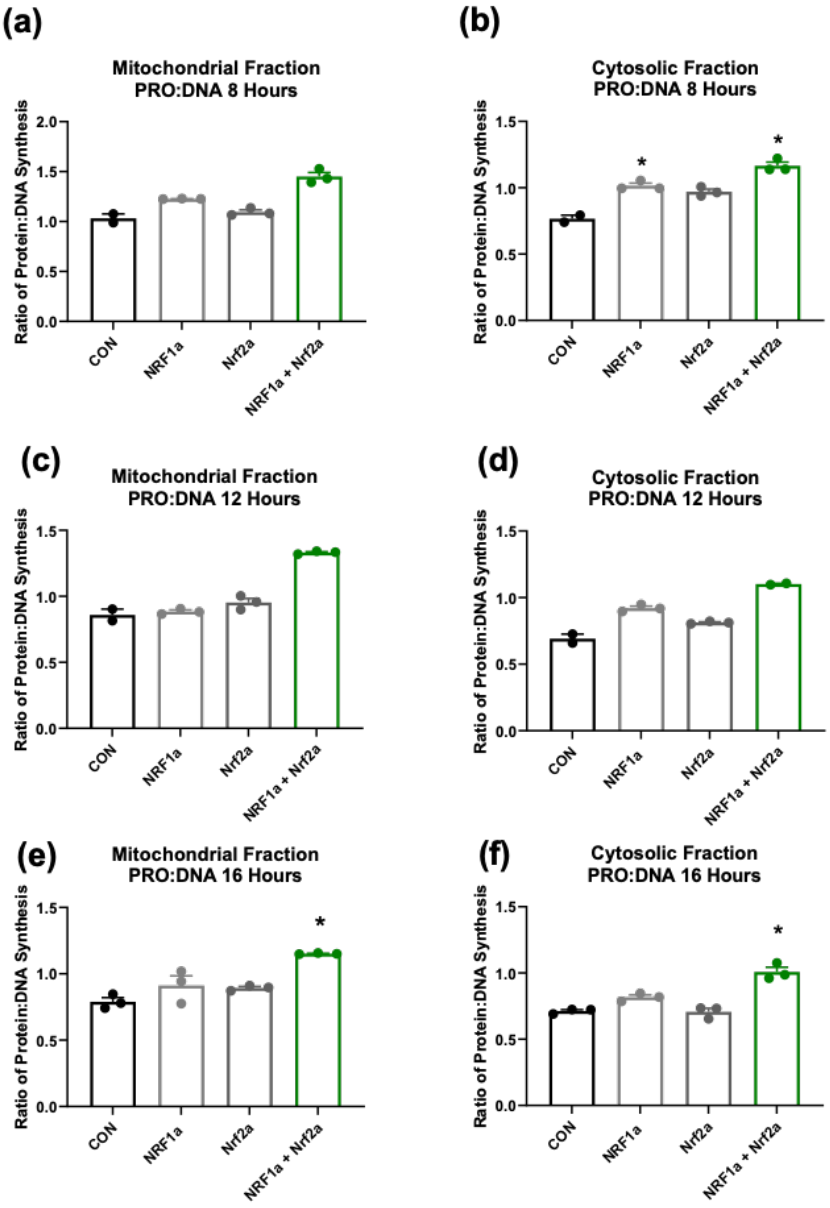

Figure S2.8. Ratio of protein to DNA synthesis in the absence of H_2O_2. In general, the beneficial effect of combined NRF1a and Nrf2a treatment on proteostatic maintenance is evident during challenge with a stress. Expressing the rates of protein synthesis relative to the rates of cell proliferation provides valuable insight into the proportion of newly synthesized proteins allocated for somatic maintenance versus for newly proliferating cells. As shown here, in the absence of H_2O_2, there are no differences in the ratio of mitochondrial protein synthesis: DNA synthesis rates at 8 or 12 hrs of treatment (a and c). In the cytosolic fraction, there was a greater ratio for the NRF1a treated and the co-treated cells compared to CON at 8 hrs (b). There were no differences in the cytosolic fraction at 12 hrs. However, after 16 hrs of combined treatment with NRF1a and Nrf2a, there was a greater ratio of mitochondrial and cytosolic protein synthesis: DNA synthesis rates, suggesting that this longer duration treatment (even in the absence of an oxidative challenge) favors proteome maintenance (e-f). *$p<0.05$ compared to CON

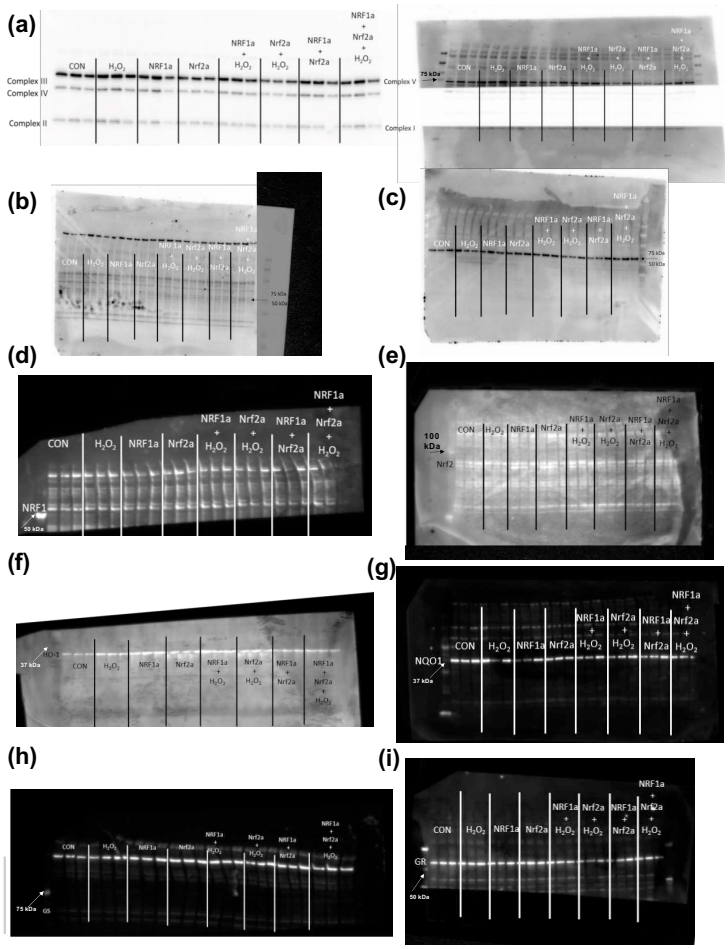

Figure A.9. Representative western blot images from data provided in Figures 4-6. C2C12 myoblast whole cell lysates (2.5 µg of protein/lane) were separated on 4-20% criterion gels followed by transfer to PVDF membranes. Representative full western blots for all proteins presented in Figures 4-6 are as follows: (a) the 5 OXPHOS complexes shown in 2 separate exposures, (b) AMPK phosphorylated at Th172, (c) total AMPK, (d) NRF1, (e) Nrf2, (f) heme oxygenase-1; HO-1, (g) NAD(P)H quinone dehydrogenase; NQO1, (h) glutathione synthetase, (I) glutathione reductase. Arrows denote the appropriate molecular weight markers.

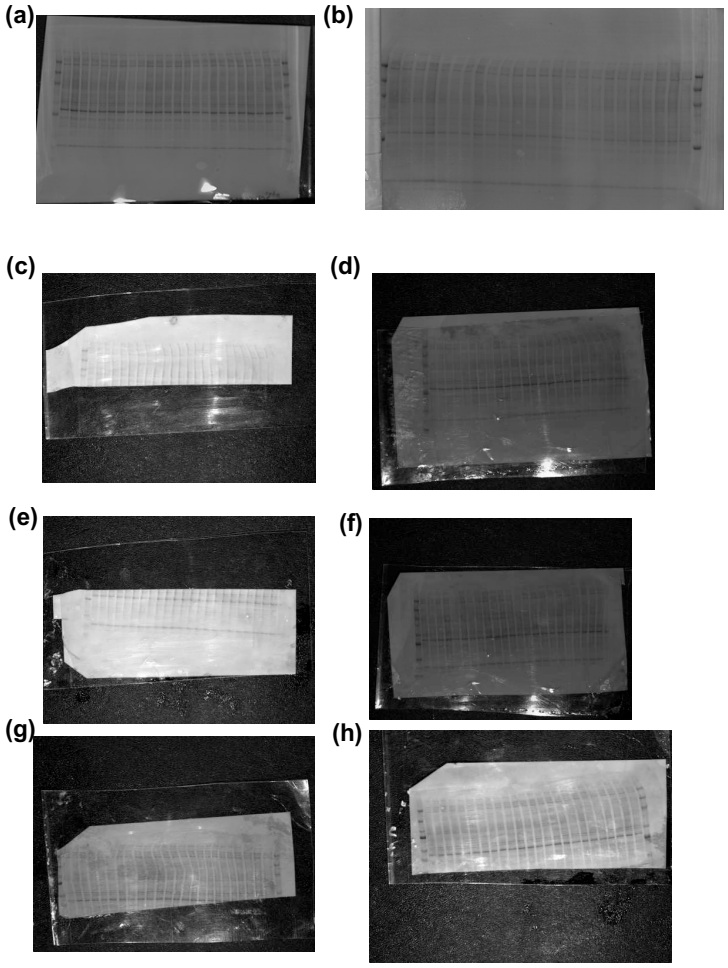

Figure A.10. Representative amido black stains for total protein content. Following completion of immunoblotting for proteins, PVDF membranes were stained with amido black and then used for total protein normalization. Representative full western blots for total protein quantification presented in Figures 4-6 are as follows: (a) the 5 OXPHOS complexes, (b) AMPK phosphorylated at Th172, which was then stripped before probing for total AMPK, (c) NRF1, (d) Nrf2, (e) heme oxygenase-1; HO-1, (f) NAD(P)H quinone dehydrogenase; NQO1, (g) glutathione synthetase, (h) glutathione reductase.

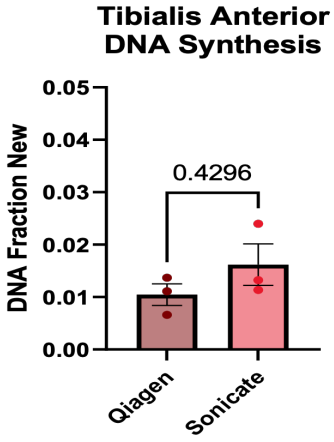

Figure B.1. Comparison of two methods for DNA extraction for downstream GCMS analysis of isotope labeling. For assessments incorporation of deoxyribose with the deuterium label into newly synthesized DNA we needed a crude DNA isolation from tissue homogenates. Because DNA quality is not a priority, we employed a faster and more cost-effective method of isolating DNA through sonication. Briefly samples (< 5 mg of powdered tissue suspended in 200 ul of MiliQ water) were sonicated for 10 seconds 6 times allowing samples to cool on ice in between repetitions. To confirm that the fraction new of the deoxyribose derivative is similar a subset of samples was analyzed using sonication and a Qiagen DNA Kit extraction (QIAmp DNA Kit) for the tibialis anterior (A) $p>0.05$ indicating the methods were not different.

Supplemental Table B.1 Western Blotting Conditions. This table presents the western blotting conditions for each protein that was probed for using previously reported methods. Approximately 20 µg of protein was loaded into a 4% - 20% Criterion pre-cast gel (Bio-Rad, Hercules, CA, USA) and resolved at 120 V for 120 min. The proteins were then transferred at 60 V for 105 min in transfer buffer (20% w/v methanol, 0.02% w/v SDS, 25 mM Tris Base, 192 mM glycine, pH 8.3). Membranes were then blocked and incubated with primary antibodies on a shaker overnight in 4^{o}C. Membranes were rinsed and then incubated with appropriate secondary antibodies. See supplemental table 1 for all western blotting conditions. After the membranes were rinsed, Western Lightening ECL Enhanced (Perkin Elm NEL 104001EA) was applied and the membranes were subsequently imaged using a FluorChem E Chemiluminescence Imager (Protein Simple, San Diego, CA, USA). Total protein was either quantified using Ponceau S or amido black.

Antibody	Block Reagent	Primary Cat #	Primary Reagent	Primary concentration	Secondary Cat #	Secondary Reagent	Secondary concentration	Exposure time
Nrf2	1% milk in 1xTBST	Santa Cruz: 365949	1% milk in 1xPBS	1:1,000	Santa Cruz: 2005	5% BSA in 1xTBST	1:10,000	2:40 (min:sec)
NQO1	1% milk in 1xTBST	Novus: 208200	1% milk in 1xPBS	1:1,000	Santa Cruz: 2005	5% BSA in 1xTBST	1:10,000	0:40 – 2:40 (min:sec)
OXPHOS	5% BSA in 1xTBST	Abcam: 110413	1% milk in 1xPBS	1:1,000	Santa Cruz: 2005	5% BSA in 1xTBST	1:10,000	0:35 – 1:57 (min:sec)
Phospho-eIF2	5% BSA in 1xTBST	Cell Signaling: 3579S	5% BSA in 1xTBST	1:1,000	Proteintech: SA00001-2	5% BSA in 1xTBST	1:10,000	2:40 (min:sec)
Total eIF2	5% BSA in 1xTBST	Cell Signaling: 5324S	5% BSA in 1xTBST	1:1,000	Proteintech: SA00001-2	5% BSA in 1xTBST	1:10,000	00:40 (min:sec)
p21	5% milk in 1xTBST	Santa Cruz: 6246	5% milk in 1xTBST	1:1,000	Santa Cruz: 2005	5% milk in 1xTBST	1:3,000	00:40 (min:sec)
Cyclin D	5% milk in 1xTBST	Proteintech: 26939	5% milk in 1xTBST	1:1,000	Proteintech: SA00001-2	5% milk in 1xTBST	1:10,000	00:40 (min:sec)
Phospho-H2AX	5% milk in 1xTBST	Cell Signaling: 9718	5% milk in 1xTBST	1:1,000	Proteintech: SA00001-2	5% milk in 1xTBST	1:1,000	2:40 (min:sec)

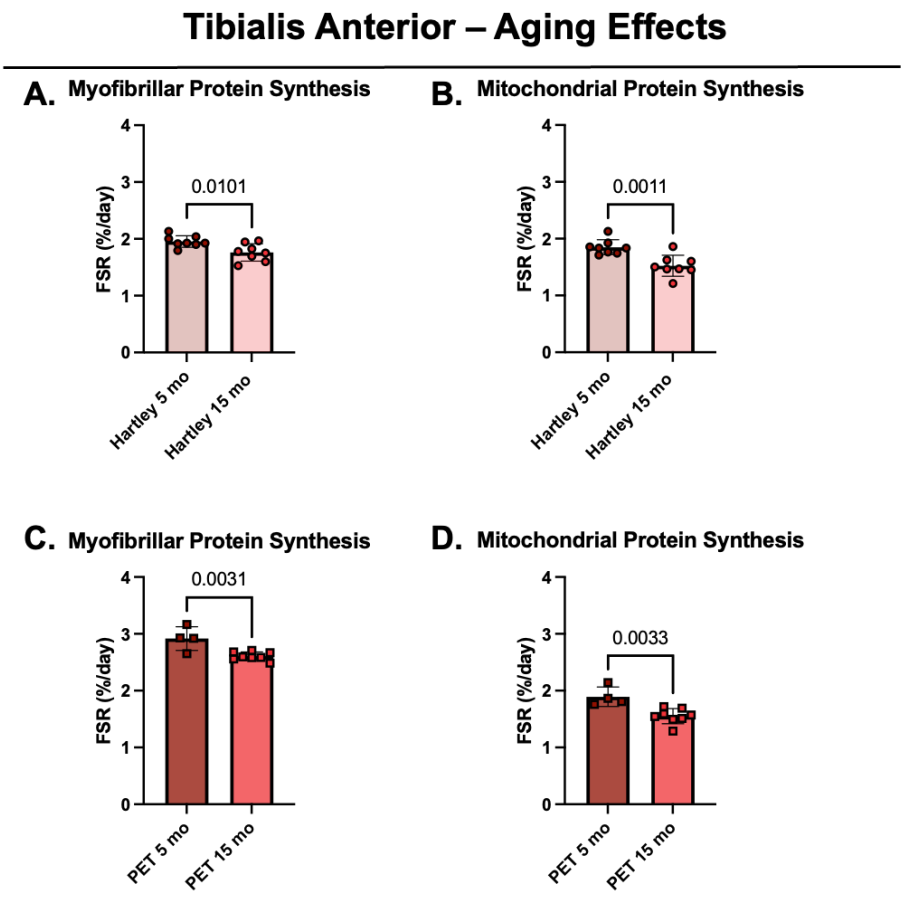

Figure B.2. Hartley and PET guinea pigs experience age-related decreases in rates of tibialis anterior protein synthesis. A subset (n=8/group to match PET n-value) of 5 and 15 mo Hartley guinea pigs were used to determine age-related changes in rates of protein synthesis. Rates of tibialis anterior myofibrillar (A) and mitochondrial (B) protein synthesis in Hartley guinea pigs significantly decreased from 5 to 15 mo of age. Additionally, rates of tibialis anterior myofibrillar (C) and mitochondrial (D) protein synthesis in PET guinea pigs significantly decreased from 5 to 15 mo of age.

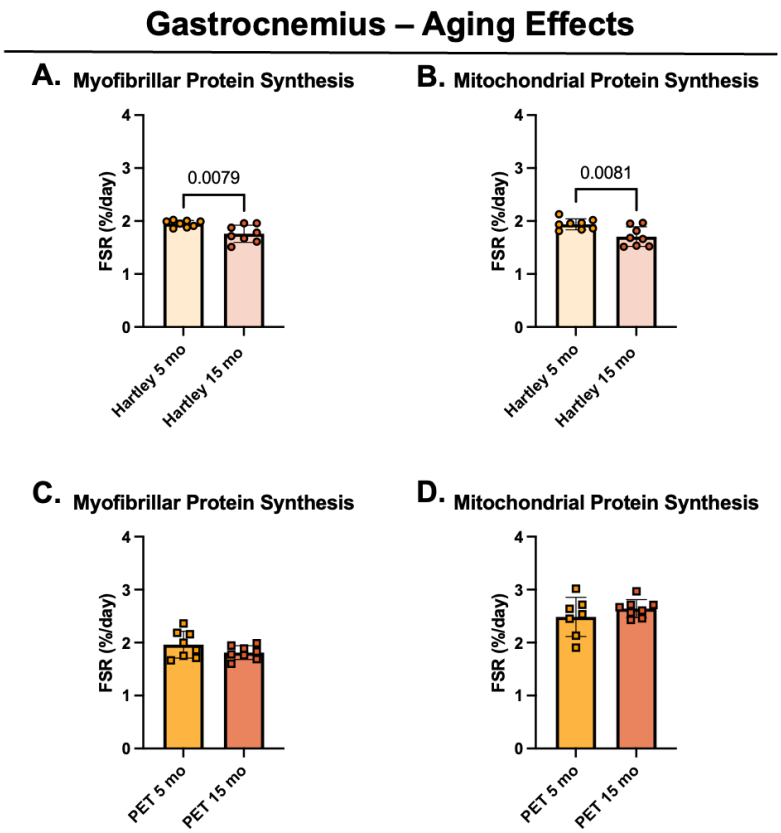

Figure B.3. Hartley and PET guinea pigs experience age-related decreases in rates of gastrocnemius protein synthesis. A subset (n=8/group to match PET n-value) of 5 and 15 mo Hartley guinea pigs were used to determine age-related changes in rates of protein synthesis. Rates of gastrocnemius myofibrillar (A) and mitochondrial (B) protein synthesis in Hartley guinea pigs significantly decreased from 5 to 15 mo of age. However, rates of gastrocnemius myofibrillar (C) and mitochondrial (D) protein synthesis in PET guinea pigs were maintained from 5 to 15 mo of age.

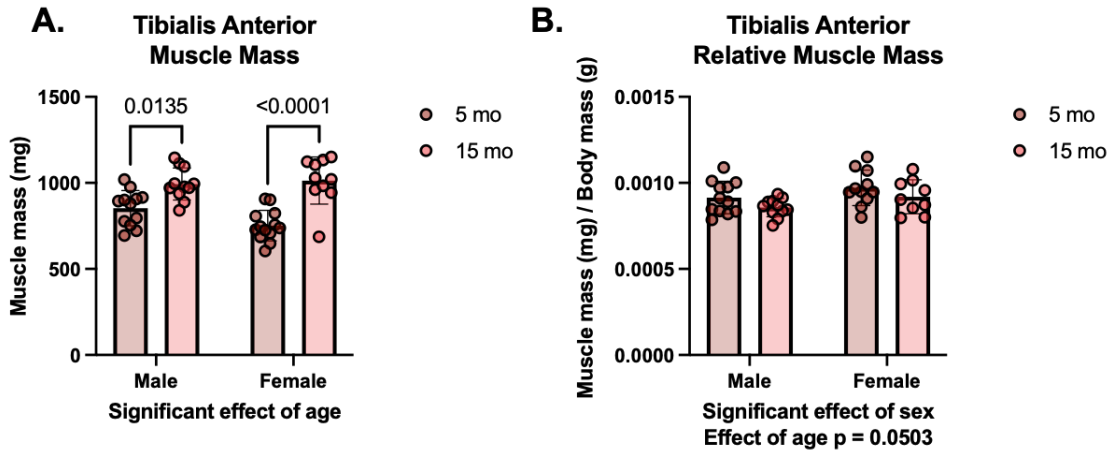

Supplemental Figure B.4 Age-related changes in tibialis anterior muscle mass. There was an increase from 5 to 15 mo in tibialis anterior skeletal muscle mass in Hartley guinea pigs (A). However, when muscle mass was expressed relative to body mass there was a trend to decrease relative muscle mass ($p = 0.0503$) and an overall effect of sex that relative muscle mass in female Hartley guinea pigs was higher than male Hartley guinea pigs (B).

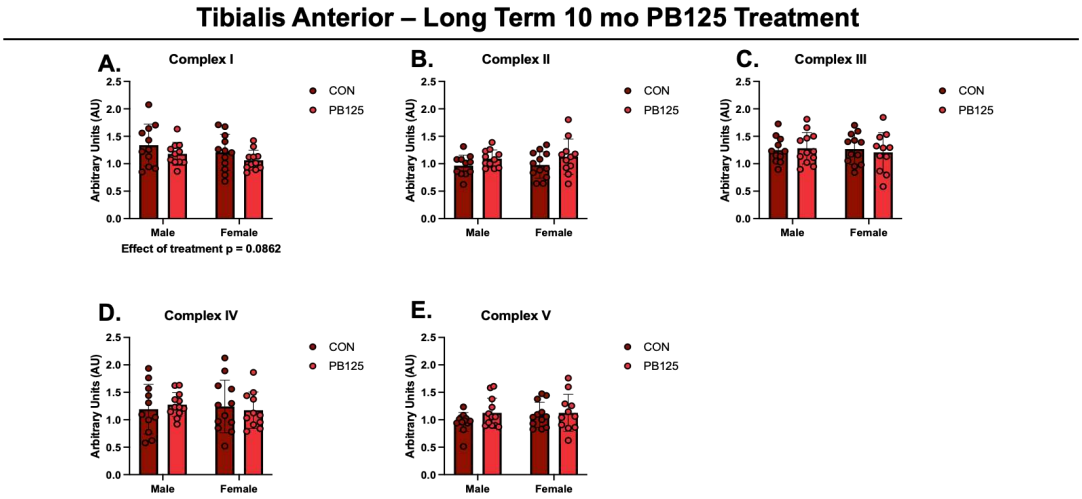

Figure B.5. Long-term 10 mo PB125 treatment maintains rates of tibialis anterior protein synthesis. Rates of myofibrillar (A), mitochondrial (B), cytosolic (C), and collagen (D) protein synthesis were maintained with 10 mo of daily PB125 treatment.

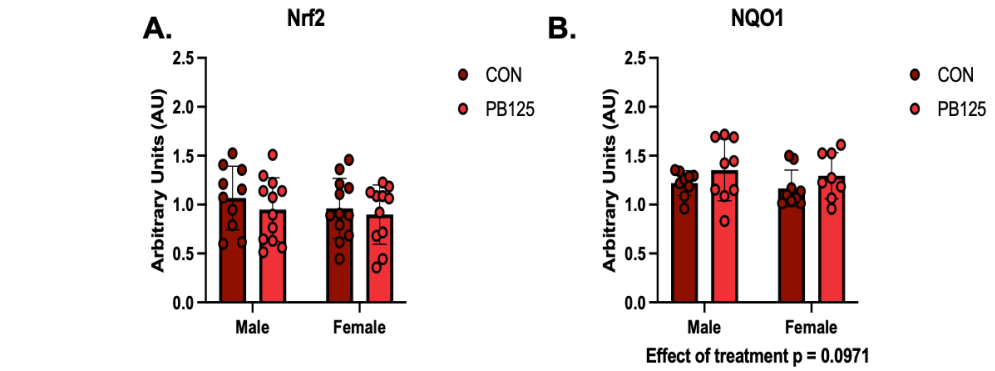

Figure B.6. Long-term 10 mo PB125 treatment does not increase Nrf2 or NQO1. Given we treated Hartley guinea pigs with a Nrf2 activator we wanted to examine if increases in Nrf2 protein content mediated some of these changes in tibialis anterior mechanisms of proteostasis. We did not observe an effect of treatment in the Nrf2 (A) or NQO1 (B) protein after 10 mo of PB125 treatment.

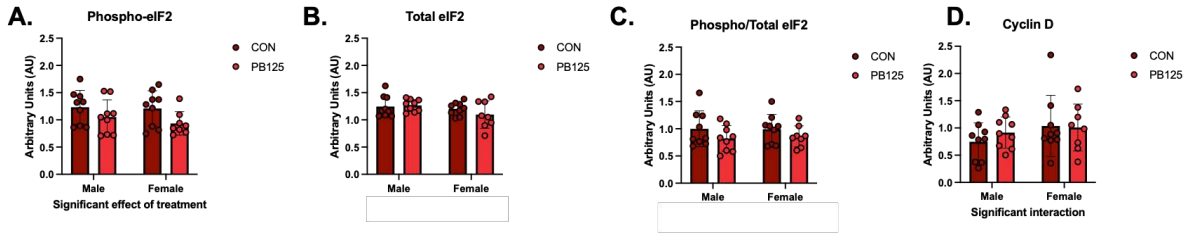

Figure B.7. Long-term 10 mo PB125 treatment does not alter the phosphorylation state of eIF2 or cyclin D. Because we observed an overall effect of PB125 treatment increased ribosomal biogenesis (driven by male Hartley guinea pigs) we examined if the phosphorylation state of eIF2, a protein critical for translation, was altered. Opposite to what we would expect there was a significant effect of PB125 treatment to decrease phosphorylated eIF2 (A). However, there were no differences in total eIF2 (B) or the ratio of phosphorylated to total eIF2 (C). Collectively, this suggests that the phosphorylation state of eIF2 was not altered. However, there was a significant interaction of sex by treatment for cyclin D protein content (D). When t-tests were performed in males and females there were no differences in cyclin D protein content (data not shown). Therefore, we conclude that 10 mo of PB125 treatment did not alter cyclin D protein content.

Tibialis Anterior – Long Term 10 mo PB125 Treatment

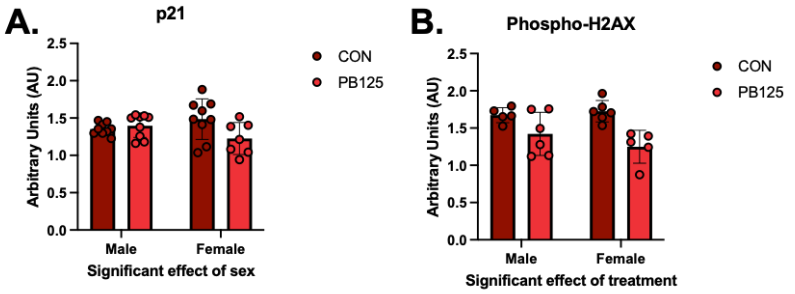

Figure B.8. Long-term 10 mo PB125 alters markers of skeletal muscle cellular senescence and senescence-associated DNA damage in a sex-specific manner. Because rates of DNA synthesis were decreased with PB125 treatment we interrogated markers of senescence and senescence associated DNA damage. There was an overall effect of sex on p21, a marker of cellular senescence (A). There was also an overall effect of treatment to decrease phospho-H2AX, a marker of senescence associated DNA damage (B). Because of the sex and PB125 treatment by sex interactions we additionally analyzed treatment differences within a given sex (Figure 3.6).

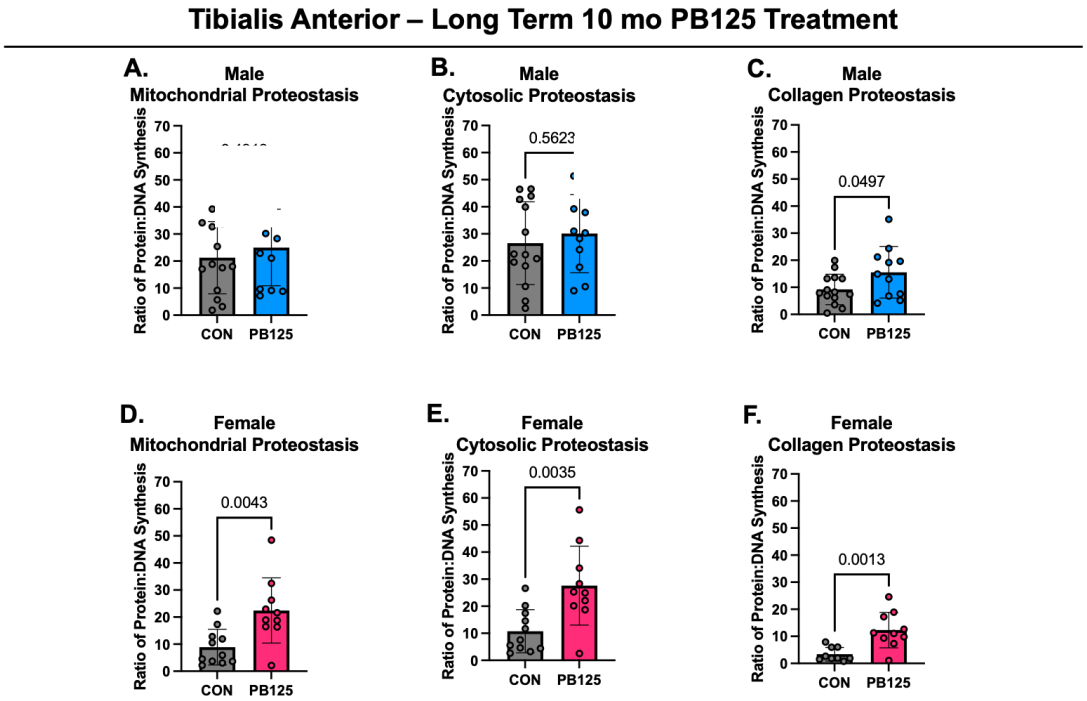

Figure B.9. Long-term 10 mo PB125 increased mechanisms of proteostasis in a sex-specific manner. When sexes were analyzed separately, PB125 did not increase mechanisms of mitochondrial (A) and cytosolic (B) proteostasis in male Hartley guinea pigs but it did increase mechanisms of mitochondrial (D) and cytosolic (E) proteostasis in female guinea pigs. PB125 increased mechanisms of collagen proteostasis in both male (C) and female (F) Hartley guinea pigs.

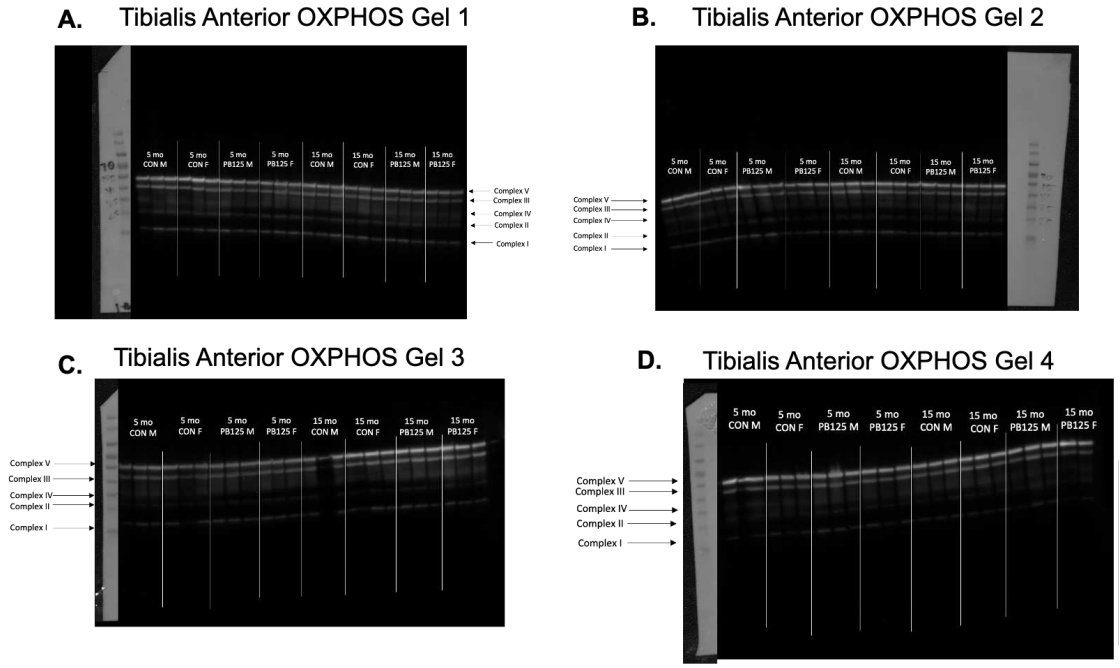

Figure B.10. Unedited and annotated full western blots for OXPHOS.

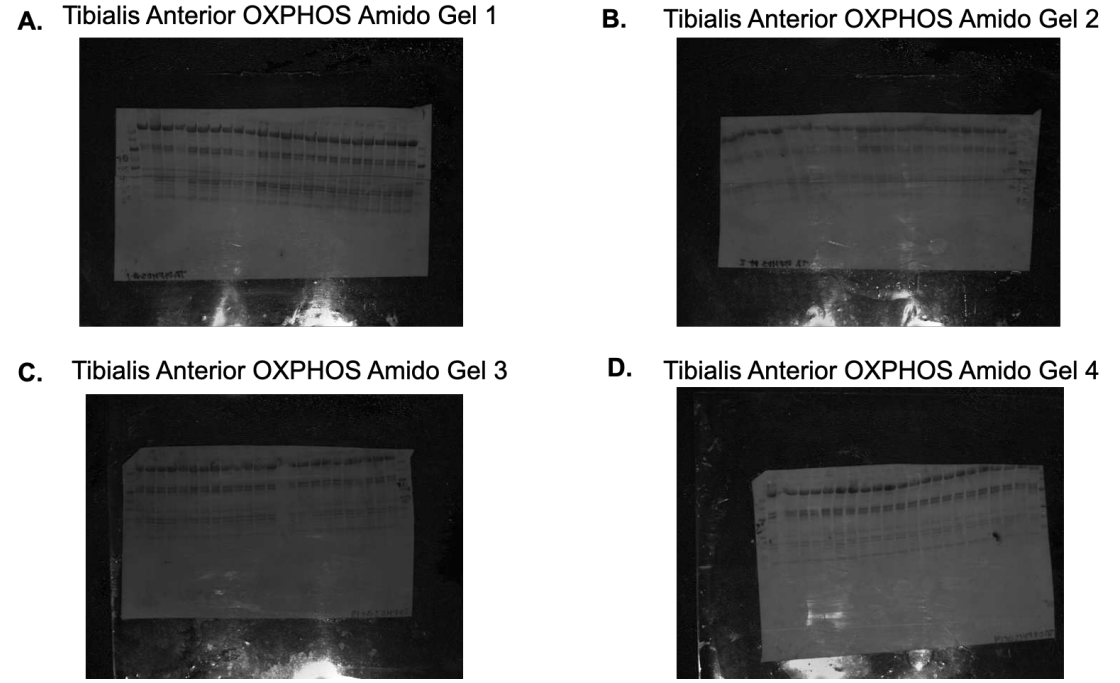

Figure B.11. Unedited full western blots for OXPHOS total protein stain, Amido Black.

A. Tibialis Anterior Nrf2 Gel 1

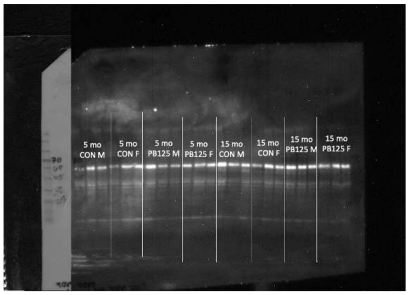

B. Tibialis Anterior Nrf2 Gel 2

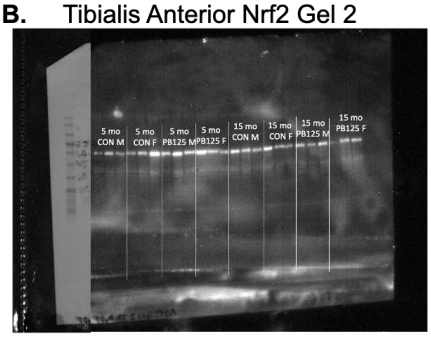

C. Tibialis Anterior Nrf2 Gel 3

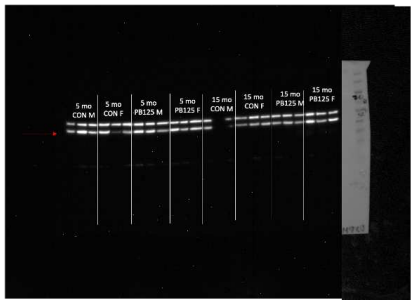

D. Tibialis Anterior Nrf2 Gel 4

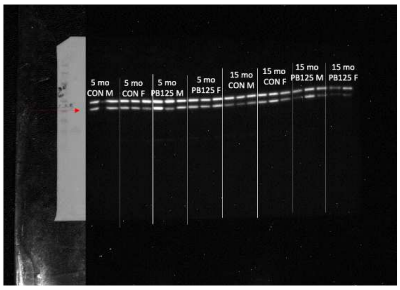

Figure B.12. Unedited and annotated full western blots for Nrf2.

A. Tibialis Anterior Nrf2 Amido Gel 1

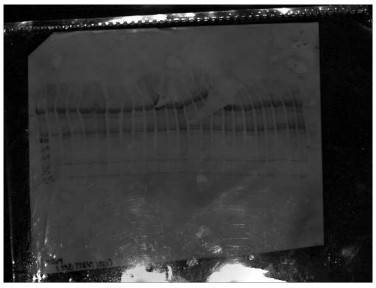

B. Tibialis Anterior Nrf2 Amido Gel 2

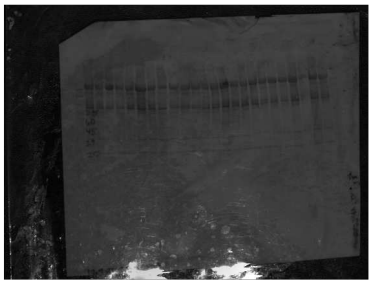

C. Tibialis Anterior Nrf2 Amido Gel 3

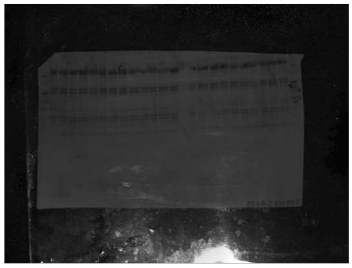

D. Tibialis Anterior Nrf2 Amido Gel 4

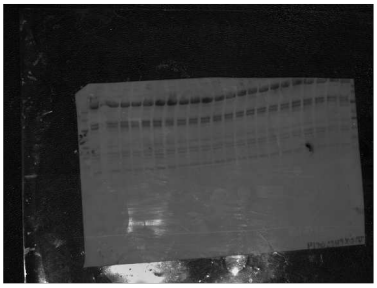

Figure B.13. Unedited full western blots for Nrf2 total protein stain, Amido Black.

A. Tibialis Anterior NQO1 Gel 1

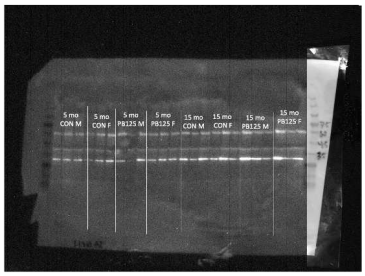

B. Tibialis Anterior NQO1 Gel 2

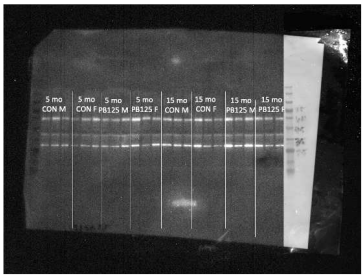

C. Tibialis Anterior NQO1 Gel 3

Due to resource constraints, we were not only able to perform the NQO1 Western Blot for Gel 3

D. Tibialis Anterior NQO1 Gel 4

Figure B.14. Unedited and annotated full western blots for NQO1. Resource constraints included running out of supplies.

A. Tibialis Anterior NQO1 Amido Gel 1

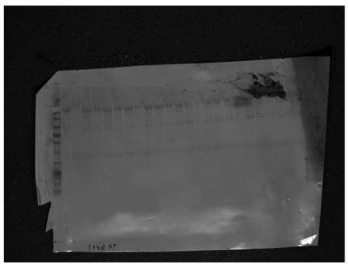

B. Tibialis Anterior NQO1 Amido Gel 2

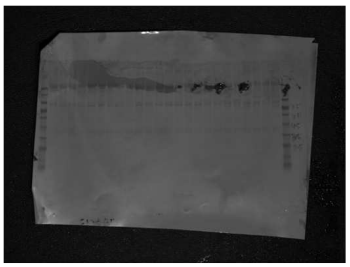

C. Tibialis Anterior NQO1 Amido Gel 3

Due to resource constraints, we were not only able to perform the NQO1 Western Blot for Gel 3

D. Tibialis Anterior NQO1 Amido Gel 4

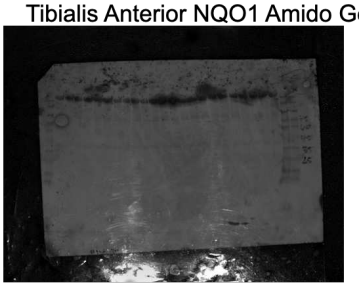

Figure B.15. Unedited full western blots for NQO1 total protein stain, Amido Black. Resource constraints included running out of supplies.

A. Tibialis Anterior p-eIF2 Gel 1

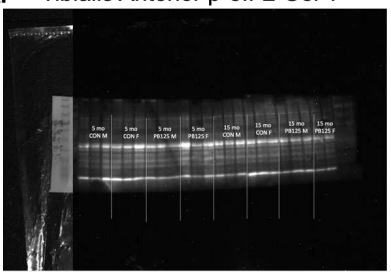

B. Tibialis Anterior p-eIF2 Gel 2

Due to resource constraints, we were not only able to perform the phospho eIF2 Western Blot for Gel 2

C. Tibialis Anterior p-eIF2 Gel 3

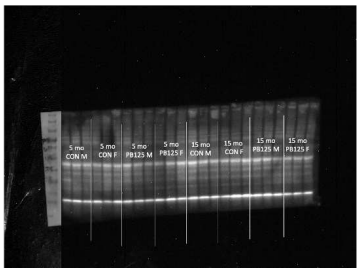

D. Tibialis Anterior p-eIF2 Gel 4

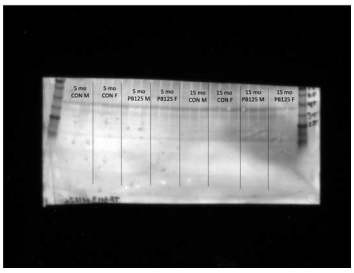

Figure B.16. Unedited and annotated full western blots for phospho-eIF2. Resource constraints included running out of supplies.

A. Tibialis Anterior t-eIF2 Gel 1

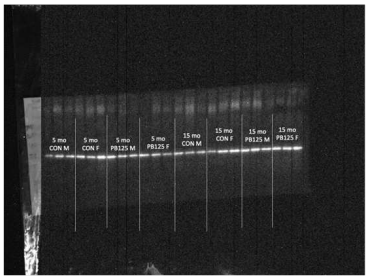

B. Tibialis Anterior t-eIF2 Gel 2

Due to resource constraints, we were not only able to perform the total eIF2 Western Blot for Gel 2

C. Tibialis Anterior t-eIF2 Gel 3

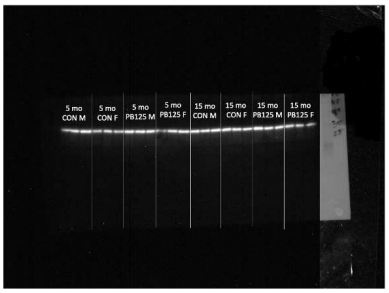

D. Tibialis Anterior t-eIF2 Gel 4

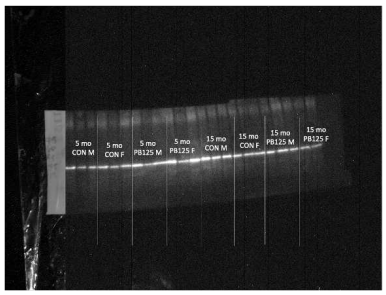

Figure B.17. Unedited and annotated full western blots for total eIF2. Resource constraints included running out of supplies.

A. Tibialis Anterior p/t eIF2 Amido Gel 1

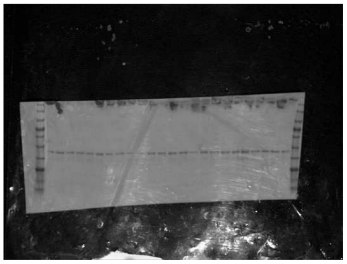

B. Tibialis Anterior p/t eIF2 Amido Gel 2

Due to resource constraints, we were not only able to perform the phospho and total eIF2 Western Blot for Gel 2

C. Tibialis Anterior p/t eIF2 Amido Gel 3

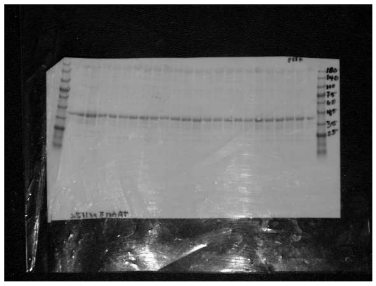

D. Tibialis Anterior p/t eIF2 Amido Gel 4

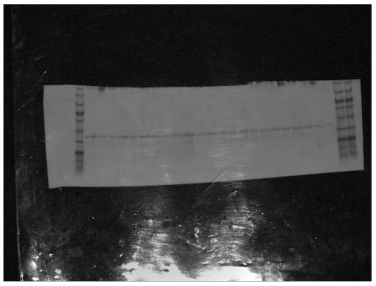

Figure B.18. Unedited full western blots for phosphor and total eIF2 total protein stain, ponceau. Resource constraints included running out of supplies.

A. Tibialis Anterior cyclin D Gel 1

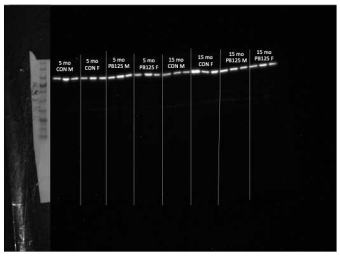

B. Tibialis Anterior cyclin D Gel 2

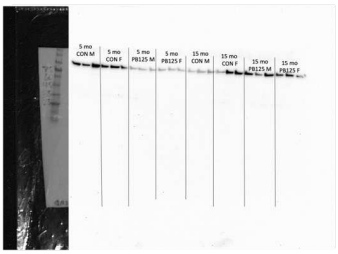

C. Tibialis Anterior cyclin D Gel 3

Due to resource constraints, we were not only able to perform the cyclin D Western Blot for Gel 3

D. Tibialis Anterior cyclin D Gel 4

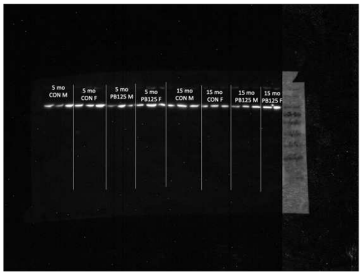

Figure B.19. Unedited and annotated full western blots for cyclin D. Resource constraints included running out of supplies.

A. Tibialis Anterior cyclin D Amido Gel 1

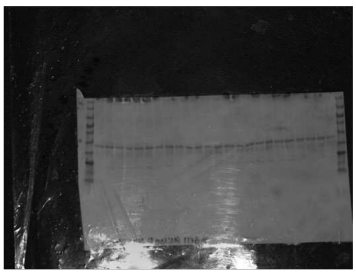

B. Tibialis Anterior cyclin D Amido Gel 2

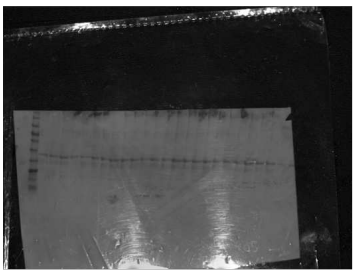

C. Tibialis Anterior cyclin D Amido Gel 3

Due to resource constraints, we were not only able to perform the cyclin D Western Blot for Gel 3

D. Tibialis Anterior cyclin D Amido Gel 4

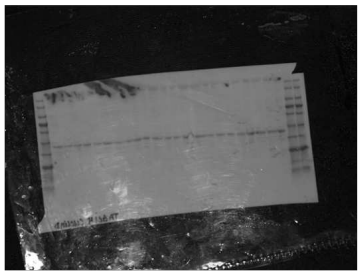

Figure B.20. Unedited full western blots for cyclin D total protein stain, ponceau. Resource constraints included running out of supplies.

A. Tibialis Anterior p21 Gel 1

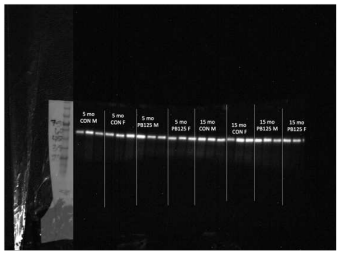

B. Tibialis Anterior p21 Gel 2

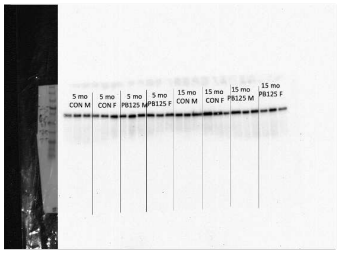

C. Tibialis Anterior p21 Gel 3

Due to resource constraints, we were not only able to perform the p21 Western Blot for Gel 3

D. Tibialis Anterior p21 Gel 4

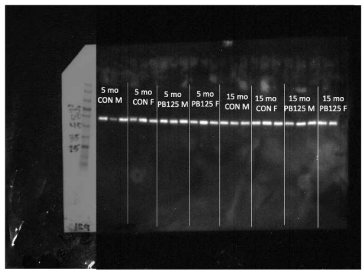

Figure B.21. Unedited and annotated full western blots for p21. Resource constraints included running out of supplies.

A. Tibialis Anterior p21 Amido Gel 1

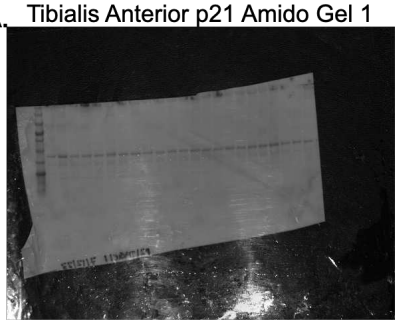

B. Tibialis Anterior p21 Amido Gel 2

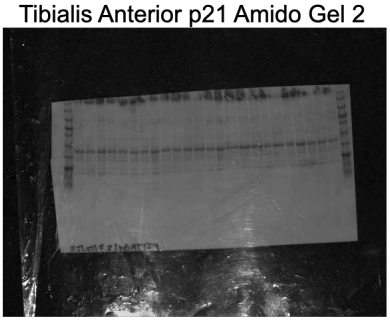

C. Tibialis Anterior p21 Amido Gel 3

Due to resource constraints, we were not only able to perform the p21 Western Blot for Gel 3

D. Tibialis Anterior p21 Amido Gel 4

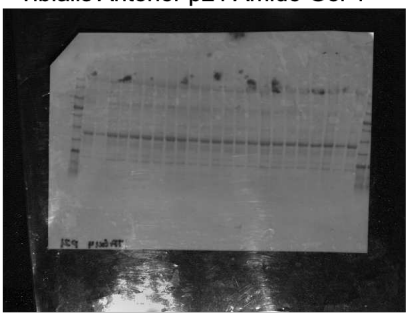

Figure B.22. Unedited full western blots for p21 total protein stain, ponceau. Resource constraints included running out of supplies.

A. Tibialis Anterior Phospho-H2AX Gel 1

Due to resource constraints, we were not only able to perform the P-H2AX Western Blot for Gel 1

B. Tibialis Anterior Phospho-H2AX Gel 2

Due to resource constraints, we were not only able to perform the P-H2AX Western Blot for Gel 2

C. Tibialis Anterior Phospho-H2AX Gel 3

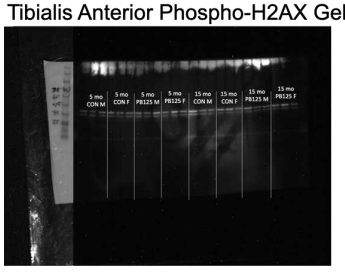

D. Tibialis Anterior Phospho-H2AX Gel 4

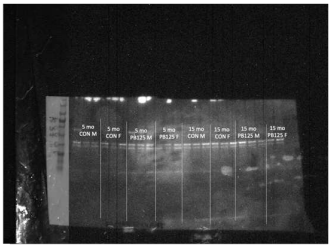

Figure B.23. Unedited and annotated full western blots for phospho-H2AX. Resource constraints included running out of supplies.

A. Tibialis Anterior Phospho-H2AX Amido Gel 1

Due to resource constraints, we were not only able to perform the P-H2AX Western Blot for Gel 1

B. Tibialis Anterior Phospho-H2AX Amido Gel 2

Due to resource constraints, we were not only able to perform the P-H2AX Western Blot for Gel 2

C. Tibialis Anterior Phospho-H2AX Amido Gel 3

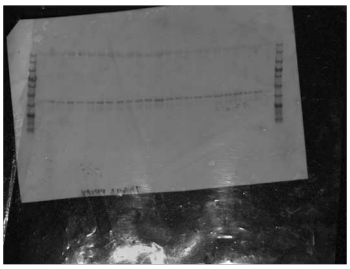

D. Tibialis Anterior Phospho-H2AX Amido Gel 4

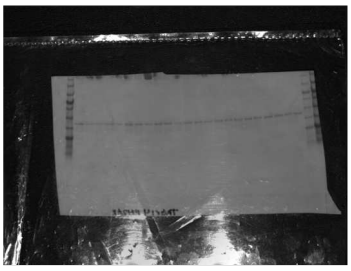

Figure B.24. Unedited full western blots for Phospho-H2AX total protein stain, ponceau. Resource constraints included running out of supplies.

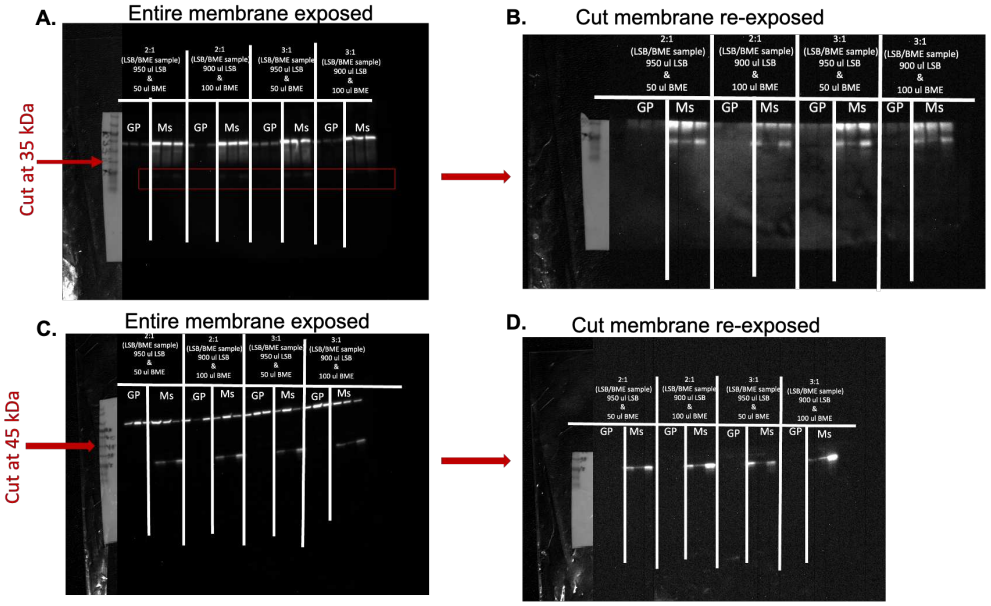

Figure B.25. Guinea pig versus mouse molecular weights variability for p21 (A and B) and cyclin D (C and D). As noted on the membranes various dilutions of 2-Mercaptoethanol (BME) and laemmli sample buffer (LSB) were used to determine if a greater amount of reducing reagent altered the resolution of the bands at the respective molecular weights. Additionally, guinea pig samples were run alongside skeletal muscle mouse samples to determine why in the guinea pig species there is only a band at three times the molecular weight for p21 (predicted molecular weight 21 kDa; guinea pig band 21*3 = ~63 kDa) and for cyclin D (predicted molecular weight 34 kDa; guinea pig band 21*3 = ~100 kDa). We suspected it this is a trimer. We concluded that changing the dilutions did not affect the molecular weights when the membrane was cut for p21 at 35 kDa (A) and re-exposed (B) or for cyclin D at 45 kDa (C) and re-exposed (D). Because the guinea pig species is not commonly utilized there are not many antibodies that are confirmed to be compatible with the guinea pig. We acknowledge this as a limitation.

APPENDIX C – CHAPTER 4 SUPPLEMENTAL FIGURES

Table C.1. Histology reagents. This table presents the immunohistochemistry and immunofluorescence conditions for each antibody that was probed for using previously reported methods. See methods for details regarding incubation time and temperature.

Probe	Block	1° Ab	1° Ab Cat #	1° Reagent	2° Ab	2° Cat #	2° Reagent	DAB/Fluoro
Iba1	10% donkey serum in Tris A/2% BSA	Rabbit 1:400	Quire:QAB10278	Tris A/2% BSA	Donkey 1:250	706-0650147	10% goat serum in 0.05M TBS	4:30 – 5:00
S100B	2% goat serum in Tris A/2% BSA	Mouse 1:500	Ab: 212816	2% goat serum 0.05M TBS	Goat 1:500	Invitrogen: A21422	2% goat 0.05M TBS	Alexa 555
C3	2% donkey serum in Tris A/2% BSA	Rabbit 1:100	Ab: 181147	2% donkey serum 0.05M TBS	Donkey 1:500	Invitrogen: A31573	2% donkey 0.05M TBS	Alexa 647
GFAP	2% goat serum 0.05M TBS	Rabbit 1:250	Dako: Z0334	2% goat serum 0.05M TBS	Goat 1:500	Invitrogen: A11008	2% goat 0.05M TBS	Alexa 488

Table C.2 Western Blotting Conditions. This table presents the western blotting conditions for each protein that was probed for using previously reported methods. Approximately 20 µg of protein was loaded into a 4% - 20% Criterion pre-cast gel (Bio-Rad, Hercules, CA, USA) and resolved at 120 V for 120 min. The proteins were then transferred at 60 V for 105 min in transfer buffer (20% w/v methanol, 0.02% w/v SDS, 25 mM Tris Base, 192 mM glycine, pH 8.3). Membranes were then blocked and incubated with primary antibodies on a shaker overnight in 4°C. Membranes were rinsed and then incubated with appropriate secondary antibodies. See supplemental table 1 for all western blotting conditions. After the membranes were rinsed, Western Lightening ECL Enhanced (Perkin Elm NEL 104001EA) was applied and the membranes were subsequently imaged using a FluorChem E Chemiluminescence Imager (Protein Simple, San Diego, CA, USA). Total protein was either quantified using amido black as previously described.

Antibody	Block Reagent	Primary Cat #	Primary Reagent	Primary concentration	Secondary Cat #	Secondary Reagent	Secondary concentration	Exposure time
Nrf2	1% milk in 1xTBST	Santa Cruz: 365949	1% milk in 1xPBS	1:1,000	Santa Cruz: 2005	5% BSA in 1xTBST	1:10,000	2:40 (min:sec)
NQO1	1% milk in 1xTBST	Novus: 208200	1% milk in 1xPBS	1:1,000	Santa Cruz: 2005	5% BSA in 1xTBST	1:10,000	0:40 (min:sec)

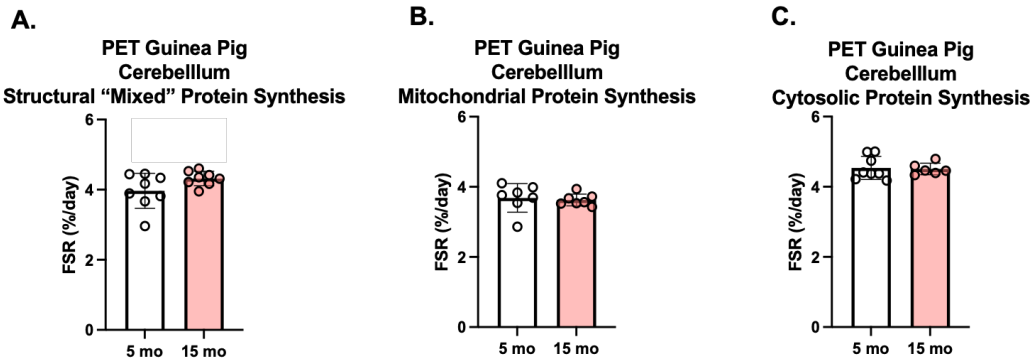

Figure C.1. Age-related changes in cerebellar protein synthesis in PET guinea pigs. From 5 to 15 months rates of structural or mixed (A), mitochondrial (B), and cytosolic (C) proteins were maintained in PET guinea pigs.

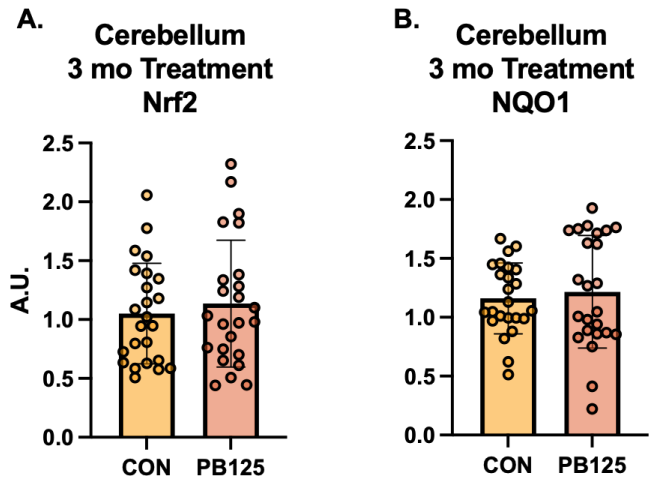

Figure C.2. Short-term PB125 treatment does not alter Nrf2 of NQO1 protein content. PB125, a purported Nrf2 activator, did not change Nrf2 protein (A) or NQO1, a downstream antioxidant of Nrf2, protein content (B) after 3 mo of treatment in the cerebellum of Hartley guinea pigs.

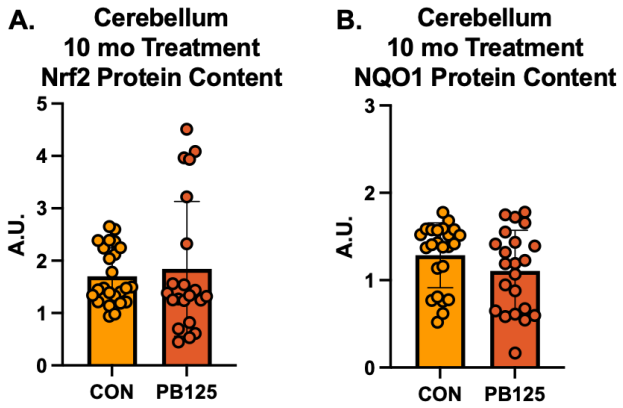

Figure C.3. Long-term PB125 treatment does not alter Nrf2 of NQO1 protein content. PB125, a purported Nrf2 activator, did not change Nrf2 protein (A) or NQO1, a downstream antioxidant of Nrf2, protein content (B) after 10 mo of treatment in the cerebellum of Hartley guinea pigs.

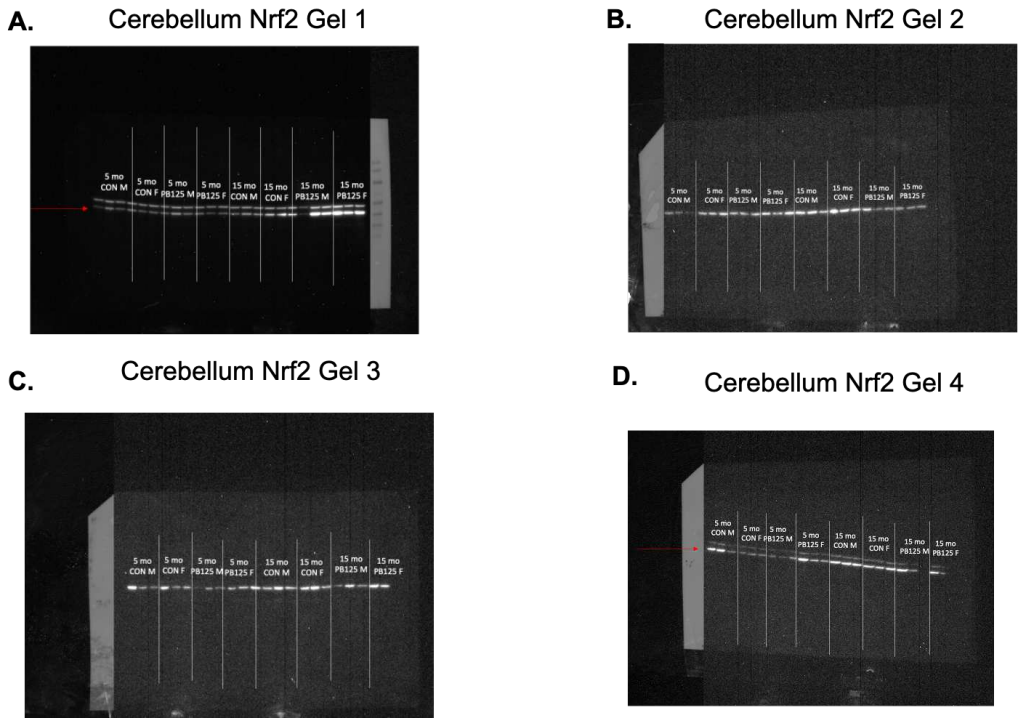

Figure C.4. Unedited and annotated full western blots for Nrf2.

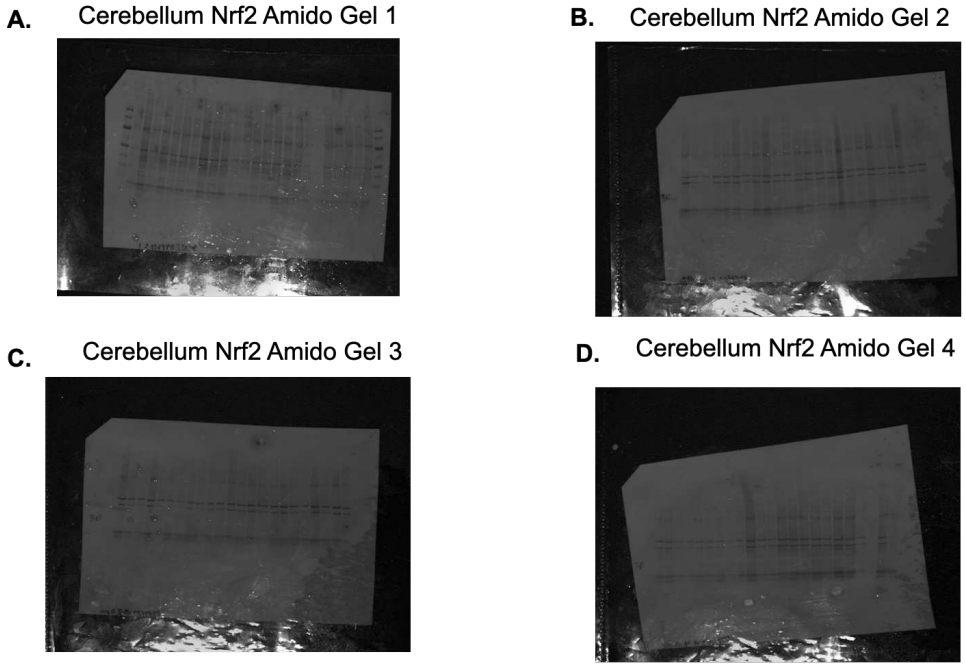

Figure C.5. Unedited full western blots for Nrf2 total protein stain, Amido Black.

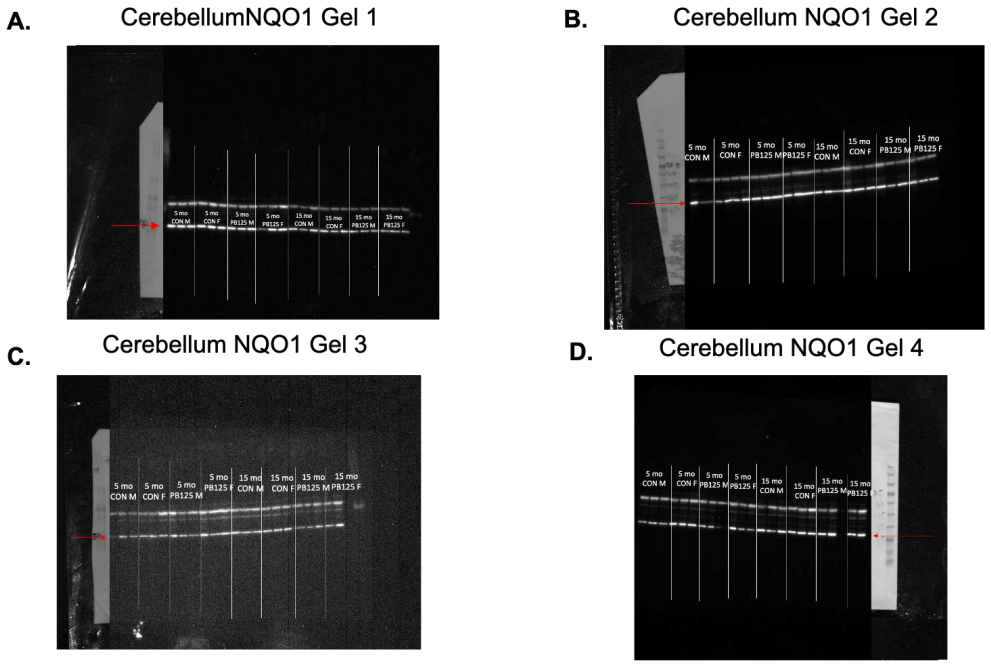

Figure C.6. Unedited and annotated full western blots for NQO1.

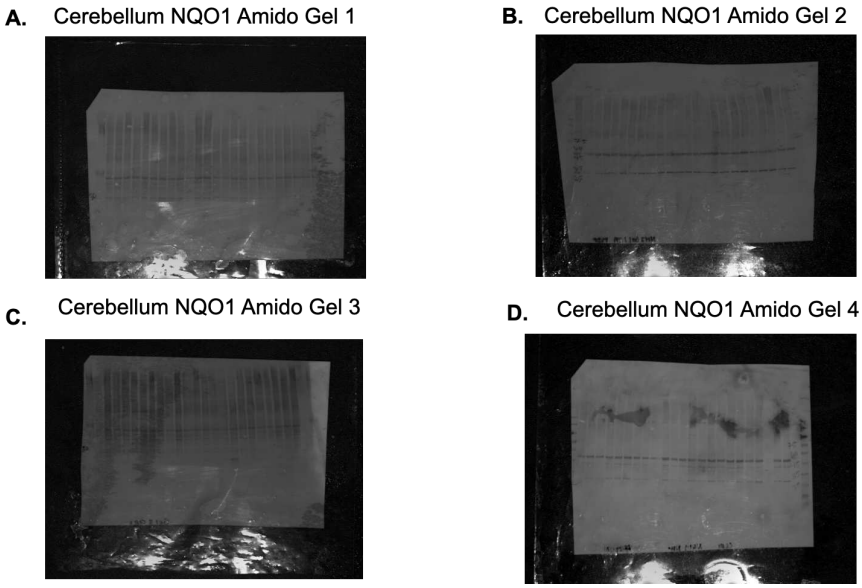

Figure C.7. Unedited full western blots for NQO1 total protein stain, Amido Black.

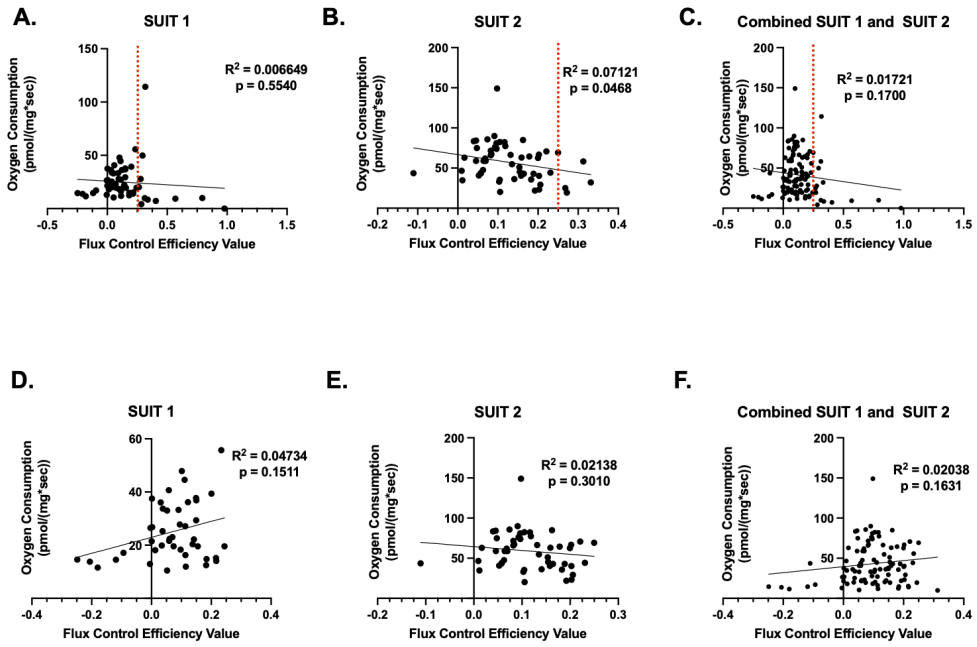

Figure D.1. Calculation of cytochrome C efficiency values. Given this is the first time that guinea pigs hippocampal samples have been respired in an Oroboros O2k we sought to determine the appropriate flux control efficiency value for inclusion of O2k runs through the addition of cytochrome c which is added to chambers to test mitochondrial membrane integrity in line with best practices. The flux control efficiency value is defined as the flux after addition of the cytochrome c titration (reference state) minus flux before the cytochrome c titration (background state) divided by flux after the cytochrome c addition (reference state). If samples are over-permeabilized, either through mechanical or chemical means, mitochondrial cytochrome c is lost resulting in a non-biological loss of respiration. When exogenous cytochrome c is subsequently added, this over-permeabilization is evidenced by a “meaningful” increase in oxygen flux (i.e., flux control efficiency value). A threshold for the flux control efficiency value must be established for each experimental paradigm to determine how large of an increase in oxygen flux is indicative of over-permeabilization necessitating exclusion from data analysis. This “meaningful” cytochrome c threshold varies across cell-types, tissues, and species. The threshold is based on the presence of a negative linear relationship between the flux control factor and the titration step right before the addition of cytochrome c. Values that are greater than (X%) flux control should, therefore, be removed from analysis to prevent biasing the outcomes by over-permeabilization. The reference state is graphed for each flux control efficiency value for the SUIT 1 ADP titration protocol (A), SUIT 2 protocol (B), and combined SUIT 1 and 2 protocols (C) where a significant negative linear relationship exists for the SUIT 2 (B) and combined SUIT 1 and 2 protocols (C). When we removed values greater than 0.25 (denoted by the red dashed line) the negative linear relationship dissipated ($p>0.05$) and minimally influence variance (minimize R^2 value) for SUIT 1 ADP titration protocol (D), SUIT 2 protocol (E), and the combined SUITs 1 and 2 (F). This threshold of 0.25 is also what has been reported in permeabilized samples from guinea pig skeletal muscle.

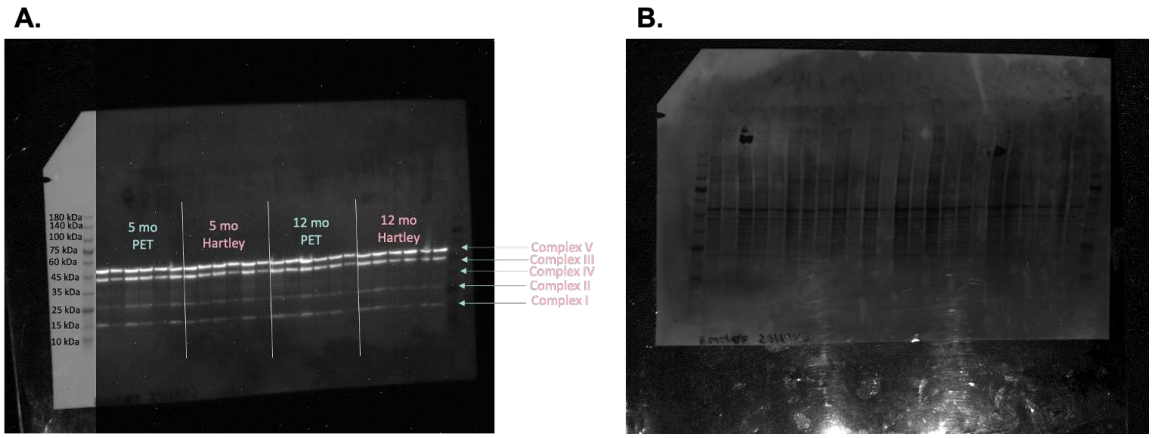

Figure D.2. OXPHOS Western Blot. Western blotting was used to measure relative content of OXPHOS proteins in a subset of tissues as previously described by our group. Panel A shows the entire unedited blot. 15 - 30 mg portions of the hippocampus (n=6 per treatment group to ensure all comparisons were made on the same gel/membrane) were homogenized in a Bullet Blender with zirconium beads and 0.3 mL of radioimmunoprecipitation assay (RIPA) buffer (150 mM NaCl, 0.1 mM EDTA, 50 mM Tris, 0.1% sodium deoxycholate, 0.1% SDS, 1% Triton X-100, pH = 7.50) with HALT protease inhibitors. Protein concentration was determined with BCA assay (ThermoFisher 23225). Samples were reduced (50 µL of B-mercaptoethanol and 950 µL of 2x laemmli sample buffer BioRad 1610737) and heated at 50^{o}C for 10 min. Approximately 20 µg of protein was loaded into a 4% - 20% Criterion pre-cast gel (Bio-Rad, Hercules, CA, USA) and resolved at 120 V for 120 min. The proteins were then transferred at 60 V for 105 min in transfer buffer (20% w/v methanol, 0.02% w/v SDS, 25 mM Tris Base, 192 mM glycine, pH = 8.3). Membranes were then blocked (5% BSA in TBST) and incubated with primary antibodies (1% non-fat milk in PBS; 1:1,000) against total OXPHOS proteins (Abcam 110413, Lot # Q5039) on a shaker overnight in 4^{o}C. Membranes were rinsed and then incubated with appropriate secondary antibodies for (5% BSA in TBST; 1:10,000) OXPHOS (goat anti-mouse Santa Cruz 2005, Lot # D1614). After the membranes were rinsed, Western Lightening ECL Enhanced (Perkin Elm NEL104001EA) was applied and the membranes were subsequently imaged using a FluorChem E Chemiluminescence Imager (Protein Simple, San Diego, CA, USA). Analysis of densitometry was completed using AlphaView SA Software. Units are expressed as density of primary antibody relative to density of amido black as shown in panel B.

Table D.1 Summary of high resolution SUIT1 respirometry experiment using Oroboros O2k. A table highlighting SUIT 1 (ADP Titration) protocol used in the study. Further explanations of these respiratory states and measurements can be found in Pesta & Gnaiger, 2011 or at the Oroboros website: www.bioblast.at.

Table D.1		
SUIT 1 ADP Titration – A complex I supported ADP titration evaluating ADP sensitivity as well as maximal respiration, followed with non-coupled respiration.		
Respiratory State	Substrates	Description
State 2 [PGM]	5 mM pyruvate (P), 10 mM glutamate (G), 0.5, mM malate (M)	LEAK respiration in the presence of complex I substrates. The amount of oxygen consumption as a consequence of protons leaking across the membrane.
State 3 [PGM]	Previous steps + addition of ADP such that [ADP] progressively increased as follows: from 0.05 mM, 0.1 mM, 0.15 mM, 0.2 mM, 0.25 mM, 0.5 mM, 1 mM, 2 mM, 4 mM, 8 mM	Respiration associated with ATP production. NADH is generated through the oxidation of PGM, donating electrons to complex I, and creating a proton gradient where ADP is the limiting factor for ATP production. The amount of oxygen consumed is a consequence of ADP being phosphorylated to ATP. Initial titrations are sub-saturating concentrations of ADP increasing to maximal ADP stimulated respiration.
State 3 [Cyt C]	Previous step + 5 mM Cytochrome C	During permeabilization, the outer membrane of mitochondria can be damaged, resulting in loss of cytochrome C. An increase in oxygen consumption is indicative of cytochrome C release during chemical permeabilization.
State 3 [PGM + S]	Previous step + 10 mM succinate (S)	Same as previous step but now both NADH and $FADH_2$ are generated through the oxidation of complexes I (PGM) and II (S) substrates yielding maximal ADP stimulated respiration.
ETS [CI – CIV]	Previous step + 1.0 mM FCCP	FCCP is a protonophore allowing hydrogen ions through the inner-mitochondrial membrane, uncoupling the proton gradient from ATP production through ATP synthase. This reflects the maximal or reserve capacity of complexes I – IV, unconstrained from ATP synthase activity.
ETS [CII – CIV]	Previous step + 5 µM rotenone (Rot)	Rotenone is an inhibitor of complex I. Therefore, non-coupled oxygen consumption is indicative of complex II – IV capacity.
ROX	2.5 µM Antimycin A (Ama)	Antimycin A inhibits complex III thus shutting down the electron transfer pathway. Residual oxygen consumption (ROX) is the remaining oxygen consumed from other pathways independent of complex IV.
Calculated Ratios	Calculation	Description
Respiratory Control Ratio (RCR)	State 3[PGM] / State 2[PGM]	The ratio of maximally stimulated ATP production to LEAK respiration. Respiratory Control Ratio (RCR) is a metric of mitochondrial coupling efficiency. A higher ratio is indicative of greater mitochondrial efficiency of oxygen consumption coupled to ATP production.
Cytochrome C Efficiency Value	(State 3 [Cyt C] – State 3 [PGM]) / State 3 [Cyto C]	As a quality control, adding cytochrome C to the SUIT protocol evaluates the extent in which the membrane was damaged and/or over-permeabilized. Refer to Methods: *Mitochondrial Respirometry* and Supplemental Figure D.1 for additional information.

Table D.2 Summary of high resolution respirometry SUIT 2 experiment using Oroboros O2k. A table highlighting SUIT 2 protocol used in the study. Further explanations of these respiratory states and measurements can be found in Pesta & Gnaiger, 2011 or at the Oroboros website: www.bioblast.at. Abbreviations: P – pyruvate; G – glutamate; M – malate; S – succinate; ADP – adenosine diphosphate; Cyt C – cytochrome C; ATP – adenosine triphosphate; Rot – rotenone; FCCP – Trifluoromethoxy carbonylcyanide phenylhydrazone; Ama – Antimycin A; ETS – electron transport system; CI – complex I; CII – complex II; CIII – complex III; CIV – complex IV; CV – complex V or ATP Synthase; ROX – residual oxygen consumption; RCR – respiratory control ratio; NADH – reduced nicotinamide adenine dinucleotide; $FADH_2$ – reduced flavin adenine dinucleotide

Table D.2		
SUIT 2 – A protocol measuring coupled and non-coupled respiration in the presence of carbohydrates.		
Respiratory State	Substrates	Description
State 2 [PGM]	5 mM pyruvate (P), 10 mM glutamate (G), 0.5, mM malate (M)	LEAK respiration in the presence of complex I and II substrates including carbohydrates. The amount of oxygen consumption as a consequence of protons leaking across the membrane.
State 2 [PGM + S]	Previous step + 10 mM succinate (S)	Same as previous step with the addition of the complex II substrate, succinate (S).
State 3 CI - CIV [Sub + 0.5D]	Previous step + 0.5 mM ADP	Respiration associated with ATP production. NADH and $FADH_2$ is generated through the oxidation of PGMS electrons to complexes I and II, and creating a proton gradient where ADP is the limiting factor for ATP production. The amount of oxygen consumed is a consequence of ADP being phosphorylated to ATP with a sub-saturating bolus of ADP.
State 3 CI - CIV [PGMS + 1.0D]	Previous step + 0.5 mM ADP	Same as previous step. The final concentration of ADP is higher but still sub-saturating stimulated respiration.
State 3 CI - CIV [PGMS + 6D]	Previous step + 5 mM ADP	Same as previous step, however, the final concentration of ADP (6.0 mM) is a saturating does, maximally stimulating mitochondrial respiration and ATP production.
State 3 CI - CIV [Cyt C]	Previous step + 5 mM Cytochrome C	During permeabilization, the outer membrane of mitochondria can be damaged, resulting in loss of cytochrome C. An increase in oxygen consumption is indicative of cytochrome C release during chemical permeabilization.
State 3 CI – CIV [PGMS+ 6D]	Previous step + 5 µM rotenone (Rot)	Rotenone is an inhibitor of complex I. Oxygen consumption is due to maximally stimulated ADP respiration of complexes II – IV.
ETS CII - CIV [PGMS+ 6D]	Previous step + 1.0 mM FCCP	FCCP is a protonophore allowing hydrogen ions through the inner-mitochondrial membrane, uncoupling the proton gradient from ATP production through ATP synthase. This is the maximal or reserve capacity of the mitochondria for complexes II – IV.
CIV	Previous step + 2 mM ascorbate + 0.5 mM TMPD	TMPD reduces cytochrome c to assess CIV activity and ascorbate is added to maintain the reduced state of TMPD
Calculated Ratios	Calculation	Description
Cytochrome C Control Efficiency Value	(State 3 [Cyt C] – State 3 [PGMS+ 6.0D]) / State 3 [Cyto C]	As a quality control, adding cytochrome C to the SUIT protocol evaluates the extent in which the membrane was damaged and/or over-permeabilized. Refer to Methods: *Mitochondrial Respirometry* and Supplemental Figure S1 for additional information.

APPENDIX E – A PRACTICAL PERSPECTIVE ON HOW TO DEVELOP, IMPLEMENT, EXECUTE, AND REPRODUCE HIGH-RESOLUTION RESPIROMETRY EXPERIMENTS: THE PHYSIOLOGIST'S GUIDE TO AN OROBORS O2K

INTRODUCTION

Initially referred to as the "powerhouse of the cell [1]" decades of subsequent research led to the coining of a new term to describe the mitochondrial reticulum: the mitochondrial information processing system (MIPS) [2]. Mitochondrial function is multifaceted including respiration for ATP production [3]. calcium handling [4]. electron leak [3]. and fatty acid synthesis [5]. These processes are all energy dependent. Thus, ATP production via oxidative phosphorylation (i.e., mitochondrial respiration) remains a primary function of mitochondria, enabling them to energetically support all MIPS functions.

High-resolution respirometry (HRR) is arguably the most rigorous approach for assessing mitochondrial respiratory control or studying cellular oxygen kinetics in response to the provision of specific electron donating substrates, proton ionophores, and/or mitochondrial complex inhibitors. This approach holds great promise for expanding understanding of cellular energetics and how targeting mitochondrial respiration can improve organismal health [6–8]. However, the predominance of resources available to those aiming to incorporate HRR into their research are difficult to comprehend if an individual does not have an advanced understanding of the HRR technology, biochemistry, and mitochondrial biology, impeding progress in the field of metabolism and bioenergetics. A simple analogy is trying to follow a recipe to caramelize onions without the knowledge of how to properly execute the steps of the recipe. Cooks can easily turn on and crank the heat, but they will not get a desirable product. Due to the lack of an easy to follow "O2k Cookbook," users may heedlessly follow a protocol instead of carefully

[3] Published in The FASEB Journal authored by Maureen A. Walsh, Robert V. Musci, Robert A. Jacobs, Karyn L. Hamilton

designing one to specifically address their research question(s). Thus, they risk not assessing the correct conditions and drawing false conclusions. Further, not taking steps to ensure reproducibility or maximizing transparency with clearly communicated methods when publishing studies muddles the field, hindering progress in understanding metabolism and bioenergetics. Therefore, the goals of this perspective are: 1. Describe how to develop effective mitochondrial respiration assays using an Oroboros O2k; 2. Highlight methodological considerations when executing mitochondrial respiration assays; and 3. Suggest ways to implement procedures to ensure reproducible data and decrease sample variability. Readers should possess a basic understanding of cellular bioenergetics and metabolism to understand concepts present here – see references as needed [9–11]. Finally, this perspective should not replace intensive in-person training on operating an O2k, conducting routine maintenance/calibrations, and running the assays.

HISTORY, ADVANTAGES, AND DISADVANTAGES OF ASSESSING MITOCHONDRIAL RESPIRATORY CONTROL

The first measures of mitochondrial oxygen consumption were reported in 1955 [12]. However, the rise in the number of published assessments of respiratory control did not occur until years later with exponential increases in related research each decade from the 1990s until the 2020s. This increase is in part due to refinements in technology and increased instrument accessibility. Two common instruments used to assess respiratory control are the Seahorse XF Analyzer, a plate-based phosphorescence system, and the Oroboros Oxygraph 2000 (O2k), a chamber-based Clark-type amperometric system. Recently, Divakaruni and Jastroen suggested ways to increase the transparency and reproducibility of mitochondrial assays with a strong emphasis on the plate-based system [13]. However, the plate-based system only allows for the addition of up to four substrates, inhibitors, or uncouplers, limiting the degree of flexibility and number of questions that can be addressed in one assay. Plate-based systems are certainly merited for relatively high throughput measures of broad respiratory potential in adherent or

suspended cells. However, it is noteworthy that mitochondria seldom operate in the conditions that they are subjected to in a Seahorse (i.e., substrate availability/concentration, number of substrates, temperature, etc.). Further, this plate-based platform is not feasible for respiring permeabilized samples, thus requiring users to select the O2k for experiments with permeabilized tissues (discussed in the next section). Unlike the O2k, plate-based systems do not have tandem fluorescence attachments to measure other mitochondrial functions such as hydrogen peroxide emissions, calcium retention, and ATP synthesis. For questions regarding the spatial and temporal scrutiny of respiratory control, one may favor the use of a system that provides fewer limitations in terms of questions answered in a single assay. Therefore, we will discuss the O2k system in addressing the goals of this perspective.

The O2k was created in 1992 by Dr. Erich Gnaiger, who has contributed to the development of helpful resources specific to the study of respiratory control and mitochondrial bioenergetics [14,15]. One of the biggest advantages of the O2k is the ability to design experimental conditions that best answer the scientific questions of interest. The respiration media in which mitochondrial samples are analyzed during O2k experiments is intended to mimic microenvironmental conditions while devoid of electron donating substrates and adenylate pool(s) necessary to facilitate oxidative phosphorylation. Thus, the O2k user has the flexibility to design experiments examining aspects of submaximal and/or maximal respiratory control specific to various electron donating sources through a series of carefully planned titrations of substrates and inhibitors. Users can select the order, concentration, and number of substrate titrations. Further, they can incorporate the use of proton ionophores to uncouple electron transport across the electron transfer system (ETS) from ATP synthesis (i.e., decoupling oxidative phosphorylation) and/or mitochondrial inhibitors to block the flow of electrons across specific ETS complexes. This approach enables one to assess many aspects of respiratory control in a given cell type and metabolic state.

The O2k system is not ideal for all experiments. First, it is an investment to purchase instruments and supplies (base O2k model ~$43,000). However, the cost per assay is relatively inexpensive ($10 – 20/assay depending on protocol) compared to the plate-based assays ($300-500/assay at an internal core facility and base model ~$75,000). Second, proper use of the O2k is time intensive. To ensure high quality data, O2ks require daily calibrations prior to each experiment to correct for room air oxygen concentrations and for the background correction of flux variability at high oxygen concentrations (i.e., > 160 μM of O_2) [14]. Additionally, the cleaning protocols after each experiment are critical and procedure-specific, requiring from 30 minutes to 3 hours, yet these protocols are rarely described in published research. When instruments are not cleaned properly it can shorten the life of the oxygen sensors and increase retention of chemical inhibitors affecting the respiration values of subsequent assays. Finally, while the O2k provides high-resolution measures, it is a low throughput piece of equipment, only having the capacity to run one sample in duplicate (See Jujiao, 2022 for the need for technical replicates) [16]. If performing measurements on animal or human specimens, this limits the number of experiments that can be performed per day since it is necessary to respire freshly acquired samples. In fact, the low throughput is such a notable weakness, that it may be more advantageous for users who are only aiming to measure maximal oxidative capacity and supra-physiological substrate concentrations to consider plate-based assays. Despite these limitations, the information obtained using an O2k can meaningfully expand understanding of the role of mitochondrial respiration in physical performance, health, and disease.

PREPARATION AND EXECUTION OF SAMPLES FOR MITOCHONDRIAL RESPIRATION

The research questions should always drive decisions regarding sample preparation and protocol development (Table E.1). During the planning process, taking steps to ensure reproducibility and decrease variability (Table E.2) is important for experimental rigor. Figure A1 serves as a roadmap for each of the considerations discussed in the sections that follow. We

also must acknowledge the comprehensive published work of Schmidt and colleagues [17] who initiated the discussions around assumptions and limitations of certain bioenergetic research platforms including the O2k. In this perspective we hope to expand on certain recommendations from prior work to ultimately improve development, implementation, execution, and reproducibility of O2k assays for those looking to make critical, tangible improvements in the quality and understanding of their O2k data. We discuss prior work to demonstrate that, when authors made thoughtful decisions about the protocols developed to address their proposed questions, the resulting data produced outcomes more translatable to physiology.

Sample preparation

A critical step in planning respirometry studies is deciding on the sample preparation, which includes tissue/cell-type (first decision) and mitochondrial preparation (second decision). Oroboros outlines six different mitochondrial preparations including isolated mitochondria, submitochondrial particles, tissue homogenate, permeabilized muscle fibers, permeabilized tissues, and permeabilized cells [15]. Further, they have created the Oroboros Ecosystem as an internal search engine for finding previous publications of various sample preparations, species, and physiological/pathological states. We suggest considering cellular mitochondria shape[18]. and/or metabolite biosynthesis when determining the appropriate mitochondrial preparation.

Specifically, permeabilized sample preparations may be preferred when addressing physiological queries in cells with robust reticular networks and many organelle contact sites that mitochondrial isolation procedures disrupt (extensively reviewed by Glancy et al., 2020) [19]. The rationale is that permeabilized sample preparations allow for scrutiny of intact mitochondrial networks in their normal intracellular position and assembly, preserving essential interactions and signaling events that can influence respiration [20]. An example illustrating this important point is one focused on skeletal muscle lactate metabolism. Originally, based on data from experiments with mitochondria isolated from muscle samples, it was concluded that

skeletal muscle could not oxidize lactate [21]. However, methods for isolating mitochondria remove the intracellular components that aid in tissue metabolism which exposes samples to conditions that are different than their *in vivo* environments. In a subsequent study utilizing permeabilized muscle fibers instead of isolated mitochondria, the authors found that skeletal muscle could indeed oxidize lactate, facilitated by the cytosolic enzyme lactate dehydrogenase [22].

Alternatively, isolated mitochondrial preparations may be appropriate to compare bioenergetics in cell types with simpler reticular networks and/or with relatively few contact sites across other sub-cellular structures. It also may be beneficial to choose an isolated mitochondrial preparation when interested in normalizing respiratory rates to direct measures of mitochondrial protein (i.e., rates of cellular respiration). In contrast, respiratory rates in permeabilized tissue are typically expressed relative to wet or dry tissue weights. It is important to note, however, that the mitochondrial isolation process increases production of reactive oxygen species (ROS) [23] and alters fatty acid oxidation [24]. Thus, mitochondrial isolation could be a confounding factor and contraindicated for studies involving ROS emission and/or fatty acid oxidation. For example, the isolation process might mask treatment differences as the surrounding cells removed by mitochondrial isolation might have had a greater concentration of antioxidant enzymes.

Sample variability is a critical consideration for deciding on mitochondrial preparation and when considering sample sizes required to detect differences (statistical power). Due to the increased transparency of statistical reporting in published manuscripts, we were able to calculate the coefficient of variation (%CV) of data resulting from HRR in isolated mitochondria versus permeabilized tissue preparations in murine left ventricle and red gastrocnemius at similar maximally stimulated conditions in a recent study published by the Petrick and colleagues [25]. In isolated mitochondria, the %CV was 15.2% and 25.2% for the left ventricle and red gastrocnemius, respectively. Interestingly, in permeabilized samples from these same

animals, the %CV was 24.3% and 7.0% for the left ventricle and red gastrocnemius, respectively. In permeabilized myofibers from human muscle samples, intra-individual (i.e., chamber to chamber) variability of maximally stimulated state 3 coupled respiration has been reported as 15.3% for an n = 68 [26] and 15.2% for an n = 25 [27]. Inter-laboratory variability in similar cohorts of humans is higher at 26.0%, [28]. owing to increased biological and methodological variation, which is similar to other laboratory-based techniques used for fiber-specific or skeletal muscle enzymatic assessments [29]. However, to date there has not been a rigorous study examining the coefficient of variation of permeabilized versus isolated mitochondria from the same sample and protocol with discussion about why differences across preparations may occur. The point to glean from these data is that experiments that assess mitochondrial respiratory capacity require a large number of samples. For example, the most robust intervention to improve mitochondrial function is exercise training [30]. However, given the substantial variability, to achieve a 6% effect size at 80% power a study would require 75 participants (with technical replicates of samples obtained from each participant) [26]. In summary, the research questions should guide decisions for the best mitochondrial preparation to follow, and care should be taken with power calculations or sample size determinations, falsely confirming or rejecting the null hypothesis.

Protocol Design

A considerable strength of the O2k is the ability to tailor reagents and protocols to test specific research questions. To assist users, Oroboros created a master protocol site as a starting point, however it is not an exhaustive list of all protocols. Additionally, Oroboros nicely outlines common substrates, uncouplers, and inhibitors as well as standard final concentrations for assays on their website.

An important consideration in designing an O2k protocol to test physiological questions, is to contemplate what experimental conditions are most likely to lead to data most reflective of *in vivo* bioenergetics. Standard assay conditions established with single titrations of supra-

physiological ADP concentrations likely limit understanding of the entire spectrum of metabolic demand and complementary bioenergetics. For example, compared to skeletal muscle from younger adults, older adults have lower submaximal mitochondrial respiration with 25 μM ADP, a concentration reflective of that in resting skeletal muscle [31–33]. However, the authors did not observe significant differences between younger and older adults at maximal ADP concentrations (i.e., 175 μM ADP), which is a concentration substantially lower than most other protocols which use 5,000 μM ADP [31]. Therefore, submaximal ADP concentrations might be more meaningful when translating mitochondrial respirometry data sets to *in vivo* mitochondrial bioenergetics. Data resulting from a single saturating bolus of ADP in respiratory protocols should be considered in the context of biological relevance, study design, and interpretation.

Further, protocols can be designed to interrogate both submaximal and maximal respiratory rates specific to certain substrates across a range of ADP titrations [31,34,35]. Traditionally, the ADP titration includes additions of glutamate, malate, and pyruvate followed by increasing submaximal boluses of ADP until there is no further increase in oxygen consumption. However, the specific respiratory states, and thus substrates used to assess the sensitivity of ADP-driven respiration, are variable and should also be specific to a study's research questions. These ADP titration data are fit to a Michaelis-Menten curve to calculate maximal oxygen consumption, ADP V_{max}, as well as ADP sensitivity, Km. A higher Km value is indicative of a greater amount of ADP to achieve ½ of ADP V_{max}, thus indicating a lower ADP sensitivity. The premise of Michaelis-Menten kinetics can also be used for other substrates with submaximal or maximal ADP concentrations titrated in prior to the substrate of interest. Ocantoylcarnitine, a medium chain fatty acid, has been used to determine the submaximal and maximal kinetics of this substrate as a metric of fatty acid oxidation when titrated in combination with malate [36,37]. Furthermore, substrates such as glutamate and succinate can be titrated into an assay to examine kinetics of complexes I and II, respectively. For example, one research group utilized this approach to identify that, compared to lean controls, participants with type 2 diabetes have

impaired maximal kinetics of succinate and ocantoylcarnitine as well as submaximal kinetics of glutamate, suggesting differences in both substrate and specific mitochondrial complex activity [36]. Therefore, the approach of using submaximal titrations is malleable based on the experimenters' research questions regarding substrates or bioenergetic pathways.

Another important aspect of tailoring O2k assays is designing the substrate, uncoupler, and inhibitor titration (SUIT) protocols. A SUIT protocol describes the use of substrates (e.g., glutamate, malate, pyruvate, ocantoylcarnitine, succinate, etc.), uncouplers (e.g., FCCP or CCCP), and inhibitors (e.g., rotenone, antimycin A, etc.) to assess specific aspects of respiratory control. An ADP titration protocol that also includes FCCP and rotenone, for example, is considered a SUIT protocol. The ability to assess complex-specific respiration using inhibitors gives experimenters the advantage of determining if respiratory differences or alterations associated with an experimental treatment exist at the level of a specific mitochondrial complex or across the entire ETS, providing additional mechanistic insights. For example, we were able to show that low, physiologically relevant concentrations of hydrogen peroxide significantly decrease non-coupled respiration in muscle precursor cells [38]. However, by using the complex I specific inhibitor, rotenone, which abolished these differences, we were able to conclude that hydrogen peroxide constrains respiration specific to mitochondrial complex I. Using a similar SUIT protocol, Davis and Barrett examined the effects of exercise training on Alaskan sled dog skeletal muscle mitochondrial respiration.[39] They observed a significant effect of exercise training on complex I and II respiration at various temperatures [39]. However, upon addition of rotenone the differences were eliminated suggesting that the effects of exercise primarily improve complex I function in this impressive model of mitochondrial function [39].

Designing an O2k protocol should also include consideration for other aspects of the cell environment that can influence respiration and, therefore, lead to false interpretation of data if not accounted for in the design. Scalable *in vivo* variables that influence respiratory control may not be captured in all HRR-protocols. Specifically, if one is looking to best replicate resting

conditions or situations reflecting maximal electron flow across the ETS, cellular and/or mitochondrial temperature ranges should be considered [28,40]. For example, exercise-induced improvements in skeletal muscle respiratory control are more apparent when assessed at temperatures mimicking skeletal muscle during exercise, 40°C, when compared to temperatures reflecting resting muscle, 35°C [40]. Table E.1 outlines critical considerations and top priorities when beginning O2k assays using a new tissue or species. Such methodological considerations provide opportunities to examine the same respiratory state across various conditions. For more extensive discussions detailing how to control for these cellular conditions with HRR, readers are referred to outstanding previous publications [17,28,41].

In sum, HRR using an O2k provides experimental autonomy in designing protocols to specifically test research questions. We [42,43] and others [44–46] publish information outlining the details of protocols used (i.e., concentration, order of reagents, sample tracings, and respiration states) and encourage other users to similarly provide detailed protocols, either directly in methods or in supplemental text/figures. This information is imperative for readers as they interpret the findings of primary research articles. We refer authors and reviewers to the Mitochondrial Pathways report by Dr. Gnaiger for reporting respiration states and experimental conditions [15].

O2k Data Rigor and Reproducibility

By following best practices of sample preparation, O2k experiment execution, and scientific reporting it becomes easier to interpret reference values for species and tissues. Therefore, we encourage authors to incorporate procedures that maximize experimental rigor, enhance reproducibility, and decrease variability. Table E.2A outlines recommendations for increasing reproducibility based on previously published work. Table E.2B includes points for decreasing variability. While the table is not an exhaustive list, we believe they are important considerations when designing studies. Finally, we acknowledge that enhancing reproducibility

and decreasing variability are quite similar and thus improving one may, in turn, improve the other.

Critical and under-reported components of O2k assays that impact reproducibility are cytochrome c responses and the associated flux control efficiency values. When working with permeabilized samples, it is necessary to add exogenous cytochrome c to the respiration chambers to test mitochondrial membrane integrity. If samples are over-permeabilized, either through mechanical or chemical means, mitochondrial cytochrome c is lost resulting in a non-biological loss of respiration. When exogenous cytochrome c is subsequently added, this over-permeabilization is evidenced by a "meaningful" increase in oxygen flux (i.e., flux control efficiency value). Lanza and Nair nicely demonstrate this in a prior publication showing sample tracings of over-permeabilized samples [41]. A threshold for the flux control efficiency value must be established for each experimental paradigm to determine how large of an increase in oxygen flux is indicative of over-permeabilization necessitating exclusion from data analysis. This "meaningful" cytochrome c threshold varies across cell-types, tissues, and species. The threshold is based on the presence of a negative linear relationship between the flux control factor and the titration step right before the addition of cytochrome c. Values that are greater than (X%) flux control should, therefore, be removed from analysis to prevent biasing the outcomes by over-permeabilization [14]. For example, over-permeabilized human skeletal muscle had been consistently reported at an increase of 0.1 – 0.15 (or 10 – 15%) flux control efficiency value [47,48]. However, permeabilized skeletal muscle samples from guinea pigs [43] and dogs [49] have a flux control efficiency value of about 0.25 (25%) and 0.3 (30%), respectively. The flux control efficiency value is defined as the flux after addition of the cytochrome c titration (reference state) minus flux before the cytochrome c titration (background state) divided by flux after the cytochrome c addition (reference state) [34,48].

$$\frac{(After\ cytochrome\ c - Before\ cytochrome\ c)}{After\ cytochrome\ c} \times 100$$

When establishing protocols for interpreting flux control efficiency value in less well-studied cell types, tissues, or species, we recommend plotting the oxygen consumption at the step before cytochrome c relative to the flux control efficiency value, to determine the flux control efficiency value at which the significant negative relationship dissipates ($p>0.05$ and R^2 value >0.05) [38,43]. Upon removal of these values the negative linear relationship should dissipate or minimally influence variance (minimize R^2 value) [43]. While there are other factors that we outline in Table E.2 to enhance reproducibility, we believe that using cytochrome c and establishing flux control efficiency values is necessary for all experiments. Finally, we have only highlighted considerations for sample preparation and protocol selections; however, data normalization (i.e., tissue wet weight, tissue dry weight, citrate synthase protein/activity, etc.) and processing are additional items that require careful attention when establishing experimental designs; these points are effectively summarized by Schmidt and colleagues [17].

FUTURE DIRECTIONS

Here we outline ways to develop, implement, execute, and reproduce HRR experiments using an O2k. Making decisions about O2k assays by simply repeating protocols from past publications, rather than designing specific protocols to address mitochondrial mechanisms that are key to the experimental questions being tested, significantly limits the value of HRR-derived data. However, thoughtful design and execution of O2k experiments results in data that become a powerhouse for addressing many mitochondrial respiration research questions. We hope this perspective serves as a resource for scientists new to this method, veterans considering incorporation of different cell types, tissues, or species in their studies, and manuscript/grant proposal peer reviewers. Given the increasing number of O2k instruments in labs worldwide, we seek to encourage users to report more detailed methods and think critically about sample collection, protocol execution, and biological interpretation. Finally, we challenge scientists to continually work together to help better standardize HRR and create lab resources to propagate the use of O2ks.

FIGURES

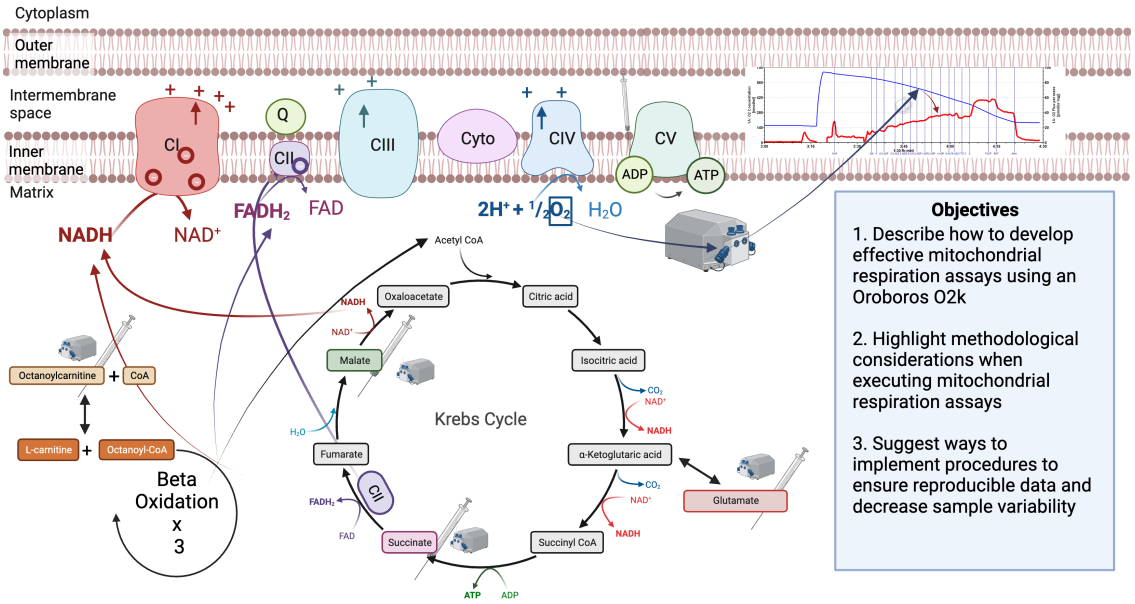

Figure E.1. Graphical abstract. Mitochondrial respiration is stimulated by titration of substrates and exogenous ADP in an Oroboros O2k (denoted by Hamilton syringes). We encourage users to test their research questions with the most relevant bioenergetic pathway through the inclusion/exclusion of carefully selected substrates and chemicals that specifically inhibit or uncouple respiration. The “Objectives” box summarizes the main points of this perspective to increase the standardization of O2k experiments.

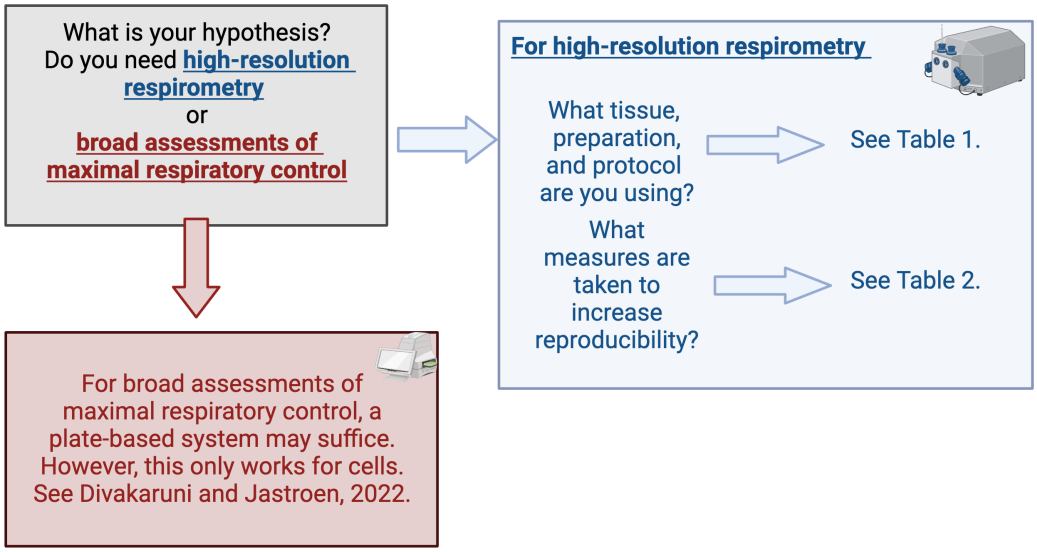

Figure E.2. Overview of steps for mitochondrial oxygen consumption Experiments. We suggest answering these questions as an initial roadmap for development and execution of mitochondrial respiration experiments.

Table E1. Questions for Considering Top Priorities When Designing New Protocols or Assessing New Tissues

Question(s)	Examples
What is your (specific) research questions? How are you going to test it?	Almost any titration in an O2k assay is a metric of mitochondrial respiration. Therefore, simply stating, "We predict XX treatment will improve mitochondrial respiration." is not specific. Further, it does not challenge scientists to think about the ample questions that can be addressed in a single O2k assay. Instead, questions should be specific indicating what aspects of mitochondrial respiration (i.e., complex I submaximal respiration or complex I and II submaximal respiration with carbohydrate and fatty acid fuel sources) are increased or decreased within a specific experimental paradigm.
What do you know about your experimental condition (i.e., genotype, treatment, age)? Do you have preliminary data?	If studying preclinical models of Alzheimer's Disease human studies demonstrate evidence of impairments at complexes II and IV [50]. Thus, it would be fruitful to design assays to assess these complexes. If you have preliminary data (e.g., transcriptomics or proteomics) are certain mitochondrial complexes altered (e.g., complex I) or specific key enzymes to target a substrate preference (e.g., carnitine palmitoyl transferase)? This information could help design protocols to better highlight differences in existing data.
What is the most/least abundant fuel source of the tissue?	The brain does not oxidize fatty acids but has high concentrations of glutamate.
Based on assay decisions thus far, what aspects of mitochondrial bioenergetics are you sacrificing?	You cannot address every bioenergetic pathway in one assay. However, by adding only saturating concentrations and not submaximal to maximal titrations of substrates, you may be losing the translatability to *in vivo* conditions.
Is the order of substrates/inhibitors preventing your ability to assess an outcome that is critical to your study?	If performing an ADP titration should substrates fueling complexes I and II be added prior to increasing boluses of ADP? For example, by only adding complex I substrates to an ADP titration the kinetics data are only translatable to complex I function; however, *in vivo* complexes I and II always operate in tandem. If adding a protonophore to uncouple respiration, is it added before or after certain complexes are inhibited? For example, if rotenone (a complex I inhibitor) is added prior to uncoupling (FCCP) the reserve capacity is only examining complex II uncoupled respiration.
What issues arise with the current protocols?	Do you have enough time to clean instruments between assays? For example, if using chemical uncouplers (FCCP) and inhibitors (rotenone and antimycin) we suggest ~45 minute cleaning protocol with 3*5 min rinses in 70% EtOH, 1*15 min rinse in 100% EtOH, and 3*5 min rinses with water prior to adding the respiration buffer (MiR05 or Buffer Z) to equilibrate with room air for the next assay. Are there enough personnel to ensure experiments flow smoothly if performing multiple assays per day or per sample?

Table E2. Steps to ensure reproducibility and decrease variability of O2k experiments

Steps to Ensure Reproducibility of O2k Experiments (A)	
Category	Our Recommendation
User differences	The same user should prepare all respiratory samples in a respective study. However, data analysis can be performed by two separate users [51].
Buffers	Batch prepare all buffers/substrates for a given study ensuring proper pH at respective temperatures [17].
Freeze-thaws	Aliquot all buffers/substrates for one day of experimentation and do not refreeze [41].
Cytochrome c responses – flux control efficiency value	The meaningful increase prompting exclusion of data due to over-permeabilization is tissue- and species-dependent. For example, permeabilized human skeletal muscle is consistently reported at an increase of 0.1 – 0.15 (10% - 15%) flux control factor efficiency value [47,48]. However, when establishing preparations and protocols in less well-studied species, plot the flux at the titration prior to cytochrome c addition and the flux control efficiency value to determine the flux control efficiency value where there is a drop off in oxygen consumption [43].
Amount of tissue loaded per chamber	Be consistent in the ranges of tissue loaded and report ranges (e.g., XX mg – XX mg) in the methods section. Others have shown it is challenging to detect subtle differences between titration steps when a small tissue weight (~0.8 mg) is added; too large a sample weight (>4.0 mg) can result in diffusion limitations and a steady state that is difficult to achieve [52].
Steps to Decrease Variability of O2k Experiments (B)	
Category	Our Recommendation
Time in BIOPS or Buffer X	While no studies have reported a thorough time-course for sample viability in preservation buffer, one study did observe non-significant decreases in white adipose tissue respiration from 3 to 24 hours.[51] We speculate that max duration of viability is tissue dependent, ranging from 30 minutes to 24 hours.
Lapse of time from euthanasia to sample collection in animal studies	The lapse of time between euthanasia and sample collection have been reported by some [25,53] and longer durations have yielded negative effects on mitochondrial function [54].
Fasting duration of animals and humans	Fasting conditions should be considered based on tissue of interest.
Temperature Correction	Historically, it is most common to respire O2k assays at 37°C [55]. However, recent reports demonstrate that temperature corrections mimicking exercise [56] or *in vivo* mitochondrial temperature [28,57] align better with whole body maximal oxygen update.
Confluency of cells	We and others [38,58] have previously reported harvesting cells for assays at a consistent confluence. When respiring cells at lower confluences (independent of cell count) we noticed higher cytochrome c flux control efficiency values in pilot experiments.
Circadian phase	It is known skeletal muscle oxidative potential demonstrates a day-night rhythm [59]. Therefore, in line with best practices tissues should, at minimum, be collected at similar times of day.
Management of chamber oxygenation	In permeabilized systems hyper-oxygenation (>160 μM of O_2) is required to allow for a sufficient concentration gradient to facilitate mitochondrial respiration. Users should attempt to select a starting value that will last the duration of the experiment, as re-oxygen (i.e., addition of exogenous hydrogen peroxide to the respiration buffer with catalase) may influence subsequent measures of respiratory control. If necessary, re-oxygenation should always occur at the same step of the SUIT protocol. Users should also always report the oxygen range used for all assays (e.g., 250 – 450 μM of O_2) in the publication.
Chamber cleaning protocols	Differing SUIT protocols require different cleaning protocols. Insufficient cleaning between experiments can greatly influence subsequent measures, complicating meaningful interpretations for differences or changes observed in relation to altered biological function *per se* or methodological oversight. Cleaning protocols should be described in sufficient detail to replicate across laboratories.
Statistical power analyses	The likelihood of demonstrating an experimental group difference is directly related to a measure's statistical power. Conduct a priori power analyses to aid in powering your research appropriately. Moreover, report effect sizes (i.e., Cohen's d or eta squared), alongside p-values to aid in our collective interpretation of statistical versus biological relevance.

REFERENCES

1. Siekevitz P. Powerhouse of the Cell. *Scientific American*. 1957;197(1). https://www.jstor.org/stable/24940890

2. Picard M, Shirihai OS. Mitochondrial signal transduction. *Cell Metab*. 2022;34(11):1620-1653. doi:10.1016/j.cmet.2022.10.008

3. Brand MD, Orr AL, Perevoshchikova IV, Quinlan CL. The role of mitochondrial function and cellular bioenergetics in ageing and disease. *Brit J Dermatol*. 2013;169:1-8. doi:10.1111/bjd.12208

4. Balderas E, Eberhardt DR, Lee S, et al. Mitochondrial calcium uniporter stabilization preserves energetic homeostasis during Complex I impairment. *Nat Commun*. 2022;13(1):2769. doi:10.1038/C1467-022-30236-4

5. Nowinski SM, Solmonson A, Rusin SF, et al. Mitochondrial fatty acid synthesis coordinates oxidative metabolism in mammalian mitochondria. *Elife*. 2020;9:e58041. doi:10.7554/elife.58041

6. Coen PM, Musci RV, Hinkley JM, Miller BF. Mitochondria as a Target for Mitigating Sarcopenia. *Front Physiol*. 2019;9:1883. doi:10.3389/fphys.2018.01883

7. Musci RV, Hamilton KL, Miller BF. Targeting mitochondrial function and proteostasis to mitigate dynapenia. *Eur J Appl Physiol*. 2018;118(1):1-9. doi:10.1007/s00421-017-3730-x

8. Singh A, Faccenda D, Campanella M. Pharmacological advances in mitochondrial therapy. *EBioMedicine*. 2021;65:103244. doi:10.1016/j.ebiom.2021.103244

9. *Biochemistry (Lippincott's Illustrated Reviews Series)*. 7th Edition.; 2014.

10. Brooks G, Fahey T, Baldwin K. *Exercise Physiology. Human Bioenergetics and Its Applications*. 4th Edition. McGraw-Hill; 2005.

11. *Biochemistry Primer for Exercise Science*. Human Kinetics; 2012.

12. CHANCE B, WILLIAMS GR. A Simple and Rapid Assay of Oxidative Phosphorylation. *Nature*. 1955;175(4469):1120-1121. doi:10.1038/1751120a0

13. Divakaruni AS, Jastroch M. A practical guide for the analysis, standardization and interpretation of oxygen consumption measurements. *Nat Metabolism*. Published online 2022:1-17. doi:10.1038/C2255-022-00619-4

14. Pesta D, Gnaiger E. Mitochondrial Bioenergetics, Methods and Protocols. *Methods Mol Biology*. 2011;810:25-58. doi:10.1007/978-1-61779-382-0_3

15. Gnaiger E. Mitochondrial Pathways and Respirometry Control An Introduction to OXPHOS Analysis. *Bioenerg Commun*. 2020;(5th ed). doi:10.26124/bec:2020-0002

16. Kuang J, Saner NJ, Botella J, et al. Assessing mitochondrial respiration in permeabilized fibres and biomarkers for mitochondrial content in human skeletal muscle. *Acta Physiol*. Published online 2022:e13772. doi:10.1111/apha.13772

17. Schmidt CA, Fisher-Wellman KH, Neufer PD. From OCR and ECAR to energy: perspectives on the design and interpretation of bioenergetics studies. *J Biol Chem*. 2021;297(4):101140. doi:10.1016/j.jbc.2021.101140

18. Ahmad T, Aggarwal K, Pattnaik B, et al. Computational classification of mitochondrial shapes reflects stress and redox state. *Cell Death Dis*. 2013;4(1):e461-e461. doi:10.1038/cddis.2012.213

19. Glancy B, Kim Y, Katti P, Willingham TB. The Functional Impact of Mitochondrial Structure Across Subcellular Scales. *Front Physiol*. 2020;11:541040. doi:10.3389/fphys.2020.541040

20. Brand MD, Nicholls DG. Assessing mitochondrial dysfunction in cells. *Biochem J*. 2011;435(Pt 2):297-312. doi:10.1042/bj20110162

21. Rasmussen HN, Hall G, Rasmussen UF. Lactate dehydrogenase is not a mitochondrial enzyme in human and mouse vastus lateralis muscle. *J Physiology*. 2002;541(2):575-580. doi:10.1113/jphysiol.2002.019216

22. Jacobs RA, Meinild AK, Nordsborg NB, Lundby C. Lactate oxidation in human skeletal muscle mitochondria. *Am J Physiol-endoc M*. 2013;304(7):E686-E694. doi:10.1152/ajpendo.00476.2012

23. Picard M, Taivassalo T, Ritchie D, et al. Mitochondrial Structure and Function Are Disrupted by Standard Isolation Methods. *Plos One*. 2011;6(3):e18317. doi:10.1371/journal.pone.0018317

24. Pande SV, Blanchaer MC. Preferential loss of ATP-dependent long-chain fatty acid activating enzyme in mitochondria prepared using nagarse. *Biochimica Et Biophysica Acta Bba - Lipids Lipid Metabolism*. 1970;202(1):43-48. doi:10.1016/0005-2760(70)90216-x

25. Petrick HL, Brunetta HS, Pignanelli C, et al. In vitro ketone-supported mitochondrial respiration is minimal when other substrates are readily available in cardiac and skeletal muscle. *J Physiology*. 2020;598(21):4869-4885. doi:10.1113/jp280032

26. Jacques M, Kuang J, Bishop DJ, et al. Mitochondrial respiration variability and simulations in human skeletal muscle: The Gene SMART study. *Faseb J Official Publ Fed Am Soc Exp Biology*. Published online 2020. doi:10.1096/fj.201901997rr

27. Cardinale DA, Gejl KD, Ørtenblad N, Ekblom B, Blomstrand E, Larsen FJ. Reliability of maximal mitochondrial oxidative phosphorylation in permeabilized fibers from the vastus lateralis employing high-resolution respirometry. *Physiological Reports*. 2018;6(4):e13611. doi:10.14814/phy2.13611

28. Jacobs RA, Lundby C. Contextualizing the biological relevance of standardized high-resolution respirometry to assess mitochondrial function in permeabilized human skeletal muscle. *Acta Physiol*. 2021;231(4):e13625. doi:10.1111/apha.13625

29. Simoneau JA, Bouchard C. Human variation in skeletal muscle fiber-type proportion and enzyme activities. *Am J Physiol-endoc M*. 1989;257(4):E567-E572. doi:10.1152/ajpendo.1989.257.4.e567

30. Memme JM, Erlich AT, Phukan G, Hood DA. Exercise and mitochondrial health. *J Physiol*. 2021;599(3):803-817. doi:10.1113/jp278853

31. Holloway GP, Holwerda AM, Miotto PM, Dirks ML, Verdijk LB, Loon LJC van. Age-Associated Impairments in Mitochondrial ADP Sensitivity Contribute to Redox Stress in Senescent Human Skeletal Muscle. *Cell Reports*. 2018;22(11):2837-2848. doi:10.1016/j.celrep.2018.02.069

32. Perry CGR, Heigenhauser GJF, Bonen A, Spriet LL. High-intensity aerobic interval training increases fat and carbohydrate metabolic capacities in human skeletal muscle. *Appl Physiology Nutrition Metabolism*. 2008;33(6):1112-1123. doi:10.1139/h08-097

33. Phillips SM, Green HJ, Tarnopolsky MA, Heigenhauser GJ, Grant SM. Progressive effect of endurance training on metabolic adaptations in working skeletal muscle. *Am J Physiol-endoc M*. 1996;270(2):E265-E272. doi:10.1152/ajpendo.1996.270.2.e265

34. Konopka AR, Laurin JL, Schoenberg HM, et al. Metformin inhibits mitochondrial adaptations to aerobic exercise training in older adults. *Aging Cell*. 2019;18(1):e12880. doi:10.1111/acel.12880

35. Elliehausen CJ, Minton DM, Nichol AD, Konopka AR. Skeletal muscle mitochondrial respiration in a model of age-related osteoarthritis is impaired after dietary rapamycin. *Exp Gerontol*. 2021;155:111579. doi:10.1016/j.exger.2021.111579

36. Larsen S, Stride N, Hey-Mogensen M, et al. Increased mitochondrial substrate sensitivity in skeletal muscle of patients with type 2 diabetes. *Diabetologia*. 2011;54(6):1427-1436. doi:10.1007/s00125-011-2098-4

37. Batterson PM, McGowan EM, Stierwalt HD, Ehrlicher SE, Newsom SA, Robinson MM. Two weeks of high-intensity interval training increases skeletal muscle mitochondrial respiration via complex-specific remodeling in sedentary humans. *J Appl Physiol*. 2023;134(2):339-355. doi:10.1152/japplphysiol.00467.2022

38. Walsh MA, Zhang Q, Musci RV, Hamilton KL. The combination of NRF1 and Nrf2 activators in myoblasts stimulate mechanisms of proteostasis without changes in mitochondrial respiration. *Redox Muscle Physiology Exerc Sport*. Published online 2022:100001. doi:10.1016/j.rimpes.2022.100001

39. Davis MS, Barrett MR. Effect of conditioning and physiological hyperthermia on canine skeletal muscle mitochondrial oxygen consumption. *J Appl Physiol*. 2021;130(5):1317-1325. doi:10.1152/japplphysiol.00969.2020

40. Fiorenza M, Lemminger AK, Marker M, et al. High-intensity exercise training enhances mitochondrial oxidative phosphorylation efficiency in a temperature-dependent manner in human skeletal muscle: implications for exercise performance. *Faseb J*. 2019;33(8):8976-8989. doi:10.1096/fj.201900106rrr

41. Lanza IR, Nair KS. Chapter 20: Functional Assessment of Isolated Mitochondria In Vitro. *Methods Enzymol*. 2009;457:349-372. doi:10.1016/s0076-6879(09)05020-4

42. Jacobs RA, Aboouf MA, Koester-Hegmann C, et al. Erythropoietin promotes hippocampal mitochondrial function and enhances cognition in mice. *Commun Biology*. 2021;4(1):938. doi:10.1038/C2003-021-02465-8

43. Musci RV, Andrie KM, Walsh MA, et al. Phytochemical compound PB125 attenuates skeletal muscle mitochondrial dysfunction and impaired proteostasis in a model of musculoskeletal decline. *J Physiology*. Published online 2022. doi:10.1113/jp282273

44. Scalzo RL, Schauer IE, Rafferty D, et al. Single-leg exercise training augments in vivo skeletal muscle oxidative flux and vascular content and function in adults with type 2 diabetes. *J Physiology*. Published online 2021. doi:10.1113/jp280603

45. Spendiff S, Vuda M, Gouspillou G, et al. Denervation drives mitochondrial dysfunction in skeletal muscle of octogenarians. *J Physiology*. 2016;594(24):7361-7379. doi:10.1113/jp272487

46. Gouspillou G, Godin R, Piquereau J, et al. Protective role of Parkin in skeletal muscle contractile and mitochondrial function. *J Physiology*. 2018;596(13):2565-2579. doi:10.1113/jp275604

47. Gonzalez-Freire M, Scalzo P, D'Agostino J, et al. Skeletal muscle ex vivo mitochondrial respiration parallels decline in vivo oxidative capacity, cardiorespiratory fitness, and muscle strength: The Baltimore Longitudinal Study of Aging. *Aging Cell*. 2018;17(2):e12725. doi:10.1111/acel.12725

48. Porter C, Hurren NM, Cotter MV, et al. Mitochondrial respiratory capacity and coupling control decline with age in human skeletal muscle. *Am J Physiol-endoc M*. 2015;309(3):E224-E232. doi:10.1152/ajpendo.00125.2015

49. Miller B, Hamilton K, Boushel R, et al. Mitochondrial respiration in highly aerobic canines in the non-raced state and after a 1600-km sled dog race. *Plos One*. 2017;12(4):e0174874. doi:10.1371/journal.pone.0174874

50. Troutwine BR, Strope TA, Franczak E, et al. Mitochondrial function and Aβ in Alzheimer's disease postmortem brain. *Neurobiol Dis*. Published online 2022:105781. doi:10.1016/j.nbd.2022.105781

51. Sahl RE, Helms EFH, Schmücker M, et al. Reliability and variation in mitochondrial respiration in human adipose tissue. *Adipocyte*. 2021;10(1):605-611. doi:10.1080/21623945.2021.1991617

52. Herbst EAF, Holloway GP. Permeabilization of brain tissue in situ enables multiregion analysis of mitochondrial function in a single mouse brain. *J Physiology*. 2015;593(4):787-801. doi:10.1113/jphysiol.2014.285379

53. Hughes MC, Ramos SV, Turnbull PC, et al. Early myopathy in Duchenne muscular dystrophy is associated with elevated mitochondrial H2O2 emission during impaired oxidative phosphorylation. *J Cachexia Sarcopenia Muscle*. 2019;10(3):643-661. doi:10.1002/jcsm.12405

54. Zhang Y, Dong Y, Wu X, et al. The Mitochondrial Pathway of Anesthetic Isoflurane-induced Apoptosis*. *J Biol Chem*. 2010;285(6):4025-4037. doi:10.1074/jbc.m109.065664

55. Gnaiger E. Capacity of oxidative phosphorylation in human skeletal muscle New perspectives of mitochondrial physiology. *Int J Biochem Cell Biology*. 2009;41(10):1837-1845. doi:10.1016/j.biocel.2009.03.013

56. Boushel R, Gnaiger E, Calbet JAL, et al. Muscle mitochondrial capacity exceeds maximal oxygen delivery in humans. *Mitochondrion*. 2011;11(2):303-307. doi:10.1016/j.mito.2010.12.006

57. Chrétien D, Bénit P, Ha HH, et al. Mitochondria are physiologically maintained at close to 50 °C. *Plos Biol*. 2018;16(1):e2003992. doi:10.1371/journal.pbio.2003992

58. Robinson MM, Sather BK, Burney ER, et al. Robust intrinsic differences in mitochondrial respiration and H2O2 emission between L6 and C2C12 cells. *Am J Physiology Cell Physiology*. Published online 2019. doi:10.1152/ajpcell.00343.2018

59. Moorsel D van, Hansen J, Havekes B, et al. Demonstration of a day-night rhythm in human skeletal muscle oxidative capacity. *Mol Metab*. 2016;5(8):635-645. doi:10.1016/j.molmet.2016.06.012

APPENDIX F – AN ABBREVIATED OVERVIEW OF THE EFFECTS OF SHORT TERM PB125 TREATMENT ON MECHANISMS OF PROTEOSTASIS IN HARTLEY GUINEA PIGS

OVERVIEW

Chapter 3 reported changes in mechanisms of proteostasis after long-term (10 mo) PB125 treatment in the tibialis anterior, gastrocnemius, and soleus of male and female Hartley guinea pigs. However, there was an additional arm of the study that examined the short-term (3 mo from 2 to 5 mo of age) PB125 treatment effects in delaying the onset of skeletal muscle aging in male and female Hartley guinea pigs. To not muddy the results presented in Chapter 3, I created Appendix F to showcase the short-term data with figures presented in a similar fashion to the long-term study, followed by a short discussion. All methods are described in Chapter 3 as well as unedited western blot images. Figures for Appendix F are located after the "Results and Discussion" section to keep formatting consistent with other chapters.

RESULTS AND DISCUSSION

Appendix F, an arm of a larger parent project, examined the short-term (3 mo) effects of daily PB125 treatment on mechanisms of proteostasis in male and female Hartley guinea pigs. The key findings of this study were that: 1. PB125 altered the ratio of protein to DNA synthesis rates in a muscle-dependent manner; 2. PB125 treatment, a purported Nrf2 activator, increased Nrf2 protein content; 3. PB125 treatment increased semi-quantitative markers of skeletal muscle cellular senescence. Collectively, these findings represent a snapshot of how short-term PB125 treatment may alter age-related myofiber remodeling which occurs later in the lifespan of Hartley guinea pigs.

Key Finding #1: PB125 altered the ratio of protein to DNA synthesis in a muscle-dependent manner

Deuterium oxide labeling facilitates simultaneous assessment of rates of protein, RNA, and DNA synthesis in cultured cells or free-living animals/humans, giving us insight into cellular prioritization for promoting mechanisms of proteostatic maintenance [1]. Using this

methodological approach, our group has shown that treatment with purported Nrf2 activators results in a higher ratio of protein to DNA synthesis rates, suggesting a tradeoff between cell proliferation and mechanisms to maintain proteostasis [2,3]. That is, Nrf2 activator treatment promoted allocation of newly synthesized proteins for maintenance of the proteome at the expense of new cell proliferation. However, in the present study we observed an opposing effect, with a ratio of protein to DNA synthesis rates that was lower in the tibialis anterior in three out of four subcellular fractions after PB125 treatment (Figure F.6A-C). Because rates of tibialis anterior protein synthesis were maintained with treatment (Figure F.3A-D), the decrease in the ratio was driven primarily by increases in DNA synthesis rates, particularly in female Hartleys (Figure F.5B). Conversely, there was no treatment effect on the ratio of protein to DNA synthesis rates in the gastrocnemius or soleus (Figures F.6E-L). The proteostasis data presented here are similar to the results in Chapter 3, wherein PB125 was only associated with significant effects in tibialis anterior, a muscle comprised of type II myofibers; there was no treatment effect in the mixed myofiber gastrocnemius muscle or the type II myofiber soleus muscle.

However, in this study, the lower ratio of protein to DNA synthesis rates may have not resulted in increased mechanisms of maintaining proteostasis as compared to the results in Chapter 3 with 10 mo of PB125 treatment. It is important to note that both during the PB125 treatment duration (from 2 to 5 mo of age) and the deuterium oxide labeling period (from 4 to 5 mo of age) guinea pigs were growing (Figure F.2A). Additionally, guinea pigs were 5 mo at the time of euthanasia, an age where we do not observe robust age-related myofiber remodeling [4]. As mentioned in Chapter 3 rates of skeletal muscle DNA synthesis contain different cell types including multi-nucleated myonuclei that synthesize DNA [5], endothelial cells, fibrogenic cells, satellite (i.e., muscle stem) cells, and macrophages. Therefore, while PB125 treatment was associated with increased rates of DNA synthesis (Figure F.5B), we cannot be certain about which cell type(s) in the whole muscle tissue drove these changes. Taken together, it

again appears that type II myofibers have the most robust response to PB125 treatment, independent of age and treatment duration. Future studies should consider if/how a short-term treatment early in life protects organisms from long-term age/disease related changes.

Key Finding #2: PB125 increased Nrf2 protein content

The phytochemical compound, PB125, composed of carnosol, luteolin, and withaferin A, is a purported Nrf2 activator. In a prior publication we report that after PB125 dosing these active ingredients were detected in the blood of Hartley guinea pigs and it resulted in significant increases in Nrf2 protein content in the gastrocnemius muscle driven by the younger guinea pigs [6]. In this data set we observe a similar effect of increased Nrf2 protein content in the tibialis anterior after 3 mo of PB125 treatment (Figure F.7A). However, in other studies by our group (Chapters 2 and 3 of this dissertation) and by others [7], there were no detectable differences in Nrf2 protein content. The variability in findings related to accumulation of Nrf2 protein following treatment might be, in part, due to the skeletal muscle studied (i.e., type I soleus versus type II tibialis anterior in the present study) and/or treatment duration of purported Nrf2 activators. Furthermore, the half-life of Nrf2 is approximately 20 minutes [8], again making it challenging to capture increases in Nrf2 protein content. The project reflected in Chapters 3 and 4 (and manuscripts already published [6,9]) was designed to capture short and long-term PB125 treatment effects and not acute changes in Nrf2 activation following daily dosing.

Key Finding #3: PB125 increased semi-quantitative markers of cellular senescence

Senescent cells often referred to as “zombie cells” are those that have permanently exited cell cycling [10]. In the present study we assessed skeletal muscle cellular senescence with semi-quantitative measures of p21 and phospho-H2AX. PB125 increased p21 and phospo-H2AX markers of senescence and senescence associated DNA damage, respectively (Figures F.9A and C). Interestingly, exercise reportedly has similar effects on increasing markers of skeletal muscle senescence [11]. While cellular senescence is a hallmark of aging [12], it appears that acute hormetic increases in measures of cellular senescence (in the case of

exercise) might prime the cell to be more resistant or resilient to future stressors. While we did not age the guinea pigs after short-term PB125 treatment, there is the possibility that this short-term 3 mo PB125 treatment protected against cell senescence later in life as we know these markers of senescence increases with age in these guinea pigs (data presented in Chapter 3 as Figure 3.7A, B, E, F).

Conclusions and Future Directions

Developing therapeutics to delay the onset and/or slow the progression of age-related changes in muscle health are critical. In the present data set, we demonstrated that PB125 treatment, a purported Nrf2 activator, known to improve mechanisms of proteostasis resulted in different effects between predominantly type I and type II myofibers. Taken together, these data suggest that PB125 treatment earlier in the lifespan might have some protective effects against the development of skeletal muscle senescence associated with age at least in the Hartley guinea pig, a preclinical model of musculoskeletal decline.

FIGURES

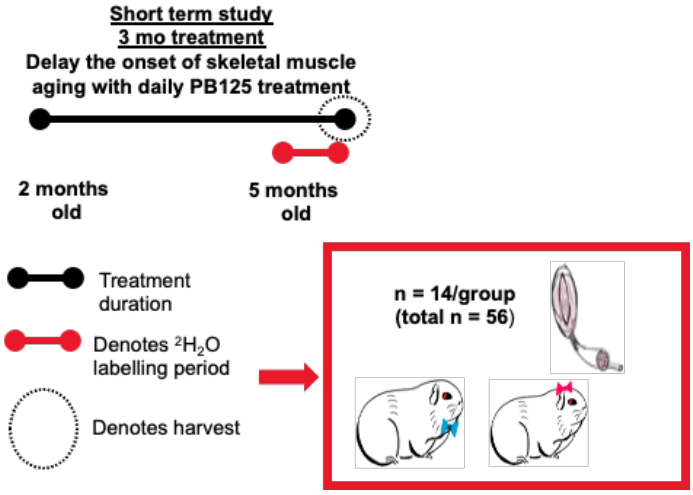

Figure F.1. Study design. Male (n = 14/group) and female (n = 14/group) Hartley guinea pigs were either treated with PB125 or a vehicle control for 3 mo (from 2 to 5 mo) to delay the onset of skeletal muscle (black line). During the final month of treatment (red line line) guinea pigs were labeled with deuterium oxide (^2H_2O) to assess long-term rates of protein, RNA, and DNA synthesis. Guinea pigs were sacrificed at 5 mo of age and plasma, tibialis anterior, gastrocnemius, and soleus samples were collected for analysis.

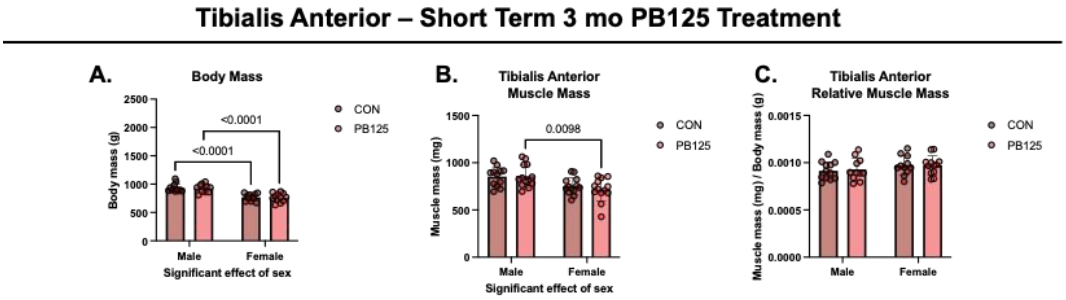

Figure F.2. 3 mo of PB125 treatment does not alter body mass, muscle mass, or relative muscle mass. Independent of treatment, male Hartley guinea pigs were larger than female Hartley guinea pigs (A) as were their skeletal muscle masses (B). However, when muscle mass was expressed relative to body mass there were no sex or treatment effects (C).

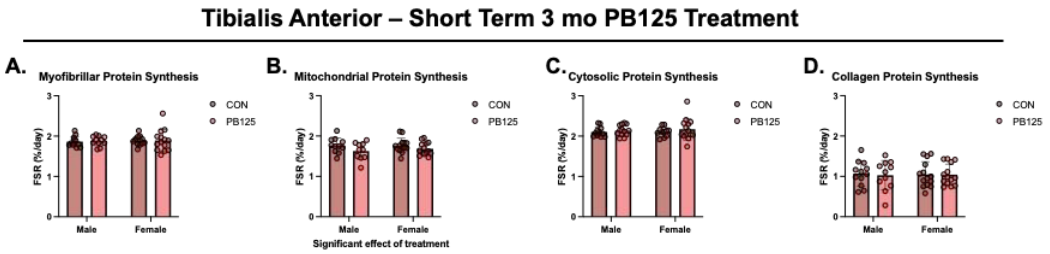

Figure F.3. Rates of tibialis anterior protein synthesis with 3 mo of PB125 treatment. Rates of myofibrillar (A), cytosolic (C), and collagen (D) proteins were maintained with 3 mo of PB125 treatment in younger Hartley guinea pigs. However, rates of mitochondrial proteins were significantly lower in guinea pigs treated with PB125 (B), suggesting that the quality of the mitochondria were better lending to lower rates of protein synthesis. There were no differences between male and female guinea pigs in any of the fractions.

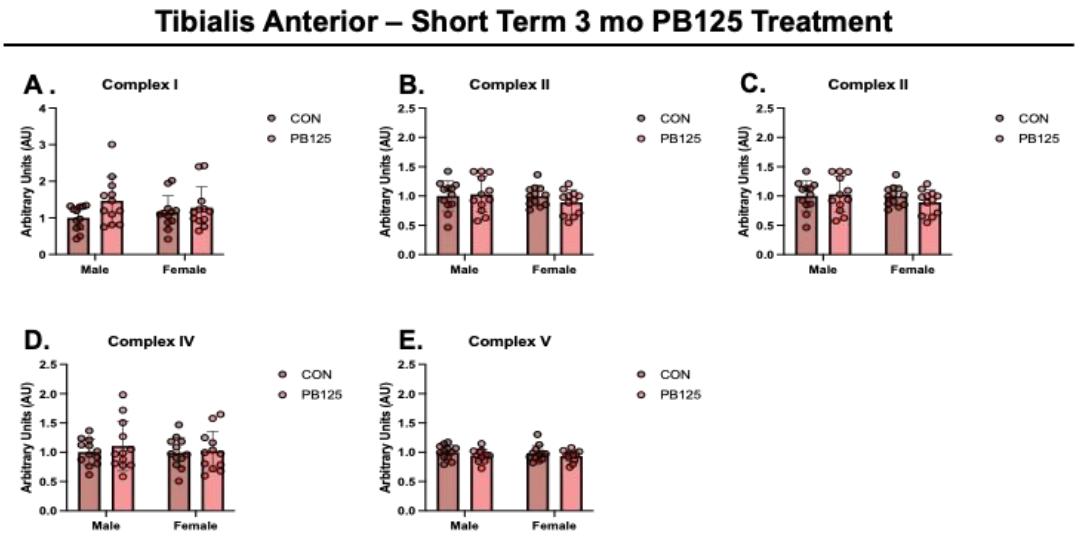

Figure F.4. Mitochondrial protein content does not change with 3 mo of PB125 treatment. An OXPHOS western blot semi-quantitively determined the relative protein content of one component of each of the five distinct mitochondrial protein complexes. There were no effects of treatment or sex on any in any of the five complexes which suggests that despite decreases in mitochondrial protein synthesis with PB125 treatment (Figure B.3C) mitochondrial protein breakdown was matched.

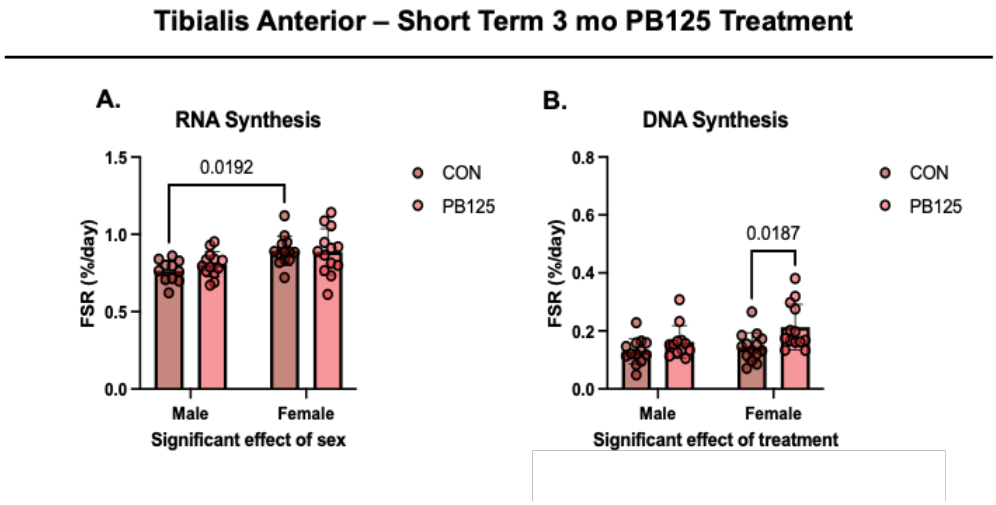

Figure F.5 Rates of tibialis anterior ribosomal biogenesis and DNA synthesis with 3 mo of PB125 treatment. We enriched body water with deuterium oxide (^2H_2O) to facilitate dynamic and simultaneous monitoring of rates of newly synthesized RNA and DNA. Independent of PB125 treatment there was an overall effect of sex that female Hartley guinea pigs had higher rates of ribosomal biogenesis than male Hartley guinea pigs (A). There was an overall effect of treatment to increase rates of DNA synthesis, a measure of cellular proliferation that was largely driven by the female Hartley guinea pigs (B).

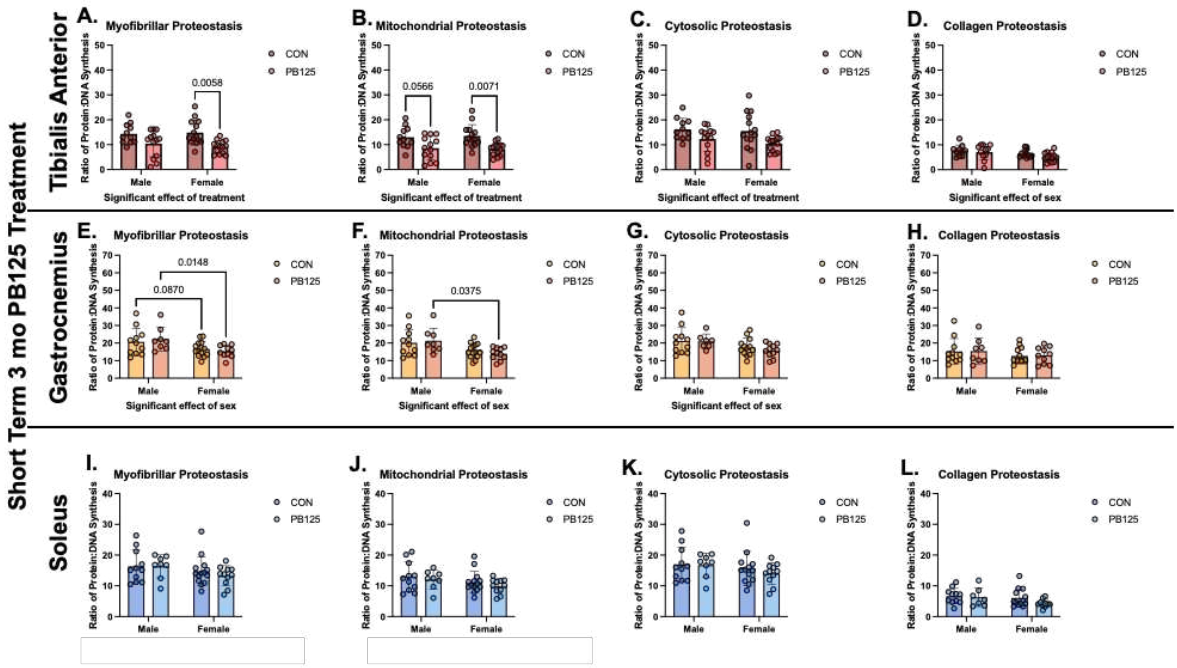

Figure F.6. Mechanisms of proteostasis in tibialis anterior favor growth compared to the gastrocnemius and soleus with 3 mo of PB125 treatment. We have previously highlighted the importance of considering protein synthesis rates relative to cellular proliferation when interpreting mechanisms of proteostatic maintenance [1]. Therefore, we expressed rates of protein synthesis relative to DNA synthesis as a ratio. Additionally, we re-analyzed previously published data in the gastrocnemius and soleus from these same guinea pigs [6], to compare responses to treatment with a Nrf2 activator between muscles of different fiber types [7]. We found that PB125 decreased the ratio of protein to DNA synthesis rates, suggesting that allocation of newly synthesized myofibrillar (A), mitochondrial (B), and cytosolic (C) proteins was likely for growth, with less investment in proteostatic maintenance. There was an overall effect of sex in the collagen fraction in that females had a lower ratio of protein to DNA synthesis compared to males (D). Conversely, there were no effects of PB125 treatment in all fractions of the gastrocnemius or soleus (E – L). There was an overall effect of sex in the gastrocnemius myofibrillar (E), mitochondrial (F), and cytosolic (G) fractions in that females had a lower ratio of rates of protein to DNA synthesis.

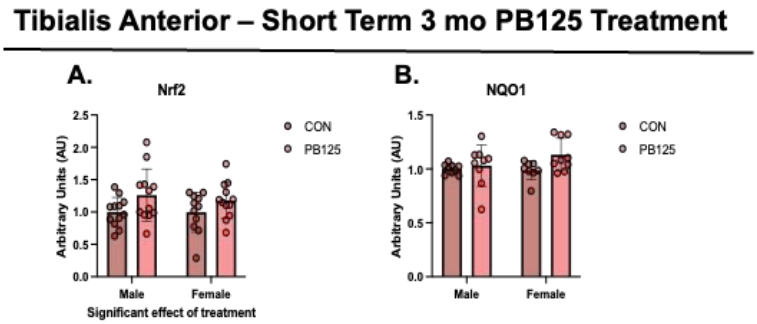

Figure F.7. 3 mo of PB215 treatment increase Nrf2 protein content but not a downstream antioxidant. Given we treated Hartley guinea pigs with a Nrf2 activator we wanted to examine if increases in Nrf2 protein content mediated some of these changes in tibialis anterior mechanisms of proteostasis. We indeed observed an overall effect of treatment in the Nrf2 protein after 3 mo of PB125 treatment (A). However, there were no effects on NQO1, a downstream antioxidant of Nrf2 (B).

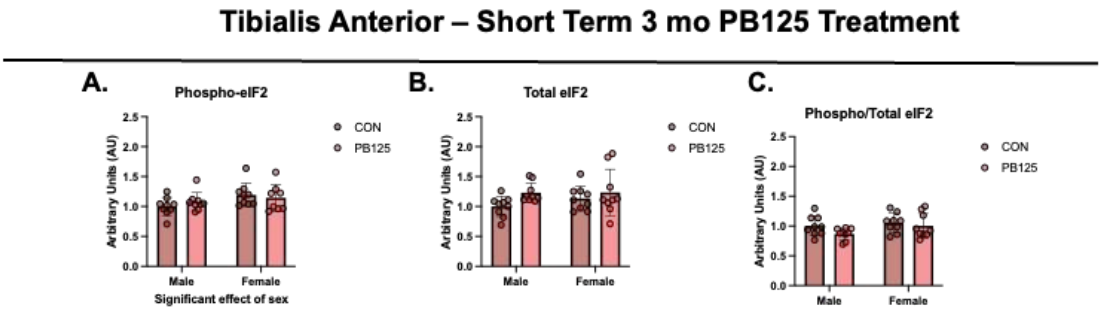

Figure F.8. The phosphorylation state of eIF2 was not altered with 3 mo of PB125 treatment. Because we observed that females had higher rates of ribosomal biogenesis we examined if the phosphorylation state of eIF2, a protein critical for translation, was altered. Parallel to increases rates of ribosomal biogenesis there was increased phosphorylated eIF2 in females (A). However, there were no differences in total eIF2 (B) or the ratio of phosphorylated to total eIF2 (C).

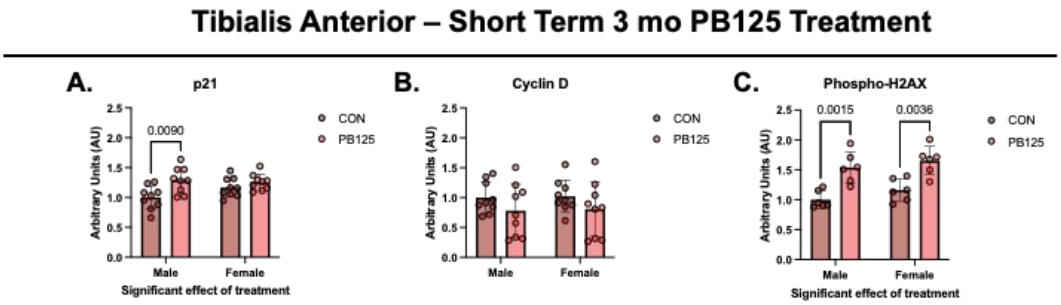

Figure F.9. Markers of senescence and senescence associated DNA damage were increased with 3 mo of PB125 treatment. Because rates of DNA synthesis were increased with PB125 treatment we interrogated markers of cell cycle regulation and senescence associated DNA damage. Contrary to what we would expect was that PB125 increases p21, a marker of cellular senescence (A), but there were no differences in cyclin D, a cell cycle regulator (B). Paralleling the increased p21, PB125 also increases phospho-H2AX, a marker of senescence associated DNA damage (C).

REFERENCES

1. Miller BF, Drake JC, Naylor B, Price JC, Hamilton KL. The measurement of protein synthesis for assessing proteostasis in studies of slowed aging. Ageing Res Rev. 2014;18:106-111. doi:10.1016/j.arr.2014.09.005

2. Walsh MA, Zhang Q, Musci RV, Hamilton KL. The combination of NRF1 and Nrf2 activators in myoblasts stimulate mechanisms of proteostasis without changes in mitochondrial respiration. Redox Muscle Physiology Exerc Sport. Published online 2022:100001. doi:10.1016/j.rimpes.2022.100001

3. Bruns DR, Ehrlicher SE, Khademi S, et al. Differential Effects of Vitamin C or Protandim on Skeletal Muscle Adaptation to Exercise. J Appl Physiol. Published online 2018. doi:10.1152/japplphysiol.00277.2018

4. Musci RV, Walsh MA, Konopka AR, et al. The Dunkin Hartley Guinea Pig Is a Model of Primary Osteoarthritis That Also Exhibits Early Onset Myofiber Remodeling That Resembles Human Musculoskeletal Aging. Front Physiol. 2020;11:571372. doi:10.3389/fphys.2020.571372

5. Borowik AK, Davidyan A, Peelor FF, et al. Skeletal muscle nuclei in mice are not post-mitotic. Funct. Published online 2022. doi:10.1093/function/zqac059

6. Musci RV, Andrie KM, Walsh MA, et al. Phytochemical compound PB125 attenuates skeletal muscle mitochondrial dysfunction and impaired proteostasis in a model of musculoskeletal decline. J Physiology. Published online 2022. doi:10.1113/jp282273

7. Wang Z, Xu H, Zhou H, et al. Long term detraining reverses the improvement of lifelong exercise on skeletal muscle ferroptosis and inflammation in aging rats: fber type dependence of the Keap1/Nrf2 pathway. Biogerontology. Published online 2023. doi:10.1007/s10522-023-10042-1

8. Kobayashi M, Yamamoto M. Nrf2–Keap1 regulation of cellular defense mechanisms against electrophiles and reactive oxygen species. Adv Enzyme Regul. 2006;46(1):113-140. doi:10.1016/j.advenzreg.2006.01.007

9. Andrie KM, Palmer DR, Wahl O, et al. Treatment with PB125® Increases Femoral Long Bone Strength in 15-Month-Old Female Hartley Guinea Pigs. Ann Biomed Eng. Published online 2023:1-11. doi:10.1007/s10439-023-03415-7

10. Dungan CM, Wells JM, Murach KA. The life and times of cellular senescence in skeletal muscle: friend or foe for homeostasis and adaptation? Am J Physiol-Cell Physiol. 2023;325(1):C324-C331. doi:10.1152/ajpcell.00553.2022

11. Saito Y, Chikenji TS, Matsumura T, Nakano M, Fujimiya M. Exercise enhances skeletal muscle regeneration by promoting senescence in fibro-adipogenic progenitors. Nat Commun. 2020;11(1):889. doi:10.1038/C1467-020-14734-x

12. López-Otín C, Blasco MA, Partridge L, Serrano M, Kroemer and G. Hallmarks of aging: An expanding universe. Cell. Published online 2023. doi:10.1016/j.cell.2022.11.001